REPORT NO.
UCB/EERC-82/05
JUNE 1982

EARTHQUAKE ENGINEERING RESEARCH CENTER

MODEL STUDY OF EFFECTS OF DAMAGE ON THE VIBRATION PROPERTIES OF STEEL OFFSHORE PLATFORMS

by

F. SHAHRIVAR
J. G. BOUWKAMP

Report to the National Science Foundation

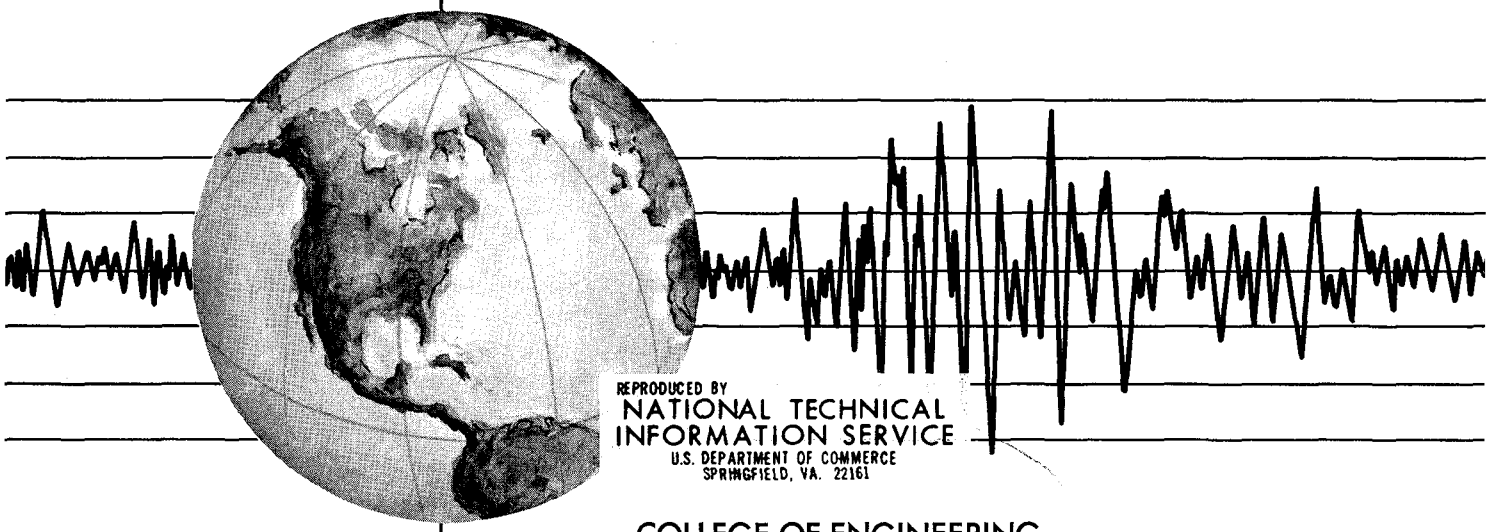

COLLEGE OF ENGINEERING

UNIVERSITY OF CALIFORNIA · Berkeley, California

For sale by the National Technical Information Service, U.S. Department of Commerce, Springfield, Virginia 22161.

See back of report for up to date listing of EERC reports.

DISCLAIMER

50272-101

REPORT DOCUMENTATION PAGE	1. REPORT NO. NSF/CEE-82012	2.	3. Recipient's Accession No. PB83 148742
4. Title and Subtitle: Model Study of Effects of Damage on the Vibration Properties of Steel Offshore Platforms			5. Report Date: June 1982 6.
7. Author(s): F. Shahrivar and J. G. Bouwkamp			8. Performing Organization Rept. No. UCB/EERC-82/05
9. Performing Organization Name and Address: Earthquake Engineering Research Center, University of California, Berkeley, 47th Street and Hoffman Blvd., Richmond, Calif. 94804			10. Project/Task/Work Unit No. 11. Contract(C) or Grant(G) No. (C) (G) PFR-79-08257
12. Sponsoring Organization Name and Address: National Science Foundation, 1800 G Street, N.W., Washington, D.C. 20550			13. Type of Report & Period Covered 14.

15. Supplementary Notes

16. Abstract (Limit: 200 words)

The selected vibration properties of an offshore platform model were studied considering both damaged and undamaged conditions. The platform model was a 1/50th scale, three dimensional tower possessing the key features of a typical, eight legged, k-braced steel offshore platform. Changes in the vibration frequencies and mode shapes of fixed offshore platforms can be used to detect damage. In this study, for the first time, quantitative information on mode shapes was utilized leading to improved damage detection capabilities.

The scaling considerations, the model and the experimental method are described. The experimental results are complemented with analytical results and show excellent correlation. In general, emphasis is placed on the vibration frequencies and deck modal displacements of the first two translational modes and the first torsional mode. The effects of a variation in deck mass are assessed both experimentally and analytically. Also, the the effects of shifts in the position of the deck center of mass are assessed analytically.

Both experimental and analytical results support the potential application of mode shape monitoring to detect structural damage. This study illustrates that when both frequencies and mode shapes are considered, damage related changes differ in characteristics from variations not related to damage.

17. Document Analysis a. Descriptors

b. Identifiers/Open-Ended Terms

c. COSATI Field/Group

18. Availability Statement: Release Unlimited	19. Security Class (This Report): UNCLASSIFIED	21. No. of Pages: 213
	20. Security Class (This Page): UNCLASSIFIED	22. Price

(See ANSI-Z39.18) *See Instructions on Reverse*

OPTIONAL FORM 272 (4-77)
(Formerly NTIS-35)
Department of Commerce

MODEL STUDY OF EFFECTS OF DAMAGE ON THE VIBRATION PROPERTIES OF STEEL OFFSHORE PLATFORMS

by

F. Shahrivar

and

J. G. Bouwkamp

Report to the National Science Foundation

Report No. UCB/EERC-82/05

Earthquake Engineering Research Center
University of California
Berkeley, California

June 1982

ABSTRACT

Changes in the vibration frequencies and mode shapes of fixed offshore platforms can be used to detect damage. The selected vibration properties of an offshore platform model were studied considering both damaged and undamaged conditions. The platform model was a 1/50th scale, three dimensional tower possessing the key features of a typical, eight legged, k-braced steel offshore platform. In this study, for the first time, quantitative information on mode shapes was utilized leading to improved damage detection capabilities.

The scaling considerations, the model and the experimental method are described. The experimental results are complemented with analytical results and show excellent correlation. In general, emphasis is placed on the vibration frequencies and deck modal displacements of the first two translational modes and the first torsional mode. The effects of a variation in deck mass are assessed both experimentally and analytically. Also, the effects of shifts in the position of the deck center of mass are assessed analytically.

Both experimental and analytical results support the potential application of mode shape monitoring to detect structural damage. Results demonstrate that modal displacements of the deck and the vibration frequencies for the first two translational modes and the first torsional mode of the structure are sufficient for monitoring structural integrity. Findings show that frequency changes of only a few percent are accompanied by changes of more than 30% in the normalized modal displacements of the deck when certain members are damaged. Because the ability to detect damage through changes in vibration properties is potentially hampered by significant variations not related to damage, it is important that such variations be distinguishable from changes caused by damage. This study is an illustration that when both frequencies and mode shapes are considered, damage related changes differ in characteristics from variations not related to damage.

ACKNOWLEDGEMENTS

The research reported herein was submitted by the senior author in partial satisfaction of the requirements for the degree of Doctor of Philosophy in Engineering. The study was carried out under the supervision of Professor Jack G. Bouwkamp through the sponsorship of the National Science Foundation under grant PFR-7908257. The authors gratefully acknowledge this grant. The valuable suggestions and review of the manuscript by Professor Ray W. Clough are greatly appreciated. The advice of Professor John R. Paulling and assistance of the Department of Naval Architecture in providing the ship model towing tank for the tests were of great help to the project.

The implementation of the project required the assistance of several staff members; Lou Trescony, Dave Wasley and Roy M. Stephen provided assistance during the operations. The help of these people, the assistance of the graduate students, and the efforts and help of the technical staff of the SESM machine shop are appreciated.

Thanks are due to Messrs. Xin Sen Lu and Ben Burke for their contributions through rewarding discussions, and to Dr. J.A. Ruhl of Shell Oil Co. who provided design drawings of a Shell tower.

The senior author wishes to express his gratitude to his father, Mr. Mohammad Shahrivar, for his supportive assistance and consultation throughout the dynamic tests. The first author also wishes to thank his wife for her help and support during the course of the project.

TABLE OF CONTENTS

CHAPTER 1

INTRODUCTION

1.1 Overview

The discovery of offshore oil and gas reservoirs and the increased demand for energy in recent decades have caused considerable efforts to explore, drill, and develop these offshore resources. In the last decade oil production in the North Sea has had a significant positive impact on the economy of the western European nations. Meanwhile, the increased production in North American waters has also been notable. Increased development of offshore oil and gas resources is apt to continue in North American waters and worldwide.

Most offshore oil production facilities are installed on steel towers which are supported by the ocean floor or seabed. The steel towers or platforms, considered in this study, are three dimensional trusses constructed from tubular members with circular cross sections. These structures serve as drilling and/or production platforms, and house the necessary plant facilities at several deck levels located at their uppermost part. Furthermore, they provide lateral support at different levels along their height for the conductor pipes which house the production risers that extend from the ocean floor to the deck level. The main body of these towers, called the jacket (Fig. 1.1), is secured to the ocean floor by means of piles. Some piles are driven through the hollow legs into the ocean floor (leg piles), and others (skirt piles) through sleeves that are connected to the lower portion of the jacket (Fig. 1.1). Although grouting is used to bond the skirt piles to their sleeves, it is not always used for the leg piles to which the deck assembly (truss cap, refer to Fig. 1.1) is welded.

These structures are proportioned to withstand expected environmental loads [1] which vary depending on geographic location; e.g., for towers in the Gulf of Mexico wave and wind loads generated by hurricanes need to be considered, for those in the Gulf of Alaska

forces due to waves and winds generated by extratropical storms should be taken into account, and for towers in seismic regions, such as the coastal waters of California or Alaska, loads caused by earthquakes of certain intensity and duration (possessing certain spectral characteristics) need to be considered. During the life of a platform the environmental loads may cause structural damage in the tower, notably fatigue. In addition, unexpected accidents during erection, pile driving, or the final stages of construction at the ocean site could also cause damage. Further, a tower is not immune to damage in the event of collision with a ship or an iceberg.

Higher towers are being constructed as the search for offshore gas and oil is pursued into deeper waters and more hostile environments. Platforms subjected to more arduous conditions have a higher probability of structural failure and are more difficult to repair. The increased capital cost of these towers and the consequences of a catastrophic failure make a strong appeal for any technique that will give advance warning of failures that could possibly lead to total loss of the platform. In addition to the significant economic losses, safety of personnel and environmental considerations dictate that platforms be safe from collapse. Damage detection techniques will allow the implementation of procedures both to safeguard personnel and to protect the environment when collapse is imminent. In addition, repairs can be carried out in a timely fashion to prevent further damage or collapse. Such techniques will considerably benefit the planning and control of production processes, particularly for those platforms which are in remote locations [2]. Damage detection at earlier stages will greatly facilitate undersea repairs and reduce repair costs and other economic losses.

In the past, periodic subsea divings have been used for detecting damage to offshore towers. Despite improvements in diving equipment and expertise, the technique has its limitations. It cannot guarantee a thorough and reliable inspection of any tower. The effectiveness is limited by hostile environments and it cannot be pursued at very great depths.

The dynamic characteristics of an offshore platform, such as natural frequencies of vibration and mode shapes, depend upon the tower stiffness and mass distribution. Failure of any structural member can alter the platform stiffness and dynamic characteristics; so that a change in the dynamic characteristics can be used to infer damage to the integrity of the structure. To be useful, such changes must be significant enough to be detected with ease. In addition, changes not due to damage, such as variations in the deck mass, and marine growth, could affect the dynamic characteristics, so one must be able to distinguish changes caused by damage from those not caused by damage.

Dynamic characteristics of a structure can be evaluated either by performing a controlled test and analyzing the resulting response, or by analyzing the structure's response to a broad spectrum of random, dynamic loads due to waves and wind. In either case, the vibration information is evaluated with respect to the vibration modes which are excited. In general, vibration monitoring can be effective and easier to apply if waves, which are the most commonly encountered input, excite the vibratory response. However, it must be realized that in areas where the sea is generally calm (Gulf of Mexico and coastal waters of Southern California) little dynamic excitation is to be expected most of the time, and for this reason forced excitation may be necessary.

When the vibration information is to be obtained by performing a dynamic test, several factors must be considered prior to selecting the type of test. Generally these factors include some prior knowledge of the features and properties of the structure (which can be obtained by preliminary tests), and the specific dynamic characteristics that are to be evaluated. For example, depending on the need and also the practicality, one may cause significant excitation in a single mode only, by performing a snapback type of test. Likewise, one may excite several modes at the same time by inducing shock, or one may measure the steady state response of a tower to resonant excitation and obtain transfer functions which are functions of the natural frequencies, their associated mode shapes, and their damping [3]. The vibratory response to ambient excitation is generally sufficient for evaluat-

ing the characteristics of at least several vibration modes and can be used for continuous monitoring of these characteristics.

By using measurements at appropriate locations on a tower in its ambient vibration state or during a well planned, controlled dynamic test, one can obtain quantitative information on the dynamic characteristics of the structure. If the data are gathered at appropriately selected locations, information may be obtained which is pronounced and sensitive to damage. By examining relevant characteristics one could be in a position to infer damage by observing the changes in these quantities.

1.2 Background

In this report the term "monitoring" implies keeping track of the changes or lack of change in the appropriate dynamic properties of a tower to infer damage. Frequencies (periods) and mode shape information may be monitored for this purpose. Properties of global modes, which are mainly the lower modes, as well as higher modes of local nature, may be used in the monitoring.

In general, breakage or complete severance of a leg or of a vertical or diagonal member, which functions as one of the lateral stiffness and load resisting elements in the tower, can cause changes in the global mode characteristics [4,5,6,7]. Local cracks (usually near the joints in the braces), which cause flooding, have practically no effect on the overall lateral stiffness of the steel towers, but cause a local increase in the mass of the tower. This type of damage may cause detectable changes in some of the higher global modes of the structure but generally not in the lower ones [4]. Stress concentrations in the cracked areas and the corrosive environment can cause progression in the crack and lead to complete severance. On the other hand, local cracks which affect the end condition of members and change their effective mass, can be detected by monitoring the local modes [4].

There has been considerable industrial research to gain experience and to examine the feasibility of integrity monitoring of existing towers. Investigators have obtained natural

vibration frequencies of offshore platforms from vibration measurements and have attempted to detect and observe changes in the frequency values. Most of the investigators have relied on ambient excitation of the vibratory response. Forced vibrations, which have been commonly carried out on buildings [8,9,10], have also been employed [3]; boat impact and pulling have also been used to excite towers [11].

Spectral methods appropriate for the analysis of random data [12,13,14,15] have been employed to obtain and evaluate vibration information from ambient acceleration measurements. The task of evaluating vibration frequencies by such techniques is practical and easy [16]. Accelerations measured at a single location can provide several vibration frequencies, and measurements at only a few locations suffice to evaluate frequencies of the excited modes and to identify their mode shapes.

Earlier investigations have been mainly concerned with the lower modes of vibration [16,17,18], and have relied on measurements taken at the deck and above the water level. This is in part due to the fact that for the usual towers the ocean waves and the ambient conditions easily excite these modes, and the accelerations (as well as the displacements and velocities) resulting from the fundamental vibrations are largest at the deck level, which is the most convenient location for taking measurements. In later investigations, attempts were made to obtain and to identify higher modal frequencies. The vibration measurements taken on the deck and above the water level, were complemented with below water measurements [3,4]. Mathematical models were developed in conjunction with these studies and were refined to correlate better with the observations. These computer models served as the primary means of assessing the quantitative frequency changes in case relevant members were completely severed because of the scarcity of opportunities resulting from modification, repairs, or for other reasons [4,6]. Recently attention was diverted to local frequency monitoring [3,4], an area in which there is continuing research.

An early study by Vandiver in 1974, which was used to confirm the lack of member breakage in a 150 foot tall Coast Guard tower standing in 70 feet of water, showed that it

was possible to detect damage by employing vibration frequency values [17]. Later, investigations of three platforms in 100 feet of water demonstrated that frequencies of the lowest translational modes along with some higher modes, which could include up to the third translational modes, could be obtained from measurements at the deck level (above water) [16]. These frequencies were in the 0.4 to 10 Hz range, and were stable to within 3%. A minor modification to one of these towers resulted in frequency changes of up to 15%. Later work, reported in 1978, examined the natural periods of four towers in deeper waters (up to 373 feet) and compared measured results with analytical results [11]. The analytical investigation included parametric studies of deck mass and pile stiffness variations to evaluate their effect on vibration periods.

In a later investigation, a platform owned by Shell Oil Company in 327 feet of water was studied extensively [5]. It was instrumented at 17 locations above the water level for ambient vibration measurements. Twenty-four modes were detected, ranging from 0.65 to 4.5 Hz. These included the fundamental up to the third translational modes and other complex modes. Uncertainties in the parameters affecting the vibration periods were discussed. The thresholds for damage detection were believed to be about 1% for the fundamental frequencies and about 2% for frequencies of well-identified higher modes. That is, changes larger than these values would indicate more than 90% likelihood of failure. Measured frequencies of the fundamental modes in rough seas were 1 to 2% lower than those measured in calm seas. For a given sea state the frequencies were detectable to within 0.5 to 0.8%. An analytical model of the tower was developed and was successively refined. Failure studies on the refined analytical model were conducted. It was concluded that breakage of some vertical diagonals on the periphery of the jacket or failure of a leg pile could be detected from shifts in the frequency values.

In another investigation, three towers in 212 feet, 375 feet, and 213 feet of water - referred to here as the first, second, and third towers, respectively - were studied [6]. Data were gathered on these platforms during several visits and were evaluated using spectral

techniques. Ambient measurements on the first tower showed an excellent stability of frequencies for the different visits. For the second tower machinery noise dominated the measurements and no conclusions were made concerning the frequency stability. In the third platform three bracing members were replaced. Ambient measurements were taken before the repairs were carried out as well as during the intervals when members were removed, and after the new members were installed. This tower was modeled analytically and the analytical model was tuned to correlate better with the observed properties. Parameter studies and member removal analyses (which included the members that were replaced) were carried out. The considered frequencies ranged from about 0.65 to 4.60 Hz. The analysis indicated significant changes in the higher frequencies, and in some cases in the order of some of the higher modes, as a result of damage. Some limited modal information for the response shapes was obtained by applying the data analysis technique described in Reference 19 to the ambient measurements. The investigators encountered some problems in correlating the analytical frequencies to the results from measurements, but this perhaps was related to the mass modeling at the deck. The tower had a large oil storage tank located eccentrically at its uppermost deck. The tank when full, weighed 2100 K, which was a substantial portion of the total deck weight. With the fundamental frequencies ranging from about 0.65 to 1.0 Hz, shifts by as much as about 10% were observed. However, the investigators were unable to detect removal of bracing members from their ambient vibration (frequency) results.

The removal of a four-legged gas producing platform from the North Sea provided another good opportunity to assess the effectiveness of vibration monitoring. The tower was located in about 75 feet of water and was about 170 feet high. It was not a typical platform. The feasibility of both local monitoring and global monitoring for this tower was investigated [4]. Ambient vibration measurements were taken before and after a member was completely severed at one end. Intermediate measurements mainly for monitoring the local modes were taken as the member was progressively cut. The tower was instrumented both

above and below water level. Eight below-water level accelerometers were placed on a group of four members in the panel where the member was to be cut. These were located in groups of two, on the individual members (and between the joints) to detect local in-plane and out-of-plane modes of vibration. The measured global frequencies, which included the second group of frequencies, ranged from about 1.3 Hz to 4.0 Hz and were believed to be stable and accurate to within 1% to 2%. Two separate analytical models were used. One was used to study relevant local modes ([4], p. 113), and the other was used for the global modal analysis. The flooding as the member was being cut was easily detected by the changes in the frequencies of the local modes. These frequencies, which were analytically determined to within 3%, changed more than 12%. Severance (a complete cut), as well as some general conclusions regarding its general location, were also easily confirmed by using the global modes. Measured changes in the frequencies of the fundamental modes were as large as 15%.

Very limited work has been done to employ quantitative mode shape information for monitoring purposes. A method described in Reference 19 uses the matrix of cross and auto spectral density functions [12] (which can be obtained from random data measurements in the ambient state) to obtain quantitative information on the response shapes at the frequencies where peaks occur in the spectra. The results are obtained iteratively using a least squares method. In application [6,19] some difficulties were reported with closely spaced modes or where two modes make significant contributions; the method was otherwise satisfactory in obtaining good estimates of mode shape information.

Collectively the investigations reported show that for some smaller towers global frequency monitoring above the water can be used successfully to identify damage. However, it provides little help for inferring damage in deep water platforms. This is principally due to the fact that changes in these frequencies resulting from damage are small, and that small variations in dynamic parameters, such as deck mass, also cause frequency shifts. The global frequency changes due to damage are directly related to the change in the overall

stiffness of the platform. For higher towers the reduction in the overall lateral as well as in the torsional stiffness, resulting from severance of a single member, will be smaller. Thereby, the global frequency monitoring method is successful in detecting damage only with smaller towers.

So far the effects of damage on quantitative mode shape information have not been investigated. Mode shape information has been used qualitatively in general for the purpose of modal identification. How large are the quantitative changes in mode shape information when damage occurs? Are there also relatively significant variations due to non-damage phenomena, such as alterations in the deck mass? If the changes due to damage are large they will also provide some latitude to distinguish significant non-damage type variations from those resulting from damage. Hence, these concepts are important and should be investigated.

1.3 Objectives

The purpose of the program described in this report was to study mode shapes and frequencies under undamaged and damaged conditions using a three dimensional laboratory model. The laboratory model was designed so that it possessed the key features and properties of a typical steel offshore platform. The specific objectives of this program are listed as follows:

1. To assess the possibility of inferring damage by observing the changes in the vibratory characteristics, namely the frequencies and mode shapes, of the tower.
2. To assess the relative usefulness of mode shapes and frequencies in detecting damage by comparing the quantitative changes in the frequencies with the quantitative changes in the mode shapes when damage occurs.
3. To assess what the above changes can reveal as to location of damage.
4. To examine how well the changes can be predicted analytically.

5. To examine the effect of deck mass on these characteristics and their variation as a result of damage.

6. To observe and/or examine other phenomena, such as the effect of submergence on the dynamic characteristics (frequencies and mode shape, for example) and how well they correlate with analytical predictions, when such prediction opportunities are provided.

7. To provide some information and also gain insight on some of the local vibration phenomena that are relevant to integrity monitoring.

1.4 Method and Scope

A typical steel offshore tower was chosen and the portion above the skirt pile section (to which the skirt pile sleeves were connected, refer to Fig 1.1) was selected as the prototype of the test structure. Then a three dimensional laboratory model based on the prototype was designed and constructed. Finally a mathematical model of the laboratory structure was formulated for analytical correlation.

The study encompassed the complete severance of one bracing member for each damage case considered. During the test program, four diagonal bracing members were severed, one at a time, by removing a small section near the lower end to simulate complete failure of the member. In the undamaged case and in the four damaged cases the tower was submerged. Two deck mass conditions, namely the maximum and the minimum loadings, were considered in each case. In all cases these masses were non-eccentric (i.e., in plan view the position of the center of mass of the deck coincided with the center of rigidity of the undamaged structure). Both frequency and mode shape information were considered in the study. Emphasis was placed on the three fundamental modes (two translational and one torsional), considering their mode shapes as indicated by deck displacement measurements.

The effect of submergence on the dynamic characteristics was assessed for the tower in the (undamaged) minimum deck mass condition. The effect of deck mass eccentricity as

well as an additional case of damage was examined analytically by using the mathematical model. Further details of the research program are presented in Chapters 2 through 5.

CHAPTER 2

THE EXPERIMENTAL MODEL

2.1 Introduction

Experimentations on actual structures, to better understand their behavior, is generally impractical when it involves modifying or damaging the structure. In many engineering applications small scale replicas (models) of actual structures (the prototypes) are employed instead for this purpose. Generally the model is much more economical to construct and easier to test, and its behavior reveals the (key) features of the prototype behavior. These concepts were pertinent to this investigation, in which a small scale three-dimensional model was to be employed in place of a full scale steel platform. The model was to be tested in a ship model towing tank which could hold water up to a depth of 5.5 feet, while the water depth for the (typical) prototype was to be greater than 200 feet. Considering the overall as well as the typical member sizes in offshore platforms, the size of the testing facilities (which included the water depth in the tank and the room required for the base apparatus onto which the model was to be fixed), the available material properties and also tubing sizes that could be used to construct a model, a geometric scale of 1/50th was selected. In using such a small model, concepts related to scaling had to be considered.

The purpose behind designing the model was to come up with a test structure which possessed the important features common to the class of platforms the model was to represent. To meet this purpose a typical steel offshore platform was selected as prototype, but the scaling (similitude) requirements, which render an exact one-to-one correspondence of every important variable in the prototype and its model, were used only as a general guide in designing the model. Hence the model was not intended to simulate the behavior of the particular steel tower selected, but only to behave similarly to a typical structure.

In this chapter basic concepts related to scaling are summarized, and the necessary similitude requirements for a model structure are presented. The guidelines followed in

designing the experimental model are described. Also, the selection of material for constructing the model is discussed. Finally, the model structure is described and its relevant features are discussed with reference to the corresponding features in the selected full scale structure.

2.2 Basic Concepts

Similarity of a model and its prototype implies a one-to-one correspondence in their key properties and behavior. Every value of a key variable in the model, such as time, corresponds to a unique value of the similar variable in its prototype. These corresponding values are defined as homologs. The ratios of homologous parameters are constants called scale factors. They are defined here as the ratio of the variable in the prototype to its homolog in the model.

Allowing length, time, and mass to be the three fundamental dimensional quantities of mechanics, all other dimensional quantities can then be expressed in terms of these three, denoted by the symbols L, T, and M. Using the list of all variables that can have a bearing on the behavior of a prototype, a set of independent, dimensionless terms called Pi terms can be formed, where each Pi term is formed by the products and ratios of a subset of the variables.

As long as the corresponding Pi terms in a prototype and its model have the same values, the model will simulate the prototype behavior. The only restriction will be on the values of the Pi terms in the model and not on the values of individual variables. So that for a given geometric scale factor, any set of scale factors for the homologs that provides the required Pi term values is permissible. This set of scale factors defines the similitude requirements and is used for designing a model. For a model that is designed to simulate the vibratory properties of its prototype, and that complies with the necessary similitude requirements, homologous parts will experience homologous forces at homologous times, and corresponding forces will have the same ratio in the model and prototype. A comprehensive presentation of the theory of models, and a strategy for deriving Pi terms

and similitude requirements can be found in References 20, 21, and 22.

To derive Pi terms for the study of mode shapes and frequencies of a platform, the variables that affect the quantities under study are needed. The length, wall thickness, outer diameter for every member, and the elastic modulus control the stiffness of the tower and the elastic forces during vibrations. The mass distribution of the tower will then be defined by the mass density for the members and the mass of the deck (which will be designed and also assumed to behave as a rigid unit in this program). The inertial contributions from the fluid in which the tower is submerged are dependent on the outer diameters of the tubular members (also inner diameters for the flooded legs) in the structure, and the mass density of the fluid. The preceding completes the list of important variables in the study.

The Reynolds number which defines the ratio of inertial forces to viscous forces in the fluid medium [23] could not be the same for a prototype and its model in this study, due to the fact that tests could be carried out in water only (instead of a fluid with a much smaller coefficient of kinematic viscosity [23,24]), and therefore, forces arising from the fluid viscosity would be exaggerated. Viscosity had a very small effect, if any, on the vibration mode shapes and frequencies of the platform, which was subjected to small amplitude vibrations during the tests, although it may have contributed in damping out the vibrations of the model platform. However, damping measurements in both air and water indicated less than one percent of critical damping in the model for the primary vibration modes. This amount of damping affects the undamped vibration frequencies by less than 0.005%, does not affect the mode shapes, and is therefore not a concern in the study.

The list of important variables in the study can be summarized as follows:

Parameter		
Independent variables	**Symbol**	**Dimension**
Tower deck mass	m	M
Mass density of the material for structural members	ρ_s	$M\ L^{-3}$
Length for members	l	L
Outer diameter for members	D	L
Wall thickness for members	t	L
Modulus of elasticity for members	E	$M\ L^{-1}\ T^{-2}$
Mass density of the fluid medium	ρ_f	$M\ L^{-3}$
Dependent variables		
Vibration frequencies	f	T^{-1}
Normalized modal displacements (non-dimensional)	ϕ	–

The six Pi terms: $P1 = \frac{\rho_s}{\rho_f}$, $P2 = \frac{D}{l}$, $P3 = \frac{t}{l}$, $P4 = \frac{m}{l^3 \rho_f}$,

$P5 = (f\sqrt{\rho_f}\, l)/\sqrt{E}$ and $P6 = \phi$ can be obtained from these.

Since water is used for simulating the fluid environment

$$\frac{(\rho_f)_{model}}{(\rho_f)_{prototype}} = \frac{\rho_{fm}}{\rho_{fp}} = \frac{1}{\rho_{fr}} = 1$$

and from the first Pi term $\left(\frac{\rho_s}{\rho_f}\right)_{model} = \left(\frac{\rho_s}{\rho_f}\right)_{prototype}$ is required. Therefore $\rho_{sr} = \rho_{sp} / \rho_{sm} = \rho_{fp} / \rho_{fm} = \rho_{fr} = 1$ will demand the same mass densities for the members in the prototype and its model. Using the chosen geometric scale $l_r = 50$, the second and also the third Pi terms, $D_r = l_r = t_r = 50$ will be required. Similarly, using P4, $m_r = \rho_{fr} (l_r)^3 = 50^3$ is demanded for the deck mass. So that $\phi_r = 1$ (the same normalized modal displacements in the model and prototype) and

$$f_r = \frac{\sqrt{E_r}}{l_r \sqrt{\rho_{fr}}} = \frac{\sqrt{E_r}}{50}$$

will hold true for the model. The preceding comments are summarized in Tables 2.1 and 2.2.

According to this analysis there is no restriction on the value of E for the model. To choose this value, the acceleration of gravity is added to the list of variables. The acceleration of gravity g, controls the fluid motions near the water surface. This variable will have some influence on the hydrodynamic inertial forces (i.e. the inertial contributions from the water) that act on the members near the free water surface during vibrations of the platform. This is a minor effect for the type of platform considered and causes very small amplitude waves that propagate radially outward from the legs (and bracing members), at the free water surface, during the platform vibrations. By including g, the additional Pi term P7 = (g l ρ_f)/E results from which $E_r = g_r \rho_{fr} l_r = (1)(1)50 = 50$ will be desired.

2.3 Material Selection

As noted above, a 600 Ksi (30,000/50 Ksi) modulus of elasticity is desirable for a 1/50 - geometric scale model. However, it was difficult to obtain a material with a modulus of exactly 600 Ksi. Further, it was also impractical to expect the member wall thicknesses to be as thin as 1/50th of those in a prototype; therefore a modulus lower than 600 Ksi would be suitable to compensate for the resulting increase in the stiffness of the model due to the

thicker member walls. These limitations confine the choice of model material to plastics, which have moduli that can range from 270 to 600 Ksi. It should be borne in mind that the material should have linear elastic behavior during the testing. Two materials were considered suitable: acrylic resin (Plexiglas) or polycarbonate.

All plastics can show creep behavior under sustained stresses, particularly at elevated temperatures. In vibration problems, however, plastics can behave practically as linear elastic material. Previously Plexiglas had been used in laboratory tests at the University laboratories. It was known that in vibration problems Plexiglas behaves as a material whose modulus is frequency dependent below some frequency and independent of frequency above this value [25].

Preliminary tests of limited scope were carried out to assess the general behavior of polycarbonate, so that from knowledge of the general behavior of both polycarbonate and Plexiglas the material which was suited best for use could be selected. Two polycarbonate specimens and one Plexiglas specimen were tested under sinusoidal axial forces. Each tubular specimen had an outer diameter of 3/4" and a wall thickness of 1/16". By means of an oscilloscope equipped with a camera, traces of axial force versus axial strain were photographed. These defined the elastic modulus, since the specimen cross sectional areas were known. The accuracy of the calculated moduli was estimated to be 7% to 5%. Because temperatures within 60° to 65° F. were expected in the towing tank, where the model was to be tested, the specimens were submerged in a water bath with a controlled temperature during these tests. For each cyclic test, the frequency of the simusoidal force was also controlled.

Test frequencies ranged from 0.1 Hz to 20 Hz during which the polycarbonate specimens showed linear elastic behavior. Test results showing the measured moduli for the Plexiglas as well as one of the polycarbonate specimens, are presented in Fig. 2.1. During these tests the temperature was held between 60° and 64° F for the Plexiglas specimen, and within 60° F to 63° F for the polycarbonate specimen. Subsequently, the polycarbonate specimen was also tested at temperatures of 59° F, 62° F, and 65° F respectively. At each

temperature, as illustrated in Fig. 2.2, four cyclic tests at different frequencies, ranging from 0.1 Hz to 15 Hz, were performed. The measured moduli were within 5% of the mean value of modulus for the first test (60° F to 63° F), and indicated no decrease in modulus as the temperature increased. Tests on the second polycarbonate specimen, with the temperature ranging from 60° to 69° F, indicated moduli within 5% of a mean of 333 Ksi. This specimen indicated the same type of behavior as the first polycarbonate specimen (refer to Fig. 2.2).

Several tests were carried out on both the Plexiglas and polycarbonate specimens to compare their material damping character. Using the log-decrement method [26] the polycarbonate was found to exhibit the lower material damping of the two.

Based on these findings it was concluded that polycarbonate behaves as a linear elastic material for frequencies higher than 0.1 Hz. It was also concluded that its modulus could be assumed constant for temperatures ranging from 60° F to 70° F. A further conclusion was that for frequencies above 6 Hz the value of the modulus for polycarbonate was considerably lower than that for Plexiglas. Even though the value of the modulus can vary somewhat from one tube to another, because this depends on the manufacturing processes, the preceding conclusion held true. Later, static tests on the model, taking up to ten minutes from loading to unloading, also confirmed the behavior of polycarbonate as being practically linear elastic. The preliminary dynamic tests on the model (and tubes used for its construction) also confirmed the aforementioned conclusions.

The vibration frequencies of the model were expected to be higher than 6.0 Hz. For these frequencies, as discussed above, the value of modulus for Plexiglas was expected to be close to the value desired (600 Ksi) for a 1/50th geometric scale model, whereas the modulus for polycarbonate was considerably lower than this value. Further, the available wall thicknesses for both polycarbonate and Plexiglas tubing were greater than what a 1/50th geometric scale demanded, and hence tended to provide a model that was stiffer than desired; Therefore, it was better to use polycarbonate (for the model) which had the lower modulus, to compensate for the resulting increase in stiffness of the model due to the

thicker member walls. In addition, desirable preliminary quasi-static verification tests (to verify the mathematical modelling of the structure with linear elastic material properties) could be carried out with a polycarbonate model, but not with a Plexiglas model, because Plexiglas behaves as a linear elastic material only in vibration tests with frequencies above approximately 5.0 Hz. In addition, the expected temperature range when testing the model in air was 66° F to 69° F, i.e., higher than the expected 60° to 65° F range when testing the model in water, and test results (described above) clearly indicated that the modulus of polycarbonate was not affected by the temperature in the 60° to 69° F range. Based on all of the preceding comments, polycarbonate was selected for constructing the model.

2.4 Selected Full Scale Tower and Description of the Model Platform

Design drawings from several typical towers were reviewed. The jacket of an eight legged, K-braced tower in 284 feet to 290 feet of water (slanted mudline) owned by Shell Oil Co. was chosen as the basic system. The portion above the 218-foot below water level, that is above the skirt pile section (refer to Fig. 1.1), was selected as the prototype to serve as a guide in designing the model platform.

The design of the model was aimed at a 1/50 reduction in the overall dimensions of the jacket and also in the outer diameters of its members. When designing the model, certain simplifications were made. The regions where the conductor guide framing was located, and also where secondary bracing members required for launching were located, were simplified rather than duplicated exactly.

Using polycarbonate tubes, the jacket of the model was designed to meet the design objectives to the best possible extent. These tubes, from which the members were cut, were 8 feet long and were supplied by different manufacturers. A specimen cut from each 8-foot length was tested to determine the elastic modulus for that tube. The test specimens were clamped rigidly at one end as cantilever beams (of known length). Employing a vibration spectrum analyser the fundamental frequencies of the cantilevers were measured, and knowing their section properties and mass densities, their moduli were determined [26,27]. The

diagonal bracing members were cut from the same tubing in groups of at least two, so that despite the possible differences in the moduli rotational symmetry about a vertical axis was preserved. Referring to Figs. 2.3 through 2.5, Frame A was the duplicate of Frame B, Frames 1 and 4 were also duplicates, and so were Frames 2 and 3 (in both geometric properties and member moduli).

The member working lines in the designed model formed a 1/50 (geometric) scale reduction of those in the prototype. Figs. 2.3 through 2.6 illustrate the outer diameter, wall thickness, and also the modulus of every member in the jacket of the model. Principal lengths, including the overall dimensions for the model, are also supplied in these Figures. The given moduli are accurate to within 5%. Table 2.3 summarizes the member outer diameters and wall thicknesses in the prototype, the corresponding dimensions demanded by a 1/50 geometric scale, and also those actually used in the model. The minimum available wall thickness for polycarbonate tubing was 1/16 inches. The wall thicknesses in the full scale tower members are increased at the joints, but in the model they were not.

The member outer diameters used in the model (with the exception of a few horizontal bracing members) were within 6% of what a 1/50 scale reduction demanded. In the prototype, the member wall thicknesses were basically 5/8" for the legs (with the exception of two legs on the broad side which had thicker walls for launching purposes), 5/8" and 3/4" for the vertical diagonal braces, and mostly 1/2" for the secondary horizontal braces. Thus, with the 1/16" wall thickness (minimum thickness available) used in the model, the wall thicknesses in the model were considerably larger than required by a 1/50 scale reduction. They were 5 times as large for the 5/8" thick (prototype) walls, 4.2 times as large for the 3/4" walls, and 6 times for the 0.5" thick walls. The effect of these thicker walls in increasing the stiffness of the model is partially compensated by the less than 600 Ksi moduli of the polycarbonate members. These actual moduli varied from 270 Ksi to 370 Ksi and hence the model was still stiffer than desired. The distortion in stiffness controls the resulting model to prototype frequency ratios and has a small influence on the fundamental mode

shapes.

Despite the thicker member walls in the model (listed in Table 2.3), the masses of the members in the model were 4% to 40% less than the scale value for the legs (with 5/8" wall thickness) and most of the diagonal bracing members. This was due to the fact that the (volumetric) mass density required for the replica members was to be the same as that in its prototype, while the mass density for polycarbonate was only 1.2 times that of water. However, when the members are submerged, their effective mass for the jacket (including the added mass of the water) is closer to that required. For motions normal to the axis of members the effective mass, which includes the displaced water mass and internal fluid (when applicable) [23,24], is basically 80% of that demanded for the legs and 90% to 95% of that demanded for the diagonal bracing members. The model has a jacket which is lighter than required. During vibrations in air, the inertial effects arising from the jacket mass are smaller than required by similitude. However, during vibrations in water, the total inertial effects due to both the jacket mass and the water will be closer to that desired. Hence the model is more sensitive to submergence. This (intended) desirable feature provides a good opportunity to assess how well the inertial effects due to submergence can be predicted by theory.

The deck was designed and constructed as a box reinforced with webs. Polycarbonate plates were used for its fabrication. Eight aluminum plates were attached to the deck by means of machine screws. Four of these were intended for accommodating the attachment of accelerometers and the other four were used to accommodate the mounting of four removable steel blocks, which were used to stimulate the maximum deck mass condition. The deck box was designed to act as a rigid unit during vibrations in the fundamental modes. This type of behavior was verified by preliminary dynamic tests. Figures 2.7 and 2.8 illustrate the deck and provide some details as well as its overall dimensions.

Without the removable steel blocks the (minimum) deck mass was 0.065 lb - s^2 /in (center of mass at Elevation 67.1", Ref. to Fig. 2.3) during testing, weighing 25.0 lbs which

corresponds to a prototype deck mass of 3,130 K. And with all four steel blocks mounted, the (maximum) deck mass was 0.267 lb - s^2 /in (center of mass at 69.4" Elevation; see Fig. 2.3) weighing 103.0 lbs which corresponds to a prototype deck mass of 12,880 K. (refer to Table 2.4).

With the jacket and deck joined together and the legs fixed (at the bottom), the model possesses the most important features common to typical, 8-legged, K-brace towers.

2.5 Assembly of the Model

The bracing members were prepared for assembly by machining the radius of the legs at their ends. Each radius was cut by using a milling cutter set at the appropriate angles. The required angles were calculated to the nearest 1/360 of a degree. The appropriate lengths were calculated and specified to the nearest 0.001". The bracing members and legs were joined using solvent type cement. Inspections of the jacket, during the completion phase indicated that the appropriate lengths were within ± 0.02" of the design specifications. The out-of-roundness tolerances for the legs and diagonal bracing members were ± 0.007". Fig. 2.9 shows typical joint details (see also Figs. 2.3, 2.5 and 2.10).

The webs of the deck were joined to the top and bottom plates of the deck using adhesive. The completed deck was attached to the jacket using (epoxy) adhesive. Fig. 2.11 illustrates a typical leg-to-deck connection. The completed model on its base system (for testing) are shown in Figs. 2.12 and 2.13.

CHAPTER 3

EXPERIMENTAL PROGRAM

3.1 Method of Testing

3.1.1 Introduction

When a structure is dynamically excited, acceleration measurements can be taken at appropriate locations in order to evaluate characteristics of the natural modes of vibration [26,27] that are produced. The frequencies of these modes, quantitative or qualitative mode shape information, and the damping in these modes can be evaluated from the measurements, whether the excitation is the ambient condition or is induced by means of controlled dynamic tests [3,9,10,13,18,28].

In general, when dynamic testing is employed several test options are possible. Considering the information required, the prior knowledge of frequencies as well as damping, and the relative convenience in employing the different test options, the appropriate dynamic test procedure can be selected to accomplish the objectives [28,29,30,31,32].

In conducting the present test, it was necessary to use a forced excitation; i.e., dynamic testing. Two options were available: one was to induce excitation by means of shock, the other was to use a forced resonant excitation [8], produced by an electromechanical shaker.

Preliminary dynamic tests were carried out using both options. The second option (resonant excitation) was more time consuming, and rather difficult to use due to the very low damping in the modes of the tower. A shock excitation imparted at the deck could be used to excite the tower into free vibration. Several global and some local modes of vibration could be excited in this manner. Further, by imparting the impact from different directions, at different locations, the desired modes could be emphasized in each test. Due to the low damping, information on both mode shape and frequency could be evaluated (with sufficient resolution) for at least one fundamental mode, and at the same time frequencies of (some) local modes could

also be obtained from a single test, where the duration of each test was less than 24 seconds. Since considerably less time was required to complete the shock tests, and this was highly desirable, shock testing was employed.

The theoretical basis for evaluating the vibratory characteristics of the model is presented in the following sections. Further information on subjects related to the dynamic tests can be found in Refs. 33 and 34.

The instrumentation of the model, the experimental setup and the testing procedures are described at the end of this chapter.

3.1.2 Spectral Analysis of Transient Response

After a structure is excited into free vibration by impact, its accelerations during the transient response can be written as

$$\hat{a}(t) = \sum_{j=1}^{n} C_j \hat{\Phi}_j e^{-\xi_j \omega_j t} \sin(\omega_{jD} t + \theta_j) \quad , t \geqslant 0 \tag{3.1}$$

where the n-dynamic degrees of freedom [26] are sufficient to describe the accelerations at any location on the structure and where

$\hat{a}(t)$ = The acceleration vector (n-dynamic degrees of freedom)

$\hat{\Phi}_j$ = The jth mode shape vector

t^* = Time from initiation of impact

t_i = Some time after completion of wave propagation phenomena which follows the termination of impact

$t = t^* - t_i$

ω_j = Natural frequency of mode j

ξ_j = Damping ratio (percent of critical damping) for mode j

$\omega_{jD} = \omega_j \sqrt{1-\xi_j^2} \approx \omega_j$ for $\xi_j \ll 1$

θ_j = Phase angle for mode j

$C_j \geqslant 0$, a constant

The magnitude of C_j depends on the extent to which the jth mode is excited by the shock.

The acceleration at some location p on the structure during the transient response (refer to equation 3.1) can be written as

$$a_p(t) = \sum_{j=1}^{n} d_{jp}\, e^{-\xi_j \omega_j t} \sin(\omega_{jD}\, t + \theta_j) \qquad , t \geqslant 0 \tag{3.2}$$

or

$$a_p(t) = \sum_{j=1}^{n} d_{jp}\, b_j(t) \qquad , t \geqslant 0 \tag{3.3a}$$

where

$$b_j(t) \equiv e^{-\xi_j \omega_j t} \sin(\omega_{jD}\, t + \theta_j) \qquad j = 1,\ n \tag{3.3b}$$

$$d_{jp} \geqslant 0 \qquad\qquad j = 1,\ n$$

The d_{jp} coefficients are constants that are linearly proportional to both C_j and the elements of $\hat{\Phi}_j$. The finite Fourier transform [34] of equation (3.3a), defined as the transient response (or acceleration) spectrum, will be

$$\begin{aligned} A_p(\omega) &\equiv \int_0^T a_p(t)\, e^{-i\omega t} dt \\ &= \sum_{j=1}^{n} d_{jp} \int_0^T b_j(t)\, e^{-i\omega t} dt \equiv \sum_{j=1}^{n} d_{jp}\, B_j(\omega) \end{aligned} \tag{3.4}$$

where

$$\omega \geqslant 0$$
$$i = \sqrt{-1}$$

and T is taken large enough so that $e^{-\xi_j \omega_j T} \approx 0$ for j = 1,n. That is, by time T the accelerations have essentially decayed to zero. For accelerations at locations m and l the ratio

$$\frac{d_{jm}\, B_j(\omega)}{d_{jl}\, B_j(\omega)} = \frac{d_{jm}}{d_{jl}} \tag{3.5}$$

will provide quantitative information for mode j. In particular, if the accelerations correspond

to the g and h degrees of freedom, then (see Eqs. 3.1 and 3.2) for mode j

$$\frac{d_{jg}}{d_{jh}} = \frac{C_j \phi_{gj}}{C_j \phi_{hj}} = \frac{\phi_{gj}}{\phi_{hj}} \tag{3.6}$$

for modal displacements corresponding to the g and h degrees of freedom.

To illustrate how the ratios in Eqs. 3.5 and 3.6 (modal displacement ratios) can be evaluated from the transient acceleration spectra (Eq. 3.4) it is necessary to examine the properties of $B_j(\omega)$. From Eqs. 3.4 and 3.3b

$$B_j(\omega) = \int_0^T b_j(t)\, e^{-i\omega t} dt = \int_0^T [e^{-\xi_j \omega_j t} \sin(\omega_{jD}\, t + \theta_j)]\, e^{-i\omega t} dt \tag{3.7}$$

Using the identity [35]

$$\sin(\omega_{jD}\, t + \theta_j) = \left[\frac{ie^{-i(\omega_{jD} t + \theta_j)} - ie^{i(\omega_{jD} t + \theta_j)}}{2}\right]$$

in Eq (3.7) leads to

$$B_j(\omega) = \int_0^T \left\{ e^{-\xi_j \omega_j t} \left[\frac{ie^{-i(\omega_{jD} t + \theta_j)} - ie^{i(\omega_{jD} t + \theta_j)}}{2}\right]\right\} e^{-i\omega t} dt$$

$$= \frac{i}{2} \int_0^T \left(e^{-[i(\omega + \omega_{jD}) + \xi_j \omega_j] t - i\theta_j} - e^{-[i(\omega - \omega_{jD}) + \xi_j \omega_j] t + i\theta_j} \right) dt$$

$$= \frac{i}{2} \left\{ - \frac{e^{-[i(\omega + \omega_{jD}) + \xi_j \omega_j] t - i\theta_j}}{i(\omega + \omega_{jD}) + \xi_j \omega_j} + \frac{e^{-[i(\omega - \omega_{jD}) + \xi_j \omega_j] t + i\theta_j}}{i(\omega - \omega_{jD}) + \xi_j \omega_j} \right\} \Bigg|_0^T$$

so that

$$B_j(\omega) = \frac{i}{2} \left\{ e^{-\xi_j \omega_j T} \left[- \frac{e^{-i(\omega + \omega_{jD})\, T - i\theta_j}}{i(\omega + \omega_{jD}) + \xi_j \omega_j} + \frac{e^{-i(\omega - \omega_{jD})\, T + i\theta_j}}{i(\omega - \omega_{jD}) + \xi_j \omega_j} \right] \right.$$

$$\left. + \left[\frac{e^{-i\theta_j}}{i(\omega + \omega_{jD}) + \xi_j \omega_j} - \frac{e^{i\theta_j}}{i(\omega - \omega_{jD}) + \xi_j \omega_j} \right] \right\} \tag{3.8}$$

Since T is taken large enough so that the accelerations have essentially decayed to zero and

$e^{-\xi_j \omega_j T} \approx 0$ for j = 1,n, Eq. 3.8 reduces to

$$B_j(\omega) \approx \frac{i}{2}\left[\frac{e^{-i\theta_j}}{i(\omega+\omega_{jD})+\xi_j\omega_j} - \frac{e^{i\theta_j}}{i(\omega-\omega_{jD})+\xi_j\omega_j}\right] \tag{3.9}$$

Multiplication and division of each term on the right hand side of Eq. 3.9 by the complex conjugate of its denominator gives

$$B_j(\omega) \approx \frac{i}{2}\left\{\left[\frac{\xi_j\omega_j - i(\omega+\omega_{jD})}{(\omega+\omega_{jD})^2+(\xi_j\omega_j)^2}\right] e^{-i\theta_j} - \left[\frac{\xi_j\omega_j - i(\omega-\omega_{jD})}{(\omega-\omega_{jD})^2+(\xi_j\omega_j)^2}\right] e^{i\theta_j}\right\} \tag{3.10}$$

For low values of damping (say $\xi_j < 0.02$) $\omega_{jD} = \omega_j\sqrt{1-\xi_j^2} \approx \omega_j$ and expression 3.10 reduces to

$$B_j(\omega) \approx \frac{i}{2}\left\{\left[\frac{\xi_j\omega_j - i(\omega+\omega_j)}{(\omega+\omega_j)^2+(\xi_j\omega_j)^2}\right] e^{-i\theta_j} - \left[\frac{\xi_j\omega_j - i(\omega-\omega_j)}{(\omega-\omega_j)^2+(\xi_j\omega_j)^2}\right] e^{i\theta_j}\right\} \tag{3.11}$$

Let $\Delta_j = \dfrac{(\omega-\omega_j)}{\omega_j}$ where $\Delta_j \geqslant -1$. Dividing the numerator and denominator of the two terms in Eq. 3.11 by ω_j and expressing the result in terms of Δ_j yields

$$B_j(\Delta_j) \approx \frac{i}{2\omega_j}\left\{\left[\frac{\xi_j - i(2+\Delta_j)}{(2+\Delta_j)^2+\xi_j^2}\right] e^{-i\theta_j} - \left[\frac{\xi_j - i\Delta_j}{\Delta_j^2+\xi_j^2}\right] e^{i\theta_j}\right\} \tag{3.12}$$

Defining

$$v_{1j} \equiv v_{1j}(\xi_j, \Delta_j) = \left[\frac{i\Delta_j - \xi_j}{\Delta_j^2+\xi_j^2}\right] \tag{3.13a}$$

$$v_{2j} \equiv v_{2j}(\xi_j, \Delta_j) = \left[\frac{\xi_j - i(2+\Delta_j)}{(2+\Delta_j)^2+\xi_j^2}\right] \tag{3.13b}$$

where $\Delta_j \geqslant 1$, and also

$$V_{1j} \equiv V_{1j}(\theta_j, v_{1j}) = \frac{i}{2\omega_j} e^{i\theta_j} v_{1j} \tag{3.14a}$$

$$V_{2j} \equiv V_{2j}(\theta_j, v_{2j}) = \frac{i}{2\omega_j} e^{-i\theta_j} v_{2j} \tag{3.14b}$$

expression 3.12 can then be written as

$$B_j(\Delta_j) \approx V_{2j}(\theta_j, v_{2j}) + V_{1j}(\theta_j, v_{1j}) \tag{3.15}$$

Thus B_j is the sum of two vectors (V_{2j} and V_{1j}) in the complex plane. From Eq. 3.14, the orientation of these vectors in the complex plane is such that their angular separation depends on the value of θ_j [35]. For a given acceleration record the value of θ_j will depend on t_i (refer to Eqs. 3.1 and 3.2). From Eq. 3.14

$$\frac{|V_{1j}|}{|V_{2j}|} = \frac{|v_{1j}|}{|v_{2j}|} \tag{3.16}$$

In addition, for $\xi_j \leqslant 0.01$ Eq. 3.13b can be well approximated by

$$v_{2j} \approx \frac{-i(2+\Delta_j)}{(2+\Delta_j)^2} = \frac{-i}{(2+\Delta_j)} \tag{3.17}$$

Fig. 3.1 illustrates $|v_{2j}|$, $|v_{1j}|$ and how they vary with Δ_j . Clearly $|v_{1j}|$ is considerably larger than $|v_{2j}|$ ($|V_{1j}|$ is considerably larger than $|V_{2j}|$, see Eq. 3.16) especially near $\Delta_j = 0$. This implies that the magnitude (and also the angle, in the complex plane) of B_j is strongly controlled by V_{1j}, and so the influence of t_i on $|B_j|$ is small. Fig. 3.1 illustrates that for a lower value of damping (ξ_j) , the peak value of $|v_{1j}|$ (therefore peak values for $|V_{1j}|$ and B_j), as well as the values of $|v_{1j}|$ (also $|B_j|$) in the vicinity of $\Delta_j = 0$ (i.e., $\omega = \omega_j$), will be higher. Whereas $|v_{2j}|$, and $|v_{1j}|$ (also $|B_j|$) in the range defined by $|\Delta_j| \geqslant 0.07$, are essentially independent of ξ_j.

Referring to Fig. 3.1, the sharp peak in a plot of $|B_j(\omega)|$ vs. ω (see Eqs. 3.11 and 3.12), which can also appear as a sharp peak in the acceleration spectra (Eq. 3.4), will mark the frequency ω_j . The large value of $|B_j(\omega)|$ for $\omega \approx \omega_j$ also implies a large $|d_{jp} B_j(\omega \approx \omega_j)|$ value (for location p) and the latter is used when evaluating the mode

shape information (refer to Eqs. 3.4, 3.5 and 3.6).

Fig. 3.2 illustrates how the angle $\alpha_{V_{1j}}$ of V_{1j} (in the complex plane) varies with Δ_j (or ω). Where the reference angle (i.e., $\alpha = 0$) corresponds to the angle of V_{1j} ($\Delta_j = 0$). Although Fig. 3.2 demonstrates the properties for ξ=0.01, it possesses the general characteristics that are common to the curves with $\xi \leqslant 0.01$. Two plateaus can be observed which are separated by nearly 180°. As illustrated, the angle $\alpha_{V_{1j}}$ approaches the two plateaus at 90°, and -90°, as Δ_j, increases from zero, or decreased from zero value, respectively. The lower the damping, the more rapidly the angles approach the two plateaus as Δ_j increases, or decreases from zero.

Fig. 3.2 also illustrates the upper and lower bounds on the possible range of the angle α_{B_j} of B_j. The angle α_{B_j} is defined by V_{1j} and V_{2j} (see Eqs. 3.14 and 3.15). So that the magnitudes of v_{1j}, v_{2j}, and the angle θ_j determine the value of α_{B_j}. As shown in Fig. 3.2, the maximum possible difference between the angles α_{B_j} and $\alpha_{V_{1j}}$ is less than a few degrees in the vicinities where the plateaus are reached from $\Delta_j = 0$. In particular, for $|\Delta_j| \leqslant 0.1$ (i.e., $0.9 \leqslant \frac{\omega}{\omega_j} \leqslant 1.1$)

$$\frac{|v_{1j}|}{|v_{2j}|} = \frac{|V_{1j}|}{|V_{2j}|} > 18 \qquad , \xi \leqslant 0.01$$

and the angle between B_j and V_{1j} (see Eq. 3.15) will be at most $\pm 3°$. Therefore the direction and magnitude of B_j is nearly the same as that of V_{1j} in the range $|\Delta_j| \leqslant 0.1$. Further, the maximum possible value of $|\alpha_{V_{1j}} - \alpha_{B_j}|$ is essentially independent of the low value of ξ in the range defined by $|\Delta_j| > 0.07$ and depends on θ_j (Eqs. 3.14, 3.15), which means that the values of α_{B_j} could be evaluated, if needed, from information at the vicinity of $\omega = \omega_j$. Information on α_{B_j} (or $\alpha_{V_{1j}}$) on the Δ_j>0 side, or on the Δ_j<0 side, is sufficient for determining the angles of the two plateaus (also θ_j). In the transient response spectra, this information can be obtained with sufficient accuracy near the peaks.

When only a single mode of vibration, k, is excited, Eq. 3.4 reduces to

$$A_p(\omega) = \sum_{j=1}^{n} d_{jp}\, B_j(\omega) = d_{kp}\, B_k(\omega)$$

and the task of obtaining modal displacement ratios is trivial. Further, by virtue of the properties of B_j, when $\xi \leqslant 0.01$ for all the excited modes the peaks in the $A_p(\omega)$ spectrum (see Eq. 3.4) are narrow and as long as

$$d_{kp} \mid B_k(\omega_k) \mid >> \sum_{j=1,\ j\neq k}^{n} d_{jp} \mid B_j(\omega_k) \mid \tag{3.19}$$

Eq. 3.4 reduces to

$$A_p(\omega_k) = \sum_{j=1}^{n} d_{jp}\, B_j(\omega_k) \approx d_{kp}\, B_k(\omega_k)$$

and can be used directly to evaluate modal displacement ratios.

3.1.3 Signal Separation in the Spectral Analysis of Transient Response

The finite Fourier transform of accelerations, at any location p, recorded during the transient response, was described by Eq. 3.4. This transform ($A_p(\omega)$) could be thought of as a summation of signals $d_{jp}\, B_j(\omega)$. Each signal, j, is produced by one of the excited modes, for which $d_{jp} \neq 0$, and possesses the properties that were described in the preceding section. In order to obtain accurate modal displacement ratios for mode k, $d_{jp}\, B_j(\omega_k)$ for j = any other significantly excited mode ($j \neq k$) must be subtracted from $A_p(\omega_k)$ (refer to Eqs. 3.4, 3.5 and 3.6). To accomplish this, $B_j(\omega)$ must be obtained for these modes. This task can be separated into two parts; one part will be obtaining $\mid B_j(\omega) \mid$ (for the frequency range desired), the other will be determining the plateaus for the angles of $B_j(\omega)$ in the complex plane.

To obtain $\mid B_j(\omega) \mid$, $\dfrac{\mid B_j(\omega) \mid}{\mid B_j(\omega_j^*) \mid}$ must first be obtained, where ω_j^* is the frequency that corresponds to the peak in the descretized spectrum. Noting that

$$\frac{\mid B_j(\omega) \mid}{\mid B_j(\omega_j^*) \mid} = \frac{\mid d_{jp}\, B_j(\omega) \mid}{\mid d_{jp}\, B_j(\omega_j^*) \mid} \tag{3.20}$$

this can be obtained from a spectrum in which signal j is strongly dominant. Where the location of the accelerometers and the mode shapes are key factors, this can generally be accomplished and can involve adding or subtracting accelerations recorded in two (different) locations in order to obtain the desired spectrum. Such spectra may be obtained from separate tests so long as ξ_j has the same value. As discussed earlier the value of θ_j has a very small effect on $| B_j(\omega) |$ and is generally not a concern. However, should the value of θ_j be important, a spectrum with the desired θ_j value can be obtained by varying t_i (see Eqs. 3.1 through 3.4).

In the case of low damping ($\xi \leqslant 0.01$) the peaks, in the plot of $| A_p(\omega) |$ against ω, defined as magnitude spectra, are narrow. Among the spectra from which the modal displacement ratios are to be evaluated, the spectrum, m, which exhibits the most pronounced peak associated with mode j is best for obtaining the angles of the plateaus (discussed earlier) for $B_j(\omega)$. As discussed earlier, the information on the angles of $A_m(\omega)$ in the vicinity of such peaks reveals the angles for the plateaus (and therefore θ_j) of $d_{jm} B_j(\omega)$ (and therefore $B_j(\omega)$).

The $| d_{jp} B_j(\omega_j^*) |$ value, of each significant signal $j \neq k$, is generally considerably larger than the contributions of other modes to $| A_p(\omega_j^*) |$ and consequently it is adequate to estimate $| d_{jp} B_j(\omega) |$ by $| A_p(\omega_j^*) | \dfrac{| B_j(\omega) |}{| B_j(\omega_j^*) |}$ for subtraction purposes. With the angles of the plateaus already determined, the contribution of signal j can be subtracted at the frequencies of interest, ω_k.

Preliminary testing and analysis indicated that in the first translational mode the tower displaces in the y direction (refer to Fig 3.3 through 3.8) and to a smaller extent in the x direction. Similarly, the modal displacements in the second translational mode were primarily in the x direction but had a small amount of displacement in the y direction. Generally, an impact parallel in direction to the x (or y) axis, and imparted at the deck, excited primarily the second (or the first) translational mode, and also to a much lesser extent the first (or the second) translational mode. The tests in which the direction of impact was parallel to the x axis will be

referred to as the x-impact tests, and the tests referred to as the y-impact tests will be those in which the direction of impact was parallel to the Y axis. If the location (i.e., the line) of impact had an eccentricity with respect to the deck center line, the first torsional mode was also excited.

By summing and differencing the acceleration time histories, measured by parallel accelerometers that were located at two extremes of the deck, the signal from the torsional mode could be separated from signals of the translational modes. The spectrum for which the torsional mode was isolated could be used to obtain the normalized form of $| B_j(\omega) |$, where j = the first torsional mode, for the frequency range in concern. The corresponding normalized forms of $| B_j(\omega) |$ for the translational modes were obtained from the acceleration time histories recorded by the accelerometers which were oriented in the direction of significant translation. For the $B_j(\omega)$ of the first translational mode (the fundamental Y sway mode) the finite Fourier transform of the acceleration time histories, from the y-impact tests, measured by the two accelerometers oriented in the y direction were used. Similarly, for the $B_j(\omega)$ of the second translational mode (fundamental x sway mode), the acceleration time histories recorded in the x-impact tests by the accelerometer which was oriented in the x direction, were used.

The measured damping ratios, ξ (using the log-decrement method), in the two sway and the torsional modes were less than 0.01. The signals $B_j(\omega)$ in the transforms of the accelation time histories were such that the peaks were large and narrow, and revealed angles of the plateaus (and therefore θ_j) for $B_j(\omega)$. For the excited modes j, showing significant peaks, the value of $d_{jp}\, B_j(\omega_j^*)$ (ω_j^* being the frequency that corresponds to the maximum amplitude ordinate in the Fast Fourier transform) could be well approximated by using the ordinate of the peak $A_p(\omega_j^*)$ (as discussed earlier). So that the magnitudes for the expression $d_{jp}\, B_j(\omega)$ could be obtained, from the available normalized $\dfrac{| B_j(\omega) |}{| B_j(\omega_j^*) |}$, by $| d_{jp}\, B_j(\omega) | \approx | A_p(\omega_j^*) | \dfrac{| B_j(\omega) |}{| B_j(\omega_j^*) |}$, and the angles of the plateaus for B_j (obtained from the peak caused by mode j). These approximations to $d_{jp}\, B_j(\omega)$ could then be used

for the subtraction from $A_p(\omega_k^*)$ to obtain $d_{kp}\, B_k(\omega_k^*)$ with sufficient accuracy, which in turn were used for obtaining the quantitative mode shape information (equation 2.6).

3.2 Experimental Setup

Square polycarbonate plates were attached to the bottom of the tower legs using epoxy adhesive. By means of four bolts (refer to Fig. 3.9) through each plate, the legs were attached to a steel base frame. The base frame was rigidly locked into a steel base box by means of bolts. The complete system (weighing 1300 lbs.) was placed in the towing tank for testing in the submerged condition. The required position of the stationary water level was marked on the four corner legs and the base system was properly placed and adjusted so that the water level coincided with the marks on the legs. A 1/16 inch hole was drilled at the bottom as well at the top of each leg through its wall to allow flooding of the legs. The system was also used for the dynamic tests in air. Figs. 2.12 and 2.13 illustrate the model and the base system.

3.3 Instrumentation and Data Recording

Nine accelerometers were employed to record accelerations on the tower during the tests. Three strain gauge type (Statham model A39TC-5-350) accelerometers were placed on the deck as shown in Figs. 3.3 and 3.10. These were used to measure the modal displacements of the deck which behaves as a rigid unit during vibrations in the fundamental modes. Preliminary testing and analysis indicated that in order to obtain frequency information on the second torsional and the second translational modes, it was best to monitor the horizontal accelerations (on the joints) at the 30" Elevation (see Fig. 3.6), since the modal displacements in these modes would be significant at this level. Furthermore, accelerometers placed at these locations were used to evaluate the modal displacements of the joints.

Three accelerometers also were placed on members midway between the joints, with the intent to gain some insight on characteristics of local modes. In general, the local mode shapes are characterized by significant (flexural) deformations of at least one member and may involve up to several members which are connected to the same joint at one of their boundaries.

Hence the modal deformations are largest at the midspan of said members, and verifying and measuring frequencies of these modes is accomplished most easily when the accelerometers are placed at midspan. It was also of interest to observe whether any vibrations would result at neighboring joints and legs when the local modes, involving vibration of the diagonal bracing members, are excited. This concept is of importance to local mode monitoring for the purpose of verifying structural integrity.

To meet the above objectives the remaining six accelerometers were placed on the structure underwater as shown in Figs. 3.4 through 3.8 (see also Figs. 3.11 and 3.12). These were piezoelectric (Unholtz Dickie Model 75 D 21) accelerometers. Silicone paste (a heavy lubricant) was used to cover the wire leads connecting to these underwater accelerometers to provide the necessary waterproofing. As shown in Figs. 3.6 through 3.8 (see also Figs. 3.11 and 3.12), six steel weights were also placed on the jacket to preserve rotational symmetry in the mass distribution of the jacket. The accelerations, measured by the nine accelerometers during testing, were recorded simultaneously on magnetic tape by using a portable data acquisition system (Kinemetrics Digital Data System, Model DDS-1103). The amplified analog acceleration signals were directly converted and recorded in digital form on magnetic tape, and were then processed at a later time.

3.4 Testing Procedure

The shock excitation of the vibratory response was induced by manually imparting an impact to the deck (to the side of the top plate of the deck) in the two horizontal directions "S-Y" and "S-X", as illustrated in Fig. 3.3. The hammer used for the impact was a steel cylinder with a rubber tip, suspended at the appropriate level by strings. After positioning, the hammer was pulled back an appropriate distance, as illustrated in Fig. 3.13, and then released to provide the desired impact. After impact, the hammer bounced away from the deck and was caught to avoid any further contact. During each impact, several vibration modes of the tower were excited.

Data recording was initiated prior to the release of the hammer, and continued generally for about 20 seconds. However, the time period (window) that was used for evaluating the response spectra, i.e., the time during which the tower was undergoing free vibrations was about 10 seconds of the record. The actual data period was selected later during the data reduction phase; it contained the desired transient acceleration records.

During the tests, two oscilloscopes and a (frequency) spectrum analyser were used for monitoring the (magnitude of) accelerations, and vibration frequencies, respectively. The "scopes" were also used to confirm the lack of any accelerations (vibratory response) prior to excitation.

The tower was tested in the towing tank (submerged in water) and also in air in its undamaged condition. In its damaged conditions it was only tested in the towing tank. For each damage condition one of the four selected bracing members (Members 107, 94, 116 and 55 in Figs. 3.4 and 3.5) were severed. This was done by removing a slice of about 1/2" in width from the member near its lower (end) joint as illustrated in Figs. 3.4 and 3.5. After testing the member was repaired by replacing a slice of tubing, (with a close fit) that matched the cross section (and material property) of the member, attaching it with epoxy adhesive (see Fig. 3.14). The subsequent damage conditions were simulated for testing (and repaired) in the same fashion.

The two deck mass (a parameter in the consideration) cases considered for each test condition were simulated by mounting and removing the Four steel blocks, which could be locked to the deck at the appropriate locations (refer to Figs. 2.7 and 3.15).

CHAPTER 4

EXPERIMENTAL RESULTS

4.1 Introduction

This chapter presents the results of experimental studies of the vibratory properties of the model structure. General aspects are presented and discussed first, and are followed by the presentation of both the global vibration frequencies and mode shape information for the undamaged model. Subsequently, the measured changes in global frequencies and mode shapes of the model, when the selected members were sequentially damaged, are presented for each damage case. For both damaged and undamaged conditions observations on several local modes as well as a higher mode of vibration are also summarized. The measured global vibration frequencies and mode shape characteristics of the undamaged model in air are presented last. Finally, the important findings are summarized.

4.2 Overview

The vibration frequencies of interest, for all of the cases considered, were expected to be less than 50 Hz. A sampling rate of 200 Hz was used for evaluation of the acceleration spectra. The resulting folding frequency, N_f of 100 Hz [12] was found to be satisfactory since the frequency and mode shape evaluation were not jeopardized by aliasing [12]. The few cases of aliased frequencies were related to the AC power supply.

The damping in the lower modes of vibration of the model was evaluated based on the logarithmic decrement method [26]. Continuously recorded time histories of acceleration were employed. The logarithm of the peak (acceleration) amplitudes of every other fifth cycle, for anywhere from 45 to 65 cycles of the records, were plotted against their cycle numbers. The straight line fitted to the plotted points was used to evaluate the damping values. This procedure yields accurate results when the vibration mode, for which the damping is evaluated, is the only excited mode. If any other modes are also excited, beating patterns can result which might lead to inaccuracy in the calculated damping values. For the

second translational mode (Mode 1x) the direction of vibrations (motions) were primarily in the x direction (see Figs. 3.4 and 3.5) and the acceleration time histories measured by accelerometer (no.) 2 (see Fig. 3.3) had to be employed to evaluate damping. It was difficult to eliminate response in the first torsional (Mode 1t) as well as the first sway (Mode 1y) mode (in order to evaluate the damping with sufficient accuracy), when exciting the second translational mode, and several trial tests were required. Due to this difficulty and also the time limitations in the schedule of tests, the damping in the second sway mode was measured only for the tower in air. To evaluate the damping in the first translational mode, the acceleration measured by accelerometer (no.) 1 (see Fig 3.3) was subtracted from that measured by accelerometer (no.) 3. This eliminated any signal that was caused by vibrations in the first torsional mode, since the resulting quantity was equal to twice the y-acceleration (at the center) of the deck. Similarly, the sum of the accelerations measured by accelerometers 1 and 3 was a measure of the rotation of the deck about a vertical axis through the center of the deck, and was employed to evaluate the damping in the first torsional mode.

Table 4.1 summarizes the measured damping values. These values are based on free vibration decay in the undamaged model. In all cases the measured damping values were less than 0.01 (i.e., less than 1% of critical damping). The increase in the mass of the deck (maximum deck mass case) lowered the damping values. As illustrated in Table 4.1, submergence of the model in water slightly increased the damping values. In the case of a full scale structure the effects due to fluid viscosity are less pronounced (Reynolds number in the model is over 200 times that in a prototype) and any increase in damping values of the full scale structure due to the viscosity of water would be less than the measured increase in (the corresponding) damping values of the model.

The Fast Fourier Transform (FFT) method [12,34] was used to evaluate the finite Fourier transforms (spectra) of the acceleration time histories (transient response). Each spectrum was the FFT of a selected 10.24 second time period, called the time window, from an acceleration time history. The 0.0976 Hz frequency resolution in the spectra, which

results from transforming a time window of 10.24 seconds, was adequate for the evaluation of the vibratory properties of the structure. The beginning of the time windows were generally 0.5 seconds after the initiation of impact. This initial time selection was such that the acceleration records of the free vibration response did not contain undesirable high frequency modes, because they damped out quickly.

The natural frequencies of vibration were easily evaluated by an inspection of the maxima in the amplitude spectra. This evaluation will be illustrated in sections 4.3 and 4.5, for selected examples.

The evaluation of mode shapes was based on the theory presented in Chapter 3. Modal displacement ratios were calculated for the selected locations where accelerometers were placed, and for the directions in which the accelerometers were oriented, as was discussed in Chapter 3. As mentioned earlier, the vibration shape of the model in its first translational mode exhibited significant displacement in the (global) x direction (refer to Figs. 3.4 and 3.5). In a similar manner the second translational mode (Mode 1x) exhibited motions that were skewed with respect to the global X and Y axes with a predominant x component of motion. The first torsional mode shape indicated rotation of the deck about a vertical axis through its center. As mentioned in section 3.1.3 the s-x tests (refer to Section 3.4) caused predominant excitation in Modes 1x and 1t, whereas the s-y tests caused predominant excitation in Modes 1y and 1t. The modal displacement ratios for the 1y and 1t Modes were evaluated from the spectral amplitudes (magnitudes) and phase angles (in the complex plane) of the transform functions (at the discrete frequencies) of s-y tests. The modal displacement ratios for Mode 1x as well as for Mode 1t could be evaluated from the spectral amplitudes and phase angles of the transform functions of s-x tests. In general, the subtraction procedure (for interfering signals from excited modes) discussed in section 3.1.3 was necessary to evaluate the modal displacement ratios accurately. The procedure is illustrated in Appendix A.

In both of the s-x and s-y tests, some higher global modes as well as some local modes

were also excited. These modes will be discussed in sections 4.3 and 4.5. The vibration frequencies of these modes are evaluated and their mode shapes are described qualitatively.

The results of the experimental study of the vibration mode shapes and frequencies of the tower are presented in Sections 4.3 through 4.6. In these sections the (global) axes, accelerometer numbers as well as their location on the structure (such as locations A, B, C or joints 54 and 49), and member numbers will be referred to frequently. The joint numbering and member numbering is compatible with the node and member numbering in the analytical model of the platform (to be discussed in Chapter 5). The reader should refer to sections 3.3, 3.4, and Figs. 3.3 through 3.8, which identify the locations and members referred to and illustrate the directions in which accelerations were measured.

4.3 Vibratory Characteristics of the Global modes of the Model

4.3.1 Maximum Deck Mass Case

Figs. 4.1 through 4.12 illustrate a set of typical amplitude spectra for the frequency range of 3.0 Hz to 45.0 Hz. These spectra were evaluated from the transient acceleration time histories measured during s-y and s-x tests and are similar in their characteristics to the spectra of other s-y and s-x tests. The important differences among spectra were due to the changes in frequency and mode shape caused by damage to the structure.

The maxima at 7.1 Hz in the spectra of Figs. 4.1 through 4.6 are due to the excitation of Mode 1y (first sway mode). Inspection of the magnitudes of these maxima in Figs. 4.1 through 4.3 reveals that the largest displacements in this mode were measured by Accelerometers 1 and 3, which were located at the deck. Accelerometer 1 was oriented in the -y direction at location A (see Fig. 3.3), whereas Accelerometer 3 was oriented in the +y direction at location C. Fig. 4.1 indicates that Accelerometer 2, which was oriented in the -x direction at location B on the deck (Fig. 3.3), measured a small amount of x displacement in this mode. Further, inspection of Fig. 4.2 reveals that the modal displacements, (measured) in Mode 1y, on the joints of the tower, had a larger component in the y direc-

tion and a smaller component in the x direction. However, the y and x displacements are largest at the deck. Phase angles of the peaks indicated that all motions in the -x and y directions were in phase with each other for this mode. A comparison of the magnitudes of maxima in Figs. 4.1 and 4.4 reveals that this mode was strongly excited in the s-y test but weakly excited in the s-x test.

The modal displacement ratios for Mode 1y (first translational mode) were evaluated from the spectra of s-y tests. Modal displacement ratios (for the undamaged tower) were measured for three tests (Tests 144, 145, and 146) and are summarized in Table 4.2. The evaluated modal displacements in the three tests are almost identical, and indicate excellent repeatability in test results. The uncertainty in these values is less than ± 0.02 (i.e., 2% of the value of maximum modal displacement).

The maxima at 7.7 Hz in the spectra of Figs. 4.1 through 4.6 are due to the excitation of the second translational mode (Mode 1x). The magnitudes (spectral amplitudes) of these maxima, in Figs. 4.4 through 4.6, reveal that the displacements in this mode had a larger component in the x direction and a smaller component in the y direction. The phase angles of these peaks indicated that all motions in the x and y directions were in phase during vibrations. An examination of Figs. 4.1 and 4.4 reveals that, for this mode, the level of excitation in the s-x test was considerably higher than the level of excitation in the s-y test.

The normalized modal displacement ratios of Mode 1x were evaluated from the spectra of s-x tests. Results from two s-x tests are summarized in Table 4.3. The mode shape measurements made by the two tests are in excellent agreement with each other.

The maxima at 11.2 Hz in the spectra of Figs. 4.1 through 4.6 are the indication of response in the first torsional mode. As illustrated in these Figs., this mode was strongly excited in both the s-x and s-y tests. The modal displacement ratios evaluated for this mode are summarized in Table 4.4. As shown in Table 4.4, the results of the three s-y tests and the two s-x tests are identical (maximum uncertainty in the values is ± 0.02).

In Figs. 4.8, 4.9, 4.11 and 4.12 a peak caused by a single maximum ordinate at 20.0 Hz can be observed. This peak was due to noise generated by the (AC) power supply. The noise was introduced by a non-sinusoidal periodic variation in voltage, with a frequency of 60 Hz, superimposed on the analog signals. This noise caused maxima to appear in the spectra, which were different in characteristics from the maxima caused by the transient response of the tower. The maxima (due to noise) appeared at 60 Hz, and occasionally at 120 Hz and 180 Hz which were aliased at 80 Hz and 20 Hz in the evaluated spectra. The available low-pass analog filters for the piezoelectric accelerometers filtered signals above 375 Hz and this allowed a 180 Hz signal to be aliased at 20 Hz. The 20 Hz noise was present in only a few cases and did not interfere with the evaluation of results.

The second translational mode in the y direction was also excited in the tests. Spectra of time windows that began earlier in the acceleration time histories (beginning of time window less than 0.5 sec. from initiation of impact) indicated large modal displacements in the y direction at joints 49 and 54, as compared to small (modal) y displacements at locations A and C at the deck. The measured y displacements at the deck were opposite in direction to the y displacements at joints 49 and 54. A small component of motion in the x direction was also measured by Accelerometer 5, on joint 54. The frequency of vibration of this mode measured 26.8 Hz. Inspection of the maxima at 26.8 Hz in Figs. 4.8 and 4.11 reveals that the level of excitation in this mode was much lower in the s-x tests.

The s-y tests induced a higher level of excitation in the second torsional mode (Mode 2t) than the s-x tests (see maxima at 28.5 Hz in Figs. 4.8 and 4.11). The modal displacements of this mode in the y direction on joints 49 and 54 were larger than those in the y direction at locations A and C (see maxima at 28.5 Hz in Figs. 4.7 and 4.8). The vibration frequency of this mode (2t) measured 28.5 Hz.

There was no indication of excitation in the second translational mode in the x direction in the spectra of either s-x or s-y tests.

The vibration frequencies of the excited global modes of the undamage tower are

summarized in Table 4.5.

4.3.2 Minimum Deck Mass Case

The same qualitative descriptions of the vibration shapes, for Modes 1y, 1x, 1t, 2y and 2t, and also the same generalizations regarding the relative level of excitation (of the vibratory response) of these modes in the s-x and s-y tests, described for the maximum deck mass case (Section 4.3.1), apply to the minimum deck mass case.

To have the same magnitudes of acceleration in the minimum and maximum deck mass cases, the energy input by the shock that was necessary to excite the vibratory response of the tower had to be considerably less in the minimum deck mass case. Figs. 4.13 through 4.24 illustrate a set of typical amplitude spectra for the frequency range of 3.0 Hz to 45.0 Hz. These spectra were evaluated from the transient acceleration measurements of s-x and s-y tests in the minimum deck mass case and can be compared with the spectra of the maximum deck mass case in Figs. 4.1 through 4.12

The measured vibration frequencies of the global modes of the (undamaged) model in its minimum deck mass case are summarized in Table 4.5. The normalized modal displacement ratios evaluated for Modes 1y, 1x, and 1t of the undamaged model for the minimum deck mass case are summarized in Table 4.7 through 4.9.

The increase in the values of vibration frequencies, due to the decrease in deck mass, were over 75% for modes 1y, 1x and 1t, but less than 15% for modes 2y and 2t. The vibration shapes of modes 1y, 1x and 1t were also affected by the decrease in deck mass. Larger normalized modal displacements were measured at joints 54 and 49 in all three modes. The following descriptions summarize the changes in the frequencies and mode shapes of the tower resulting from the decrease in the deck mass.

In the minimum deck mass case, the frequency of mode 1y measured 13.48 Hz, which is 89% higher than the value measured in the maximum deck mass case. Also, the normalized x displacement component at the deck center in Mode 1y was larger for the minimum

deck mass case than for the maximum deck mass case.

The frequency of mode 1x measured 14.35 Hz in the minimum deck mass case, which was 1.86 times the value measured in the maximum deck mass case. The maxima of the spectra, at 14.4 Hz, in Figs. 4.13 through 4.18 are due to the vibratory response of Mode 1x. In this mode, also, the perpendicular (y) component of motion increased with the reduction of deck mass.

The decrease in deck mass increased the frequency of Mode 1t by 78%. The spectral maxima at 20.0 Hz in Figs. 4.13 through 4.18 are due to the vibratory response of Mode 1t. Accelerometer 8 measured large modal displacements on Member 60 (see Fig. 3.5). This large displacement was due to the closeness of the vibration frequency for Mode 1t and for a local mode in which Member 60 (and 109) vibrated.

In both deck mass cases vibratory responses of the second y-translational and the second torsional modes were excited by the impacts at the deck level. However, the vibratory response of Mode 2x was excited by the impacts only in the minimum deck mass case. This lack of excitation in the maximum deck mass case was related to the larger deck mass to jacket mass ratio for this case, which affected the vibration shape for mode 2x. For the minimum deck mass case the vibration frequencies were 28.5 Hz, 30.6 Hz and 32.5 Hz for Modes 2y, 2x and 2t respectively. The increases in vibration frequency values due to the decrease in deck mass were 6% for Mode 2y and 14% for Mode 2t. Maxima in the spectra of Figs. 4.19 through 4.24 at 28.5 Hz, 30.6 Hz and 32.5 Hz are due to the vibratory response of Modes 2y, 2x and 2t respectively.

4.4 Effects of Damage on the Vibratory Characteristics of Global Modes

The severance of a diagonal member in Frames B or A (see Fig. 3.4) reduces both the overall lateral stiffness of the model in the global x direction and the overall torsional stiffness of the model. In addition, the damage shifts the center of rigidity of the platform away from the frame in which the damage has occurred. The reduction in the lateral

stiffness can cause detectable reductions in the vibration frequencies for Modes 1x and 2x, whereas the reduction in the torsional stiffness can result in detectable reductions in the frequencies for Modes 1t and 2t. The shift in the center of rigidity (away from the deck center of mass) of the platform introduces a x component of modal displacement at the deck center during vibrations in Mode 1t as well as a rotation of the deck about a vertical axis (through the deck center) during the vibratory response of Mode 1x. The latter can be measured as a difference in the modal y displacements at locations A and C (see Fig. 3.3).

Severance of a diagonal brace in Frames 4 or 1 reduces the overall lateral stiffness in the y direction and also the overall torsional stiffness of the model. Further, the damage will shift the center of rigidity of the platform away from the damaged frame (4 or 1) and hence away from the center of Mass of the deck. The reductions in stiffness cause detectable reductions in the vibration frequencies of Modes 1y, 2y, 1t and 2t. The shift in the center of rigidity of the platform introduces a y component of modal displacement at the deck center during the vibratory response of Mode 1t and a rotation of the deck (about the vertical axis) during the vibratory response of Mode 1y. In general, when the damage has occurred in Frames 1 or 4 the reductions in the overall torsional stiffness and the shifts in the center of rigidity of the platform are more pronounced than the changes due to damage in Frames A or B, leading to larger effects on the vibratory properties. This is because Frames 1 and 4 are furthest from the center of rigidity of the platform.

The measured natural vibration frequencies for the global modes of the tower, for all cases tested, are summarized in Table 4.5. The measured shifts in frequencies, expressed in percent of the frequency for the undamaged tower, are summarized in Table 4.6 for values greater than 1%. The normalized modal displacements evaluated for Modes 1y, 1x and 1t, for all the damaged cases, are summarized in Tables 4.2 through 4.4 (maximum deck mass case), and Tables 4.7 through 4.9 (minimum deck mass case). The difference in the modal y displacements at locations A and C (see Fig. 3.3) divided by 2, is a measure of the rotation of the deck about the vertical axis (through the deck center) and is denoted by the

quantity $\frac{Y_A - Y_C}{2}$ in Tables 4.2 through 4.4, and 4.7 through 4.9.

Severance of the members had little effect on the vibration frequencies of Modes 2y, 2x and 2t. In only four cases were the measured reductions in the natural frequency of these modes greater than 1%. In all cases, member severance had a pronounced effect on the normalized x and y components of modal displacement measured at the deck for Modes 1y and 1x. This sensitivity of modal displacement ratios at the deck to member severance, is a property of K-braced platforms. The following descriptions summarized the effects of member severance on the vibration mode shapes and frequencies of the global modes of the model.

4.4.1 Changes Due to Severance of Member 107

The severance of Member 107, located in Frame B of the jacket (see Fig. 3.4), reduces the overall stiffness of the model in the x direction. In the maximum deck mass case this damage reduced the measured frequency of Mode 1x by 2.6% (see Tables 4.5 and 4.6). In the minimum deck mass case the frequency reduction in Mode 1x was 2.0% and the frequency of Mode 2x was reduced by 1%.

In Mode 1y, the normalized modal x displacement of the deck center increased by 36% and 60% for the maximum and minimum deck mass cases respectively, due to the damage.

In Mode 1x, the normalized modal y displacement of the deck center increased by more than 29% and 82% for the maximum and minimum deck mass cases respectively. In addition, the reduction in stiffness of Frame B in the x direction, due to the severance of Member 107, was the main factor causing a 25% and a 15% increase in the value of the normalized modal x displacement of joint 54 for the maximum and minimum deck mass cases respectively (see Tables 4.3 and 4.8). Accelerometers 1 and 3 measured different y displacements (a rotation of the deck about the vertical axis) during the vibratory response of Mode 1x (see $\frac{Y_A - Y_C}{2}$ in Tables 4.3 and 4.8).

In Mode 1t, the damage introduced x-components of modal displacement at the deck center for both deck mass cases. The modal x displacements of joint 54 increased 27% and more than 15% for the maximum and minimum deck mass cases respectively (see Tables 4.4 and 4.9), mainly due to the reduction of stiffness in Frame B in the x direction.

4.4.2 Changes Due to Severance of Member 94

The severance of Member 94 caused a reduction in the stiffness of Frame B (see Fig. 3.4). This reduced the lateral stiffness of the tower in the x direction, as well as its torsional stiffness. The measured decreases in frequency for the maximum deck mass case were 2.6% for Mode 1x and 1.7% for Mode 1t. In the minimum deck mass case the frequencies of Modes 1x and 1t were reduced by 2.7% and 1.9% respectively.

Modal displacements of Mode 1y indicated that the normalized x components of modal displacement for the deck center increased by 93%, and over 150% for the maximum and minimum deck mass cases respectively. Also, a rotation of the deck about the vertical axis was measured during the vibratory response of Mode 1y in the minimum deck mass case (Table 4.7). In Mode 1x, the measurements indicated that the normalized y component of modal displacement at the deck center increased by more than 86% and 157% for the maximum and minimum deck mass cases respectively (see Tables 4.3 and 4.8). $\frac{Y_A - Y_C}{2}$ measurements by Accelerometers 1 and 3 indicated a rotation of the deck about the vertical axis during the vibratory response of Mode 1x. In Mode 1t, the damage (to Member 94) introduced a x component of modal displacement at the deck center (see Tables 4.4 and 4.9).

4.4.3 Changes Due to Severance of Member 116

The severance of this member caused a reduction in the stiffness of Frame B (Fig. 3.4), which resulted in a decrease in the lateral stiffness of the model in the x direction as well as a decrease in its torsional stiffness. In the maximum deck mass case the measured decreases in frequency resulting from damage were 2.6% for Mode 1x, as well as for Mode

1t. In the minimum deck mass case the damage reduced the vibration frequencies of Modes 1x, 1t and 2t by 2%, 1% and 1% respectively (see Tables 4.5 and 4.6).

In Mode 1y, the normalized x components of modal displacement at the deck center increased by 100% and more than 60% for the maximum and minimum deck mass cases respectively, due to severance of this member (see Tables 4.2 and 4.7). For Mode 1x, the increases in the normalized y component of modal displacement at the deck center were more than 100% for the maximum deck mass case and 27% for the minimum deck mass case (see Tables 4.3 and 4.8). During the vibratory response of Mode 1x, Accelerometers 1 and 3 measured a rotation of the deck about the vertical axis (see $\frac{Y_A - Y_C}{2}$ in Tables 4.3 and 4.8). In Mode 3 (1t) a x component of modal displacement was introduced at the deck center by the damage (this component was small in the minimum deck mass case); the normalized modal x displacement of joint 54 decreased by 20% for both deck mass cases (see Tables 4.4 and 4.9).

4.4.4 Changes Due to Severance of Member 55

The severance of Member 55 in Frame 4 (see Fig. 3.5) reduced both the lateral stiffness of the model in the y direction, as well as its torsional stiffness. In the maximum deck mass case, the resulting decreases in the vibration frequencies were 5.5% for Mode 1y, 10.4% for Mode 1t and 1.1% for Mode 2t. In the minimum deck mass case the frequency reductions were 4.4% for Mode 1y, 7.3% for Mode 1t and 1.3% for Mode 2t.

In Mode 1y the normalized x components of modal displacement at the deck center decreased by over 57% in the minimum deck mass case, and by 57% in the maximum deck mass case. In addition, during the vibratory response of Mode 1y a rotation of the deck about the vertical axis through the deck center was measured (see $\frac{Y_A - Y_C}{2}$ in Tables 4.2 and 4.7) for both deck mass cases. In Mode 1x, the normalized y displacements of deck center decreased in value, by more than 38% for the maximum deck mass case and 54% for the minimum deck mass case (see Tables 4.3 and 4.8). A rotation of the deck about the

vertical axis was also detected during the vibratory response of Mode 1x in both deck mass cases (Tables 4.3 and 4.8)

In Mode 1t, modal y displacements were introduced at the deck center in both deck mass cases (Tables 4.4 and 4.9). In this mode, for both deck mass cases, the decrease in the normalized y displacement at joint 54 and the (new) modal y displacements at the deck, were related to each other.

4.5 Observations on Excited Local Modes

Measurements taken by accelerometers on the jacket during the tests indicated that the impacts, imparted at the deck, excited the vibratory response of several local modes of the jacket. Some of these modes were consistently excited in at least one of the s-x or s-y tests, whereas others were only weakly excited in a few of the tests and are not considered here. This section summarizes the observations pertinent to local vibration monitoring.

Members 60, 62, and 109 (see Fig 3.5) showed a tendency for vibrations in the 20 Hz to 24 Hz frequency range. This condition allowed these members to couple their vibrations and form local modes. Measurements of vibratory response by Accelerometers 8 (on Member 60) and 9 (on Member 109, see Fig. 3.5) indicated two modes that involved coupled vibrations of Members 109 and 60. In one of these modes (Mode L8/9-1) the y component of vibrations on Members 109 and 62 were in phase with each other, whereas in the other mode (Mode L8/9-2) the y components of vibration were (180°) out of phase. The vibration frequency of Mode L8/9-1 was 20.8 Hz in the maximum deck mass case and 21.1 Hz in the minimum deck mass case. The vibration frequency of Mode L8/9-2 was 24.2 Hz and 24.4 Hz in the maximum and minimum deck mass cases respectively. These frequency values indicated that the change of deck mass had little influence on the vibration frequencies of the two modes. Independence of vibration frequency from the deck mass condition is a typical feature of modes which have only localized modal displacements on the jacket. The frequencies of Modes L8/9-1 and L8/9-2 measured in all damage cases, for both of the deck mass conditions, are summarized in Table 4.10.

The severance of the four braces (discussed previously) had little influence, if any, on the end conditions of Members 109, 60, and 62, and for this reason did not affect the vibration frequencies of Modes L8/9-1 and L8/9-2.

The maxima at 20.8 Hz in Fig. 4.9, and at 21.1 Hz in Figs. 4.15 and 4.18, are due to the vibratory response of Mode L8/9-1. The maxima at 24.2 Hz in Figs. 4.9 and 4.12, and at 24.4 Hz in Figs. 4.21 and 4.24, are due to the vibratory response of Mode L8/9-2. The level of excitation of the vibratory response of these two modes was generally higher in the s-y tests. The response spectra did not indicate vibrations at joint 54 (or 49) due to the vibratory response of Modes L8/9-1 and L8/9-2.

Vibration measurements by Accelerometers 5 and 9 (see Fig. 3.4) indicated a higher mode in which joint 54 vibrated in the x direction and Member 109 vibrated with a component of motion in the x direction. The x component of vibrations on Member 109 and the vibrations of joint 54 in the x direction were in phase with each other. Small amplitude vibrations of Member 96 were also detected occasionally. The s-x impacts always excited this mode (Mode H 5/9) in the minimum deck mass case but not always in the maximum deck mass case. The frequencies of this mode were observed to range from 31.2 Hz to 31.6 Hz in the minimum deck mass case (see maxima at 31.6 Hz in Figs. 4.20, 4.21, 4.23 and 4.24) and are summarized in Table 4.11. The measurements in the minimum deck mass case indicated no significant change in the frequency for Mode H 5/9 due to severance of Members 107, 94, and 116. However, the severance of Member 55 reduced the frequency of this mode by 1%.

Preliminary testing indicated two local vibration modes in which vibrations of Members 107 and 96 were coupled with each other in the plane of Frame B. In one of these modes (Mode L7-2) Members 107 and 96 vibrated out of phase (deflecting towards and away from each other during the vibrations) and in the other mode (Mode L7-1) the members vibrated in phase with each other. Whereas both of these vibration modes were excited in the maximum deck mass case, only one was excited in the minimum deck mass

case (see Figs. 4.21 and 4.24). When the vibratory response of both of the modes was excited there was no difficulty in measuring the frequency with one accelerometer on Member 96, since the vibration frequency for Mode L7-2 is always higher than that for Mode L7-1. However, when only one of these vibration modes was excited, it was necessary to use an additional accelerometer on Member 107 to determine which mode was being excited.

In the maximum deck mass case the vibratory response of both Modes L7-1 and L7-2 (which involved significant vibrations of Member 96) were excited and caused two maxima to appear in the amplitude spectra evaluated from the acceleration time histories recorded by Accelerometer 7 as show in Figs. 4.9 and 4.12. The measured vibration frequencies of both modes, for all cases tested in the maximum deck mass case, are summarized in Table 4.11. Severance of Members 116 and 55 did not affect the end conditions of Members 107 and 96, and did not influence the frequency values for Modes L7-1 and L7-2 or their response spectra significantly (see Figs. 4.25 and 4.26). Member 107 which was free at its lower end and partially flooded by water, due to the severance, could still couple its vibrations with the vibrations of Member 96, and form new local modes. However, the shapes of the new vibration modes were such that the shocks could significantly excite the vibratory response in only one of the new modes. This resulted in the appearance of a single large peak when Member 107 was severed (instead of two large peaks prior to the severance of Member 107 and after its repair) as illustrated in Figs. 4.25 and 4.26. The severance of Member 94 caused noticeable change in the spectra of the accelerations measured by Accelerometer 7 as illustrated in Figs. 4.25 and 4.26. The severance of Member 94 (at its lower end, see Fig. 3.4) reduced the vibration frequency (i.e., the fundamental frequency of Member 94 severed at one end) below 40 Hz, and allowed it to couple its vibrations through Member 95 with the vibrations of Member 96. This affected the response spectra of the accelerations recorded on Member 96.

4.6 Vibratory Characterisics Evaluated for the Model in Air

Vibration frequency and modal displacement measurements were made on the tower in air for two reasons: to determine the effect of submergence on the vibration frequencies of Modes 1y, 1x and 1t for both deck mass cases, and to examine the capabilities of the mathematical modelling of hydrodynamic effects due to submergence through a correlative analytical study (presented in Chapter 5).

The same s-x and s-y shocks used for testing the model in water (the submerged condition) were applied to test the model in air. The vibration frequencies for Modes 1y, 1x and 1t for both the maximum and minimum deck mass conditions were measured and are summarized in Table 4.12. The normalized modal displacement ratios for Modes 1y, 1x and 1t were evaluated for the minimum deck mass case, as summarized in Table 4.13.

The submergence of the model reduced the vibration frequency values in the maximum deck mass condition by 0.10 Hz, 0.15 Hz and 0.25 Hz for Modes 1y, 1x and 1t respectively. In the minimum deck mass condition the reductions in frequency due to the submergence of the model were 1.10 Hz, 1.20 Hz and 3.60 Hz for Modes 1y, 1x and 1t respectively (see Table 4.12).

Since the vibratory properties of the model in its minimum deck mass condition are more sensitive to the effects of submergence, the mode shapes and frequencies in the minimum deck mass case are more appropriate for use to assess how well the analytical modelling accounts for the hydrodynamic effects on the vibration frequencies and mode shapes of the model. The evaluated normalized modal displacement ratios and frequencies will be used for this purpose in Chapter 5.

4.7 Summary

The vibration frequencies of Modes 1y, 1x and 1t of the model in both air and water were measured for the minimum as well as the maximum deck mass condition. In air the normalized modal displacement ratios of the 3 modes were measured for the minimum deck

mass condition, whereas in water they were measured for both deck mass conditions. In water, the vibration frequencies of Modes 2y, 2x and 2t in the minimum deck mass condition, and those for Modes 2y and 2t in the maximum deck mass condition were also measured. The same measurements taken in the undamaged condition in water were also taken when each of the four selected diagonal members were damaged, in turn, to assess the effects of damage in the submerged condition

Several local modes and one higher mode of vibration were also observed throughout the testing in water. The measurements of vibration frequencies of these modes, their description, and the effects of deck mass reduction and damage (if any) on these modes were summarized.

Based on the findings in this chapter, and also on the rotational symmetry of the model about the vertical axis through the deck center, the following generalizations and conclusions can be stated:

1. The relative change, due to damage, in the normalized modal displacements were considerably larger than the relative changes in the measured frequencies.

2. The severance of Members 107, 94 and 116 in Frame B of the model (which caused reductions in the overall torsional stiffness of the model, as well as in the lateral stiffness in the x direction), reduced the vibration frequencies by less than 3% for Modes 1x and 1t in both deck mass conditions, and had little effect on the vibration frequencies of Modes 2y, 2x and 2t.

3. The severance of Member 55 in Frame 4 of the model, which caused reductions in the torsional stiffness and lateral y direction stiffness of the model, reduced the vibration frequencies of Mode 1y by about 5% and the frequency of Mode 1t by 10.4% and 7.3% for the maximum and minimum deck mass conditions respectively, but caused a reduction of only 1% in the frequency for Mode 2t.

4. Severance of Members 107, 94 and 116 in Frame B increased the y displacement to x displacement ratios at the deck center in Mode 1x by 27% to 157% and introduced a difference in the y displacements at Locations A and C for Mode 1x, in the sense specified by (the sign in) Tables 4.3 and 4.8. In addition, these damages increased the x displacement to y displacement ratios at the deck center in Mode 1y by 36% to 150%. The severance of these members also introduced a x component of vibration at the deck center, in the direction given in Tables 4.4 and 4.9, during the vibratory response of Mode 1t.

5. A cut in Member 55 decreased the x displacement to y displacement ratios at the deck center in Mode 1y (for both deck mass cases) by over 55% and introduced a rotation of the deck about the vertical axis as shown in Tables 4.2 and 4.7. The cut also reduced the y displacement to x displacement ratios at the deck center in Mode 1x by over 38% and introduced a small rotation of the deck about the vertical axis in this mode. In Mode 1t, the damage introduced a y component of modal displacement at the deck center in the sense specified in Tables 4.4 and 4.9.

6. Due to the rotational symmetry of the tower about the vertical axis (through the deck center) the effects of severance of Members 2, 15, 36 and 52 (see Figs. 3.7 and 3.8) on the vibration frequencies of the model would be identical to those found for Members 107, 94, 116, and 55 respectively. However, for changes in mode shapes due to damage, the effects of severance in Members 2, 15, 36 and 52 will be identical to those measured for Members 107, 94, 116 and 55 respectively, except that all rotations (about the vertical axis) introduced at the deck, as well as all modal x and y displacements introduced at the deck center in Mode 1t, will be opposite in sense.

CHAPTER 5

MATHEMATICAL STUDIES

5.1 Introduction

This chapter presents the analytically evaluated vibration frequencies and mode shapes of the tested laboratory platform. The analytical evaluations were based on the finite element modeling of the laboratory platform in the tested conditions. Finite element models were developed for the maximum and minimum deck mass cases and, in each case, for the undamaged and damaged conditions of the platform structure. The hydrodynamic inertial effects due to submergence of the platform structure in water were also accounted for in the mathematical formulations.

As discussed in Chapter 4, normalized modal displacement ratios were measured for vibration Modes 1y, 1x and 1t (two translational and first torsional modes). Damage to the tower caused significant variations in the normalized modal displacement ratios of Modes 1y and 1x. Further, the damages reduced the vibration frequencies of Modes 1t, and 1x or 1y by over 1% in value, but had little influence on the measured frequencies of Modes 2t, 2y and 2x. The formulation of the mathematical model of the structure (the degree of refinement in the finite element model), to be described in Section 5.2, was aimed at simulating the vibratory properties of the structure in Modes 1y, 1x and 1t with sufficient accuracy.

Following the analytical correlation studies, the mathematical model was employed to assess the effect of severing Member 62 on Modes 1y, 1x and 1t of the structure. The analytical model was also used to assess the effects of an induced deck mass eccentricity on the vibratory properties of the undamaged structure as well as the effect of damage on the vibratory properties of the structure given the eccentricity in the deck mass. The eccentricity was induced by shifting the deck center of mass by 3.6" in the +x direction. Results of these analytical assessments are summarized and discussed following the presentation of the

mathematical correlation studies.

5.2 Mathematical Modeling and Eigenproblem Solution

SAP IV [36], a general purpose computer program, was employed to model the structure mathematically. The members and legs of the tower were idealized as three dimensional beam elements interconnected at nodes. The nodes were located at the intersections of the centroidal axes of the bracing members and legs, as well as at the base and deck connections.

The vibratory properties of several higher modes of local nature, excited during the shock tests, were described in Chapter 4. The vibration frequencies of two of these modes were lower than the frequencies of global Modes 2y, 2x and 2t. To accurately account for the vibratory characteristics of Modes 2y, 2x and 2t, and also to account for other higher vibration modes, it would have been necessary to refine the mathematical model further by adding nodes along the span of the bracing members and legs. However, the addition of these degrees of freedom would have increased the computation time, and therefore the cost of the vibration analysis. Therefore, because the purpose of the mathematical modeling was to accurately simulate the vibratory properties only of Modes 1y, 1x and 1t, nodes were not used within the spans between joints. Fig. 5.1, which shows Frame 4 of the structure in the finite element model, illustrates the typical modeling scheme used in the mathematical formulation.

The moduli of elasticity and geometric cross section properties for the bracing members and legs of the tower were described in Chapter 2 (see Figs. 2.3 through 2.6). The mass density of the polycarbonate used for constructing the structure was $0.1125 x 10^{-3} lb\_s^2/in^4$ (specific gravity = 1.202).

For the members and nodes referred to in this chapter the reader should refer to Figs. 3.4 through 3.8.

The deck (see Figs. 2.7 and 2.8) was idealized as a rigid unit and modeled as a master

node. The legs of the model were assumed fully fixed to the deck and so the degrees of freedom of the nodes located at the intersections of the leg centerlines and the deck were assumed to be dependent on the degrees of freedom of the deck master node. The inertial properties of the master node were evaluated by taking into account the inertial properties of all components of the deck, including the lumped member masses at the intersections of the legs with the deck and the mass of the accelerometers on the deck. The master node was located at the center of mass of the deck, which in plan view coincides with the geometric center of the deck (intersection of centerlines). The inertial properties and the vertical position (Elevation, see Fig. 3.7) of the master node for the maximum and minimum deck mass cases are summarized in Table 5.1. The eight nodes located at the bottom of the tower legs (Elev. -3/8", see Fig. 3.4) were assumed to be fully clamped against any motion.

The severance of a member was simulated by removing the member in the finite element model and making necessary adjustments to the lumped masses of the nodes to which the member was connected.

For every submerged member the added mass of water was assumed to be equal to the mass of fluid displaced by the member [24,37]. The added mass effect was assumed to be felt by a submerged member only for accelerations normal to its axis. That is, for every submerged member, the inertial resistance due to the added mass of the fluid applied only to the components of acceleration normal to the axis of the member. It was judged sufficient to account for the inertial effects of the fluid inside a leg only for accelerations normal to the axis of the leg. The orientation of a submerged member with respect to the global axes can be defined by the vector

$$\hat{n}^T = [\cos\theta_x \quad \cos\theta_y \quad \cos\theta_z]$$

where θ_x, θ_y, and θ_z are the direction angles for the member [38]. If the acceleration at node i of the member is $\hat{a}_i$ then the component of acceleration normal to the member is

$$\hat{a}_{in} = (I - \hat{n}\,\hat{n}^T)\,\hat{a}_i$$

where I is the 3 x 3 identity matrix. The inertial force associated with the acceleration due to the hydrodynamic added mass will therefore be

$$f_{Ii} = - \; m_i \; \hat{a}_{in} = - \; m_i \; (\; I - \; \hat{n} \; \hat{n}^T \;) \; \hat{a}_i$$

where m_i is the lumped added mass of water at node i. To account for the hydrodynamic inertial effects in Modes 1y, 1x and 1t, it was judged sufficient to account for the diagonal terms and ignore the off-diagonal terms when evaluating the global mass matrix. The resulting diagonal mass terms (translational inertia) for node i of a submerged member were

$$m_x = m_i \sin^2\theta_x$$
$$m_y = m_i \sin^2\theta_y$$
$$m_z = m_i \sin^2\theta_z$$

The finite element model had a total of 85 nodes, over 140 members, and 222 degrees of freedom (equation numbers) with a band width of 96. The vibration frequencies and mode shapes were evaluated using the subspace iteration procedure [36], where four or five iterations were carried out in a subspace of dimension 21.

5.3 Static Behavior of Model

The mathematical model of the structure demonstrated that the principal axes of the structure were not parallel to the global x and y axes. The principal axes are defined as the directions in which a unit lateral load will cause the least and the greatest lateral displacement of the structure. If the direction of the applied load does not coincide with a principal axis, the direction of the resulting lateral displacement will not coincide with the direction of the applied load. Static analysis indicated that a lateral load applied to the deck master node in the (global) y direction displaced the master node in both the y and x directions, where the ratio of the x displacement to the y displacement was -0.019. Similarly, a lateral load applied at the master node in the x direction displaced the master node with a component in the y direction, where the ratio of the y displacement to the x displacement was -0.022. This behavior is due to the arrangement of the diagonal bracing members in the periphery

of the jacket which renders the structure unsymmetric about any vertical plane but with rotational symmetry. The results of the static analysis satisfied Maxwell and Betti's Laws of reciprocal displacements.

During static tests the tower was loaded at the deck, laterally in the x and y directions, and the displacements in the direction of the applied load were measured on the side of the top plate of the deck. These measurements compared well with the analytical predictions. The results of these tests and the analytical predictions are presented in Figs. 5.2 and 5.3.

5.4 Eigenproblem Results of the Correlation Study

5.4.1 Undamaged Structure with Minimum Deck Mass

The evaluated and measured (frequency resolution = 0.05 Hz) vibration frequencies for Modes 1y, 1x and 1t of the undamaged structure with minimum deck mass in air as well as in water are summarized in Table 5.2. The corresponding evaluated and measured normalized modal displacements at the deck and at Nodes 54 and 49 (see Fig. 3.6) for Modes 1y, 1x and 1t are summarized in Table 5.3. the predicted and measured (frequency resolution = 0.098 Hz) vibration frequencies for Modes 2y, 2x and 2t of the submerged undamaged structure with minimum deck mass are given in Table 5.4.

The vibration frequency values predicted by the mathematical model were only slightly lower than the measured values for the first three modes. The predicted frequencies were 2 to 3% lower than the measured values for Modes 1y and 1x and 5% lower for Mode 1t, whether the structure was in air or in water (Table 5.2). However, the predicted vibration frequencies for Modes 2y, 2x and 2t were over 14% higher than measured, primarily due to the degree of refinement in the mathematical model which was not sufficient for accurately simulating these modes.

The predicted normalized modal displacements for Modes 1y, 1x and 1t were in good agreement with the measured values (Table 5.3). The good agreement between the experimental and analytical results indicates that the mathematical models of the structure were

capable of simulating the vibratory properties of Modes 1y, 1x and 1t accurately for the structure in air or in water.

The mathematical modelling of hydrodynamic effects, accurately predicted how placing the structure in water affected the vibratory properties of Modes 1y, 1x and 1t. The finite element models predicted reductions of 1.2, 1.3 and 3.5 Hz in the vibration frequencies of Modes 1y, 1x and 1t respectively (see Table 5.2) if the structure was placed in water (and water was allowed to fill its legs). Whereas the measured reductions in the vibration frequencies of Modes 1y, 1x and 1t, due to submergence, were 1.1, 1.2 and 3.6 Hz respectively. In addition, the predicted changes in mode shape agreed closely with the measured changes, for Modes 1y, 1x and 1t, when placing the structure in water (see Table 5.3).

The analytical results indicated both x and y components of modal displacement at all nodes for Modes 1y and 1x, but one component of modal displacement was larger than the other. These relative values were similar to the relative components of modal displacement at the deck or at Node 54.

Inspection of the analytical results revealed that for mode shapes 1y, 1x and 1t the mathematical model predicted very little distortion in the horizontal cross sections of the jacket at the levels where the joints were located. These distortions in cross sections were caused by small discrepancies between the distorted and undistorted cross section. These discrepancies, if any, were generally less than 8% of the maximum modal displacement at the top of the jacket.

Figs. 5.4 through 5.6 illustrate the analytical mode shapes for Modes 1y, 1x and 1t of the structure in water. The corresponding predicted modal displacements of the deck in plan view are shown in Fig. 5.7. The corresponding measured modal displacement shapes of the deck in plan view practically overlap those given in Fig. 5.7 (see Table 5.3).

The analysis predicted lateral y - translations of the tower in Mode 2y and lateral x - translations in Mode 2x, whereas measurements taken during tests indicated lateral modal displacements in both the x and y directions for Mode 2y as well as for Mode 2x. As

mentioned earlier this discrepancy is related to the refinement in the mathematical model.

Analytical results indicated that the general characteristics of Mode shapes 1y, 1x and 1t were not changed by placing the structure in water.

5.4.2 Undamaged Structure in Water with Maximum Deck Mass

The predicted, and measured vibration frequencies of the structure for this case are summarized in Table 5.6. The predicted as well as measured normalized modal displacements of the deck and of Nodes 54 and 49 (see Fig. 3.6) for Modes 1y, 1x and 1t of the undamaged structure in water with maximum deck mass are summarized in Tables 5.8 through 5.10. In the maximum deck mass case the analysis predicted a vertical mode with a vibration frequency of 28 Hz.

As in the minimum deck mass case, the analytically predicted vibration frequencies for Modes 1y, 1x and 1t agreed closely with experimental measurements. The predicted frequencies of Modes 1y and 1x were only 3% lower than the measured values, whereas the predicted frequency of Mode 1t was 4% lower than measured. However, for Modes 2y and 2t the vibration frequencies predicted by the finite element model were 8% and 25% higher in value than the measured frequencies respectively, due to the refinement in the mathematical model which was not sufficient to accurately predict these frequencies.

The predicted normalized modal displacements were in good agreement with the measured modal displacements (Tables 5.8 through 5.10) for Modes 1y, 1x and 1t of the undamaged structure. Although the predicted normalized modal y displacements at Nodes (joints) 49 and 54 in Mode 1t were higher than measured as found for the minimum deck mass case, the mathematical model of the structure simulated the vibratory characteristics of the first three modes with good accuracy.

The vibration shapes of the first three modes, predicted by the finite element model, possessed the same general characteristics found in the minimum deck mass case but with the following differences:

The normalized modal displacements of the nodes (joints) on the jacket were lower than in the minimum deck mass case. This difference was more pronounced for nodes below the 55" Elevation (see Figs. 3.4 through 3.7), and is attributable to the larger ratio of deck mass to jacket mass. Also, at all nodes in the case of the maximum deck mass, the ratio of the x displacement to the y displacement for Mode 1y, as well as the ratio of the y displacement to x displacement for Mode 1x, were smaller than in the minimum deck mass case. Further, in the maximum deck mass case, the normalized (normalized with respect to the maximum translation of the master node in the x or y direction) modal rotation of the deck about the x axis in Mode 1y and the normalized modal rotation of the deck about the y axis in Mode 1x were 32% and 13% larger than in the minimum deck mass case respectively.

Fig. 5.8 illustrates the predicted modal displacements of the deck in plan view for the undamaged structure in water with maximum deck mass loading. The measured modal displacement shapes of the deck practically overlap the corresponding predicted shapes in Fig. 5.8.

5.4.3 Damaged Structure in Water

The predicted and measured vibration frequencies for all damage cases considered in the experimental program are summarized in Tables 5.4 and 5.6. The predicted and measured percentage reductions in the frequencies due to damage, for the first three modes are summarized in Tables 5.5 and 5.7. The predicted, as well as measured normalized modal displacements of the deck and of Nodes 54 and 49 for Modes 1y, 1x and 1t of the structure in its damaged as well as undamaged conditions are summarized in Tables 5.8 through 5.10, and Tables 5.11 through 5.13 for the maximum and minimum deck mass cases respectively. The member numbers, node (joint) numbers and locations referred to are illustrated in Figs. 3.3 through 3.8.

The predicted vibration frequency values for the first three modes of the structure in its damaged conditions for both deck mass cases agreed well with the values measured

during the experimental program (Tables 5.4 and 5.6). Considering the 0.1 Hz resolution in the frequency measurements, the predicted reductions in frequency values resulting from damage were in good agreement with the observed reductions (Tables 5.5 and 5.7).

In the maximum deck mass case the predicted normalized modal y displacements at Nodes 49 and 54 for Mode 1t were larger than the measured values. This difference for Mode 1t was also observed in the undamaged case and the predicted changes in these quantities due to damage agreed well with those indicated by measurements (see Table 5.10).

In the case of damage to Member 116, the analytical normalized modal y displacements of the deck and Node 54, in Mode 1x of the tower with minimum deck mass were larger than measured.

In the case of damage to Member 94 (see Fig. 3.4) several predicted normalized modal displacements were larger than measured during the experimental program. These were:

the modal x displacements of the deck and Node 54 in Mode 1y of the tower with minimum deck mass, the modal y displacements of the deck and Node 49 in Mode 1x for the minimum deck mass case, and the modal x displacement of Node 54 in Mode 1x in the maximum deck mass case.

The analytical normalized y displacement of the deck in Mode 1x of the tower with minimum deck mass and Member 107 damaged was lower than the value measured.

In all cases other than those mentioned above, the analytical normalized modal displacements of the first three modes had close agreement with the experimental results. Collectively, the analytical results indicated that the mathematical models of the structure were capable of simulating the effects of damage properly and with reasonably good accuracy.

The predicted modal displacements of the deck in plan view for the damaged conditions considered in the experimental program are illustrated in Fig. 5.9 through 5.12, and Figs. 5.13 through 5.16 for the maximum and minimum deck mass cases respectively. To illustrate the effects of damage the modal displacements of the deck for the corresponding

undamaged cases have also been included in these Figures. Plots of the measured deck modal displacement shapes for the damaged cases generally agree closely with the predicted shapes, or practically overlap them. Tables 5.8 through 5.13 should be used for making comparisons between the predicted and measured modal displacements of the deck.

5.5 Severance of Member 62

As illustrated in Fig. 3.5, Member 62 is located in Frame 4 of the structure and therefore contributes to the lateral stiffness of the tower in the y direction as well as its torsional stiffness. In previous studies of damage, only one of the considered members (Member 55 in Frame 4) contributed to both the lateral stiffness of the tower in the y direction and its overall torsional stiffness. The mathematical model of the structure was employed to assess how severance of Member 62 affected the vibratory properties of the structure. The results of this theoretical assessment are presented here and illustrate that the changes in vibratory properties of the structure are similar when either Member 62 or 55 is damaged.

The predicted frequencies of Modes 1y, 1x and 1t, after severance of Member 62, are summarized in Tables 5.4 and 5.6 for the minimum and maximum deck mass cases respectively. In the minimum deck mass case the frequencies of Modes 1y and 1t were predicted to decrease by 8.3% and 15.8% respectively (Table 5.5). In the maximum deck mass case the analysis indicated reductions of 2.7% and 8.8% in the frequencies of Modes 1y and 1t respectively (Table 5.7). As discussed previously, the mathematical model accurately simulated the properties of the first three modes and provided only rough estimates of frequencies for Modes 2y, 2x and 2t. The estimated frequencies of Modes 2y and 2t indicated that damage to Member 62 could strongly affect the frequencies of Modes 2y and 2t for both deck mass conditions.

The analytical normalized modal displacement ratios of the deck and Nodes (joints) 54 and 49 for the structure for both deck mass conditions with Member 62 damaged are summarized in Tables 5.8 through 5.13.

The analysis predicted the following changes in the shape of Mode 1y due to severance of member 62: a) 66% and 34% reductions in the normalized modal x displacements of the deck for the minimum and maximum deck mass cases respectively, b) significant distortion in the displaced shape of the jacket cross section at the 30" Elevation (Fig. 5.17) with over 100% increase in the normalized modal y displacement of joint 54 for both deck mass cases, due to the dramatic decrease in the y direction stiffness of Frame 4 caused by the damage (see Fig. 3.5), and c) a new rotation of the deck about the vertical axis (different modal y displacements at deck sides) for both deck mass cases, as illustrated in Tables 5.8 and 5.11.

The predicted changes in the normalized displacements of Mode 1x were: a) 83% and 36% reductions in the normalized modal y displacements of the deck for the minimum and maximum deck mass cases respectively, b) different modal y displacements at deck sides (due to rotation of the deck about the vertical axis) as indicated in Tables 5.9 and 5.12 for the two deck mass cases, and c) over 50% increase in the normalized modal y displacement of joint 54, for both deck mass cases, due to the softening of Frame 4 in the y direction resulting from the damage.

In Mode 1t the analysis indicated the introduction of modal y displacements at the deck center for both deck mass conditions as indicated in Tables 5.10 and 5.13. Further, as in the case of Mode 1y, the shape of the jacket cross section at the 30.0" Elevation (Fig. 3.6) in Mode 1t was predicted to distort dramatically with over 100% increase in the normalized modal y displacements at joint 54 (in this mode) for both deck mass cases. This was due to the softening of Frame 4 in the y direction caused by the damage.

Figs. 5.17 and 5.18 illustrate the predicted distortions in the cross section of the jacket at the 30" Elevation, for the first and third mode shapes, caused by the damage. As mentioned above, these distortions were attributed to the drastic reduction in the stiffness of Frame 4 and of joint 54 in the y direction caused by severance of Member 62.

The changes in the normalized modal displacement ratios of the deck, summarized above, due to severance of Member 62, were similar to the changes caused by severance of

Member 54, but with different magnitudes. Figs 5.19 and 5.20 illustrate the effects of damage in Member 62 on the modal displacements of the deck in plan view.

5.6 Effect of Deck Mass Eccentricity

The mathematical model was employed to assess what changes occur in the vibratory properties of the structure when the position of the deck center of mass shifts by 3.6" in the +x direction (see Figs. 2.7 and 3.4). In all cases considered previously, the deck center of mass coincided with the deck geometric center in plan view. The analytical assessment encompassed the effects of the eccentricity on the vibratory properties of Modes 1y, 1x and 1t. The 3.6" eccentricity was 10% of the breadth of the jacket at its top (10% of the distance between Frames 1 and 4 at the 64.32" Elevation, see Fig. 2.3) and was believed to be a large eccentricity. Results of the evaluation are summarized in this section.

5.6.1 Undamaged Structure

The predicted vibration frequencies of the undamaged structure for the eccentric deck mass case are summarized in Table 5.14. In both deck mass cases the eccentricity reduced the frequency of Mode 1y but increased the frequency of Mode 1t (see predicted vibration frequencies for the undamaged cases in Tables 5.4, 5.6 and 5.14).

The predicted normalized modal displacements of the deck and of joints 54 and 49 for the eccentric deck mass case with no damage are summarized in Tables 5.16 through 5.18 for Modes 1y, 1x and 1t respectively.

In Mode 1y the deck mass eccentricity increased the predicted normalized modal displacements on the side towards which the deck center of mass was shifted, and decreased the normalized modal displacements on the opposite side. This was reflected in the larger normalized modal y displacements at joint 54 as compared to those at joint 49, which were smaller (see Tables 5.8, 5.11 and 5.16). Further, the resulting modal rotation of the deck about the vertical axis in Mode 1y, caused by the deck mass eccentricity, was relatively large for both deck mass cases (see $\frac{Y_A - Y_C}{2}$ in Tables 5.8, 5.11 and 5.16).

At the deck, the eccentricity decreased the ratio of modal x displacement to y displacement in Mode 1y and also the ratio of modal y displacement to x displacement in Mode 1x for both deck mass cases. However, these predicted decreases were generally considerably smaller than the similar predicted decreases when Members 55 and 62 were severed in the non-eccentric deck mass case (see Tables 5.8, 5.9, 5.11, 5.12, 5.16 and 5.17).

In both deck mass cases relatively large normalized modal y displacements were introduced at the deck center in Mode 1t as well as normalized $\frac{Y_A - Y_C}{2}$ in Mode 1y due to the deck mass eccentricity. When smaller magnitudes of normalized modal y displacement were introduced at the deck center in Mode 1t or the same magnitudes of normalized $\frac{Y_A - Y_C}{2}$ were introduced in Mode 1y due to damage in the non-eccentric deck mass case, they were accompanied with dramatic reductions in the frequency of Mode 1t. But, as mentioned earlier, the analysis predicted the deck mass eccentricity to increase the frequency of Mode 1t.

5.6.2 Damaged Structure

The effect of damage on the vibration frequencies and shapes of Modes 1y, 1x and 1t of the structure having the eccentricity in its deck mass were evaluated analytically. For the minimum deck mass case all damage cases considered previously (in Section 5.4.3) were also considered here. However, for the maximum deck mass case, the severance of Members 55 and 107 were considered. The predicted vibration frequencies are summarized in Table 5.14 and the predicted shifts in the frequencies, expressed in percent of the frequency for the undamaged tower, are summarized in Table 5.15 for values greater than 1%. The analytical normalized modal displacements of the deck and of joints 54 and 49, for the damaged structure, are summarized in Tables 5.16 through 5.18 for Modes 1y, 1x and 1t respectively.

The predicted changes in frequencies due to damage were similar to those predicted and measured for the non-eccentric deck mass case (see Tables 5.15, 5.5 and 5.7): in either

deck mass case there were reductions greater than 1% in the frequency of Mode 1x and possibly of Mode 1t when Members 107, 94 and 116 were severed, and also reductions of greater than 1% in the frequencies of Modes 1y and 1t when Members 55 or 62 were severed. In addition, a 1.3% reduction in the frequency of Mode 1y was predicted if Member 94 was severed. This could be related to the presence of torsional behavior in Mode 1y of the undamaged structure, which was caused by the deck mass eccentricity.

The predicted changes in the normalized modal displacement ratios due to damage were also similar to those predicted and observed in the non-eccentric deck mass case.

The results indicated that damage to Members 107, 94 and 116 caused dramatic (relative) increases in the ratio of the modal x displacement to y displacement at the deck center in Mode 1y and also in the ratio of the modal y displacement to x displacement at the deck center in Mode 1x. Further, in these damage cases the normalized $\frac{Y_A - Y_C}{2}$ increased (positive increase) in Mode 1x (i.e., as shown in Table 5.17), and the normalized modal x displacement at the deck center in Mode 1t generally decreased.

The results indicated that for the modal displacements at the deck center damage to Member 55 or 62 caused dramatic (relative) decreases in the (magnitude of) ratio of modal x displacement to y displacement in Mode 1y and also in the ratio of modal y displacement to x displacement in Mode 1x. Further, the normalized $\frac{Y_A - Y_C}{2}$ decreased (negative increase) in Mode 1y (Table 5.16), and the normalized modal y displacement at the deck center increased in Mode 1t, due to severance of Member 55 or 62.

5.7 Summary

Mathematical models of the tested structure were formulated for analytical correlation studies. These models were designed to simulate the conditions under which the structure was tested. Frequencies and mode shapes were evaluated for the tower, in water, in its undamaged as well as damaged conditions, considering both the maximum and minimum

deck mass cases. Frequency and mode shapes were also evaluated for the undamaged tower in air with minimum deck mass loading. Based on how the analytical results compared with the experimental results (in Chapter 4) the following could be stated:

1. The mathematical models were capable of simulating the properties of vibration Modes 1y, 1x and 1t of the structure with reasonably good accuracy.
2. The degree of refinement in the finite element models was sufficient for accurately assessing the characteristics of the first three vibration modes.
3. The mathematical modeling of the hydrodynamic added mass accurately accounted for the changes in the frequencies and mode shapes of the structure when it was placed in water.
4. Due to its capability to simulate the effects of damage on the properties of the first three vibration modes of the structure, it is concluded that the mathematical model could be used in place of the actual structure for additional case studies.

The mathematical model of the structure was used to assess the effect of a cut in Member 62 on the vibratory properties of Modes 1y, 1x and 1t, and was also used to study the vibratory properties of the undamaged structure when the position of the deck center of mass shifted in the +x direction. Finally, the effects of damage on the first three vibration modes of the structure with the eccentric deck mass were assessed analytically. The results of these studies were summarized and discussed. The important observations were:

1. The severance of Members 62 and 55 had similar effects on the vibration properties of the first three vibration modes of the structure as indicated by the deck modal displacements, where the important changes in mode shape fell under the same classification.
2. Dramatic distortions occurred in the mode shapes at the jacket cross section at the 30" Elevation due to the reduction of stiffness at joint 54 in the y direction caused by severance of Member 62.

3. The deck mass eccentricity decreased the frequency of Mode 1y but increased the frequency of Mode 1t. This was different from the frequency changes due to damage in the non-eccentric deck mass case.

4. Considering both the mode shape and frequency information, changes due to the deck mass eccentricity in the undamaged structure were different from the changes due to damage in the non-eccentric deck mass case. The most important difference was that when damage in the non-eccentric deck mass case caused a normalized $\frac{Y_A - Y_C}{2}$ in Mode 1y of the same magnitude as that caused by deck mass eccentricity (in the undamaged structure) it also caused a significant reduction in the frequency of Mode 1t, whereas the deck mass eccentricity caused an increase in the frequency of this mode.

5. The changes in the frequency and normalized modal displacements of the deck center for Modes 1y, 1x and 1t resulting from damage were very similar whether the deck mass had an eccentricity or not.

CHAPTER 6

CONCLUSIONS

6.1 Findings

Experimental and analytical studies were conducted to assess the effects of damage on the frequencies and mode shapes of a K-braced platform model. The model was carefully prepared to possess the important dynamic features of a typical K-braced steel offshore platform. Five bracing members located in the periphery of the jacket were considered in studying the effects of damage. The effects of a variation in deck mass were assessed by considering two deck mass conditions in all cases, both experimentally and analytically. The effects of eccentricity in the location of deck mass were considered analytically. Experimental and analytical results of the study are presented and summarized in Chapters 4 and 5, respectively. The important findings and conclusions can be summarized as follows.

6.1.1 Damage Effects

A. Damage could be detected by changes in the vibratory characteristics of the first three modes (Modes 1y, 1x and 1t) of the platform. Reductions in the vibration frequencies and changes in the normalized modal displacements of the deck in the first three modes, as indicated by three accelerometers located on the deck, were sufficient for inferring damage. The normalized modal displacements of the deck center in the global x and y directions (ratio of modal x displacement to modal y displacement in Mode 1y and the inverse of this ratio in Mode 1x) and the difference in the normalized modal y displacements of two opposite sides of the deck were employed in the damage assessment strategy.

B. Changes in the normalized modal displacements of the deck were more useful in detecting damage than changes in the vibration frequencies because the percentage changes in the normalized modal x and y displacements of the deck center (in Modes 1y and 1x) were considerably larger than the percentage reductions in

frequencies caused by damage. Typically, damage reduced the vibration frequencies by only a few percent while it caused changes of over 30% (which in a few instances were over 100%) in the normalized modal x and y displacements of the deck center. From the changes in the normalized modal displacements of the deck it was possible to infer in which one of the four frames (A, B, 1 or 4) forming the periphery of the jacket the severed member was located, whereas changes in the frequencies could only indicate whether the damaged member was oriented in the global x direction or in the global y direction.

C. Damaged braces in Frame 4 (a) reduced the frequencies of Modes 1y and 1t by over 2% and 7%, respectively; (b) dramatically reduced the normalized modal x and y displacements of the deck center in Modes 1y and 1x, respectively (by over 33%); (c) caused larger normalized modal y displacements at the deck side above Frame 4 than those at the opposite side above Frame 1 during vibrations in Mode 1y; and (d) introduced (or increased the) normalized modal y-displacements at the deck center in Mode 1t for clockwise rotation of the deck about the vertical axis.

   The reductions in the frequencies of Modes 1y and 1t are attributed to decreases in the lateral y direction stiffness of the tower, and in torsional stiffness. The larger normalized modal y displacements of the deck above Frame 4 in Mode 1y as well as the normalized modal y displacements of the deck center in Mode 1t are attributed to the shift of the center of rigidity of the platform away from Frame 4. It appears that the reductions in the normalized modal x and y displacements of the deck center in Modes 1y and 1x, respectively, were due to the decrease in the overall lateral stiffness of the tower in the y direction.

D. Because of the rotational symmetry of the tower about the vertical axis, damage to diagonal bracing members in Frame 1 causes reductions in frequencies as well as in the normalized modal x and y displacements of the deck center in Modes 1y

and 1x, respectively, similar to those observed when bracing members of Frame 4 were damaged. However, in this case the changes in the difference between normalized modal y displacements above Frames 1 and 4 on the deck in Mode 1y, as well as the induced normalized y displacements at the deck center in Mode 1t, are opposite in sense to those observed when damage occurred in Frame 4. This is because the center of rigidity of the platform shifts away from Frame 1 (and towards Frame 4).

E. Damage to the selected diagonal members of Frame B (a) reduced the frequency of Mode 1x by over 1% (but less than 4%) and also that of Mode 1t by less than 3%; (b) dramatically increased the normalized modal x displacement and y displacement of the deck center in Modes 1y and 1x, respectively (generally by 30% and over); (c) caused larger normalized modal y displacements at the side of the deck above Frame 1 compared with those on the side above Frame 4 for Mode 1x (deck rotation about the vertical axis); and (d) introduced a (or caused a change of) negative normalized modal x displacement at the deck center in Mode 1t for clockwise rotation of the deck about the vertical axis.

The reductions in frequencies of Modes 1x and 1t were due to decreases in the lateral stiffness of the tower in the x direction and in torsional stiffness, respectively, caused by damage in Frame B. In this case the shift in the center of rigidity of the platform away from Frame B caused the change in the normalized modal x displacement of the deck center in Mode 1t, as well as larger normalized modal y displacements of the deck above Frame 1 than those above Frame 4 in Mode 1x. It appears that the dramatic increases in the normalized modal x and y displacements of the deck center in Modes 1y and 1x, respectively, were due to the decrease in the overall lateral stiffness of the tower in the x direction.

F. Because of rotational symmetry of the tower about the vertical axis, damage to the diagonal members in Frame A causes reductions in frequencies of Modes 1x

and 1t and dramatic increases in the normalized modal x and y displacements of the deck center in Modes 1y and 1x, respectively, similar to those observed when members of Frame B were damaged. However, the changes related to the shift in the center of rigidity, which in this case is towards Frame B (in plan view), are of the same magnitudes observed when damage was in Frame B but opposite in sign.

G. The effects of reduction in overall torsional stiffness of the platform as well as the effects of shifts in the center of rigidity of the platform, were more pronounced when damage occurred in Frame 4 or 1 (as compared to the cases in which damage was in Frame B or A). This was primarily because Frames 1 and 4 were further from the vertical axis through the deck center than were Frames B and A.

6.1.2 Mass Effects

A. The increase in deck mass (the maximum deck mass was 4.1 times the minimum deck mass) reduced the frequencies of Modes 1y, 1x and 1t by 47%, 46% and 44%, respectively, and decreased both the normalized modal x displacement of the deck center in Mode 1y and the normalized modal y displacement of the deck center in Mode 1x by 53% and 59%, respectively. Unlike the above changes, damage reduced the frequency of only one of the 1x and 1y Modes and the (percentage) changes in the normalized modal displacement of the deck center were in general over 8 times the (percentage) changes in the frequencies of Modes 1x and 1y when damage occurred.

B. Based on analytical studies, shifting the deck center of mass in the +x direction to induce a deck mass eccentricity decreased the frequency of Mode 1y by 2% and 1.4% in the maximum and minimum deck mass cases, respectively, but increased the frequency of Mode 1t by 2% and 0.7% in the maximum and minimum deck mass cases, respectively. Further, the eccentricity decreased the

normalized modal x displacement of the deck center in Mode 1y by 14% and 20% in the maximum and minimum deck mass cases, respectively, and also decreased the normalized modal y displacement of the deck center in Mode 1x by 27% and 26% for the maximum and minimum deck mass cases, respectively. When damage in the non-eccentric deck mass case introduced magnitudes of $\frac{(Y_A - Y_C)}{2}$ in Mode 1y comparable to that caused by the deck mass eccentricity, it introduced smaller normalized modal y displacements at the deck center in Mode 1t, caused considerably larger (over 40%) reductions in the normalized modal x and y displacements in Modes 1y and 1x, respectively, than caused by the deck mass eccentricity, and was accompanied by reductions of over 7% in the frequency of Mode 1t contrary to the increases in the frequency of Mode 1t caused by the eccentricity.

C. Damage in the tower with the eccentric deck mass had the same (general) effects on the frequencies and mode shapes of Modes 1y, 1x and 1t as those observed for the non-eccentric deck mass case.

6.1.3 Hydrodynamic Effects

A. The mathematical model of the structure accurately simulated the hydrodynamic inertial effects of the water surrounding the structure on the vibratory properties of Modes 1y, 1x and 1t. The vibratory properties of Modes 1y, 1x and 1t were accurately predicted by the mathematical model.

B. In the minimum deck mass case submerging the tower in water, which increased the virtual mass [24] of the submerged bracing members and legs of the platform by over 1.5 times and over 6 times, respectively, reduced the frequencies of Modes 1x and 1y by 8% and that of Mode 1t by 15%, and increased the normalized modal x displacement of the deck center in Mode 1y and the normalized modal y displacement of the deck center in Mode 1x by 76% and 94%, respec-

tively. As discussed earlier, damage reduced the frequency of only one of the two translational modes 1y and 1x, whereas here the frequencies of both of these modes were reduced.

6.2 Discussion and Recommendations

During vibrations in the first as well as the second translational mode (1y and 1x) of the structure the deck center displaced in both the x and y directions (see Figs. 3.3 through 3.6). Damage in the structure caused dramatic changes in the ratio of modal x to y displacement in Mode 1y as well as in the ratio of modal y to x displacement in Mode 1x at the deck center. These are properties that can be found in commonly used, 8-legged, K-braced, steel offshore platforms that are similar to the structure studied. Based on the findings of this study, making use of these properties can not only improve the damage detection capabilities for K-braced platforms, which have similar translational mode characteristics, but can also greatly simplify detecting damage since knowledge of modal displacements of the deck in one of the first two translational modes will be sufficient for detecting member severance. It is recommended that these properties also be studied in taller K-braced towers.

Severance of a diagonal bracing member which contributes to the overall torsional stiffness of a platform shifts the center of rigidity of the tower at the deck level. The resulting change in the distance between the centers of rigidity and mass introduces (or alters) normalized modal y (or x) displacements at the deck center in the first torsional mode, and increases the normalized modal y (or x) displacements on one side of the deck while decreasing them on the opposite side of the deck (due to rotation of the deck about the vertical axis) during vibrations in Mode 1y (or 1x) where the x and y axes would be parallel to the orientation of the frames of the tower in plan view. These effects which made it possible to identify in which one of the frames in the periphery of the structure (i.e., Frames A, B, 1 or 4 in Figs. 2.3 and 2.4) the damaged member was located, can be observed in all types of braced steel offshore platforms (4-legged or 8-legged, x-braced or K-braced platforms). In general, for a given tower, the effects are larger when the frame in which

damage has occurred is furthest from the center of rigidity. Further, for higher towers, severance of a single member will have less pronounced effects, since the reduction in the overall lateral stiffness of the damaged frame will be less when the frame is taller and has more panels. Study of the effects of damage-induced-shifts in the center of rigidity for different K-braced and x-braced platforms will provide useful information and is recommended. It is recommended that effects of member severance in interior frames of 8-legged platforms (see Frames 2 and 3 in Fig. 2.5) be investigated and the changes be compared with those caused by damage in the exterior frames which have a horizontal orientation parallel to that of the interior ones (see Frames 1 and 4 in Fig. 2.4), since magnitudes of the changes due to shifts in the center of rigidity will be larger for damage in the exterior frames and the information can be useful in distinguishing the effects of damage to the exterior frames from those caused by damage in the interior frames of 8-legged platforms.

For the structure studied, changes in the vibratory properties due to marine growth would be similar to differences between the vibratory properties of the tower in water and in air. The results of the study indicated that when both mode shape and frequency information were used changes in the vibratory properties resulting from deck mass eccentricity, differences between the vibratory properties of the structure in air and water as well as the effects of increasing the deck mass could be distinguished from the effects of damage. Additional studies of the effects of variations in deck mass, marine growth and damage on both the normalized modal displacements at the deck and vibration frequencies in K-braced platforms will be useful in assessing the effectiveness of periodic inspections of vibration characteristics to confirm structural integrity.

Based on the results of this study it is likely that for any platform an increase in deck mass eccentricity (distance between the centers of rigidity and deck mass) will increase the frequency of the first torsional mode while causing changes in mode shapes at the deck level similar to those caused by damage. This concept would be useful in damage detection and should be investigated further for different towers.

For a K-braced offshore platform the feasibility of detecting severance of diagonal bracing members from changes in the vibratory properties of the first three vibration modes can be confirmed by a mathematical study. Continuous monitoring of the deck modal displacements and the vibration frequencies for the first three modes is recommended for K-braced fixed offshore platforms. By using such a strategy the effects of marine growth which occurs gradually, and the effects of variations in the magnitude and distribution of deck mass, which can be correlated with the observed changes in mass at the deck, will not be confused with changes due to breakage of a member.

REFERENCES

1. American Petroleum Institute "Recommended Practice for Planning, Designing, and Constructing Fixed Offshore Platforms," Dallas, Texas, 7th Ed., 1976; 8th Ed., 1977; 9th Ed., 1978; 10th Ed., 1979.

2. Monk, R.G., "Machinery Vibration on Offshore Platforms," *Journal of Petroleum Technology,* April 1978, pp. 627-637.

3. Gundy, W. E., Scharton, T. D., and Thomas, R. L., "Damping Measurements on an Offshore Platform." *Proceedings,* Offshore Technology Conference, OTC 3863, Houston, Texas, 1980.

4. Kenley, R. M., and Dodds, C. J., "Detection of Damage by Structural Response Measurements," *Proceedings,* Offshore Technology Conference, OTC 3866, Houston, Texas, 1980.

5. Coppolino, R. N., and Rubin, S., "Detectability of Structural Failures in Offshore Platforms by Ambient Vibration Monitoring," *Proceedings,* Offshore Technology Conference, OTC 3865, Houston, Texas, 1980.

6. Duggan, D. M., Wallace, E. R., and Caldwell, S. R., "Measured and Predicted Vibration Behavior of Gulf of Mexico Platforms," *Proceedings,* Offshore Technology Conference, OTC 3864, Houston, Texas, 1980.

7. Marshall, P. W., "Strategy for Monitoring Inspection and Repair for Fixed Offshore Platforms," ASME Publication *Structural Integrity Technology,* May 1979.

8. Stephen, R. M., Hollings J. P., Bouwkamp, J. G., and Jurukovski, D., "Dynamic Properties of an Eleven Story Masonry Building," *EERC Report No. 75-20,* Earthquake Engineering Research Center, University of California, Berkeley, California, July 1975.

9. Petrovski, J., Stephen, R. M., Gartenbaum, and Bouwkamp, J. G., "Dynamic Behavior of a Multistory Triangular-Shaped Building," *EERC Report No. 76-3,* Earthquake Engineering Research Center, University of California, Berkeley, California, October 1976.

10. Stephen, R. M., Wilson, E. L., Bouwkamp, J. G., and Button, M., "Dynamic Behavior of a Pedestal Base Multistory Building," EERC Report No. 78-13, Earthquake Engineering Research Center, University of California, Berkeley, California, July 1978.

11. Ruhl, J. A., "Offshore Platforms: Observed Behavior and Comparison With Theory," *Journal of Petroleum Technology,* April 1978, pp.638-648.

12. Bendat, J. S., *Random Data: Analysis and Measurement Procedures,* John Wiley and Sons, Inc., N.Y., 1971.

13. Earle, E. N., "Determination of Dynamic Characteristics of Offshore Platforms From Random Variables, *Society of Petroleum Engineers Journal,* Dec. 1975, pp. 502-508.

14. Crandall, S. H., editor, *Random Vibration,* Technology Press, Cambridge, Mass., 1958.

15. Davenport, W. B., Jr., and Root, W. L., "An Introduction to the Theory of Random Signals and Noise," McGraw Hill, N.Y., 1958.

16. Loland, O., and Dodds, C. J., "Experiences in Developing and Operating Integrity Monitoring Systems in the North Sea," *Proceedings,* Offshore Technology Conference, OTC 2551, Houston, Texas, 1976.

17. Vandiver, J. K., "Detection of Structural Failure on Fixed Platforms By Measurement of Dynamic Response," *Proceedings,* Offshore Technology Conference, OTC 2267, Houston, Texas, 1975.

18. Begg, R. D., Mackenzie, A. C., Dodds, C. J., and Loland, O., "Structural Integrity Monitoring Using Digital Processing of Vibration Signals," *Proceedings,* Offshore Technology Conference, OTC 2549, Houston, Texas, 1976.

19. Burke, B. G., Sundararajan, C., and Safaie F. M., "Characterization of Ambient Vibration Data by Response Shape Vectors," *Proceedings,* Offshore Technology Conference, OTC 3862, Houston, Texas, 1980.

20. Baker, W. E., Westine, P. S. and Dodge, F. T., *Similarity Methods in Engineering Dynamics,* Hayden Book Co., Inc., New Jersey, 1978.

21. Langhaar, H. L., *Dimensional Analysis and Theory of Models,* John Wiley and Sons, Inc., N.Y., 1951.

22. Murphy, G., *Similitude in Engineering,* Ronald Press, 1950.

23. Wiegel, R. L., *Oceanographical Engineering,* Prentice-Hall, Inc., Englewood Cliffs, N.J., 1964.

24. Lamb, H., *Hydrodynamics,* Dover Publications, New York, 1945.

25. Godden, W. G., Tuncag, M. and Wasley, D. L., "Model Analysis of The Castaic Reservoir Intake Tower," *SESM Report no. 70-15,* Structures and Materials Research, Dept. of Civil Engineering, University of California, Berkeley, California, September 1970.

26. Clough, R. W. and Penzien, J., *Dynamics of Structures,* McGraw-Hill Book Co., 1975.

27. Biggs, J. M., *Introduction to Structural Dynamics,* McGraw-Hill Book Co., 1964.

28. Berman, A., "Determining Structural Parameters from Dynamic Testing," Shock and Vibration Digest, Vol. 7, Jan. 1975.

29. Ibanez, P., et. al., "Methods and Benefits of Experimental Seismic Evaluation of Nuclear Power Plants," *NUREG/CR-1443, Summary Study,* ANCO Engineers, Inc., April 1980.

30. Ibanez, P., "Review of Analytical and Experimental Techniques for Improved Structural Dynamic Models," *Welding Research Council Bulletin 249,* June 1979.

31. Stroud, R. C., Bonner, C. J. and Chambers, G. J., "Modal Testing Options for Spacecraft Developments," *Society of Automotive Engineers Technical Paper 781043,* November 1978.

32. Gundy, W. E., et. al., "A Comparison of Vibration Tests and Analysis on Nuclear Power Plant Structures and Piping," *Transactions, International Conference on Structural Mechanics in Reactor Technology,* San Francisco, August 1977.

33. Harris, C. M., and Crede, C. E., *Shock and Vibration Handbook,* McGraw-Hill Book Co., 1961.

34. Kelly, R. D. and Richman, G., *Principles and Techniques of Shock Data Analysis, SVM-5* The Shock and Vibration Information Center, United States Department of Defense, 1969.

35. Wylie, C. R., *Advanced Engineering Mathematics,* Fourth Edition, McGraw-Hill Book Co., 1975.

36. Bathe, K. J., Wilson, E. L. and Peterson, F. E., "SAP IV: A Structural Analysis Program for Static and Dynamic Response of Linear Systems," *EERC Report No. 73-11,* Earthquake Engineering Research Center, University of California, Berkeley, California, June 1973.

37. Clough, R. W., "Effects of Earthquakes on Underwater Structures," Proceedings, Second World Conference on Earthquake Engineering, Tokyo, 1960, Vol. II, pp. 815-831.

38. Penzien, J. and Tseng, S., "Three-dimensional Dynamic Analysis of Fixed Offshore Platforms," *Numerical Methods in Offshore Engineering,* John Wiley and Sons, 1978.

APPENDIX A

EVALUATION OF MODAL DISPLACEMENTS

The theoretical basis for the evaluation of modal displacement ratios from transient response spectra was described in Chapter 3. Here the method is illustrated by demonstrating the evaluation of the deck modal displacements for Modes 1x and 1t from spectra of one of the s-x tests (Test 147).

Tables A.1 through A.3 summarize the spectral amplitudes and phase angles of Fast Fourier Transform functions (FFT) from test 147 for the 6.0 Hz to 12.0 Hz range. These transform functions were evaluated from the time histories of the analog signals of acceleration outputted by Accelerometers 1, 2, and 3 during the transient vibratory response of the model. The three accelerometers were calibrated using the acceleration of gravity (commonly used for strain gauge type accelerometers), to have a sensitivity of 45 volts/g. Therefore multiplication of the analog signals by c = 0.022 g/volt provided the values of acceleration. The amplitude spectra of acceleration corresponding to Tables A.1 through A.3 are illustrated in Fig. 4.4 (for the 3.0 Hz to 19.0 Hz window).

The deck modal displacements for Test 147 can be evaluated from the information in Tables A.1 through A.3. Multiplication of the spectral amplitudes in these tables by c = 0.022 g/volt provides the values of $| A_p(\omega) |$. As discussed in chapter 3, the deck modal displacements can be evaluated from the $| d_{kp} \; B_k(\omega_k{}^*) |$ values, where k=2 (Mode 1x) or 3 (Mode 1t) and p corresponds to the locations of Accelerometers 1, 2 and 3 (Locations A, B and C, see Fig. 3.3). To subtract $d_{jp} \; B_j(\omega_k{}^*)$ vectors (only if their magnitudes cannot be neglected) from $A_p(\omega_k{}^*)$, where $j \neq k$, and evaluate $d_{kp} \; B_k(\omega_k{}^*)$ with the desired level of accuracy, i.e., to carry out the subtraction procedure described in Section 3.1.3 when necessary, the normalized functions $\dfrac{| B_j(\omega) |}{| B_j(\omega_j{}^*) |}$ are needed. Figs. A.1 through A.3 illus-

trate the $\frac{|B_j(\omega)|}{|B_j(\omega_j^*)|}$ functions for j=1, 2, and 3 (Modes 1y, 1x and 1t respectively) which will be used to evaluate modal displacements.

The $\frac{|B_j(\omega)|}{|B_j(\omega_j^*)|}$ function for Mode 1y was evaluated by differencing the acceleration time histories measured by Accelerometers 1 and 3 in Test 144 (one of the s-y tests) and using the FFT of the resulting acceleration record. The value of this function was interpolated in the 1.07 to 1.1 zone as well as the 1.55 to 1.6 zone of the $\frac{\omega}{\omega_1^*}$ domain. Similarly, the normalized function for Mode 1t (j=3) was evaluated by summing the acceleration time histories measured by Accelerometers 1 and 3 in Test 144 and using the FFT of the resulting record. For Mode 2x (j=2) the normalized function was evaluated using the time history of acceleration measured by Accelerometer 2 during Test 148 (one of the s-x tests). As summarized in Table 4.5 the natural frequencies in this case (undamaged structure with maximum deck mass) were: $\omega_1^* = 7.129$ Hz, $\omega_2^* = 7.715$ Hz and $\omega_3^* = 11.23$ Hz (see also Table A.3).

A.1 Evaluation of $d_{kp}\ B_k(\omega_k^*)$

a) Mode 2

For Locations A and C (i.e. p corresponding to locations A and C in Fig. 3.3) the values of $d_{jp}\ B_j(\omega_2^*)$, for j = 1 and 3 (Modes 1y and 1t respectively), need to be subtracted from $A_p(\omega_2^*)$. Since $\frac{\omega_2^*}{\omega_1^*} \approx 1.08$ and $\frac{\omega_2^*}{\omega_3^*} = 0.69$, from Fig. A.1 $\frac{|B_1(\omega_2^*)|}{|B_1(\omega_1^*)|} = 0.088$ and from Fig. A.3 $\frac{|B_3(\omega_2^*)|}{|B_3(\omega_3^*)|} = 0.019$.

From Table A.1, for location A,

$$|d_{1p}\ B_1(\omega_2^*)| \approx A_p(\omega_1^*)\ \frac{|B_1(\omega_2^*)|}{|B_1(\omega_1^*)|} = 26.5\ c\ (0.088)\ \text{volt–sec.}$$

$$= 2.3\ c\ \text{volt–sec.}$$

where c = 0.022 g/volt and its phase angle, i.e., the phase angle for the plateau of the signal

produced by Mode 1 on the $\omega > \omega_1$ side, is estimated from Table A.1 to be at approximately 160° (see phase angle at 7.22 Hz). Similarly,

$$| d_{3p} \; B_3(\omega_2^*) | \approx | A_p(\omega_3^*) | \frac{| B_3(\omega_2^*) |}{| B_3(\omega_3^*) |} = 115.8 \text{ c } (0.019) \text{ volt–sec.}$$

$$= 2.2 \text{ c volt–sec.}$$

and its phase angle is estimated to be 0° (see phase angles in the 9.5 Hz to 10.5 Hz range in Table A.1). Subtracting the preceding two vectors from

$$A_p(\omega_2^*) \approx \sum_{j=1}^{3} d_{jp} \; B_j(\omega_2^*)$$

provides the estimate of $d_{2p} \; B_2(\omega_2^*)$ for Location A. With $| A_p(\omega_2^*) | = 20.9$ c volt-sec. at 154.7°, the magnitude of $d_{2p} \; B_2(\omega_2^*)$ will be 20.6c volt-sec. and its phase angle will be 156°. The preceding have been summarized in Table A.4.

Similarly, for location C (using Table A.3)

$$| d_{1p} \; B_1(\omega_2^*) | \approx | A_p(\omega_1^*) | \frac{| B_1(\omega_2^*) |}{| B_1(\omega_1^*) |} = 29.3 \text{ c } (0.09) \text{ volt–sec.}$$

$$= 2.6 \text{ c volt–sec.}$$

and its phase angle is approximately 340°. Also,

$$| d_{3p} \; B_3(\omega_2^*) | \approx | A_p(\omega_3^*) | \frac{| B_3(\omega_2^*) |}{| B_3(\omega_3^*) |} = 116.4 \text{ c } (0.019) \text{ volt–sec.}$$

$$= 2.2 \text{ c volt–sec.}$$

with a phase angle of about 0°. As summarized in Table A.4 use of these two vectors leads to a magnitude of 25.1 volt-sec. and a phase angle of 336° for $d_{2p} \; B_2(\omega_2^*)$ where p corresponds to Location C.

For Location B (i.e., p corresponding to Location B) the subtraction procedure is not necessary and $d_{2p} \; B_2(\omega_2^*) \approx A_p(\omega_2^*)$.

b) Mode 3

For Locations A and C $d_{3p}\ B_3(\omega_3^*) \approx A_p(\omega_3^*)$ and the subtraction procedure is not necessary. However, for Location B, $d_{2p}\ B_2(\omega_3^*)$ should be sbtracted from $A_p(\omega_3^*)$ in order to evaluate $d_{3p}\ B_3(\omega_3^*)$ with good accuracy.

Using $\frac{\omega_3^*}{\omega_2^*} = 1.45$ in Fig. A.2, $\frac{|B_2(\omega_3^*)|}{|B_2(\omega_2^*)|} = 0.018$, and for Location B (using Table A.2)

$$|d_{2p}\ B_2(\omega_3^*)| \approx |A_p(\omega_2^*)| \frac{|B_2(\omega_3^*)|}{|B_2(\omega_2^*)|} = 171.6 \text{ c } (0.018) \text{ volt–sec.}$$

$$= 3.1 \text{ c volt–sec.}$$

with a phase angle of 250°. The $d_{3p}\ B_3(\omega_3^*)$ vector for Location B can be evaluated as summarized in Table A.5.

A.2 Evaluation of Deck Modal Displacements

As discussed in Chapter 3 the values of $|d_{kp}\ B_k(\omega_k^*)|$ provide the modal displacements. With the deck behaving as a rigid unit during vibrations in Modes 1y, 1x and 1t, the modal displacements of the deck can be evaluated as follows:

a) Mode 2 (1x)

From Table A.4 the modal displacements for the deck (see Fig. 3.3) are:

a) modal y displacement of deck center = (20.6 + 25.1) / 2 = 22.9

b) (modal y displacement at A - modal y displacement at C) / 2 =

$$\frac{(Y_A - Y_C)}{2} = (20.6 - 25.1) / 2 = -2.25$$

c) modal x displacement of deck center =

$$\text{modal x displacement at B} - (6.28"/18.88") \left[\frac{(Y_A - Y_C)}{2} \right]$$

$$= 171.6 - 0.333\ (-2.25) = 172.3$$

Normalizing the above quantities with respect to the modal x displacement of the deck center (i.e., dividing the quantities in (a) (b) and (c) by 172.3) gives the normalized modal displacements of the deck as summarized in Table 4.3 for Test (no.) 147.

b) Mode 3 (1t)

From Table A.5 the modal displacements for the deck for Mode 1t are:

a) modal y displacement of deck center = (115.8 - 116.4) / 2 = -0.3

b) $\frac{(Y_A - Y_C)}{2}$ = (115.8 + 116.4) / 2 = 116.1

c) modal x displacement of deck center = 39.0 - 0.333 (116.1) = 0.3

Dividing these quantities by 116.1 gives the normalized modal displacements of the deck as summarized in Table 4.4 for Test (no.) 147.

TABLE 2.1 Similitude Requirements

Parameter	Required Ratios (Prototype to Model)
Deck mass ratio	$m_r = 50^3$
Mass (volumetric) density ratio for members	$\rho_{sr} = 1$
Length and outer diameter ratios for members	$D_r = \ell_r = 50$
Wall thickness ratios for members	$t_r = 50$
Modulus of elasticity ratio for members	E_r, free to choose (no restriction)

TABLE 2.2 Resulting Ratios (Prototype to Model) of Dependent Quantities used in the Investigation

Parameter	Ratios That Will Hold True (Prototype to Model)
Normalized displacements for the modes of vibration	$\phi_r = 1$
Vibration frequencies of the natural modes	$f_r = \frac{\sqrt{E_r}}{50}$

TABLE 2.3 Member Outer Diameters and Wall Thicknesses in the Prototype and Model

Prototype			1/50th Scale Reduction of Prototype		Selected for Model		Ratios	
Use	Outer Diameter, D (in)	Wall Thickness, t (in)	① D (in)	② t (in)	③ D (in)	④ t (in)	③/①	④/②
Legs	65	0.625	1.30	0.0125	1.25	0.0625	0.96	5
	53	0.625	1.06	0.0125	1.00	0.0625	0.94	5
Diagonal Braces	36	0.625	0.72	0.0125	0.75	0.0625	1.04	5
	36	0.75	0.72	0.015	0.75	0.0625	1.04	4.17
	33	0.625	0.66	0.0125	0.625	0.0625	0.95	5
	30	0.625	0.60	0.0125	0.625	0.0625	1.04	5
Secondary Horizontal Braces	24	0.5	0.48	0.010	0.50	0.0625	1.04	6.25
	20	0.5	0.40	0.010	0.375	0.0625	0.94	6.25
	18	0.5	0.36	0.010	0.375	0.0625	1.04	6.25
	16	0.375	0.36	0.0075	0.375	0.0625	1.04	8.33
	16	0.5	0.32	0.010	0.375	0.0625	1.17	6.25

TABLE 2.4 Model Deck Mass Information (Includes the Mass of Three Accelerometers Used During Tests) and Corresponding Prototype Deck Weight

		Deck Mass Case	
		Maximum	Minimum
Model	Mass (lb-s^2/in)	0.267	0.065
	Center of mass elevation (in)	69.4	67.1
	Weight (lbs)	103.0	25.0
Corresponding Prototype	Weight (K)	12,880.	3,130.

TABLE 2.5 Member Sizes and Moduli

① 1.25" O.D.
$E = 0.35 \times 10^6$ PSI

② 1.00" O.D.
$E = 0.37 \times 10^6$ PSI

③ 0.75" O.D.
$E = 0.35 \times 10^6$ PSI

④ 0.625" O.D.
a. $E = 0.27 \times 10^6$ PSI
b. $E = 0.28 \times 10^6$ PSI

⑤ 0.50" O.D.
a. $E = 0.37 \times 10^6$ PSI
b. $E = 0.35 \times 10^6$ PSI

⑥ 0.375" O.D.
a. $E = 0.36 \times 10^6$ PSI
b. $E = 0.37 \times 10^6$ PSI
c. $E = 0.28 \times 10^6$ PSI

TABLE 4.1 Measured Damping Ratios in Percent of Critical Damping

a) Model in Air

Vibration Mode	Minimum Deck Mass Case	Maximum Deck Mass Case
1Y	0.33	0.28
1X	0.44	0.36
1T	0.35	0.32

b) Model in Water

Vibration Mode	Minimum Deck Mass Case	Maximum Deck Mass Case
1Y	0.58	0.50
1T	0.56	0.49

TABLE 4.2 Measured Normalized Modal Displacements. Mode 1Y, Maximum Deck Mass Case.

Test No.	Shock Direction & Type	Member Damaged	Translations at Deck Center		(Difference in y-transl. at Deck Sides)/2 $\frac{Y_A - Y_C}{2}$	Joint Translations		
						Joint 54		Joint 49
			x-dir.	y-dir.		x-dir.	y-dir.	y-dir.
144	s-y	None	-0.14	1.00	+0.00	-0.05	0.26	0.26
145	s-y	None	-0.14	1.00	+0.00	-0.05	0.26	0.25
146	s-y	None	-0.14	1.00	0.01	-0.04	0.26	0.25
264	s-y	116	-0.28	1.00	0.02	-0.08	0.27	0.25
303	s-y	94	-0.27	1.00	-0.01	-0.10	0.28	0.25
171	s-y	107	-0.19	1.00	0.01	-0.07	0.26	0.25
206	s-y	55	-0.08	1.00	-0.22	-0.05	0.22	0.20

TABLE 4.3 Measured Normalized Modal Displacements. Mode 1X, Maximum Deck Mass Case.

Test No.	Shock Direction & Type	Member Damaged	Translations at Deck Center		(Difference in y-transl. at Deck Sides)/2 $\frac{Y_A - Y_C}{2}$	Joint Translations		
						Joint 54		Joint 49
			x-dir.	y-dir.		x-dir.	y-dir.	y-dir.
147	s-x	None	1.00	0.13	-0.01	0.32	0.02	0.04
148	s-x	None	1.00	0.14	-0.01	0.32	0.02	0.04
259	s-x	116	1.00	0.28	+0.09	0.36	0.04	0.08
307	s-x	94	1.00	0.26	+0.07	0.36	0.01	0.10
179	s-x	107	1.00	0.18	+0.04	0.40	0.01	0.07
203	s-x	55	1.00	0.08	-0.05	0.32	0.01	0.01

TABLE 4.4 Measured Normalized Modal Displacements. Mode 1T, Maximum Deck Mass Case.

Test No.	Shock Direction & Type	Member Damaged	Translations at Deck Center		(Difference in y-transl. at Deck Sides)/2 $\frac{Y_A - Y_C}{2}$	Joint Translations		
						Joint 54		Joint 49
			x-dir.	y-dir.		x-dir.	y-dir.	y-dir.
144	s-y	None	-0.00	-0.01	1.00	0.15	-0.33	0.33
145	s-y	None	-0.00	-0.01	1.00	0.15	-0.33	0.33
146	s-y	None	+0.00	-0.01	1.00	0.15	-0.33	0.33
147	s-x	None	+0.00	-0.00	1.00	0.15	-0.33	0.33
148	s-x	None	-0.00	+0.00	1.00	0.15	-0.33	0.32
264	s-y	116	-0.05	+0.01	1.00	0.12	-0.32	0.30
259	s-x	116	-0.05	+0.01	1.00	0.12	-0.32	0.30
303	s-y	94	-0.05	+0.00	1.00	0.16	-0.35	0.33
307	s-x	94	-0.05	+0.00	1.00	0.16	-0.35	0.33
171	s-y	107	-0.03	+0.00	1.00	0.19	-0.33	0.33
179	s-x	107	-0.03	+0.00	1.00	0.19	-0.33	0.33
206	s-y	55	+0.02	+0.13	1.00	0.14	-0.15	0.33
203	s-x	55	+0.01	+0.13	1.00	0.14	-0.15	0.33

TABLE 4.5 Measured Natural Vibration Frequencies of Model (Hz). Frequency Resolution = 0.098 Hz.

Deck Mass	Member Severed		Mode					
	No.	Row	1y	1x	1t	2y	2x*	2t
Maximum	No Damage		7.13	7.72	11.23	26.8	—	28.5
	107	B	7.13	7.52	11.13	26.7	—	28.4
	94	B	7.13	7.52	11.04	26.8	—	28.4
	116	B	7.13	7.52	10.94	26.8	—	28.4
	55	4	6.74	7.72	10.06	26.8	—	28.2
Minimum	No Damage		13.48	14.35	20.02	28.5	30.6	32.5
	107	B	13.48	14.06	19.73	28.5	30.3	32.3
	94	B	13.38	13.96	19.63	28.5	30.5	32.4
	116	B	13.38	14.06	19.82	28.6	30.4	32.2
	55	4	12.89	14.35	18.55	28.4	30.6	32.1

*Not excited in the maximum deck mass case

TABLE 4.6 Percentage Reductions Greater than 1% in the Frequency Values Measured (Due to Damage)

Deck Mass	Member Severed		Mode					
	No.	Row	1y	1x	1t	2y	2x*	2t
Maximum	107	B	—	2.6	—	—	—	—
	94	B	—	2.6	1.7	—	—	—
	116	B	—	2.6	2.6	—	—	—
	55	4	5.5	—	10.4	—	—	1.1
Minimum	107	B	—	2.0	1.4	—	1.0	—
	94	B	—	2.7	1.9	—	—	—
	116	B	—	2.0	1.0	—	—	1.0
	55	4	4.4	—	7.3	—	—	1.3

*Not excited in the maximum deck mass case

TABLE 4.7 Measured Normalized Modal Displacements. Mode 1Y, Minimum Deck Mass Case.

Test No.	Shock Direction & Type	Member Damaged	Translations at Deck Center		(Difference in y-transl. at Deck Sides)/2 $\frac{Y_A - Y_C}{2}$	Joint Translations		
						Joint 54		Joint 49
			x-dir.	y-dir.		x-dir.	y-dir.	y-dir.
137	s-y	None	-0.30	1.00	-0.01	-0.13	0.33	0.33
139	s-y	None	-0.29	1.00	-0.01	-0.12	0.32	0.33
274	s-y	116	-0.48	1.00	-0.02	-0.18	0.34	0.31
289	s-y	94	-0.75	1.00	-0.06	-0.27	0.38	0.35
188	s-y	107	-0.48	1.00	-0.01	-0.24	0.34	0.29
197	s-y	55	-0.17	1.00	-0.22	-0.10	0.28	0.24

TABLE 4.8 Measured Normalized Modal Displacements. Mode 1X, Minimum Deck Mass Case.

Test No.	Shock Direction & Type	Member Damaged	Translations at Deck Center		(Difference in y-transl. at Deck Sides)/2 $\frac{Y_A - Y_C}{2}$	Joint Translations		
						Joint 54		Joint 49
			x-dir.	y-dir.		x-dir.	y-dir.	y-dir.
143	s-x	None	1.000	0.33	-0.02	0.39	0.09	0.11
142	s-x	None	1.000	0.33	-0.02	0.39	0.09	0.11
278	s-x	116	1.000	0.42	0.09	0.38	0.09	0.16
280	s-x	94	1.000	0.85	0.10	0.45	0.21	0.32
180	s-x	107	1.000	0.60	0.06	0.45	0.12	0.22
198	s-x	55	1.000	0.18	-0.07	0.39	0.03	0.04

TABLE 4.9 Measured Normalized Modal Displacements. Mode 1T, Minimum Deck Mass Case.

Test No.	Shock Direction & Type	Member Damaged	Translations at Deck Center		(Difference in y-transl. at Deck Sides)/2 $\frac{Y_A - Y_C}{2}$	Joint Translations		
						Joint 54		Joint 49
			x-dir.	y-dir.		x-dir.	y-dir.	y-dir.
137	s-y	None	0.01	-0.03	1.00	0.26	-0.55	0.52
139	s-y	None	0.01	-0.01	1.00	0.25	-0.55	0.54
274	s-y	116	-0.02	0.02	1.00	0.20	-0.51	0.47
289	s-y	94	-0.08	0.01	1.00	0.23	-0.55	0.50
188	s-y	107	-0.08	+0.00	1.00	0.30	-0.53	0.51
197	s-y	55	0.01	0.14	1.00	0.18	-0.22	0.48

TABLE 4.10 Measured Vibration Frequencies (Hz) of Local Modes L8/9-1 and L8/9-2

Member Severed	Mode L8/9-1		Mode L8/9-2	
	Minimum Deck Mass Case	Maximum Deck Mass Case	Minimum Deck Mass Case	Maximum Deck Mass Case
No Damage	21.1	20.8	24.4	24.2
116	21.0	20.6	24.8	24.2
94	21.0	20.5	— *	24.3
107	21.1	20.7	24.7	24.5
55	20.7	20.6	24.4	24.3

*Poorly excited (possibly at 24.2 Hz)

TABLE 4.11 Measured Vibration Frequencies (Hz) of Local Modes Consistently Excited in Only One Deck Mass Case

Member Severed	Minimum Deck Mass Case	Maximum Deck Mass Case	
	Mode H5/9	Mode L7-1	Mode L7-2
No Damage	31.6	38.0	38.8
116	31.5	37.7	39.1
94	31.4	38.1*	39.5*
107	31.4	— *	39.2
55	31.2	38.0	39.2

*Significant change in the mode shapes and/or response spectra

TABLE 4.12 Measured Vibration Frequencies (Hz) of Model in Air and in Water with Frequency Resolution = 0.05 Hz

Deck Mass	Vibration Mode	Model in Air	Model in Water
Minimum	1y	14.60	13.50
	1x	15.60	14.40
	1t	23.60	20.00
Maximum	1y	7.20	7.10
	1x	7.85	7.70
	1t	11.50	11.25

TABLE 4.13 Measured Normalized Modal Displacements of Undamaged Model in Air. Minimum Deck Mass Case.

Vibration Mode	Translations at Deck Center		(Difference in y-transl. at Deck Sides)/2 $\frac{Y_A - Y_C}{2}$	Joint Translations		
				Joint 54		Joint 49
	x-dir.	y-dir.		x-dir.	y-dir.	y-dir.
1y	-0.17	1.00	0.01	-0.05	0.32	0.27
1x	1.00	0.17	-0.02	0.29	0.04	0.05
1t	-0.03	0.01	1.00	0.13	-0.38	0.33

TABLE 5.1 Deck Master Node Inertial Properties and Elevation

Deck Mass Case	Mass ($lb\text{-}s^2/in$)	Rotational Inertia ($lb\text{-}s^2\text{-}in$)			Elevation (in)
		M_{rx}	M_{ry}	M_{rz}	
Minimum	0.0648	1.491	9.73	10.76	67.14
Maximum	0.2667	7.094	42.90	48.49	69.42

TABLE 5.2 Measured and Predicted Vibration Frequencies (Hz) of Undamaged Model with Minimum Deck Mass

	Vibration Mode	Model in Air	Model in Water
Predicted (Analytical)	1y	14.20	13.02
	1x	15.25	13.90
	1t	22.51	19.01
Measured	1y	14.60	13.50
	1x	15.60	14.40
	1t	23.60	20.00

TABLE 5.3 Predicted (Analytical) and Measured Normalized Modal Displacements of Undamaged Model with Minimum Deck Mass

		Vibration Mode	Translations at Deck Center		(Difference in y-transl. at Deck Sides)/2 $\frac{Y_A - Y_C}{2}$	Joint Translations		
						Joint 54		Joint 49
			x-dir.	y-dir.		x-dir.	y-dir.	y-dir.
Structure in Air	Analytical	1y	-0.18	1.00	0.00	-0.07	0.29	0.29
		1x	1.00	0.19	0.00	0.35	0.05	0.05
		1t	0.00	0.00	1.00	0.17	-0.37	0.37
	Measured	1y	-0.17	1.00	0.01	-0.05	0.32	0.27
		1x	1.00	0.17	-0.02	0.29	0.04	0.05
		1t	-0.03	0.01	1.00	0.13	-0.38	0.33
Structure in Water	Analytical	1y	-0.30	1.00	0.00	-0.13	0.35	0.35
		1x	1.00	0.34	0.00	0.40	0.11	0.11
		1t	0.00	0.00	1.00	0.23	-0.51	0.51
	Measured	1y	-0.30	1.00	-0.01	-0.12	0.33	0.33
		1x	1.00	0.33	-0.02	0.39	0.09	0.11
		1t	0.01	-0.02	1.00	0.26	-0.55	0.53

TABLE 5.4 Predicted (Analytical) and Measured Vibration Frequencies (Hz) of Model in Water with Minimum Deck Mass

	Member Severed		Mode					
	No.	Row	1y	1x	1t	2y	2x	2t
Predicted (Analytical)	No Damage		13.02	13.90	19.01	32.4	38.4	40.2
	116	B	12.99	13.62	18.80	32.4	36.4	39.6
	94	B	12.89	13.39	18.59	32.6	37.4	40.2
	107	B	12.98	13.56	18.79	32.4	36.8	40.1
	55	4	12.41	13.87	17.63	31.5	36.0	38.5
	62	4	11.94	13.82	16.01	25.9	38.5	36.9
Measured	No Damage		13.48	14.35	20.02	28.5	30.6	32.5
	116	B	13.38	14.06	19.82	28.6	30.4	32.2
	94	B	13.38	13.96	19.63	28.5	30.5	32.4
	107	B	13.48	14.06	19.73	28.5	30.3	32.3
	55	4	12.89	14.35	18.55	28.4	30.6	32.1

TABLE 5.5 Predicted and Measured Percentage Reductions Greater than 1%, in the Values of Vibration Frequencies

	Member Severed		Mode		
	No.	Row	1y	1x	1t
Predicted (Analytical)	116	B	—	2.0	1.1
	94	B	—	3.7	2.2
	107	B	—	2.4	1.2
	55	4	4.7	—	7.3
	62	4	8.3	—	15.8
Measured	116	B	—	2.0	1.0
	94	B	—	2.7	1.9
	107	B	—	2.0	1.4
	55	4	4.4	—	7.3

TABLE 5.6 Predicted (Analytical) and Measured Vibration Frequencies (Hz) of Model in Water with Maximum Deck Mass

	Member Severed		Mode					
	No.	Row	1y	1x	1t	2y	2x*	2t
Predicted (Analytical)	No Damage		6.92	7.49	10.80	29.0	32.8	35.7
	116	B	6.91	7.28	10.59	29.0	32.7	35.0
	94	B	6.91	7.25	10.60	29.1	31.5	35.5
	107	B	6.92	7.35	10.71	29.0	31.4	35.5
	55	4	6.61	7.49	9.70	29.0	32.8	32.9
	62	4	6.73	7.49	9.85	20.8	33.0	32.3
Measured	No Damage		7.13	7.72	11.23	26.8	—	28.5
	116	B	7.13	7.52	10.94	26.8	—	28.4
	94	B	7.13	7.52	11.04	26.8	—	28.4
	107	B	7.13	7.52	11.13	26.7	—	28.4
	55	4	6.74	7.72	10.06	26.8	—	28.2

*Not excited during tests (maximum deck mass case).

TABLE 5.7 Predicted and Measured Percentage Reductions Greater Than 1%, in the Values of Vibration Frequencies

	Member Severed		Mode		
	No.	Row	1y	1x	1t
Predicted (Analytical)	116	B	–	2.8	1.9
	94	B	–	3.2	1.9
	107	B	–	1.9	–
	55	4	4.3	–	10.2
	62	4	2.7	–	8.8
Measured	116	B	–	2.6	2.6
	94	B	–	2.6	1.7
	107	B	–	2.6	–
	55	4	5.5	–	10.4

TABLE 5.8 Measured (Experimental) and Predicted (Analytical) Normalized Modal Displacements. Mode 1Y, Maximum Deck Mass Case

	Member Damaged	Translations at Deck Center		(Difference in y-transl. at Deck Sides)/2 $\frac{Y_A - Y_C}{2}$	Joint Translations		
					Joint 54		Joint 49
		x-dir.	y-dir.		x-dir.	y-dir.	y-dir.
Predicted (Analytical)	None	-0.14	1.00	0.00	-0.06	0.27	0.27
	116	-0.25	1.00	-0.02	-0.09	0.28	0.27
	94	-0.26	1.00	-0.02	-0.11	0.29	0.26
	107	-0.18	1.00	-0.01	-0.08	0.28	0.27
	55	-0.08	1.00	-0.24	-0.06	0.24	0.21
	62	-0.09	1.00	-0.14	-0.09	0.57	0.24
Measured	None	-0.14	1.00	+0.00	-0.05	0.26	0.25
	116	-0.28	1.00	0.02	-0.08	0.27	0.25
	94	-0.27	1.00	-0.01	-0.10	0.28	0.25
	107	-0.19	1.00	0.01	-0.07	0.26	0.25
	55	-0.08	1.00	-0.22	-0.05	0.22	0.20

TABLE 5.9 Measured (Experimental) and Predicted (Analytical) Normalized Modal Displacements. Mode 1x, Maximum Deck Mass Case.

	Member Damaged	Translations at Deck Center		(Difference in y-transl. at Deck Sides)/2 $\frac{Y_A - Y_C}{2}$	Joint Translations		
					Joint 54		Joint 49
		x-dir.	y-dir.		x-dir.	y-dir.	y-dir.
Predicted (Analytical)	None	1.00	0.15	0.00	0.34	0.04	0.04
	116	1.00	0.26	0.09	0.34	0.04	0.08
	94	1.00	0.27	0.09	0.41	0.01	0.12
	107	1.00	0.19	0.04	0.40	0.02	0.07
	55	1.oO	0.08	-0.04	0.34	0.01	0.01
	62	1.00	0.10	-0.03	0.33	0.07	1.38
Measured	None	1.00	0.14	-0.01	0.32	0.02	0.04
	116	1.00	0.28	0.09	0.32	0.04	0.08
	94	1.00	0.26	0.07	0.36	0.01	0.10
	107	1.00	0.18	0.04	0.40	0.01	0.07
	55	1.00	0.08	-0.05	0.32	0.01	0.01

TABLE 5.10 Measured (Experimental) and Predicted (Analytical) Normalized Modal Displacements. Mode 1T, Maximum Deck Mass Case.

	Member Damaged	Translations at Deck Center		(Difference in y-transl. at Deck Sides)/2 $\frac{Y_A - Y_C}{2}$	Joint Translations		
					Joint 54		Joint 49
		x-dir.	y-dir.		x-dir.	y-dir.	y-dir.
Predicted (Analytical)	None	0.00	0.00	1.00	0.18	-0.37	0.37
	116	-0.05	+0.00	1.00	0.14	-0.36	0.36
	94	-0.05	-0.00	1.00	0.19	-0.39	0.38
	107	-0.03	-0.00	1.00	0.20	-0.38	0.38
	55	0.01	0.12	1.00	0.16	-0.17	0.37
	62	0.01	0.11	1.00	0.23	-0.82	0.37
Measured	None	-0.00	-0.01	1.00	0.15	-0.33	0.33
	116	-0.05	0.01	1.00	0.12	-0.32	0.30
	94	-0.05	+0.00	1.00	0.16	-0.35	0.33
	107	-0.03	+0.00	1.00	0.19	-0.33	0.33
	55	0.01	0.13	1.00	0.14	-0.15	0.33

TABLE 5.11 Measured (Experimental) and Predicted (Analytical) Normalized Modal Displacements. Mode 1Y, Minimum Deck Mass Case.

	Member Damaged	Translations at Deck Center		(Difference in y-transl. at Deck Sides)/2 $\frac{Y_A - Y_C}{2}$	Joint Translations		
					Joint 54		Joint 49
		x-dir.	y-dir.		x-dir.	y-dir.	y-dir.
Predicted (Analytical)	None	-0.30	1.00	0.00	-0.13	0.35	0.35
	116	-0.50	1.00	-0.04	-0.21	0.36	0.34
	94	-0.84	1.00	-0.09	-0.41	0.41	0.30
	107	-0.50	1.00	-0.03	-0.25	0.36	0.33
	55	-0.14	1.00	-0.25	-0.10	0.30	0.26
	62	-0.10	1.00	-0.35	-0.19	1.08	0.23
Measured	None	-0.30	1.00	-0.01	-0.12	0.33	0.33
	116	-0.48	1.00	-0.02	-0.18	0.34	0.31
	94	-0.75	1.00	-0.06	-0.27	0.38	0.35
	107	-0.48	1.00	-0.01	-0.24	0.34	0.29
	55	-0.17	1.00	-0.22	-0.10	0.28	0.24

TABLE 5.12 Measured (Experimental) and Predicted (Analytical) Normalized Modal Displacements. Mode 1x, Minimum Deck Mass Case.

	Member Damaged	Translations at Deck Center		(Difference in y-transl. at Deck Sides)/2 $\frac{Y_A - Y_C}{2}$	Joint Translations		
					Joint 54		Joint 49
		x-dir.	y-dir.		x-dir.	y-dir.	y-dir.
Predicted (Analytical)	None	1.00	0.34	0.00	0.40	0.11	0.11
	116	1.00	0.53	0.08	0.39	0.16	0.19
	94	1.00	0.94	0.12	0.48	0.24	0.39
	107	1.00	0.56	0.06	0.48	0.15	0.23
	55	1.00	0.16	-0.07	0.39	0.04	0.03
	62	1.00	0.06	-0.09	0.37	0.17	0.02
Measured	None	1.00	0.33	-0.02	0.39	0.09	0.11
	116	1.00	0.42	0.09	0.38	0.09	0.16
	94	1.00	0.85	0.10	0.45	0.21	0.32
	107	1.00	0.60	0.06	0.45	0.12	0.22
	55	1.00	0.18	-0.07	0.39	0.03	0.04

TABLE 5.13 Measured (Experimental) and Predicted (Analytical) Normalized Modal Displacements. Mode 1T, Minimum Deck Mass Case.

	Member Damaged	Translations at Deck Center		(Difference in y-transl. at Deck Sides)/2 $\frac{Y_A - Y_C}{2}$	Joint Translations		
					Joint 54		Joint 49
		x-dir.	y-dir.		x-dir.	y-dir.	y-dir.
Predicted (Analytical)	None	0.00	0.00	1.00	0.23	-0.51	0.51
	116	-0.03	+0.00	1.00	0.19	-0.49	0.48
	94	-0.09	-0.01	1.00	0.24	-0.53	0.52
	107	-0.06	-0.00	1.00	0.26	-0.52	0.51
	55	0.02	0.13	1.00	0.20	-0.23	0.50
	62	0.08	0.57	1.00	0.33	-1.05	0.60
Measured	None	0.01	-0.02	1.00	0.26	-0.55	0.53
	116	-0.02	0.02	1.00	0.20	-0.51	0.47
	94	-0.08	0.01	1.00	0.23	-0.55	0.50
	107	-0.08	+0.00	1.00	0.30	-0.53	0.51
	55	0.01	0.14	1.00	0.18	-0.22	0.48

TABLE 5.14 Analytical Vibration Frequencies (Hz) of Model in Water with Deck Center of Mass Shifted 3.6" in +x Direction

Deck Mass	Member Severed		Mode		
	No.	Row	1y	1x	1t
Maximum	No Damage		6.78	7.49	10.99
	107	B	6.77	7.35	10.91
	55	4	6.23	7.48	10.26
Minimum	No Damage		12.84	13.87	19.15
	107	B	12.78	13.55	18.92
	94	B	12.67	13.41	18.73
	116	B	12.76	13.63	18.97
	55	4	11.81	13.85	18.27
	62	4	11.44	13.81	17.09

TABLE 5.15 Percentage Reductions Greater than 1% in the Vibration Frequencies due to Damage Deck Center of Mass Shifted 3.6" in +x Direction

Deck Mass	Member Severed		Mode		
	No.	Row	1y	1x	1t
Maximum	107	B	—	1.9	—
	55	4	8.2	—	6.6
Minimum	107	B	—	2.3	1.2
	94	B	1.3	3.3	2.2
	116	B	—	1.7	—
	55	4	8.0	—	4.6
	62	4	10.9	—	10.8

TABLE 5.16 Normalized Modal Displacements Predicted for Mode 1Y with Deck Center of Mass (Master Node) Shifted 3.60" in +x Direction

Deck Mass	Member Damaged	Translations at Deck Center		(Difference in y-transl. at Deck Sides)/2 $\frac{Y_A - Y_C}{2}$	Joint Translations		
					Joint 54		Joint 49
		x-dir.	y-dir.		x-dir.	y-dir.	y-dir.
Minimum	None	-0.24	1.00	-0.21	-0.15	0.43	0.26
	116	-0.44	1.00	-0.26	-0.22	0.44	0.25
	94	-0.66	1.00	-0.29	-0.37	0.48	0.22
	107	-0.42	1.00	-0.24	-0.25	0.44	0.25
	55	-0.09	1.00	-0.48	-0.11	0.33	0.18
	62	-0.08	1.00	-0.51	-0.21	1.19	0.17
Maximum	None	-0.12	1.00	-0.23	-0.08	0.35	0.19
	107	-0.18	1.00	-0.24	-0.12	0.36	0.19
	55	-0.05	1.00	-0.48	-0.08	0.28	0.14

TABLE 5.17 Normalized Modal Displacements Predicted for Mode 1x with Deck Center of Mass (Master Node) Shifted 3.60" in the +x Direction

Deck Mass	Member Damaged	Translations at Deck Center		(Difference in y-transl. at Deck Sides)/2 $\frac{Y_A - Y_C}{2}$	Joint Translations		
					Joint 54		Joint 49
		x-dir.	y-dir.		x-dir.	y-dir.	y-dir.
Minimum	None	1.00	0.25	-0.07	0.39	0.11	0.05
	116	1.00	0.44	-0.04	0.37	0.17	0.11
	94	1.00	0.69	-0.06	0.44	0.23	0.23
	107	1.00	0.44	-0.05	0.45	0.16	0.14
	55	1.00	0.08	-0.09	0.40	0.03	-0.01
	62	1.00	0.02	-0.08	0.38	0.12	-0.03
Maximum	None	1.00	0.11	-0.04	0.34	0.04	0.01
	107	1.00	0.17	-0.01	0.39	0.04	0.05
	55	1.00	0.03	-0.05	0.34	0.01	-0.01

TABLE 5.18 Normalized Modal Displacements Predicted for Mode 1T with Deck Center of Mass (Master Node) Shifted 3.60" in the +x Direction

Deck Mass	Member Damaged	Translations at Deck Center		(Difference in y-transl. at Deck Sides)/2 $\frac{Y_A - Y_C}{2}$	Joint Translations		
					Joint 54		Joint 49
		x-dir.	y-dir.		x-dir.	y-dir.	y-dir.
Minimum	None	-0.02	0.26	1.00	0.24	-0.38	0.64
	116	-0.01	0.27	1.00	0.20	-0.36	0.62
	94	-0.07	0.27	1.00	0.24	-0.40	0.65
	107	-0.04	0.27	1.00	0.27	-0.39	0.50
	55	0.03	0.39	1.00	0.21	-0.15	0.64
	62	0.07	0.78	1.00	0.34	-0.98	0.72
Maximum	None	0.01	0.30	1.00	0.18	-0.28	0.47
	107	-0.02	0.30	1.00	0.20	-0.29	0.47
	55	0.02	0.42	1.00	0.16	-0.11	0.47

TABLE A.1 FFT OF THE ANALOG ACCELERATION SIGNALS FOR ACCELEROMETER NO. 1

FREQUENCY (HZ.)	SPECTRAL AMPLITUDE (VOLT-SEC.)	PHASE ANGLE (DEG.)
5.957	.2863E+01	11.909
6.055	.3618E+01	13.151
6.152	.3660E+01	8.995
6.250	.3520E+01	8.787
6.348	.3747E+01	16.938
6.445	.4446E+01	11.059
6.543	.5101E+01	12.845
6.641	.5341E+01	16.004
6.738	.6809E+01	14.692
6.836	.8370E+01	16.652
6.934	.1331E+02	21.330
7.031	.2877E+02	43.914
7.129	.2648E+02	136.235
7.227	.9867E+01	157.608
7.324	.5126E+01	153.804
7.422	.3777E+01	135.148
7.520	.4749E+01	117.789
7.617	.8151E+01	105.025
7.715	.2090E+02	154.735
7.812	.9775E+01	225.077
7.910	.5002E+01	242.070
8.008	.3554E+01	257.179
8.105	.2607E+01	258.909
8.203	.1758E+01	262.621
8.301	.1856E+01	281.954
8.398	.1855E+01	292.105
8.496	.1704E+01	303.734
8.594	.1583E+01	309.380
8.691	.1599E+01	315.786
8.789	.1629E+01	324.608
8.887	.1619E+01	321.987
8.984	.2102E+01	332.572
9.082	.1878E+01	318.667
9.180	.2339E+01	334.011
9.277	.2535E+01	334.560
9.375	.2536E+01	335.757
9.473	.2400E+01	353.338
9.570	.2819E+01	345.186
9.668	.2900E+01	343.895
9.766	.3216E+01	345.195
9.863	.3703E+01	347.506
9.961	.3931E+01	350.119
10.059	.4351E+01	351.852
10.156	.4574E+01	353.952
10.254	.4673E+01	352.013
10.352	.5694E+01	353.038
10.449	.6888E+01	352.250
10.547	.7638E+01	355.447
10.645	.8712E+01	356.784
10.742	.1054E+02	359.018
10.840	.1349E+02	.413
10.937	.1800E+02	2.229
11.035	.2602E+02	7.008
11.133	.4840E+02	19.635
11.230	.1158E+03	81.185
11.328	.5148E+02	149.667
11.426	.2716E+02	162.779
11.523	.1844E+02	167.042
11.621	.1393E+02	169.108
11.719	.1104E+02	170.749
11.816	.9426E+01	172.858
11.914	.8102E+01	172.454
12.012	.6683E+01	173.788

TABLE A.2 FFT OF THE ANALOG ACCELERATION SIGNALS FOR ACCELEROMETER NO. 2

FREQUENCY (HZ.)	SPECTRAL AMPLITUDE (VOLT-SEC.)	PHASE ANGLE (DEG.)
5.957	.3815E+01	70.802
6.055	.4369E+01	74.221
6.152	.4413E+01	71.099
6.250	.4762E+01	76.659
6.348	.5128E+01	81.286
6.445	.5986E+01	79.032
6.543	.6129E+01	77.491
6.641	.6504E+01	78.550
6.738	.7103E+01	78.041
6.836	.7536E+01	82.934
6.934	.8694E+01	84.840
7.031	.8145E+01	90.205
7.129	.1168E+02	80.769
7.227	.1567E+02	74.497
7.324	.1847E+02	76.020
7.422	.2450E+02	77.903
7.520	.3649E+02	84.428
7.617	.6896E+02	94.132
7.715	.1716E+03	193.856
7.812	.7776E+02	228.419
7.910	.4053E+02	240.894
8.008	.2761E+02	247.215
8.105	.2067E+02	248.652
8.203	.1689E+02	251.711
8.301	.1410E+02	255.120
8.398	.1168E+02	256.703
8.496	.1075E+02	256.758
8.594	.9459E+01	257.690
8.691	.8408E+01	257.293
8.789	.7700E+01	259.076
8.887	.7092E+01	259.244
8.984	.6575E+01	262.820
9.082	.6662E+01	267.212
9.180	.5573E+01	260.532
9.277	.5237E+01	266.528
9.375	.5317E+01	268.256
9.473	.5170E+01	268.231
9.570	.4554E+01	268.388
9.668	.4380E+01	269.325
9.766	.4011E+01	274.911
9.863	.4100E+01	275.101
9.961	.4373E+01	271.727
10.059	.3941E+01	280.031
10.156	.3825E+01	286.120
10.254	.4187E+01	280.173
10.352	.3728E+01	291.068
10.449	.3539E+01	289.309
10.547	.3189E+01	296.326
10.645	.3670E+01	305.381
10.742	.4293E+01	317.363
10.840	.4586E+01	327.924
10.937	.5257E+01	337.143
11.035	.8219E+01	353.727
11.133	.1467E+02	11.667
11.230	.3596E+02	81.221
11.328	.1616E+02	157.132
11.426	.9496E+01	175.737
11.523	.6371E+01	189.247
11.621	.5855E+01	194.224
11.719	.4565E+01	202.657
11.816	.3811E+01	201.257
11.914	.3700E+01	211.021
12.012	.3605E+01	210.184

TABLE A.3 FFT OF THE ANALOG ACCELERATION SIGNALS FOR ACCELEROMETER NO. 3

FREQUENCY (HZ.)	SPECTRAL AMPLITUDE (VOLT-SEC.)	PHASE ANGLE (DEG.)
5.957	.8035E+00	245.977
6.055	.9573E+00	238.894
6.152	.1180E+01	230.844
6.250	.1319E+01	233.081
6.348	.1559E+01	229.142
6.445	.2022E+01	228.651
6.543	.2236E+01	223.488
6.641	.2947E+01	213.152
6.738	.4272E+01	209.347
6.836	.6120E+01	208.574
6.934	.1063E+02	209.610
7.031	.2676E+02	229.430
7.129	.2933E+02	319.768
7.227	.1295E+02	342.652
7.324	.8251E+01	338.947
7.422	.6738E+01	329.647
7.520	.7362E+01	315.476
7.617	.1135E+02	298.529
7.715	.2971E+02	337.776
7.812	.1489E+02	36.505
7.910	.8652E+01	37.801
8.008	.6604E+01	34.332
8.105	.5370E+01	33.247
8.203	.5072E+01	29.750
8.301	.4516E+01	27.261
8.398	.4120E+01	22.652
8.496	.4025E+01	22.805
8.594	.3991E+01	19.060
8.691	.3964E+01	16.801
8.789	.3875E+01	18.681
8.887	.3807E+01	15.106
8.984	.3977E+01	16.107
9.082	.3782E+01	12.653
9.180	.3689E+01	12.064
9.277	.3847E+01	9.445
9.375	.3980E+01	10.231
9.473	.4021E+01	7.030
9.570	.4297E+01	9.232
9.668	.4446E+01	7.934
9.766	.4722E+01	5.171
9.863	.4928E+01	3.080
9.961	.4944E+01	5.429
10.059	.5378E+01	4.194
10.156	.5959E+01	4.822
10.254	.6286E+01	2.046
10.352	.6822E+01	3.262
10.449	.7562E+01	2.103
10.547	.8588E+01	1.761
10.645	.9776E+01	2.361
10.742	.1153E+02	3.018
10.840	.1408E+02	3.374
10.937	.1864E+02	5.022
11.035	.2701E+02	8.432
11.133	.4897E+02	19.758
11.230	.1164E+03	80.619
11.328	.5040E+02	148.614
11.426	.2643E+02	160.432
11.523	.1765E+02	164.607
11.621	.1308E+02	165.792
11.719	.1035E+02	166.886
11.816	.8594E+01	166.669
11.914	.7418E+01	166.712
12.012	.6282E+01	167.771

TABLE A.4 Evaluation of $d_{2p}B_2(\omega_2^*)$ for Mode 2 (Mode 1x), c = 0.022 g/volt

P Accelerometer Location	① $A_p(\omega_2^*)/c$		② $d_{1p}B_1(\omega_2^*)/c)$		③ $d_{3p}B_3(\omega_2^*)/c$		④ = ① - ② - ③ $d_{2p}B_2(\omega_2^*)/c$	
	Magnitude (volt-sec)	Phase Angle (deg)	Magnitude (volt-sec)	Phase Angle (deg)	Magnitude (volt-sec)	Phase Angle (deg)	Magnitude (volt-sec)	Phase Angle (deg)
A	20.9	154.7	2.3	160	2.2	0°	20.6	156
B	171.6	153.8	– †		– †		171.6	154
C	29.7	337.8	2.6	340	2.2	0°	25.1	336

†Magnitude is less than 1% of $|A_p(\omega_2^*)/c|$. Subtraction procedure is not necessary.

TABLE A.5 Evaluation of $d_{3p}B_3(\omega_3^*)$ for Mode 3 (Mode 1t), c = 0.022 g/volt

P Accelerometer Location	① $A_p(\omega_3^*)/c$		② $d_{1p}B_1(\omega_3^*)/c$		③ $d_{2p}B_2(\omega_3^*)/c$		④ = ① - ② - ③ $d_{3p}B_3(\omega_3^*)/c$	
	Magnitude (volt-sec)	Phase Angle (deg)	Magnitude (volt-sec)	Phase Angle (deg)	Magnitude (volt-sec)	Phase Angle (deg)	Magnitude (volt-sec)	Phase Angle (deg)
A	115.8	81.2	–†	–	–†	–	115.8	81.2
B	36.0	81.2	–†	–	3.1	250	39.0	80.3
C	116.4	80.6	–†	–	–†	–	116.4	80.6

†Magnitude is less than 1% of $|A_p(\omega_3^*)/c|$. Subtraction procedure is not necessary.

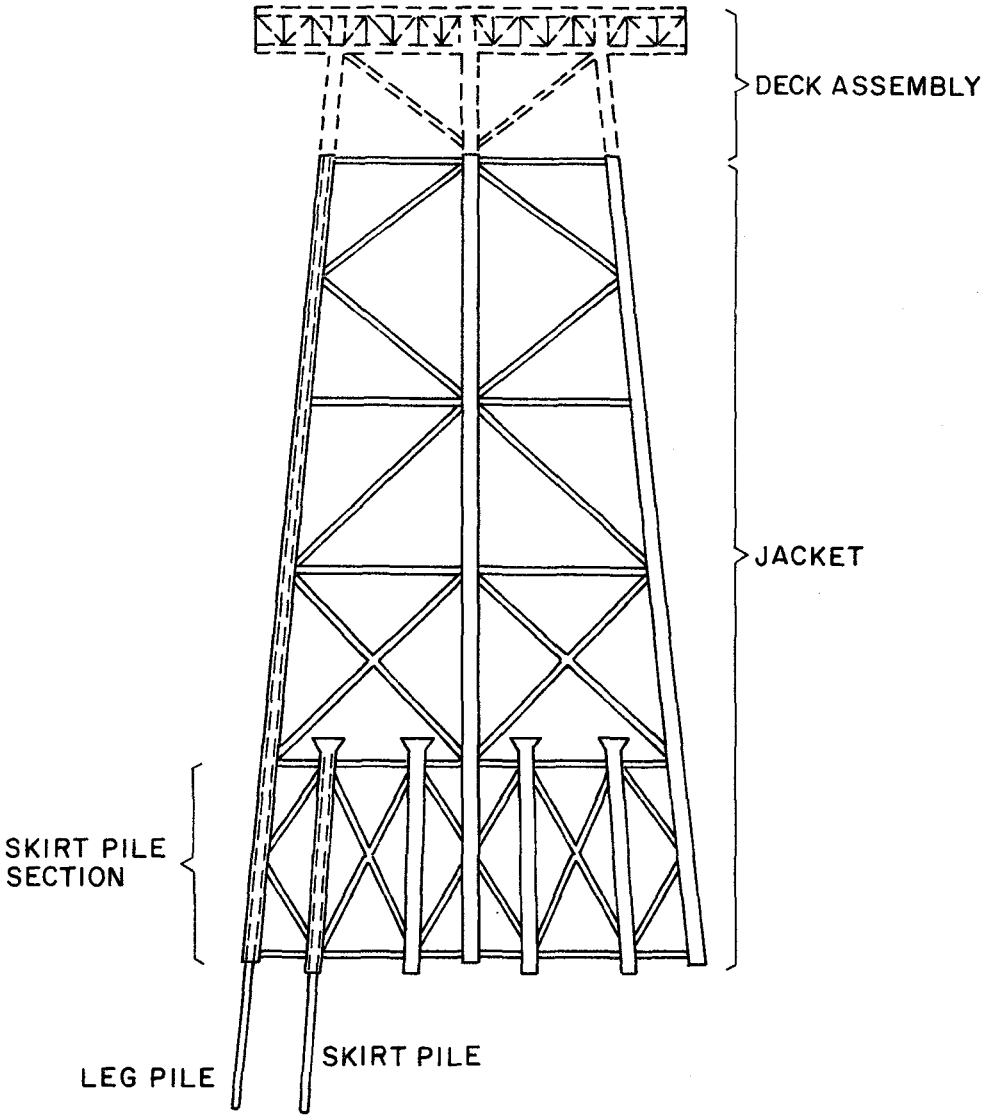

Fig. 1.1 Skirt pile section, jacket and deck assembly in a steel offshore platform

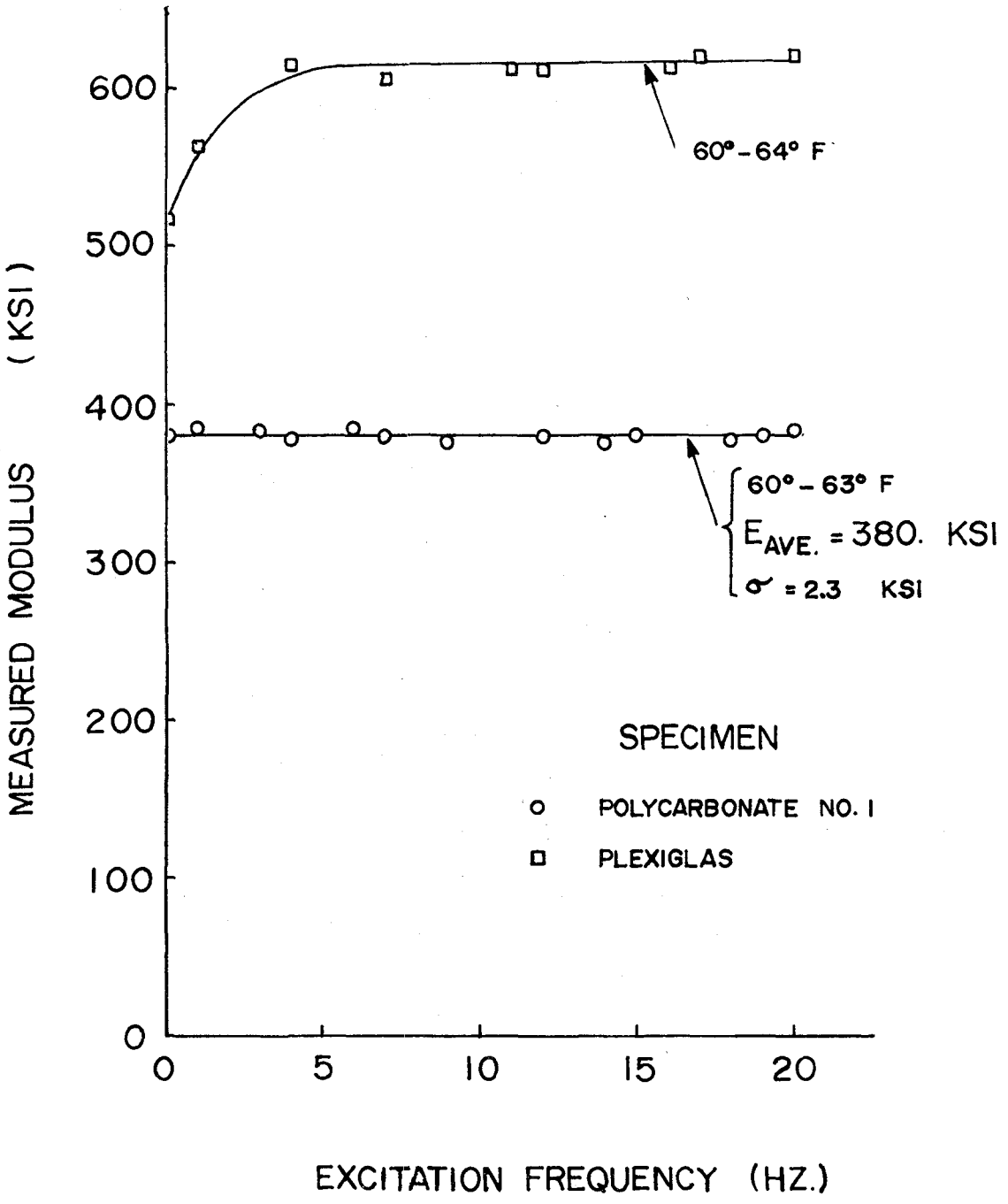

Fig. 2.1 Measured modulus of elasticity vs. excitation frequency for a Plexiglas and a polycarbonate specimen

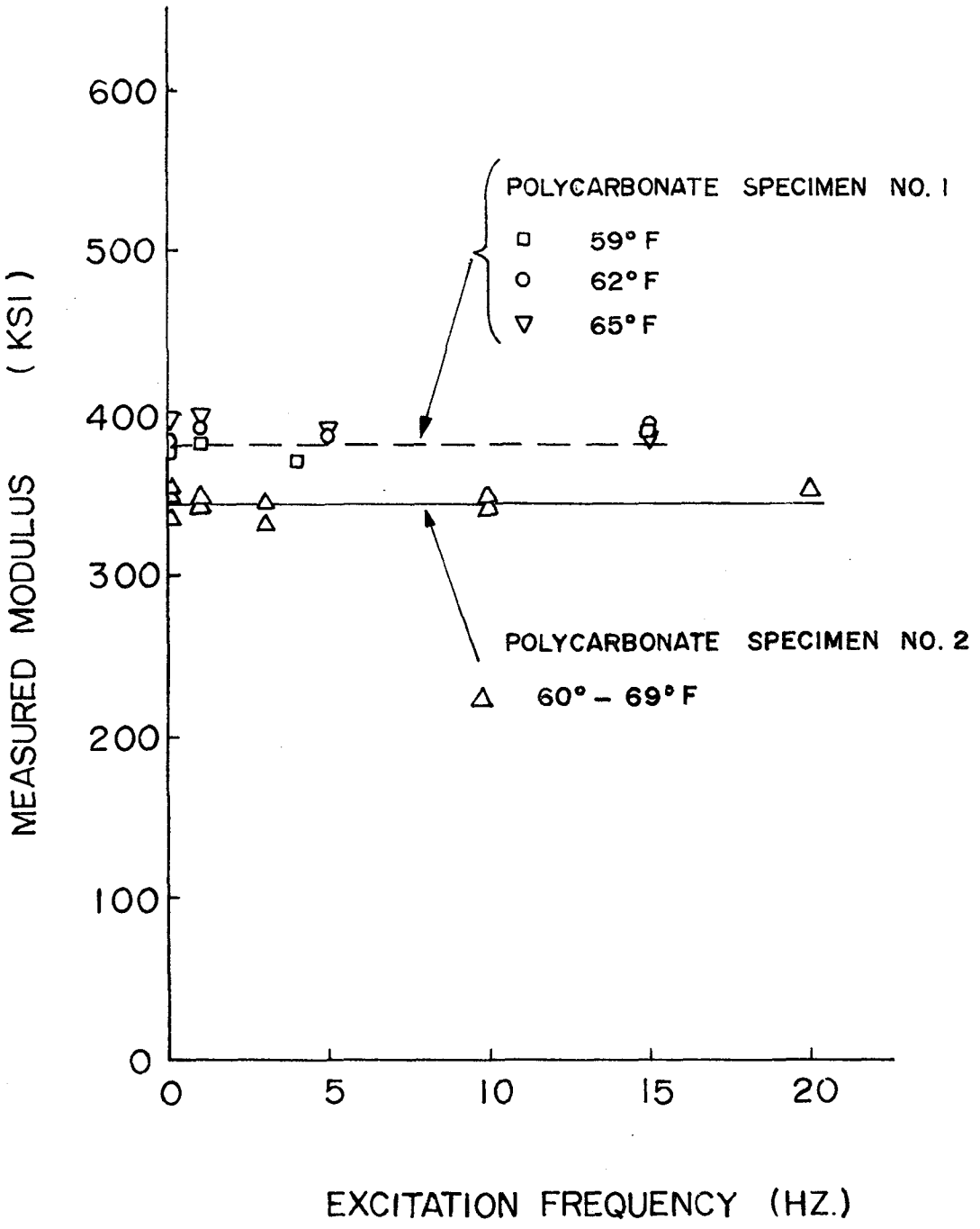

Fig. 2.2 Measured modulus of elasticity for the polycarbonate specimens

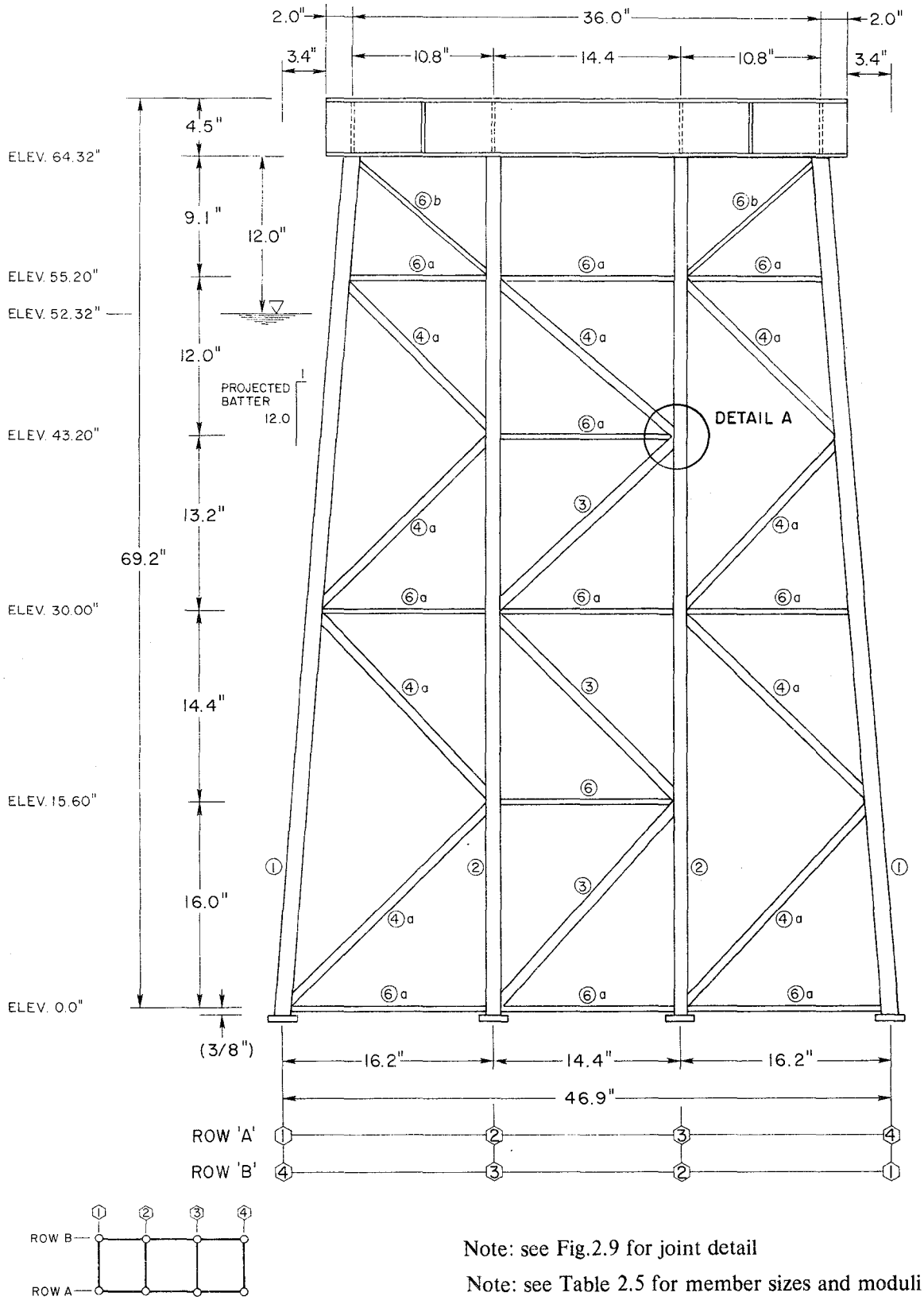

Note: see Fig.2.9 for joint detail

Note: see Table 2.5 for member sizes and moduli

Fig. 2.3 Configuration, member sizes and moduli of elasticity for Frames A and B of model platform

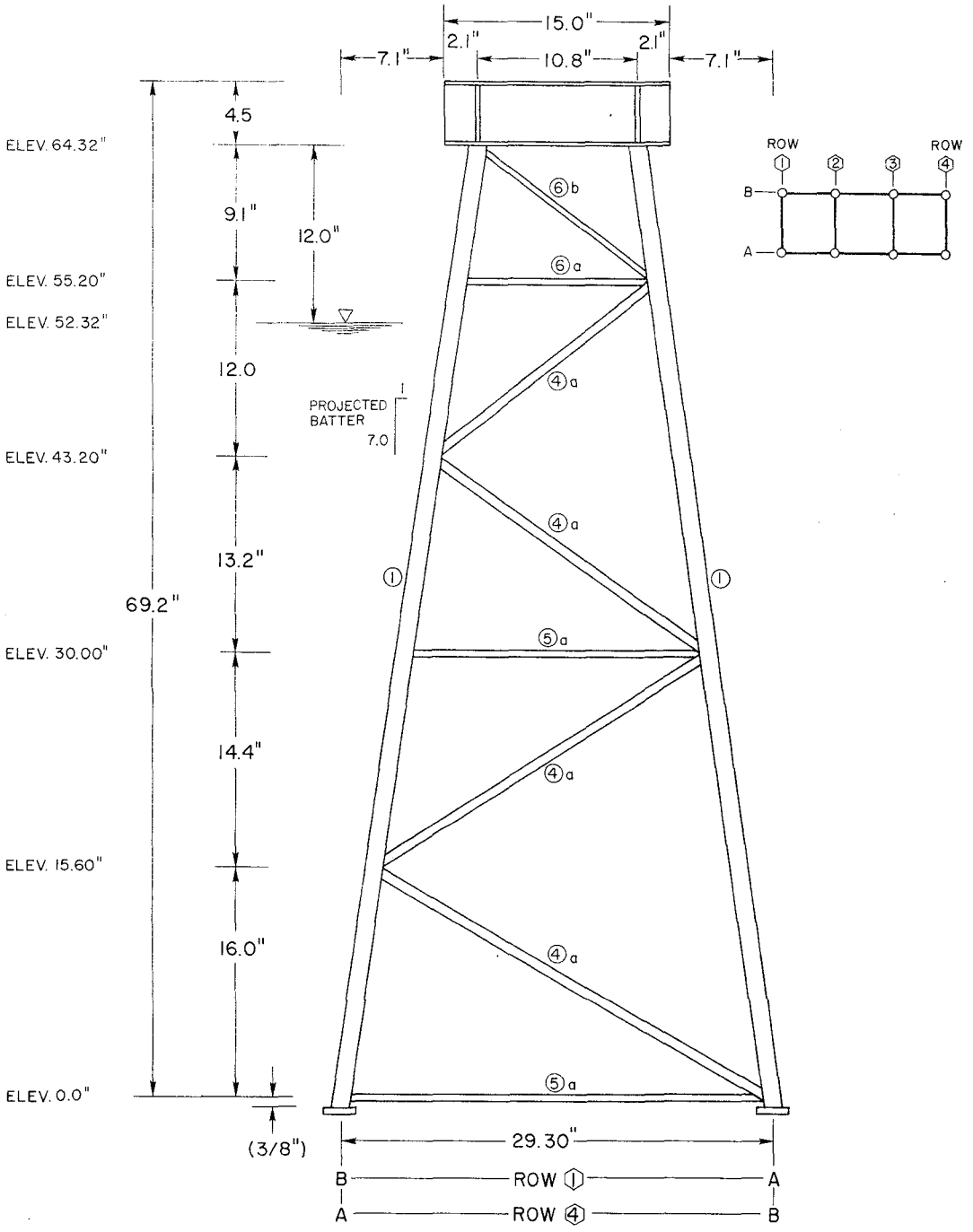

Note: see Table 2.5 for member sizes and moduli

Fig. 2.4 Configuration, member sizes and moduli of elasticity for Frames 1 and 4 of the model platform

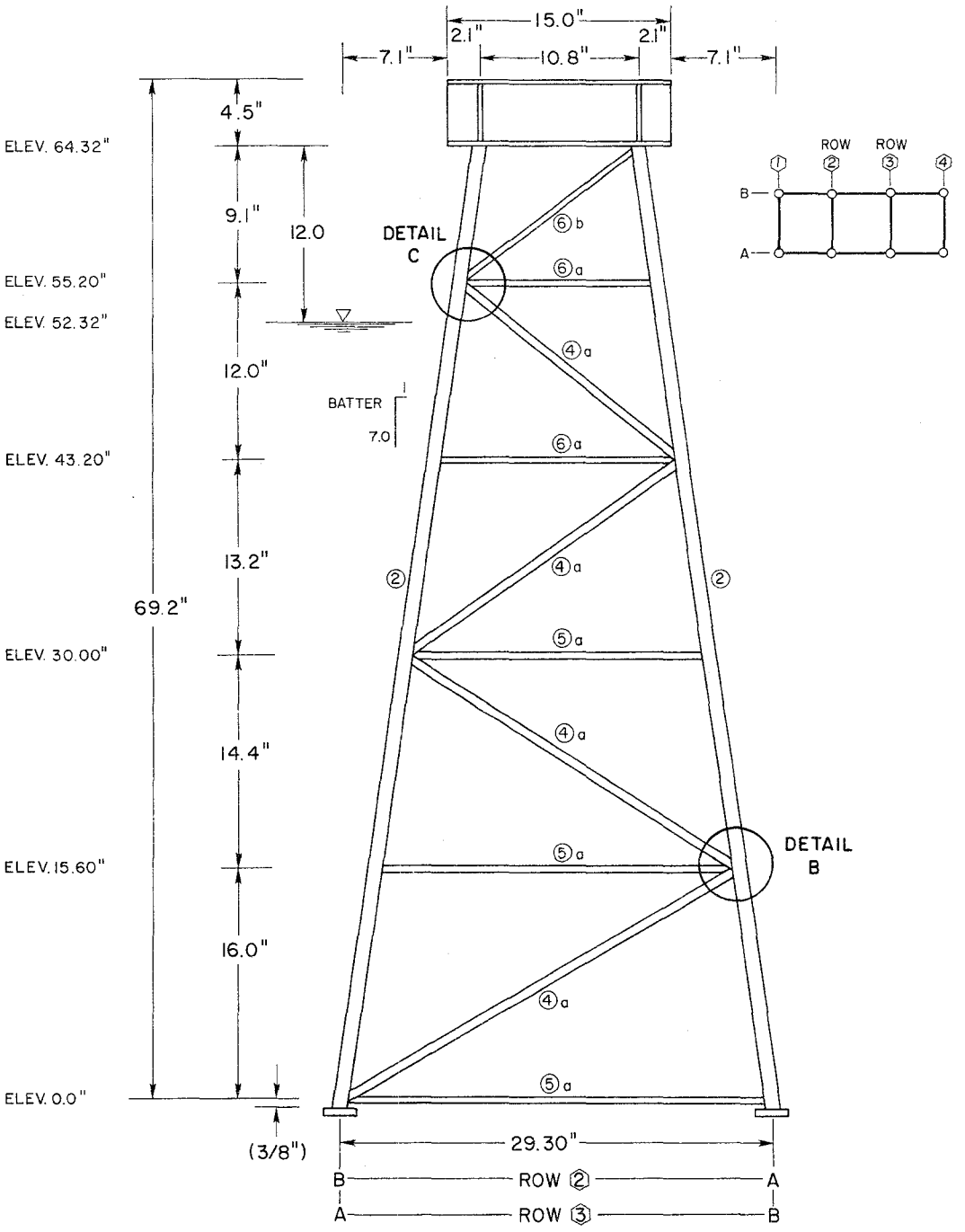

Note: see Fig.2.9 for joint details

Note: see Table 2.5 for member sizes and moduli

Fig. 2.5 Configuration, member sizes and moduli of elasticity for Frames 2 and 3 of the model platform

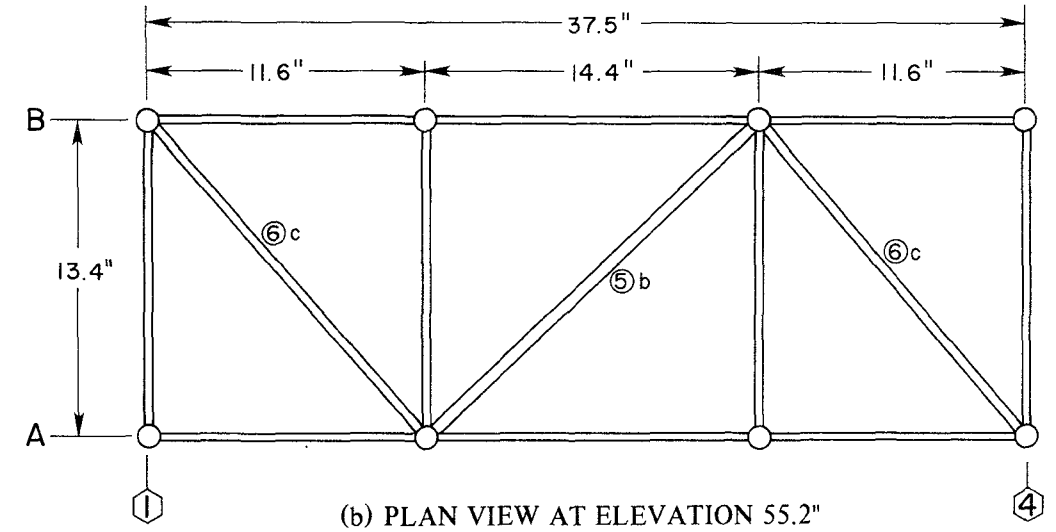

(b) PLAN VIEW AT ELEVATION 55.2"

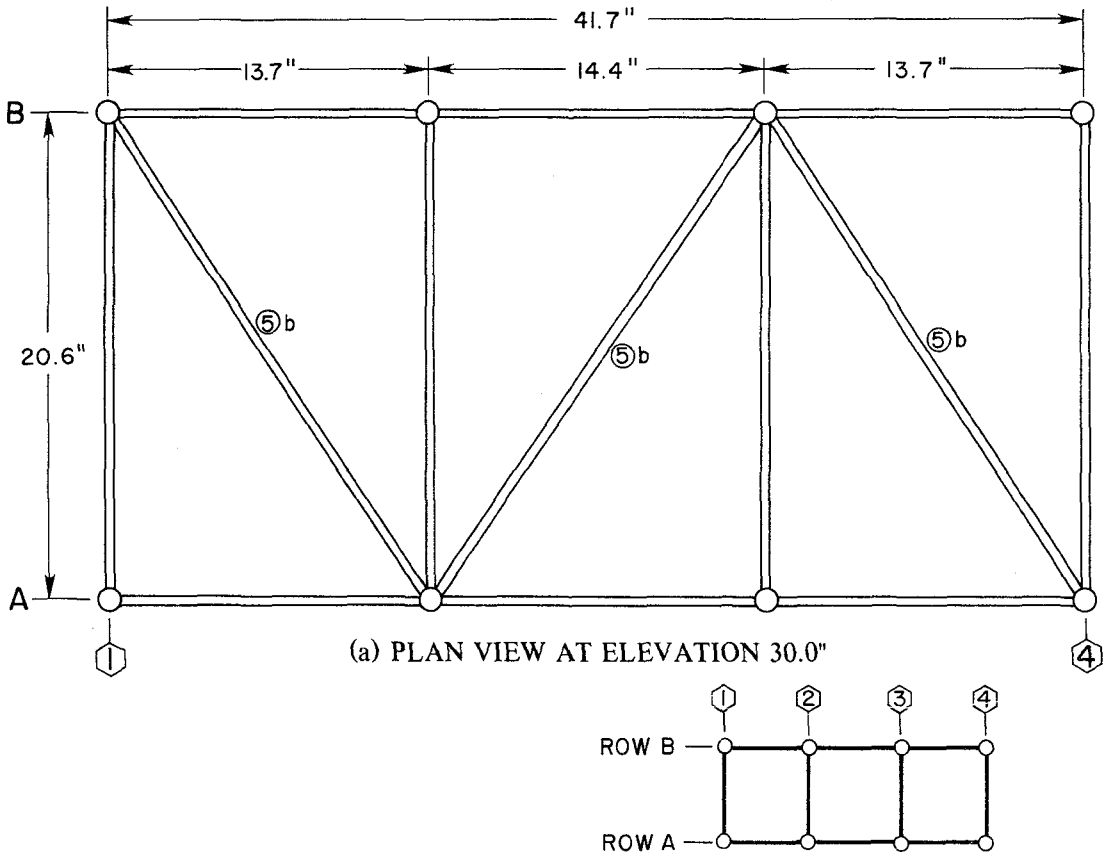

(a) PLAN VIEW AT ELEVATION 30.0"

Note: see Table 2.5 for member sizes and moduli

Fig. 2.6 Configuration, member sizes and moduli of elasticity for model platform jacket

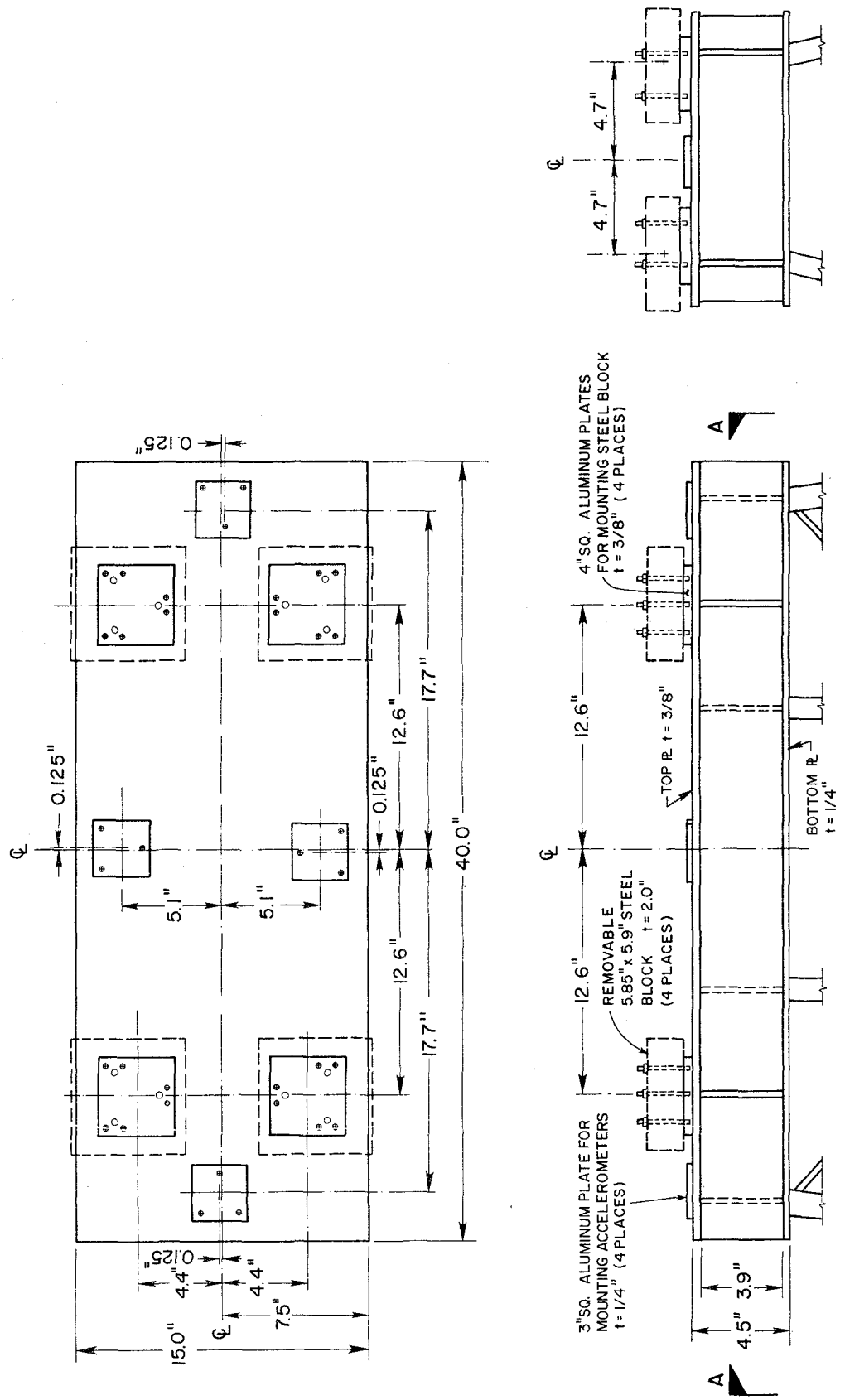

Fig. 2.7 Model platform deck configuration and details

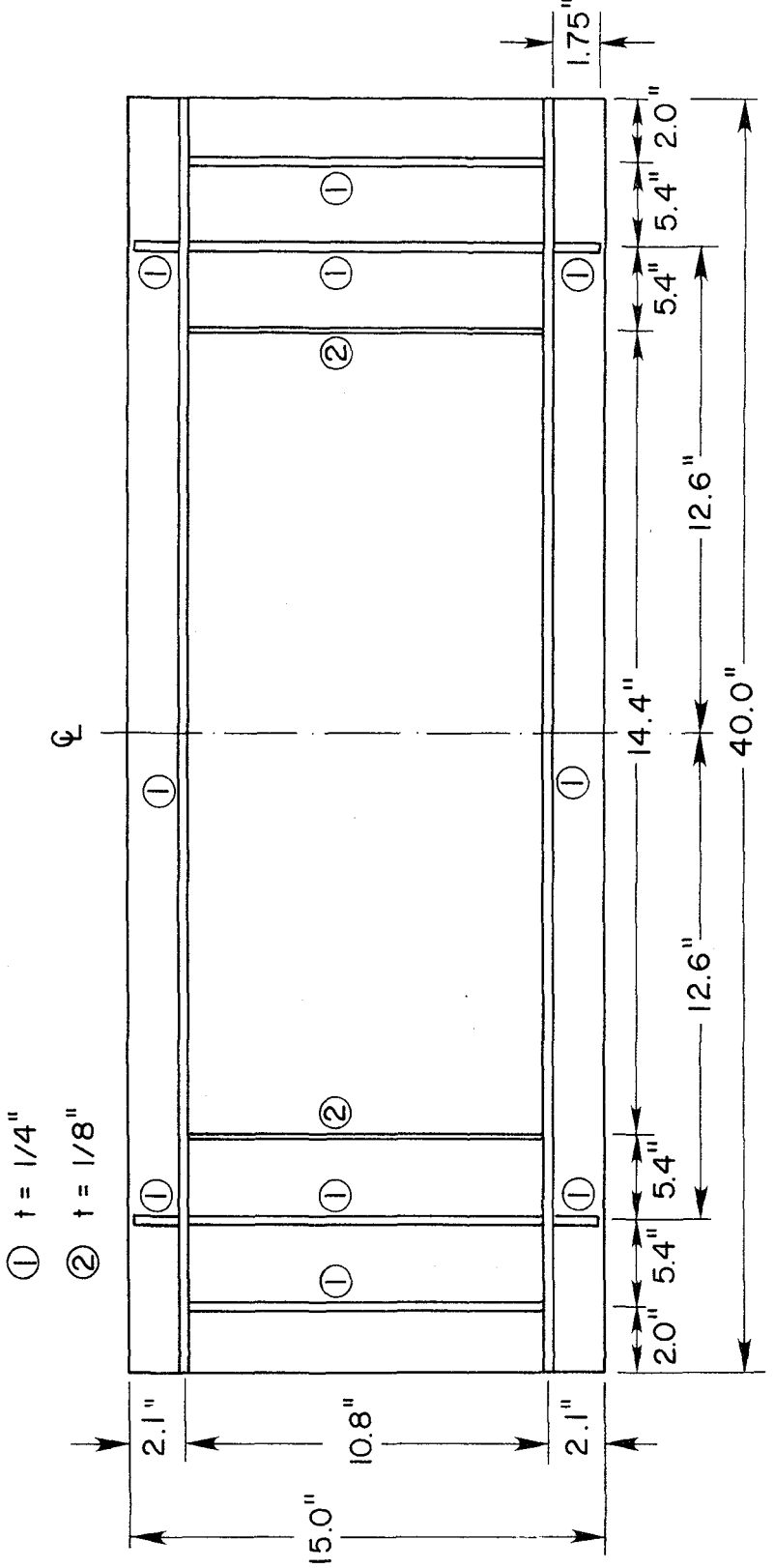

Fig. 2.8 Model platform deck webs in plan view

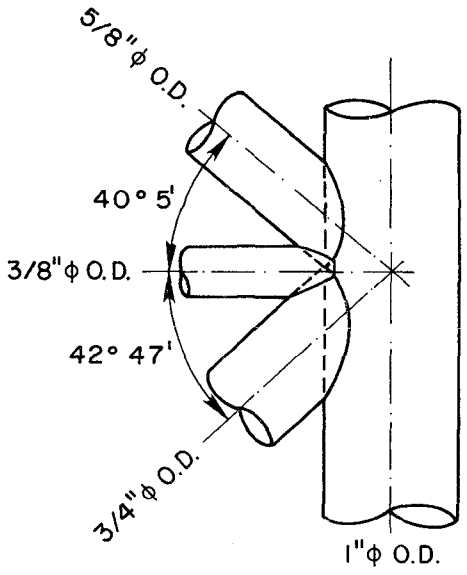

DETAIL "A"

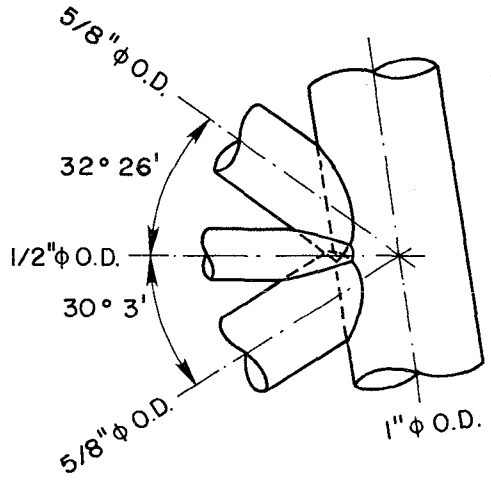

DETAIL "B"

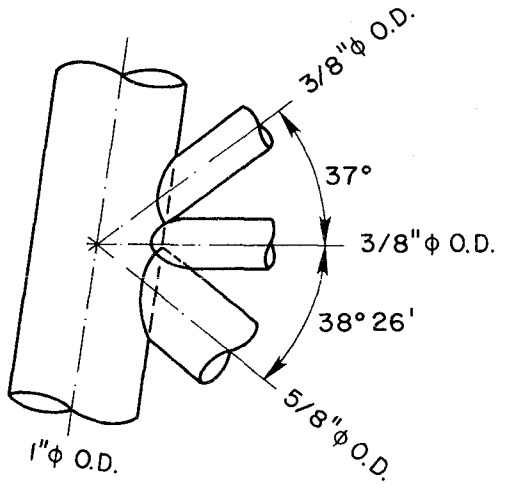

DETAIL "C"

Fig. 2.9 Typical jacket leg-brace joints of model

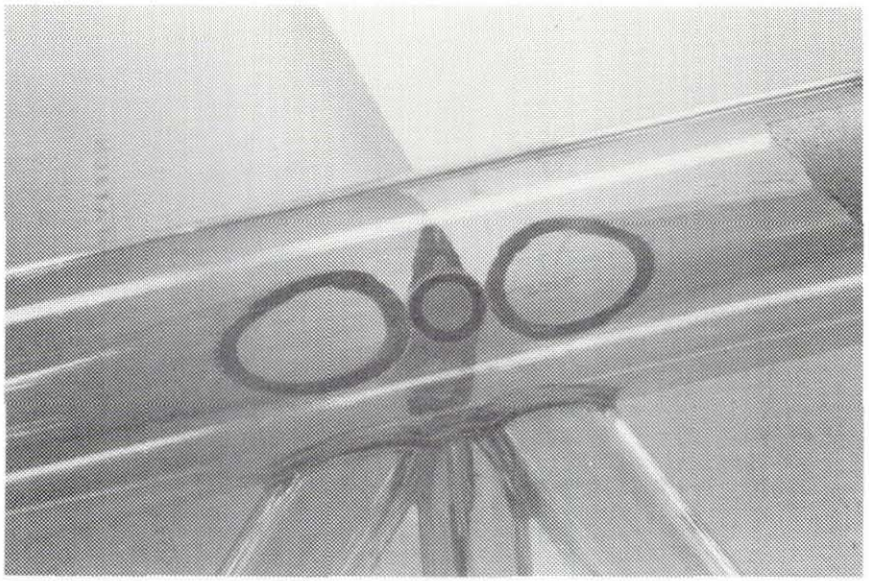

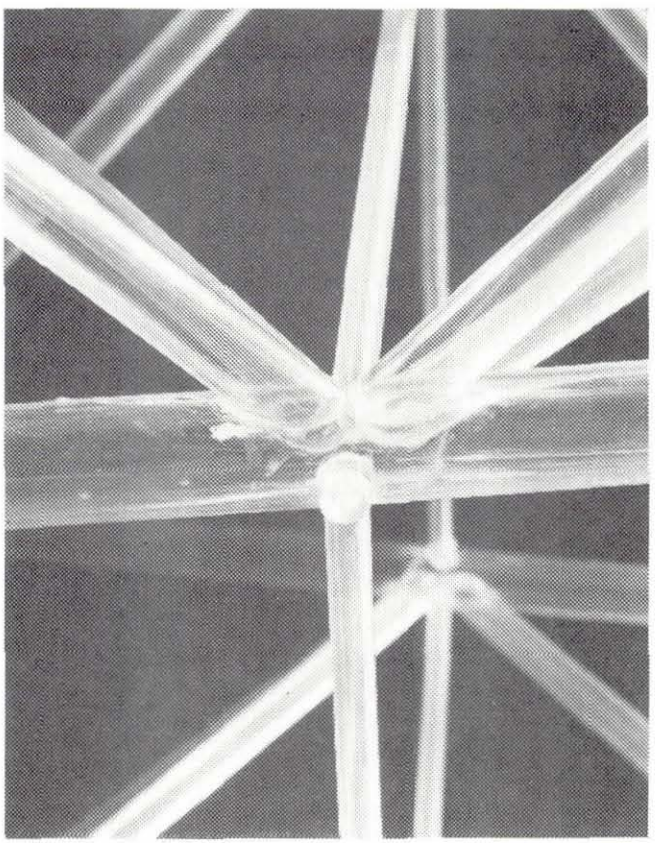

Fig. 2.10 Photographs of typical leg-brace joints of model

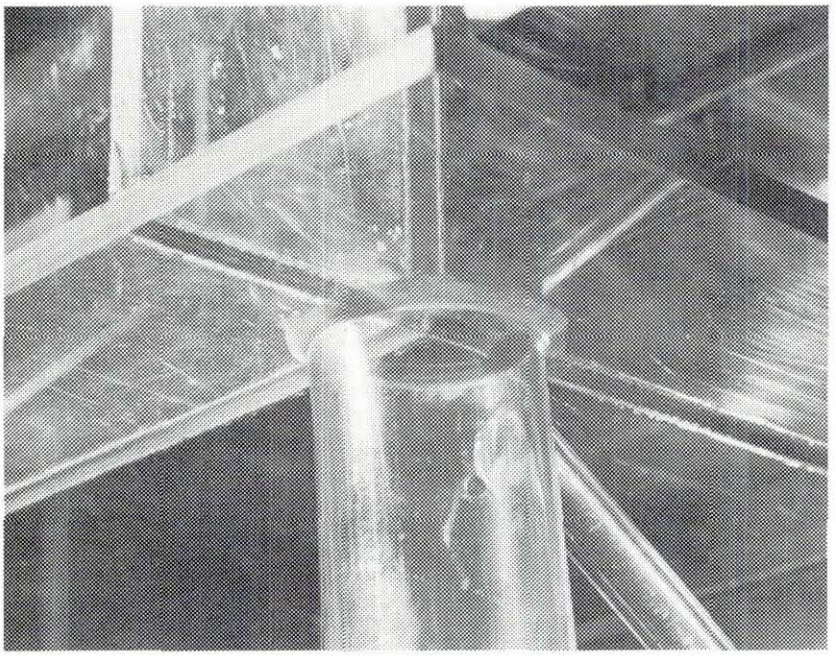

Fig. 2.11 Photograph of typical leg-to-deck connection

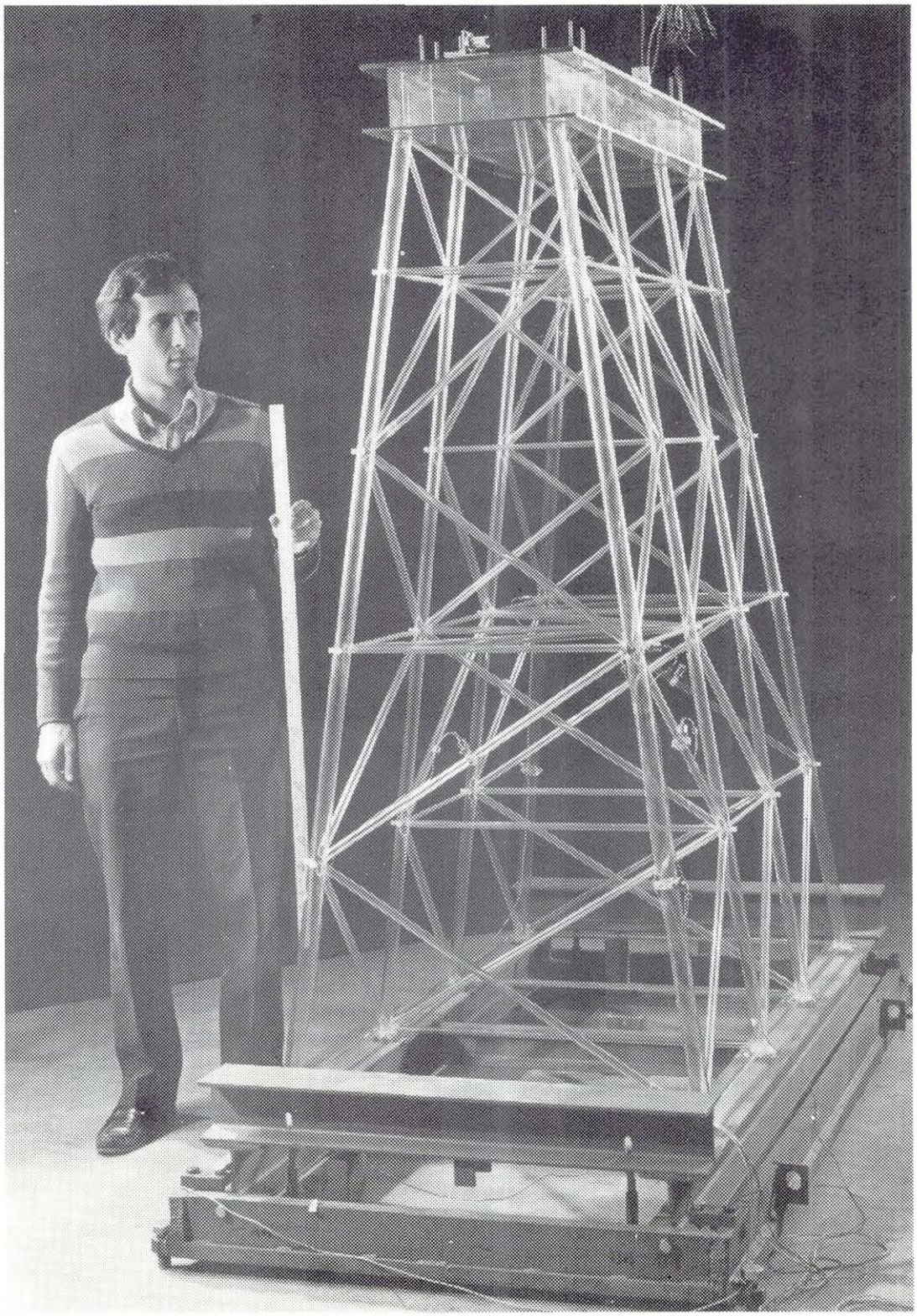

Fig. 2.12 Photograph of model platform on its base system, end-on view

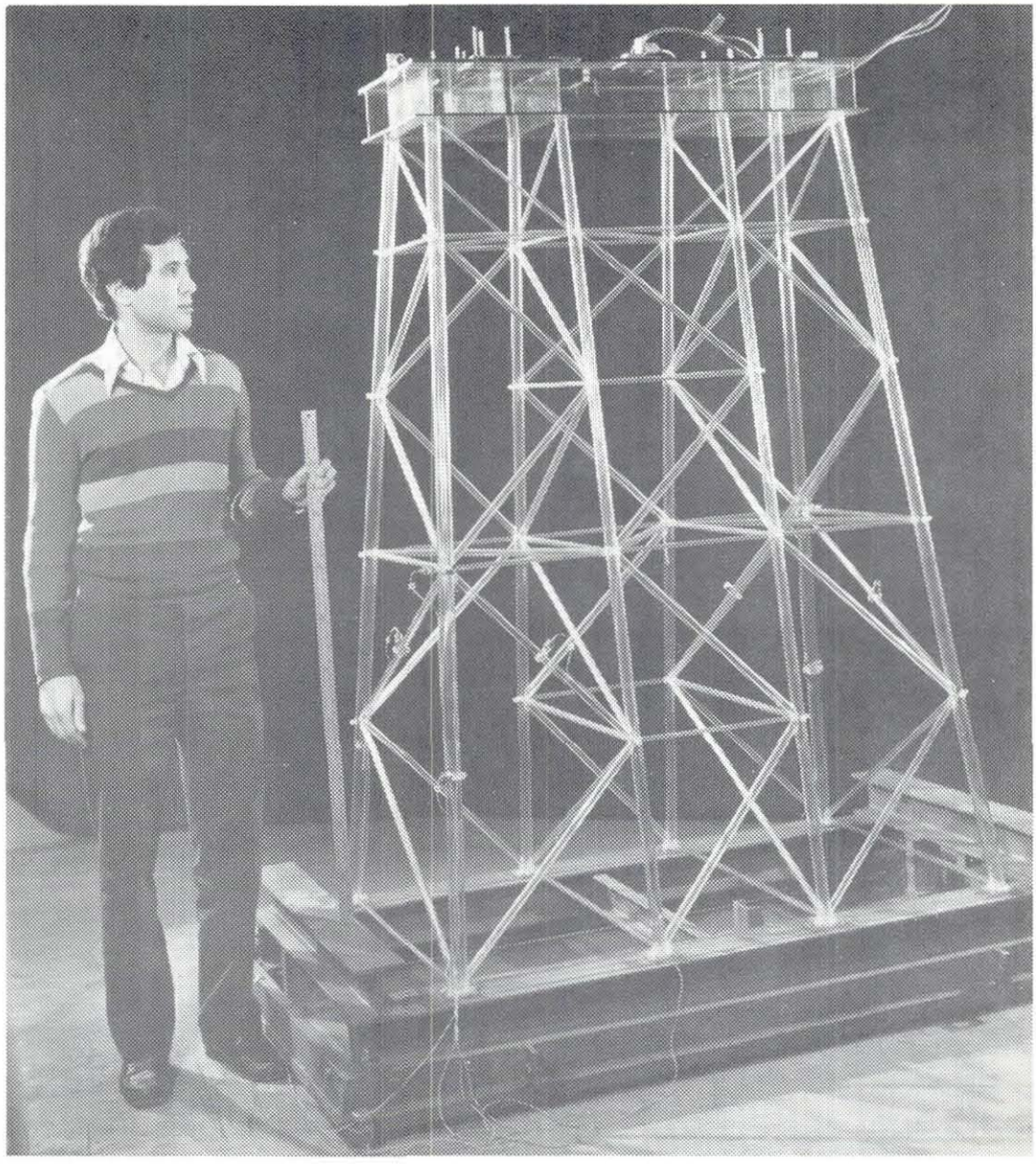

Fig. 2.13 Photograph of model platform on its base system, broad-side view

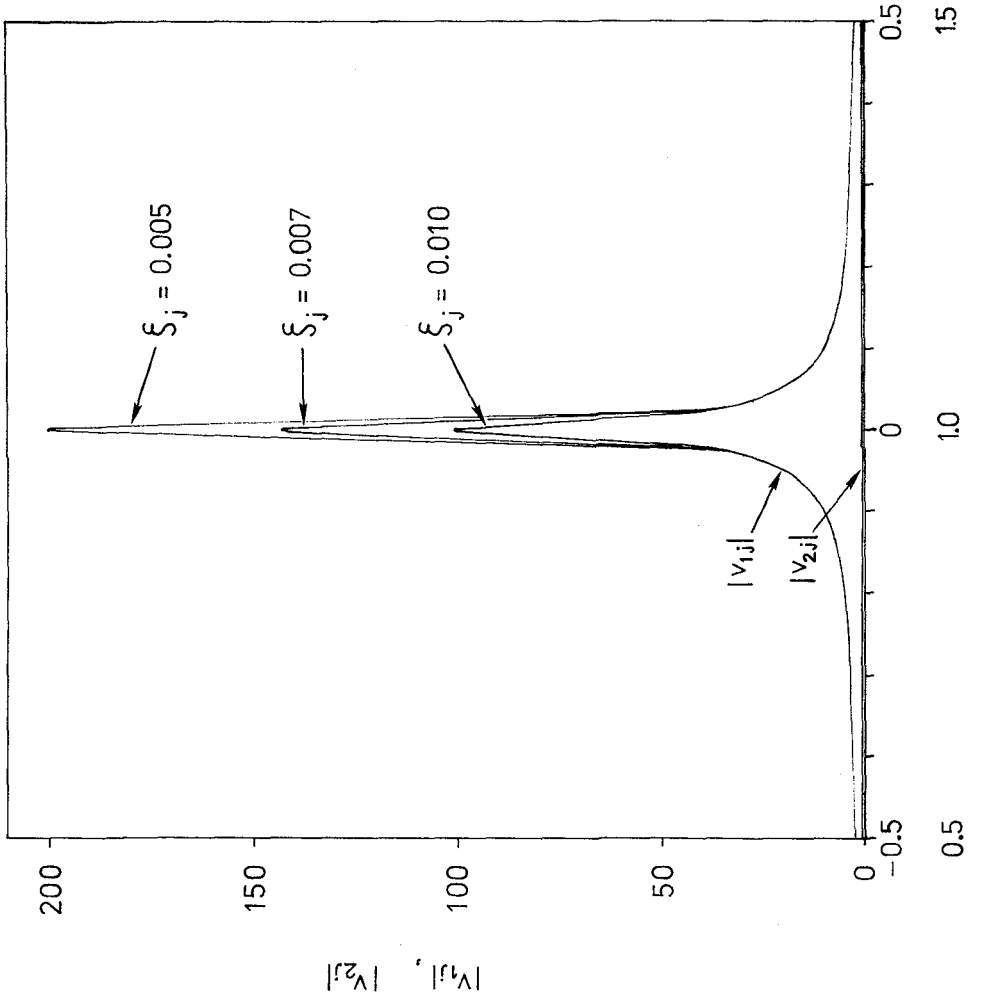

Fig. 3.1 Variation of $|v_{1j}|$ and $|v_{2j}|$ with frequency ratio

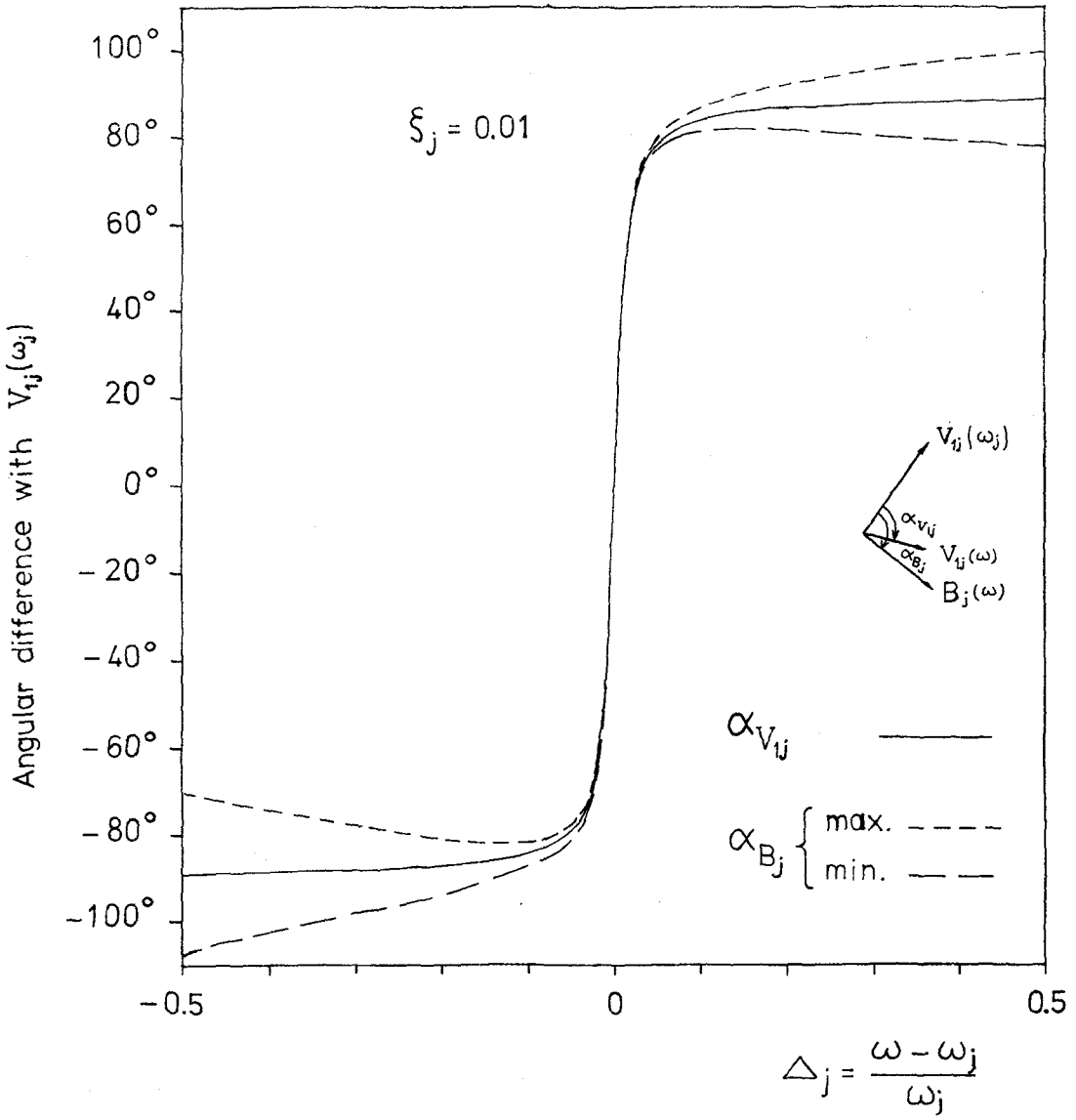

Fig. 3.2 Variation of the angle of $V_{1j}(\omega)$, $\alpha_{V_{1j}}$, and the bounds on the value of the angle of $B_j(\omega)$, α_{B_j}, with frequency ratio

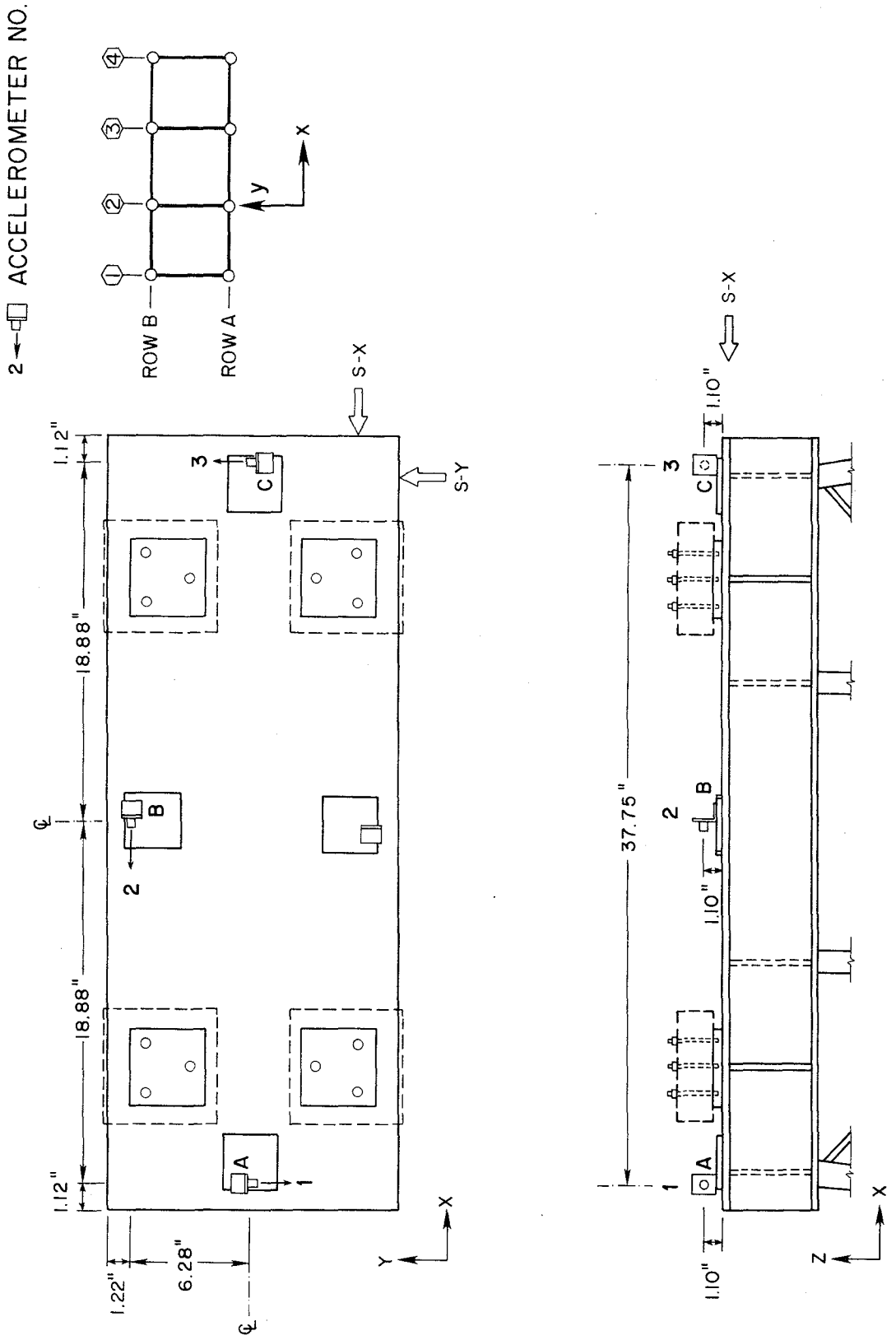

Fig. 3.3 Location of accelerometers on deck, global coordinate system and direction of impacts

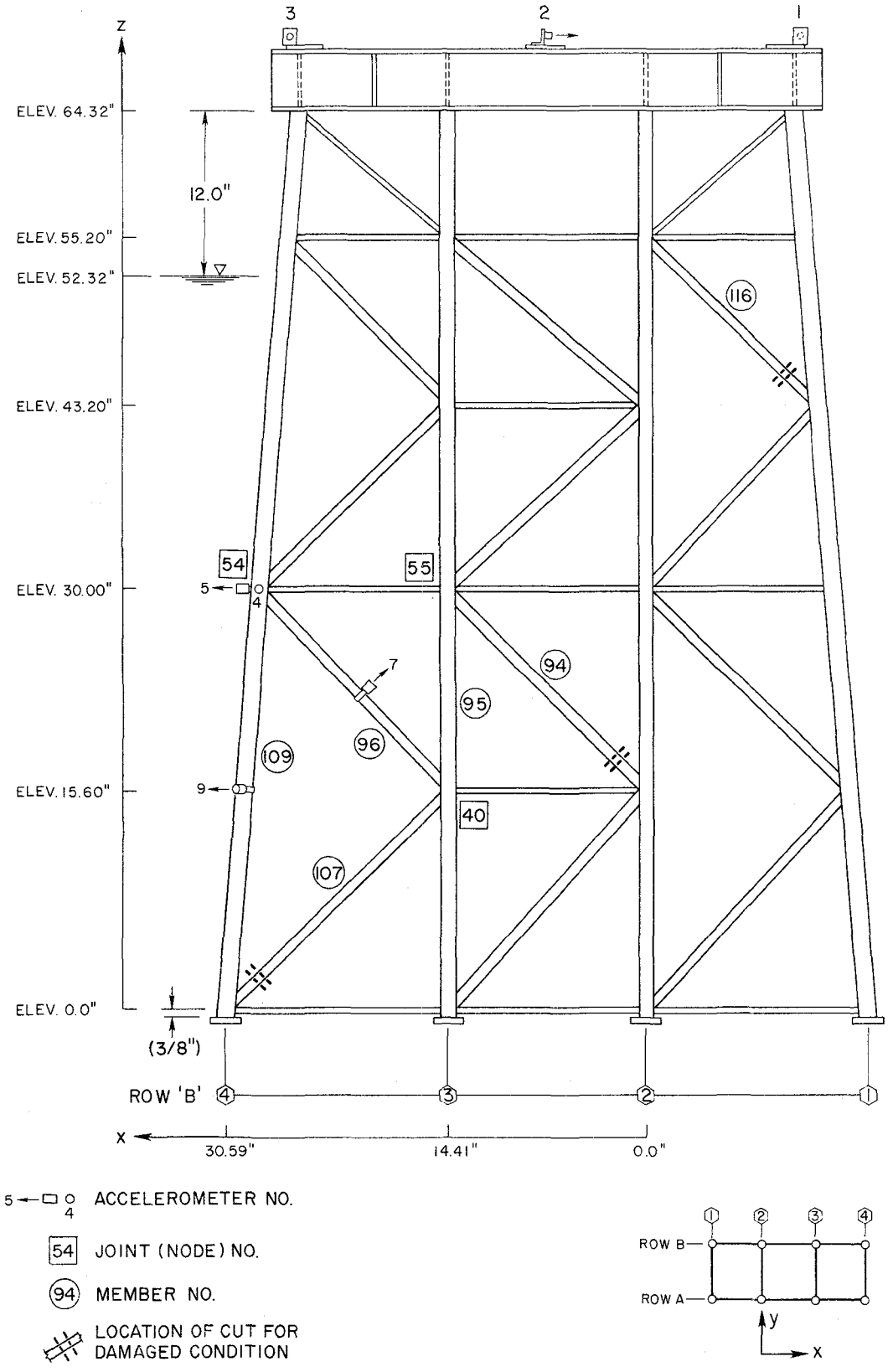

Fig. 3.4 Location of accelerometers on Frame B. Also selected joint (node) and member numbers and global coordinate system

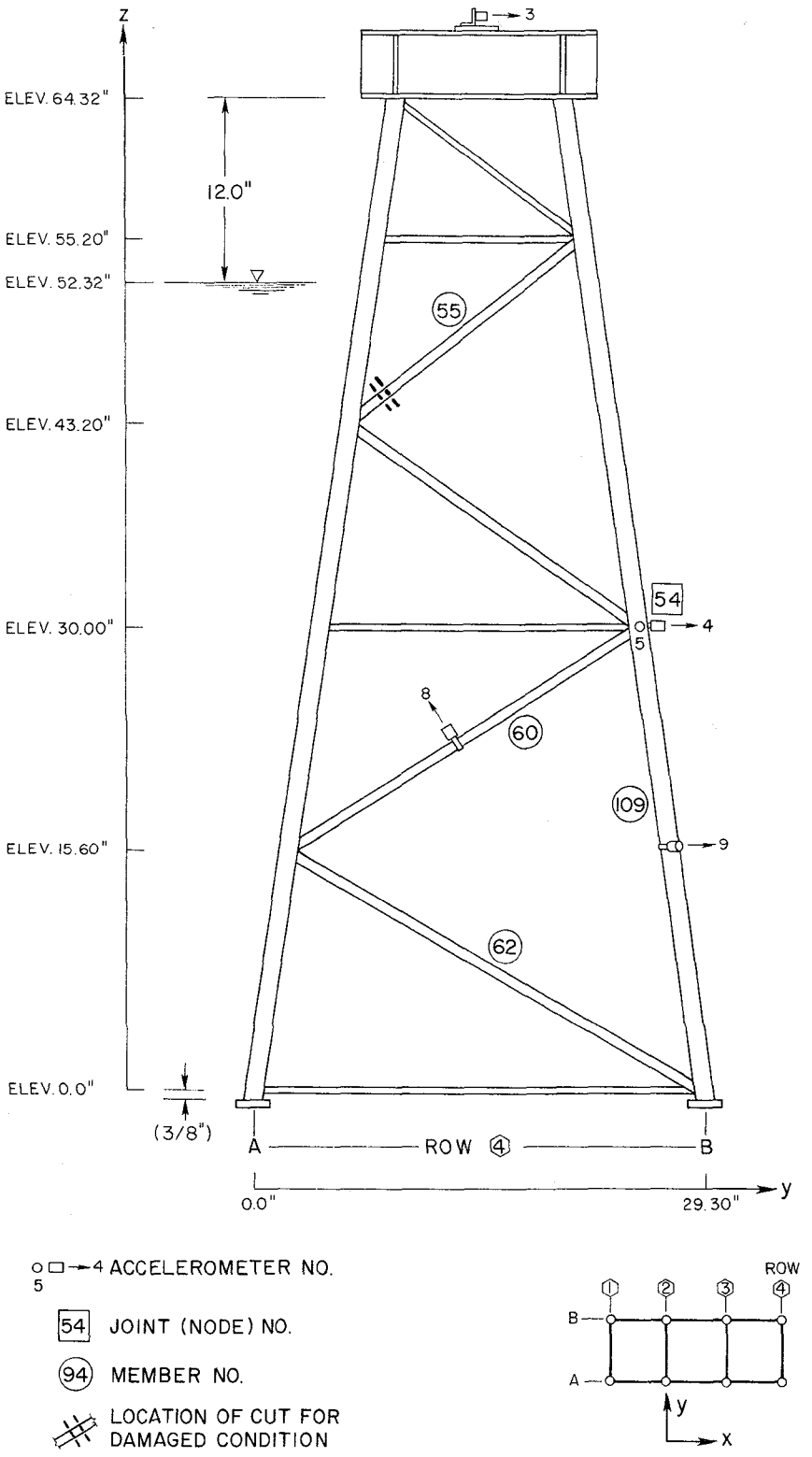

Fig. 3.5 Location of accelerometers on Frame 4. Also selected joint (node) and member numbers and global coordinate system

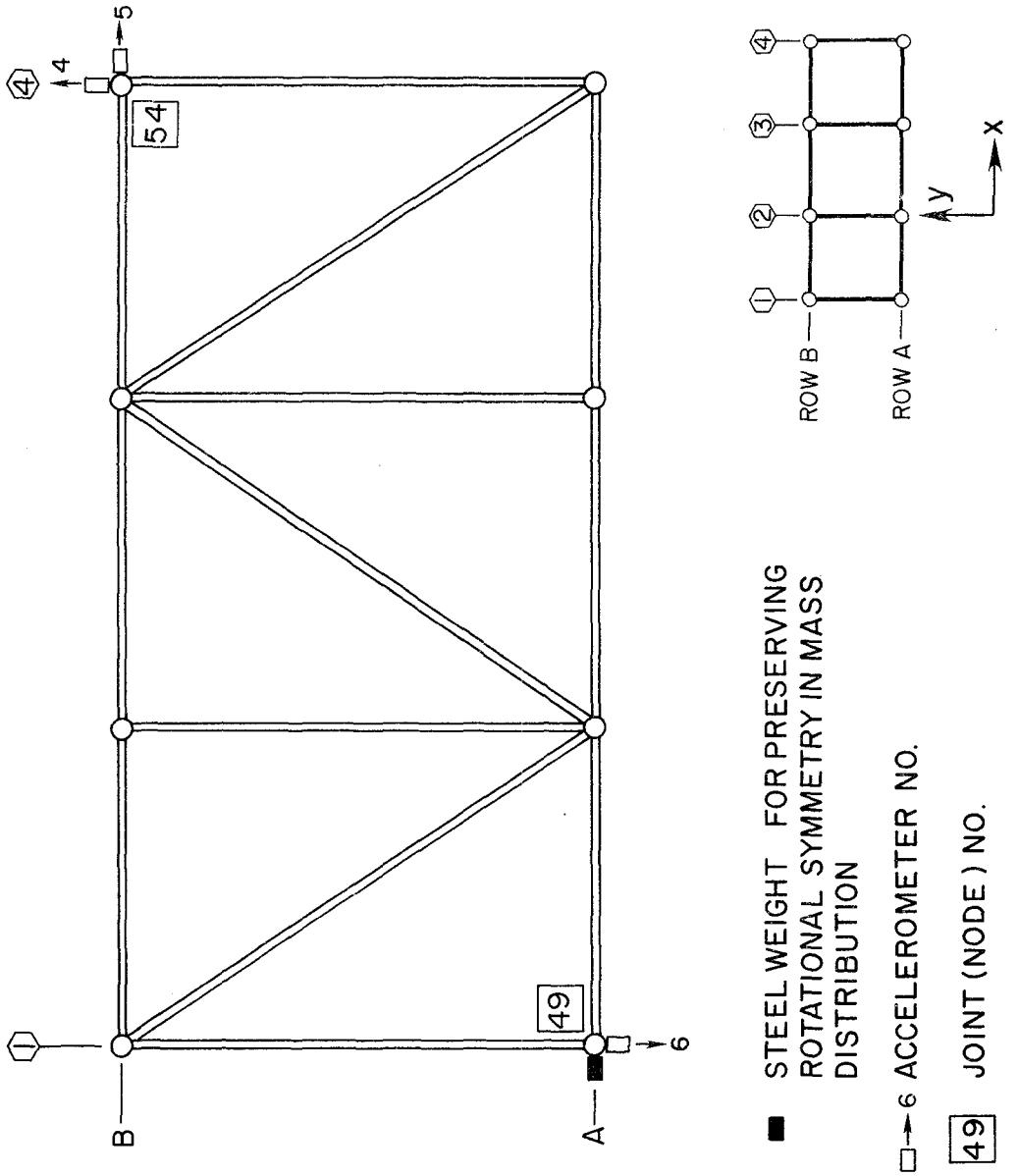

Fig. 3.6 Location of accelerometers and steel weights in plan view at Elev. 30.0"

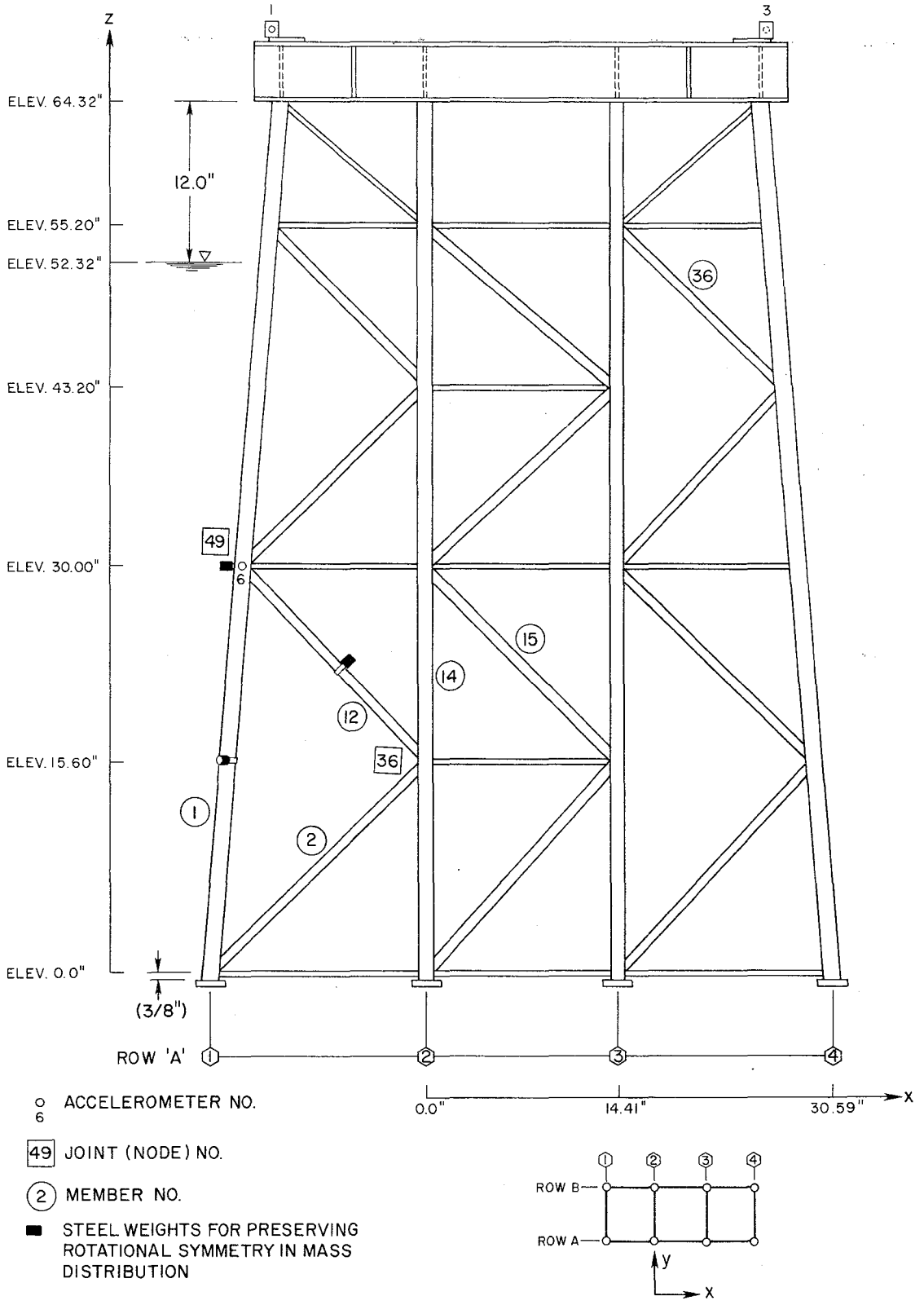

Fig. 3.7 Location of accelerometer and steel weights on Frame A. Also selected joint (node) and member numbers and global coordinate system

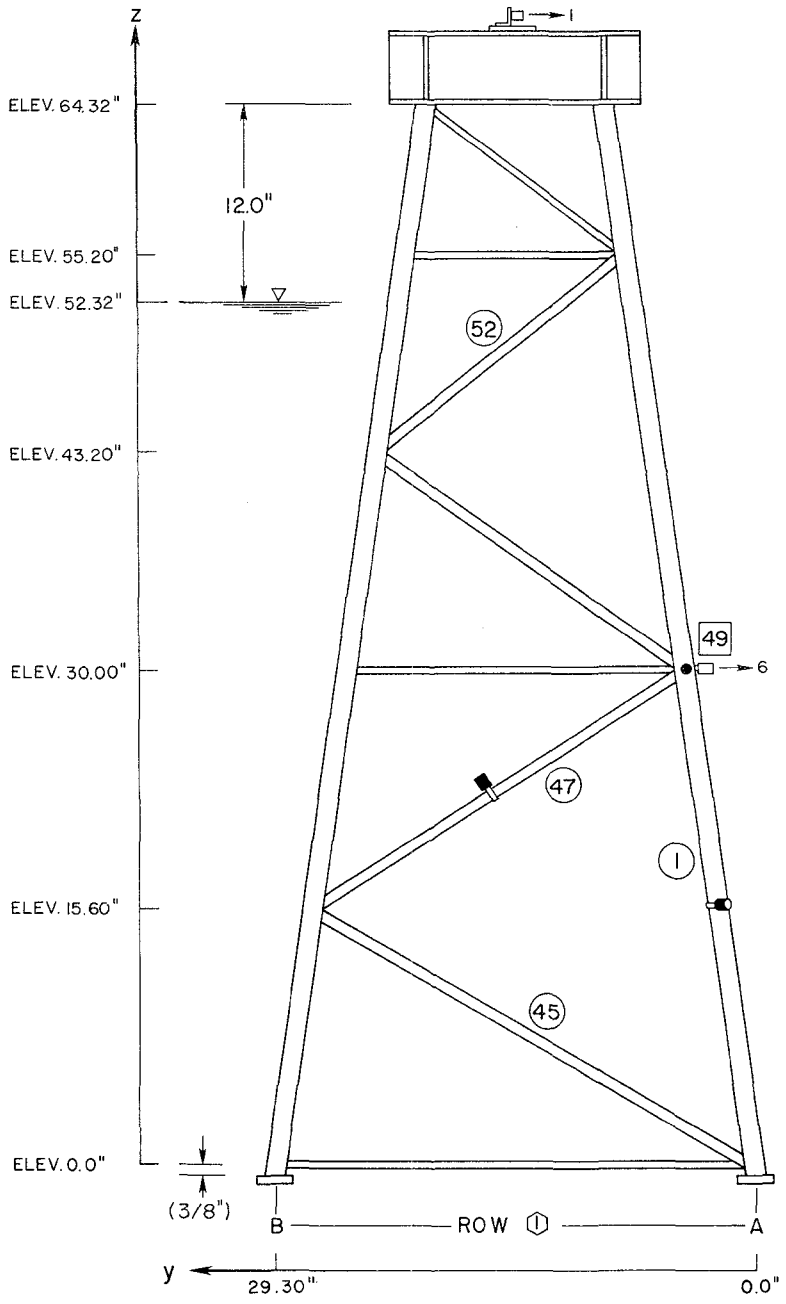

□→6 ACCELEROMETER NO.

49 JOINT (NODE) NO.

(1) MEMBER NO.

● ■ STEEL WEIGHTS FOR PRESERVING ROTATIONAL SYMMETRY IN MASS DISTRIBUTION

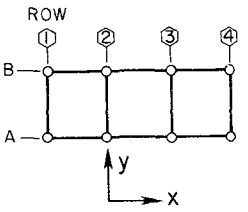

Fig. 3.8 Location of accelerometer and steel weights on Frame 1. Also selected joint (node) and member numbers and global coordinate system

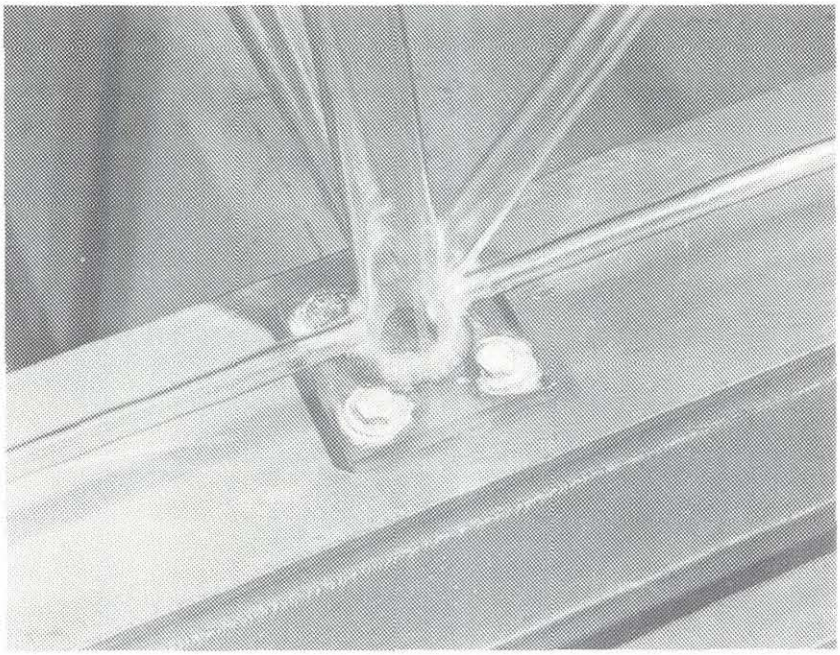

Fig. 3.9 Photograph of typical model leg-to-base frame connection

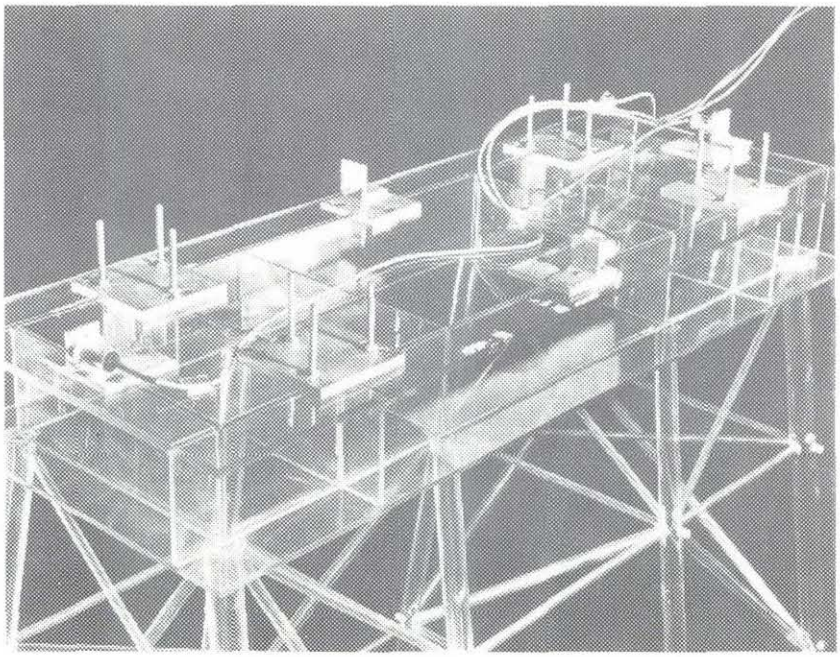

Fig. 3.10 Photograph of the accelerometers on the model deck

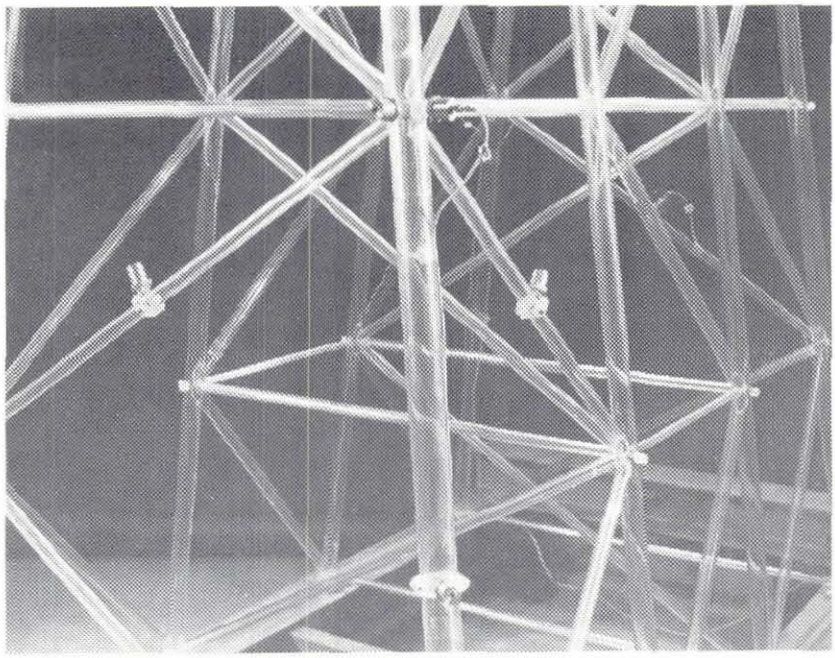

a) View of members of Frames 1 and A

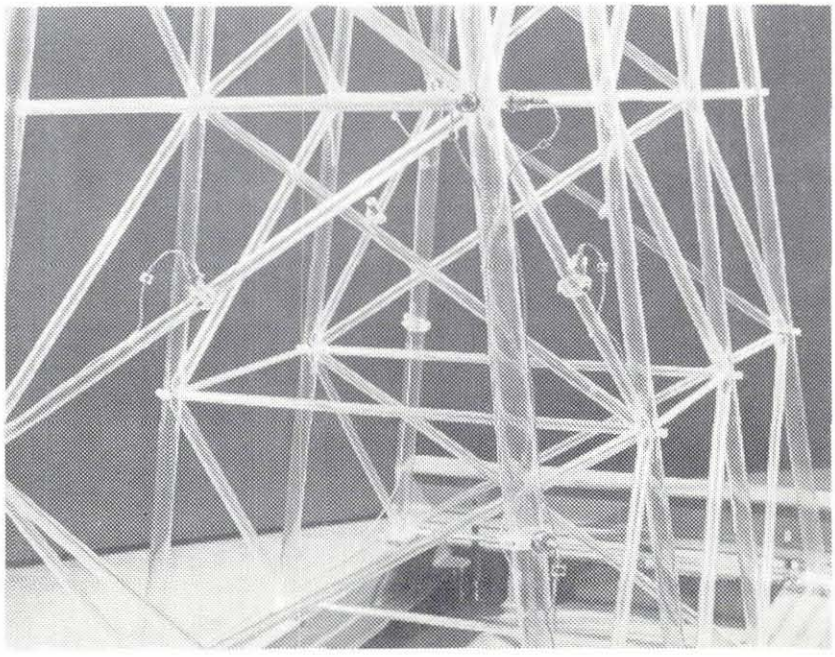

b) View of members of Frames 4 and B

Fig. 3.11 Photographs of the instrumented jacket of the model

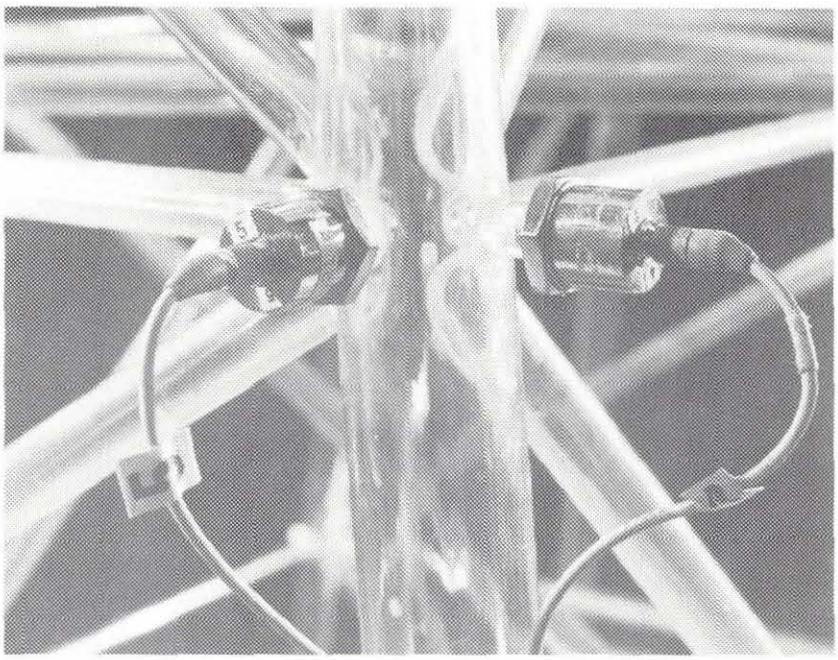

a) Accelerometers on Joint 54

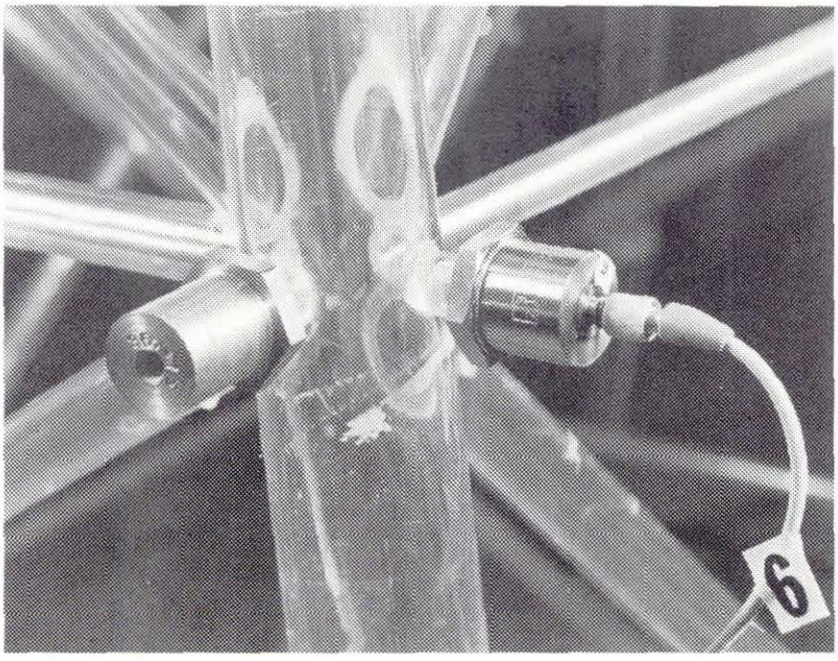

b) Accelerometer and steel weight on Joint 49

Fig. 3.12 Photographs of the instrumented joints of jacket of the model

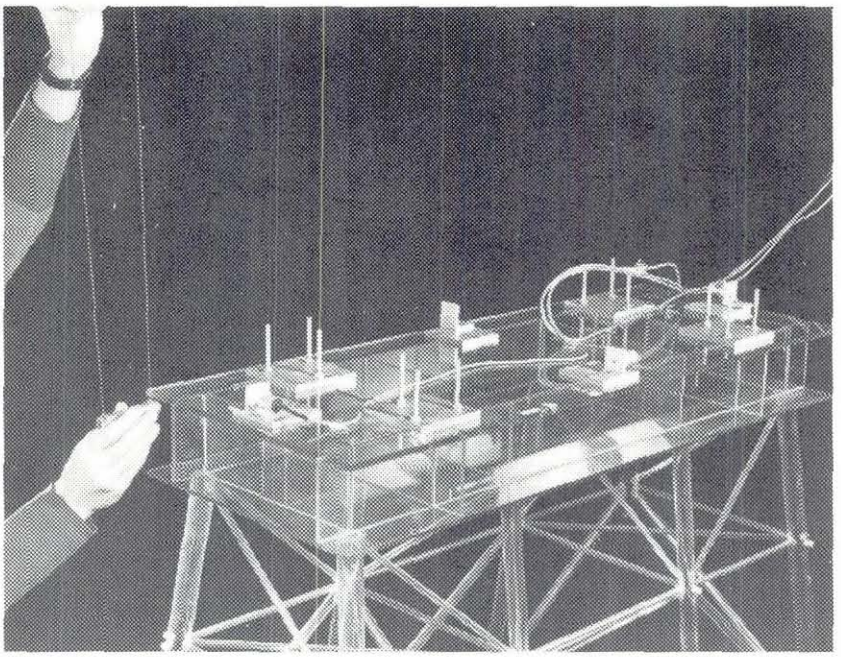

a) "S-X" test

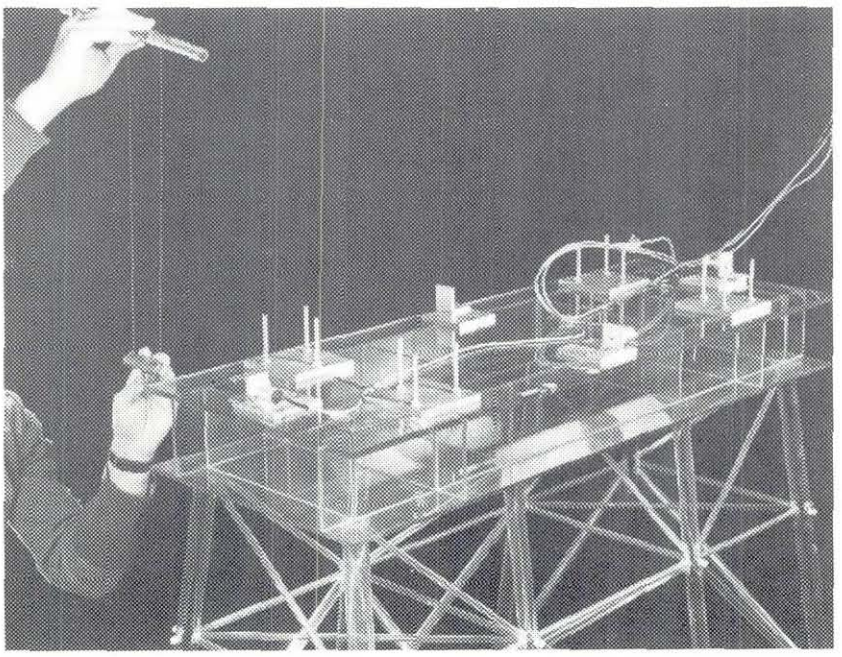

b) "S-Y" test

Fig. 3.13 Photographs illustrating positioning of hammer and direction of impacts

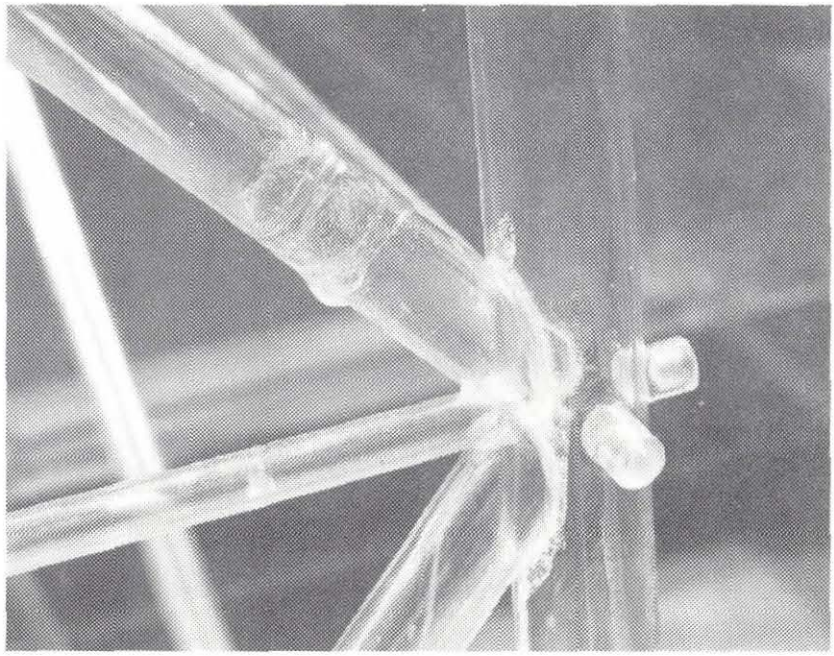

Fig. 3.14 Photograph of Member 94 after repair

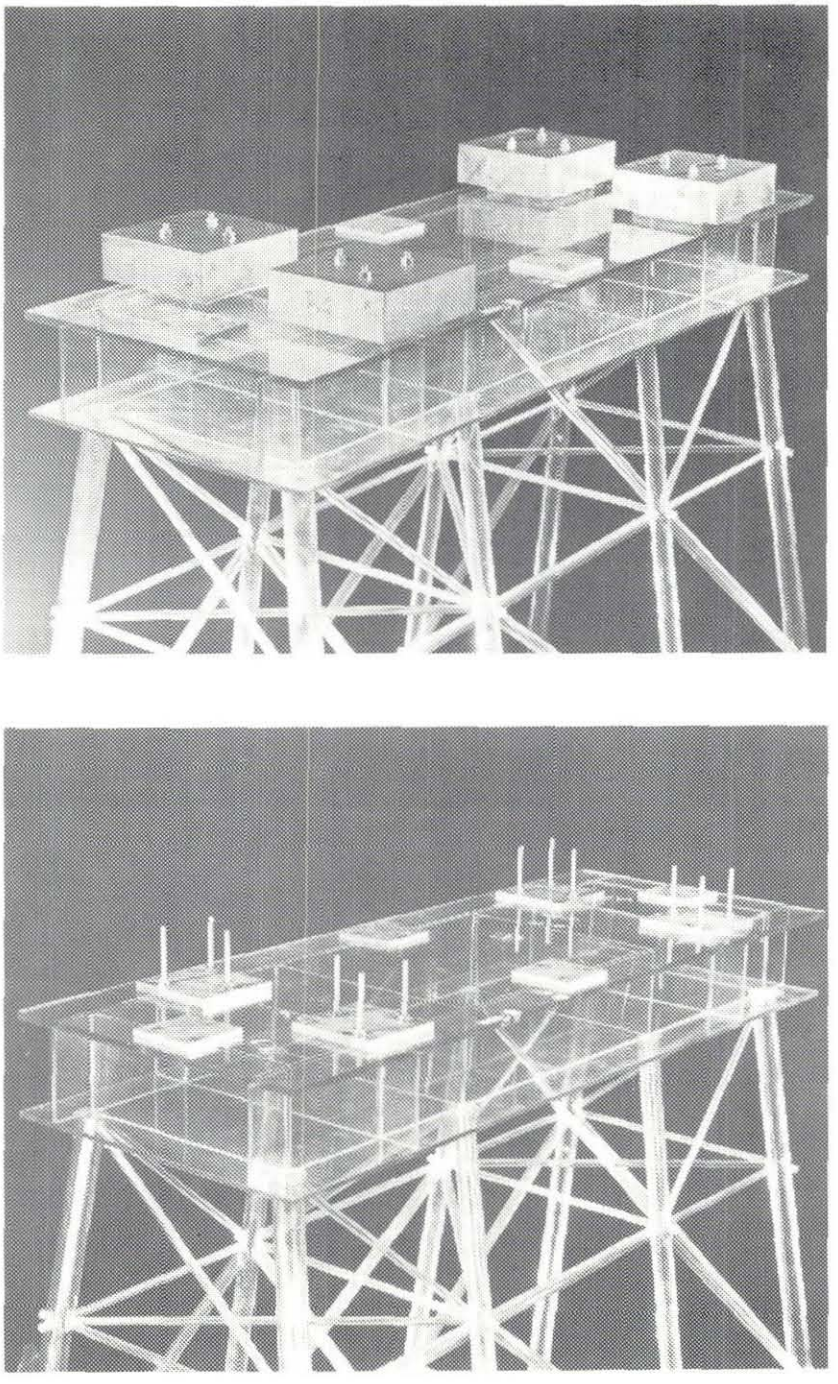

Fig. 3.15 Photographs of model deck with and without the steel blocks

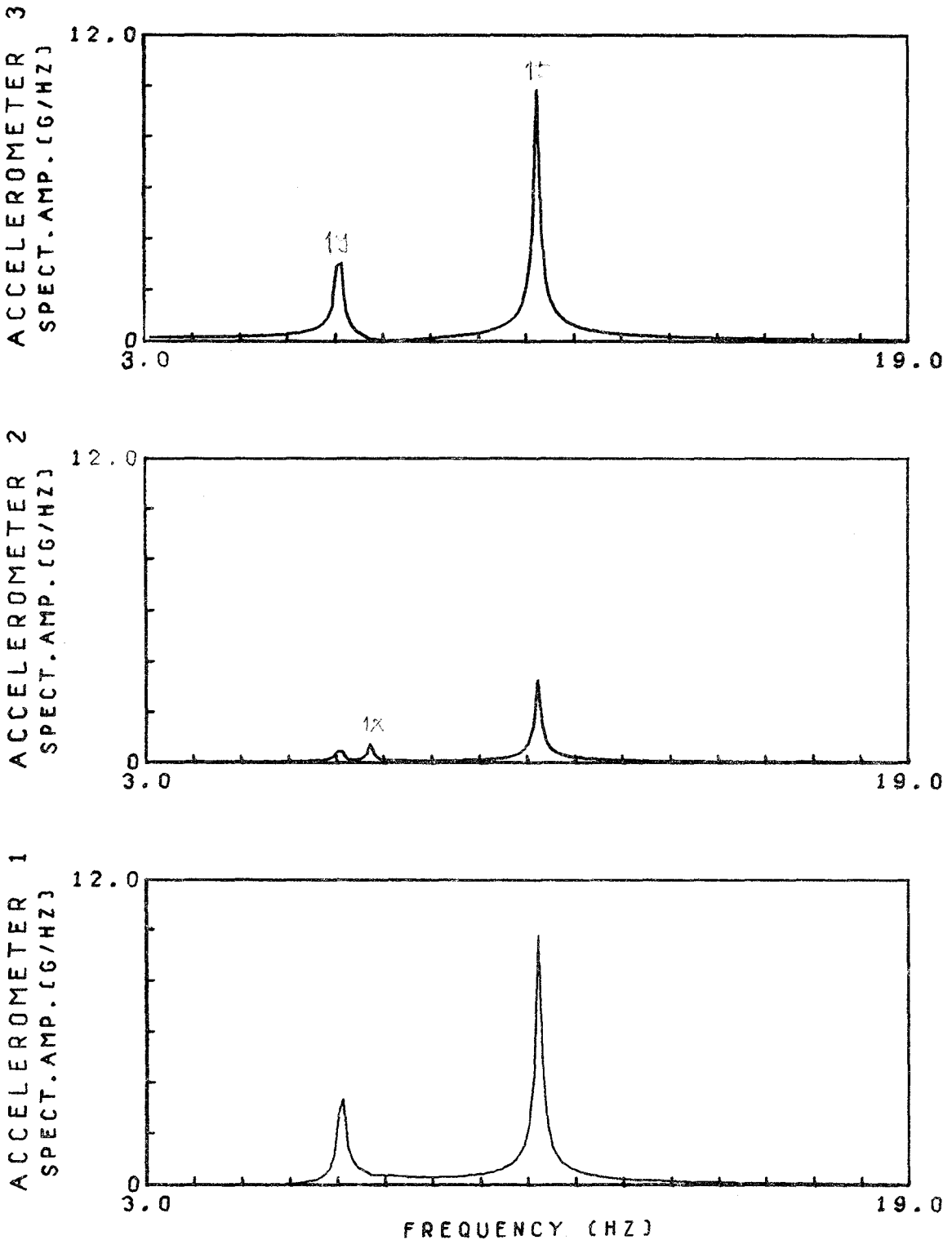

Fig. 4.1 TRANSIENT RESPONSE SPECTRA; MAXIMUM DECK MASS CASE, Y-DIRECTION SHOCK ON DECK SIDE (S-Y, TEST 144)

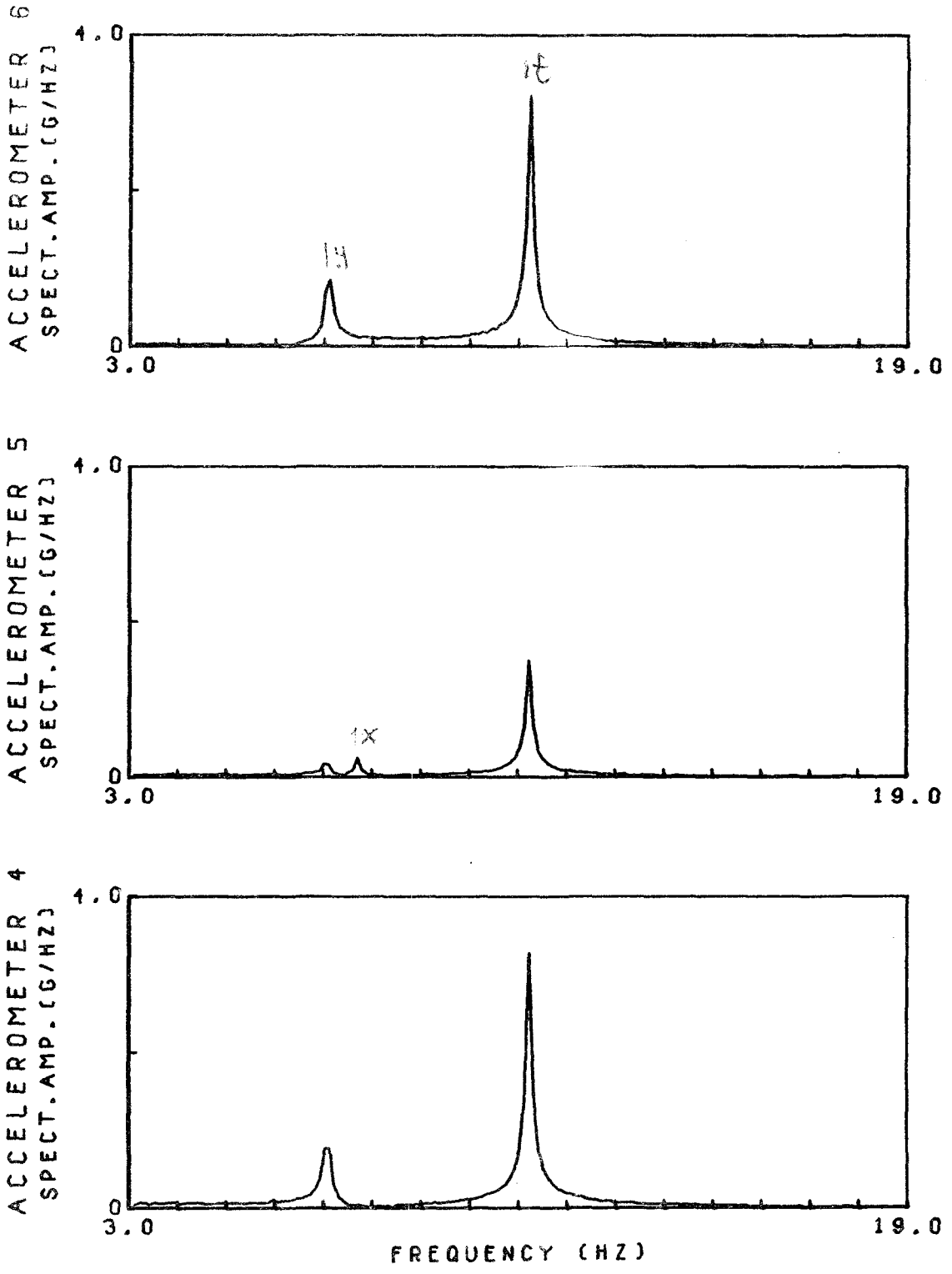

Fig. 4.2 TRANSIENT RESPONSE SPECTRA; MAXIMUM DECK MASS CASE, Y-DIRECTION SHOCK ON DECK SIDE (S-Y, TEST 144)

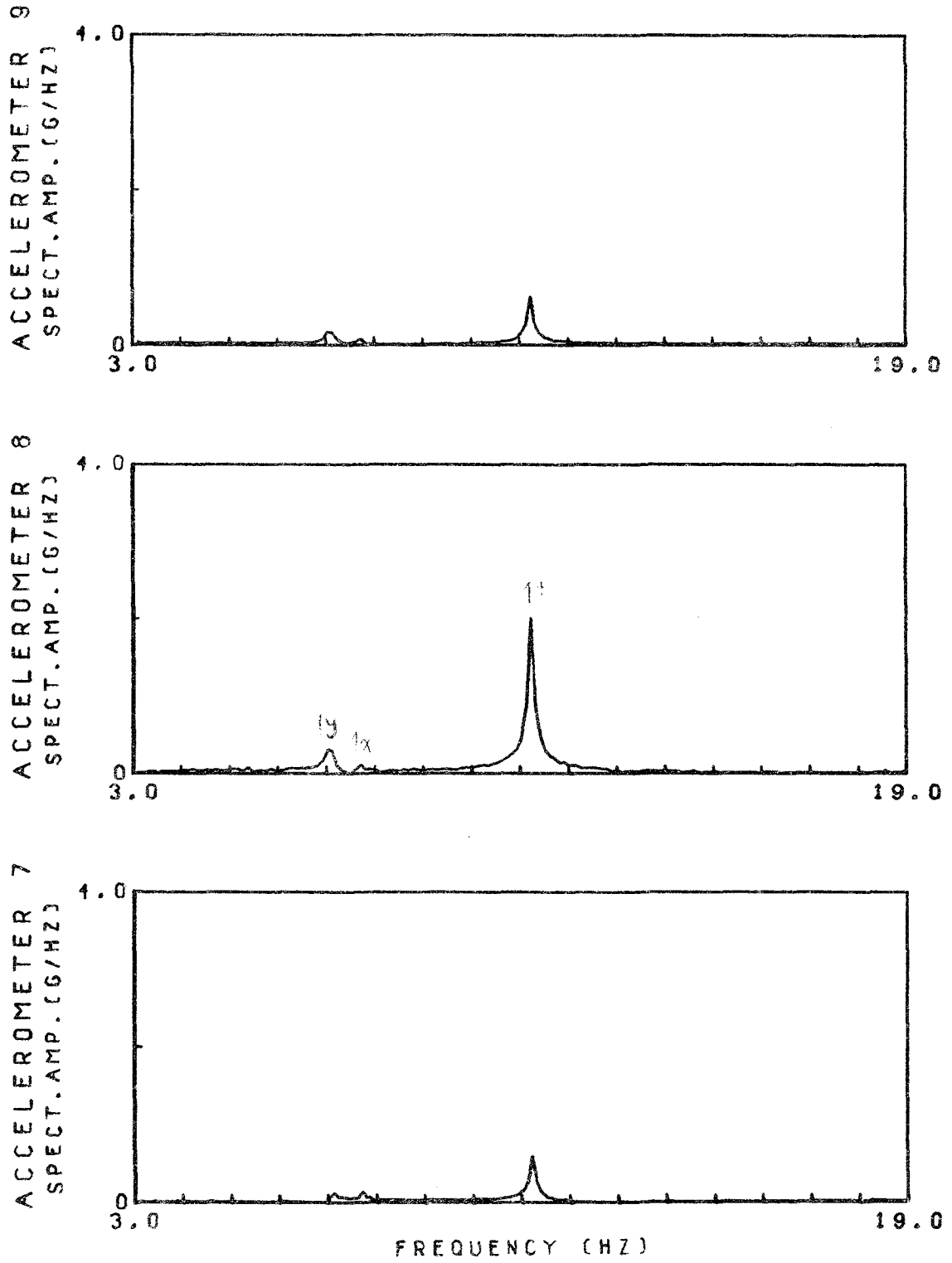

Fig. 4.3 TRANSIENT RESPONSE SPECTRA; MAXIMUM DECK MASS CASE, Y-DIRECTION SHOCK ON DECK SIDE (S-Y, TEST 144)

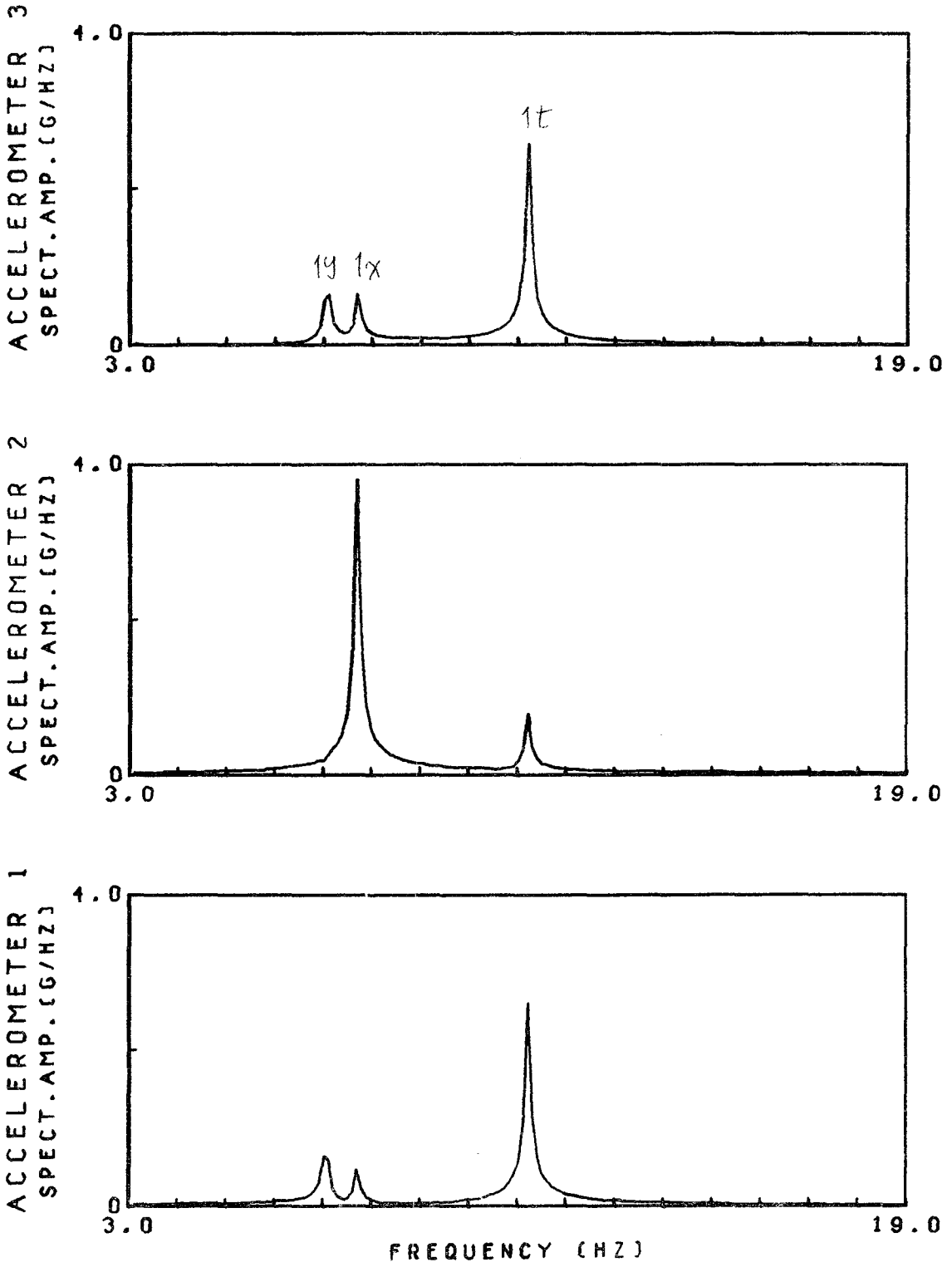

Fig. 4.4 TRANSIENT RESPONSE SPECTRA; MAXIMUM DECK MASS CASE, X-DIRECTION SHOCK ON DECK SIDE (S-X, TEST 147)

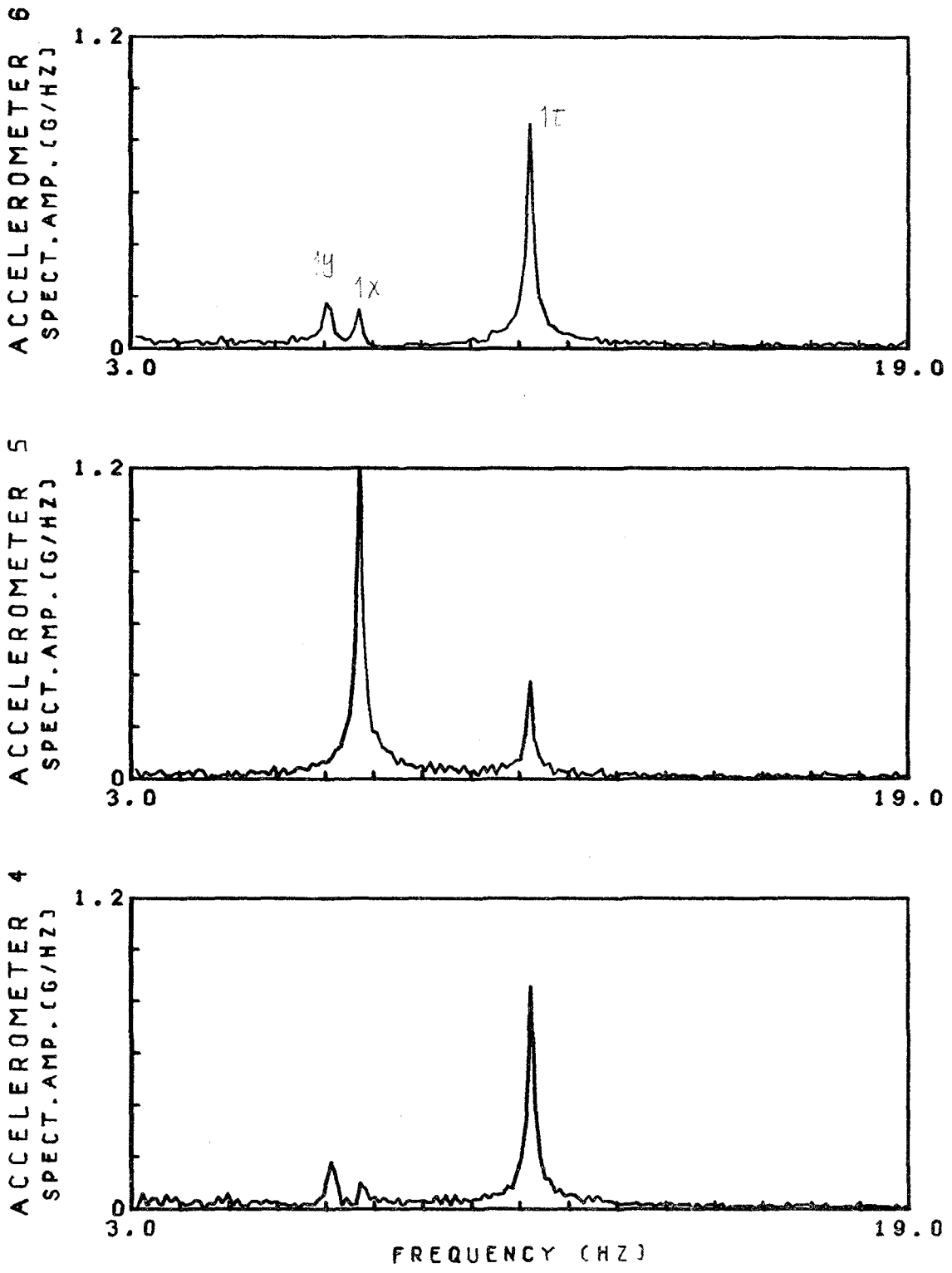

Fig. 4.5 TRANSIENT RESPONSE SPECTRA; MAXIMUM DECK MASS CASE, X-DIRECTION SHOCK ON DECK SIDE (S-X, TEST 147)

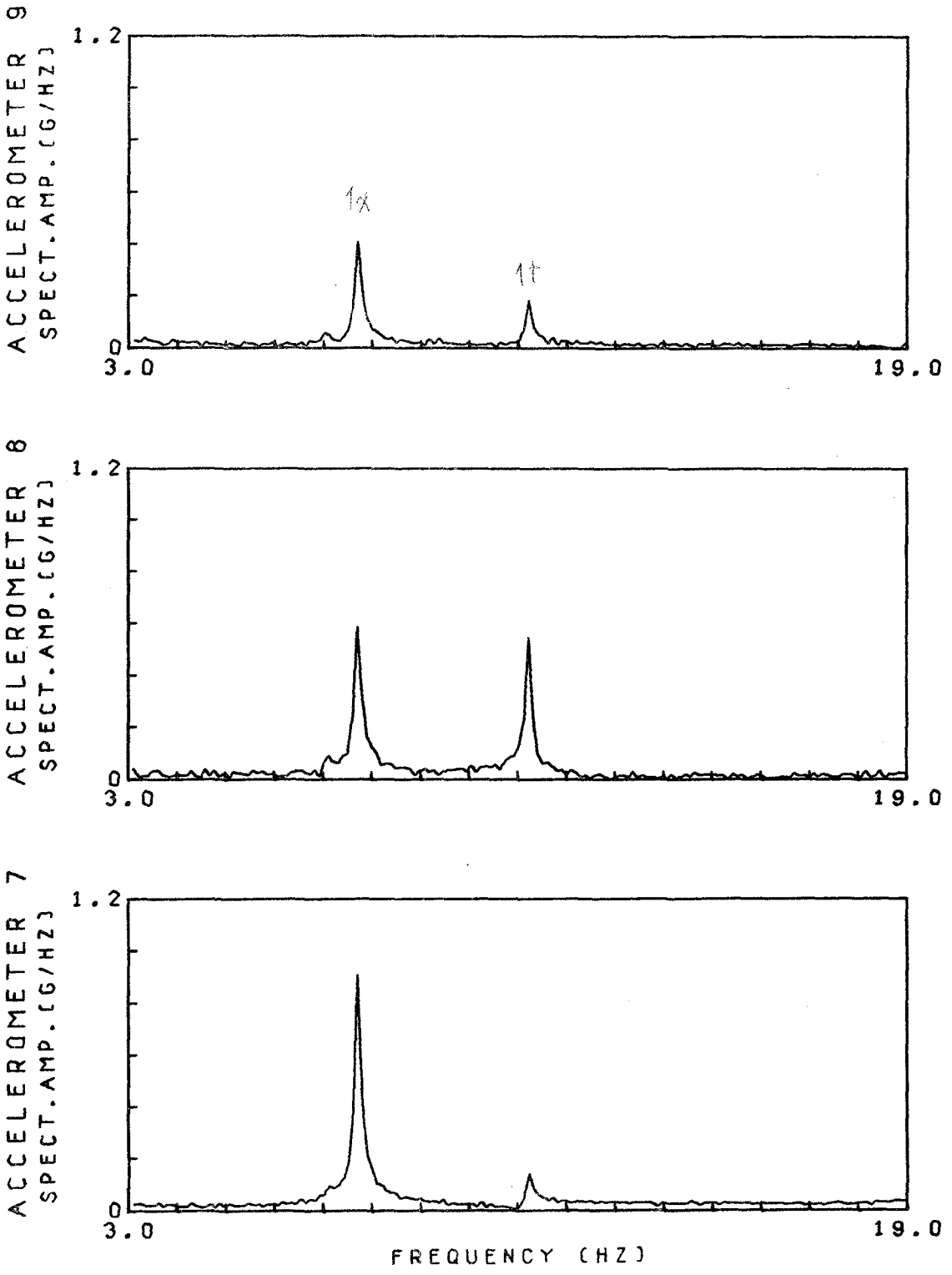

Fig. 4.6 TRANSIENT RESPONSE SPECTRA; MAXIMUM DECK MASS CASE, X-DIRECTION SHOCK ON DECK SIDE (S-X, TEST 147)

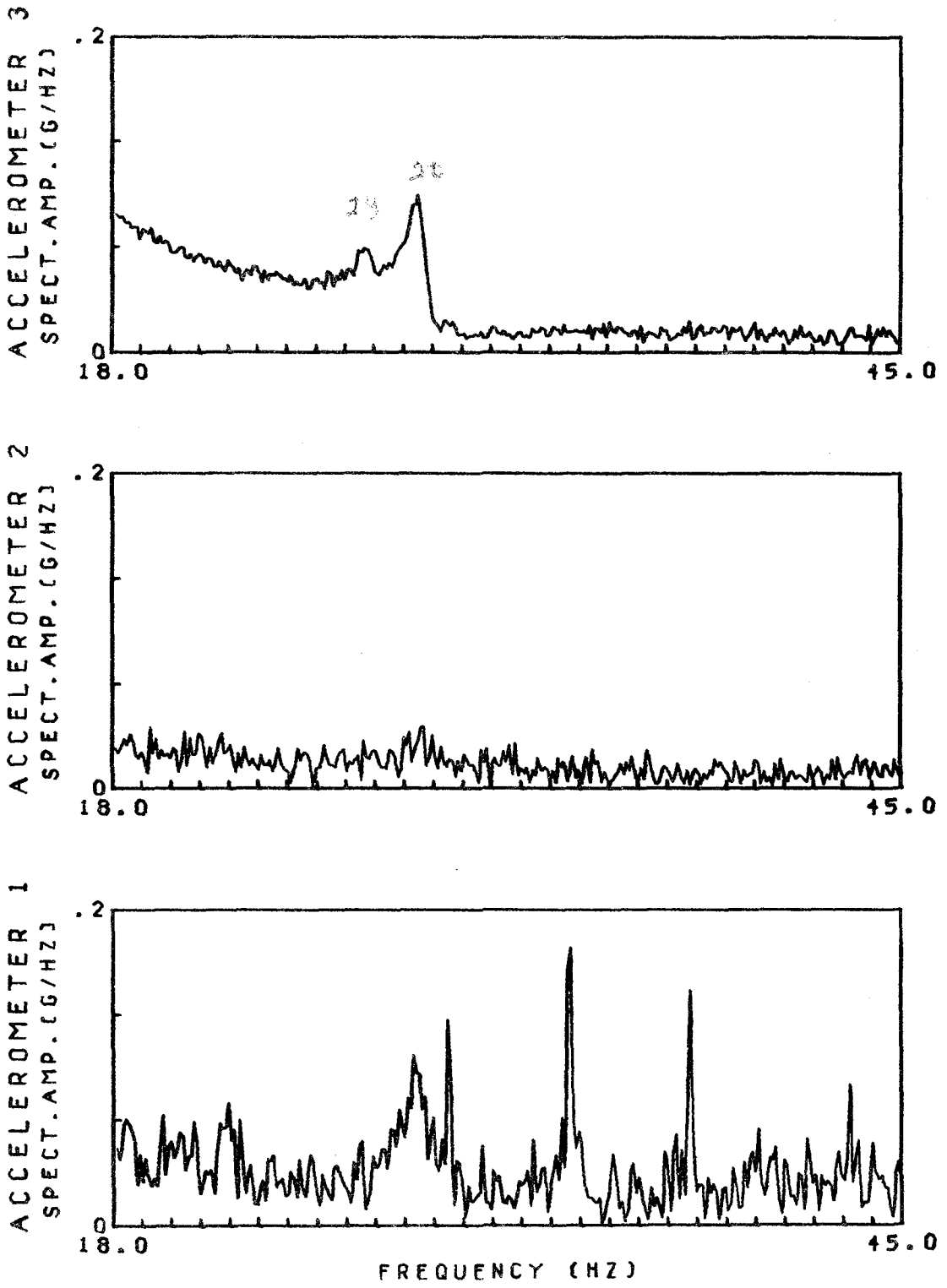

Fig. 4.7 TRANSIENT RESPONSE SPECTRA; MAXIMUM DECK MASS CASE, Y-DIRECTION SHOCK ON DECK SIDE (S-Y, TEST 144)

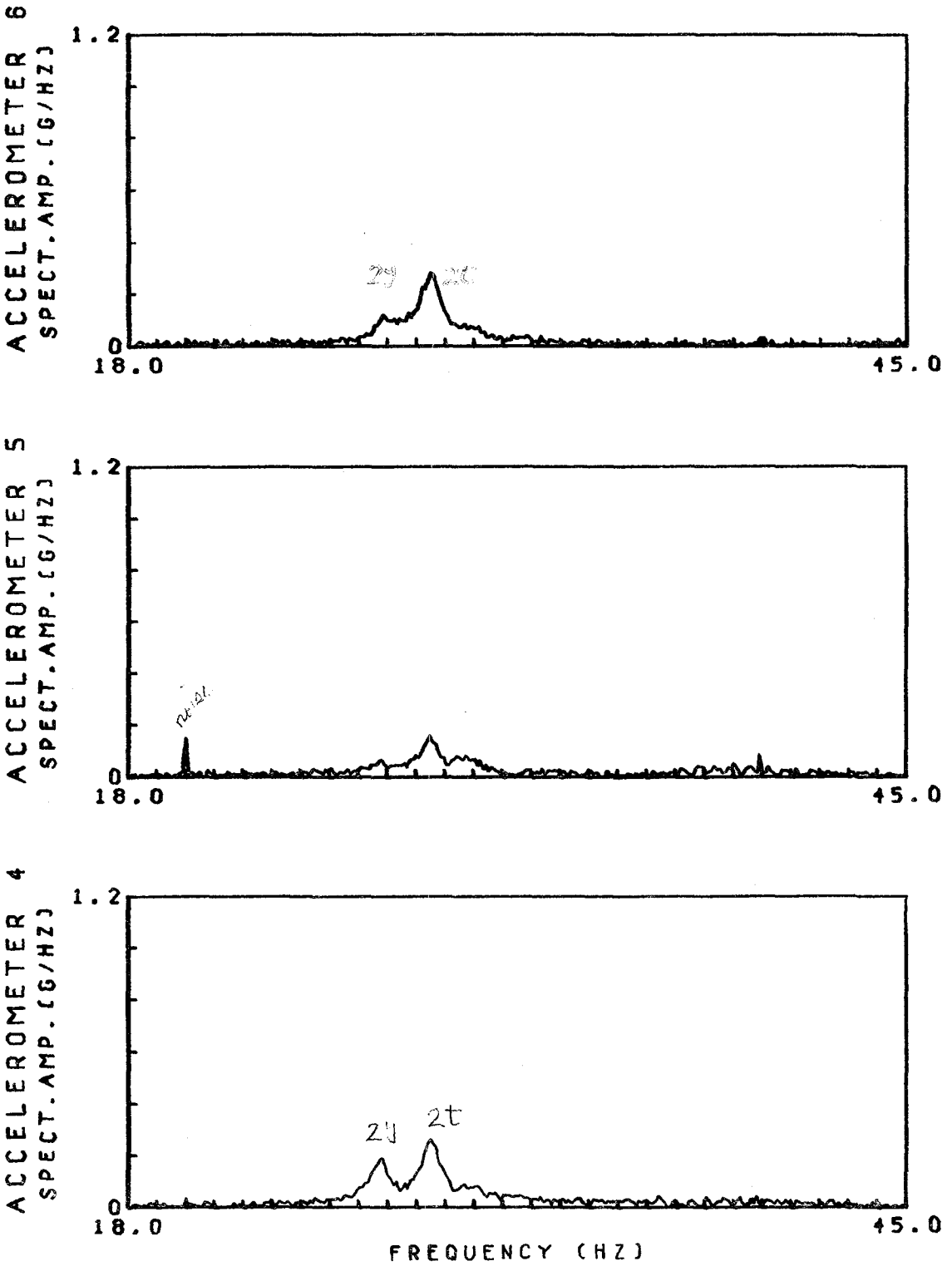

Fig. 4.8 TRANSIENT RESPONSE SPECTRA; MAXIMUM DECK MASS CASE, Y-DIRECTION SHOCK ON DECK SIDE (S-Y, TEST 144)

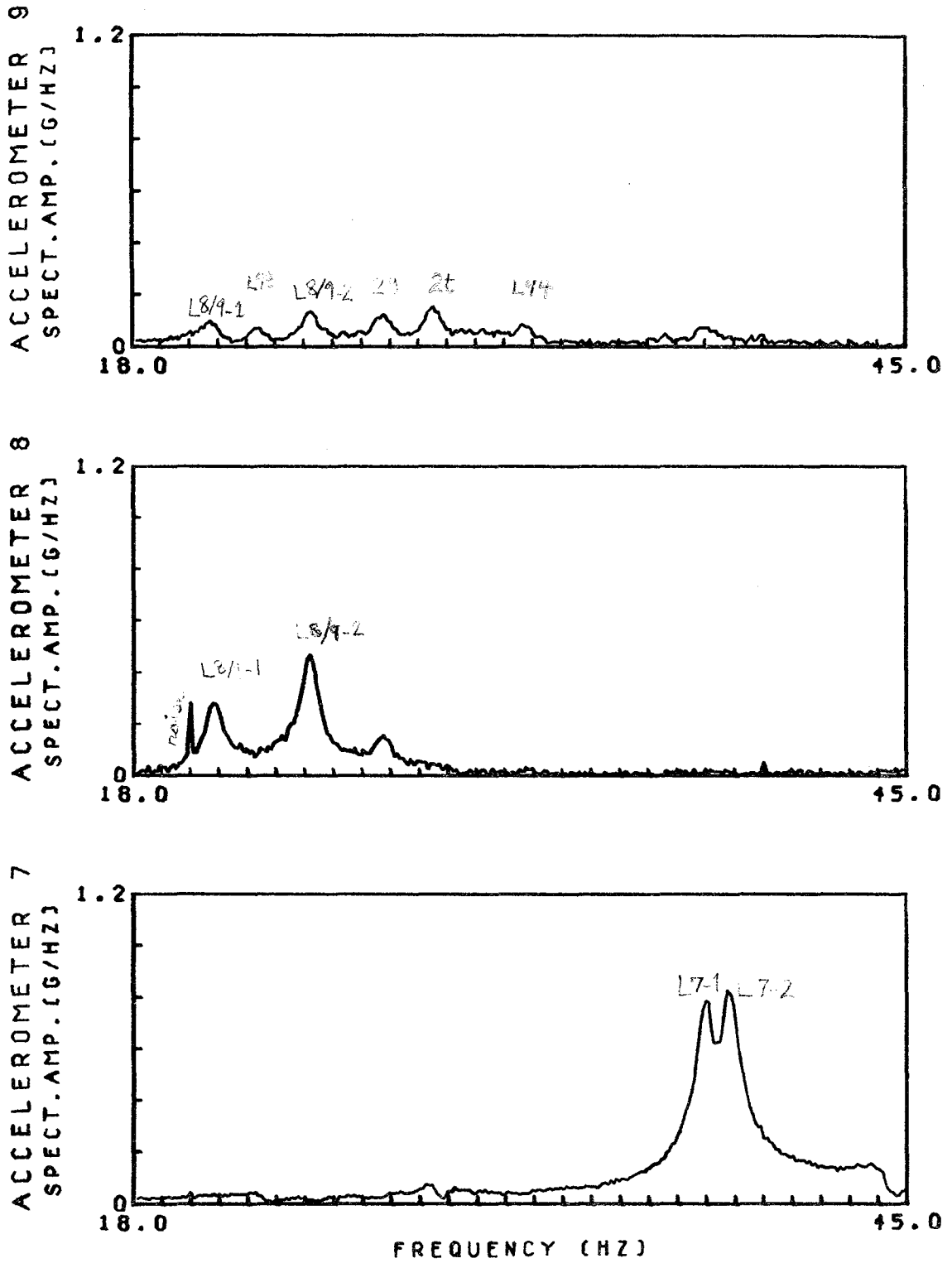

Fig. 4.9 TRANSIENT RESPONSE SPECTRA; MAXIMUM DECK MASS CASE, Y-DIRECTION SHOCK ON DECK SIDE (S-Y, TEST 144)

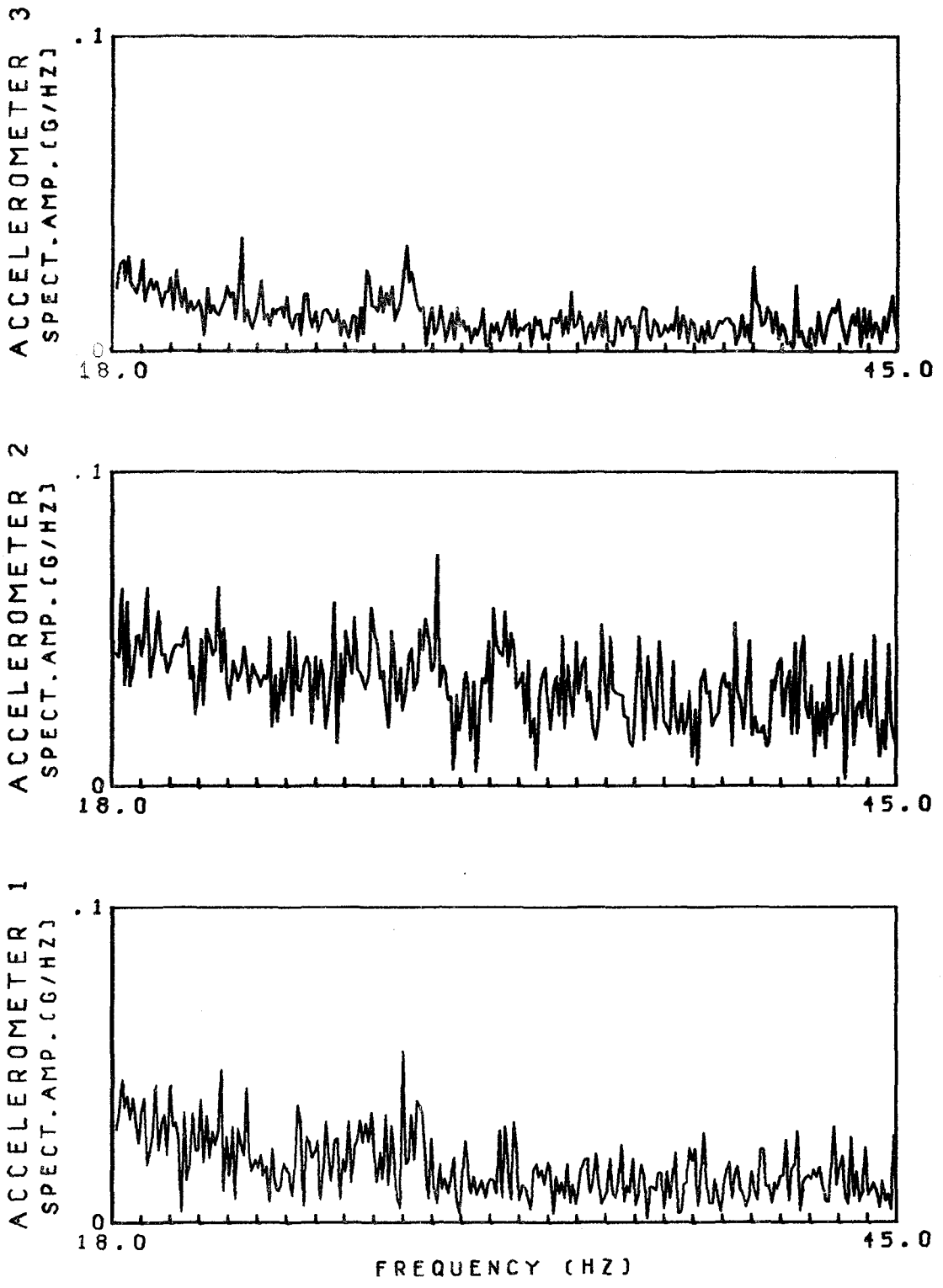

Fig. 4.10 TRANSIENT RESPONSE SPECTRA; MAXIMUM DECK MASS CASE, X-DIRECTION SHOCK ON DECK SIDE (S-X, TEST 147)

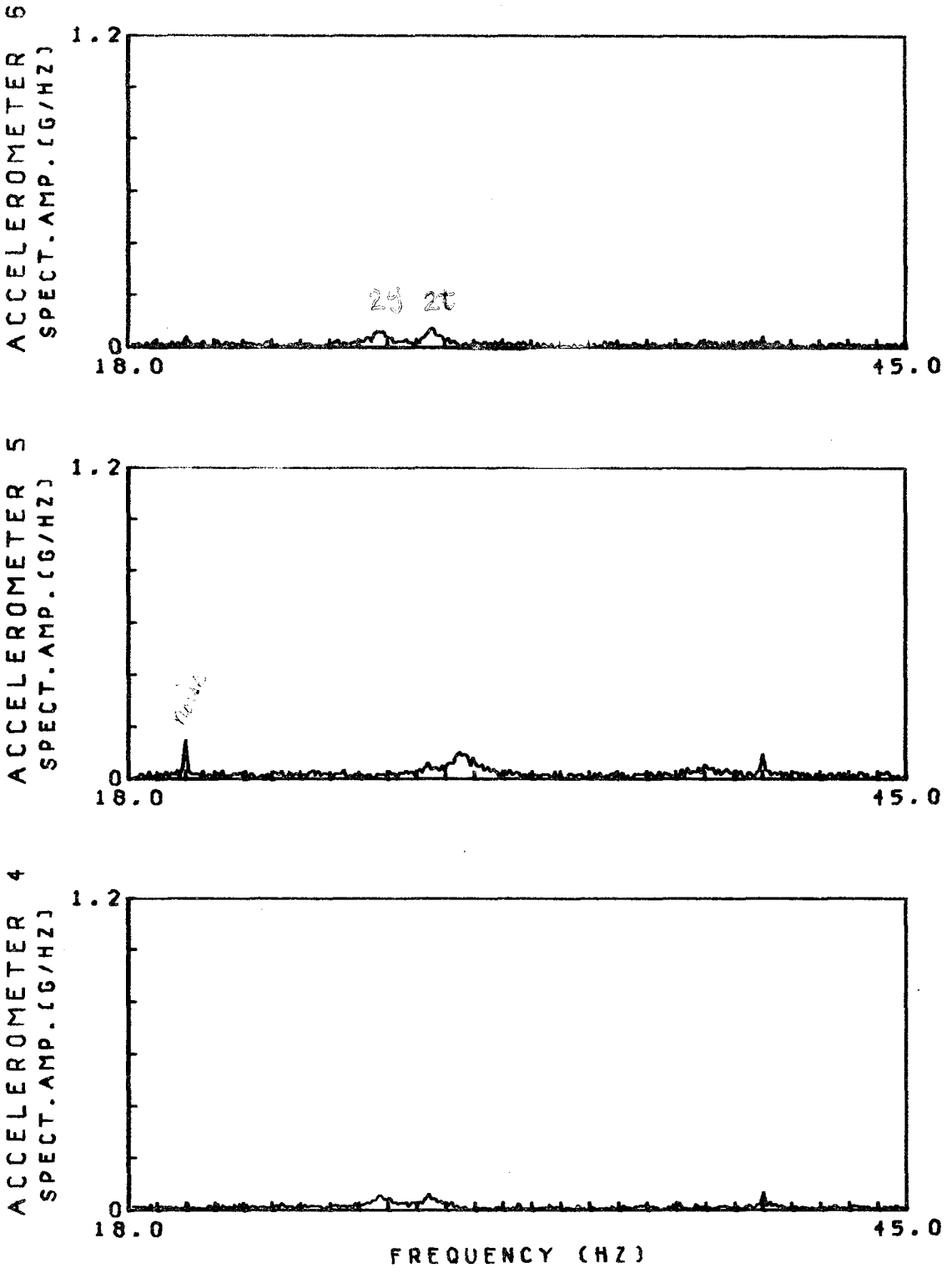

Fig. 4.11 TRANSIENT RESPONSE SPECTRA; MAXIMUM DECK MASS CASE, X-DIRECTION SHOCK ON DECK SIDE (S-X, TEST 147)

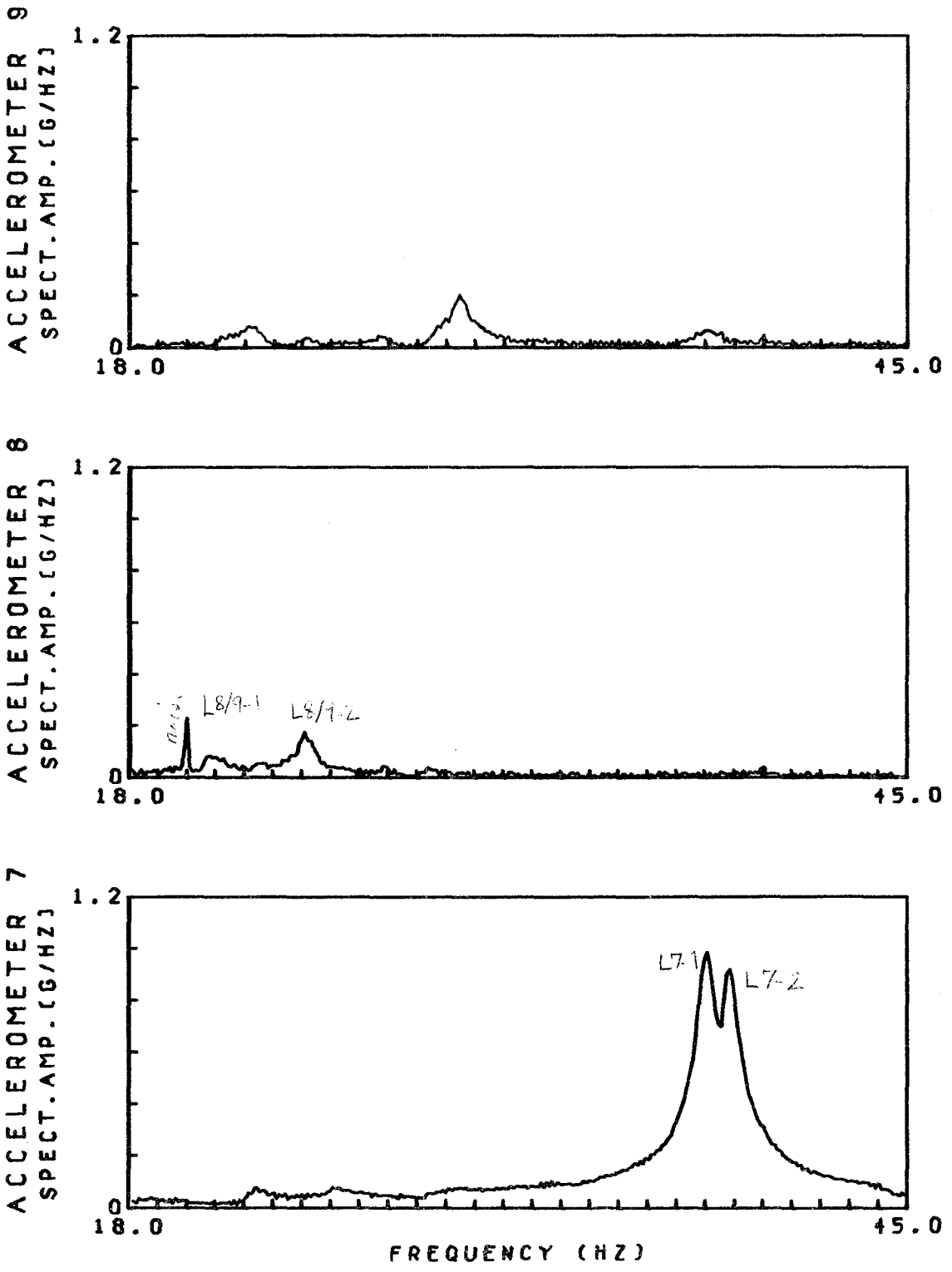

Fig. 4.12 TRANSIENT RESPONSE SPECTRA; MAXIMUM DECK MASS CASE, X-DIRECTION SHOCK ON DECK SIDE (S-X, TEST 147)

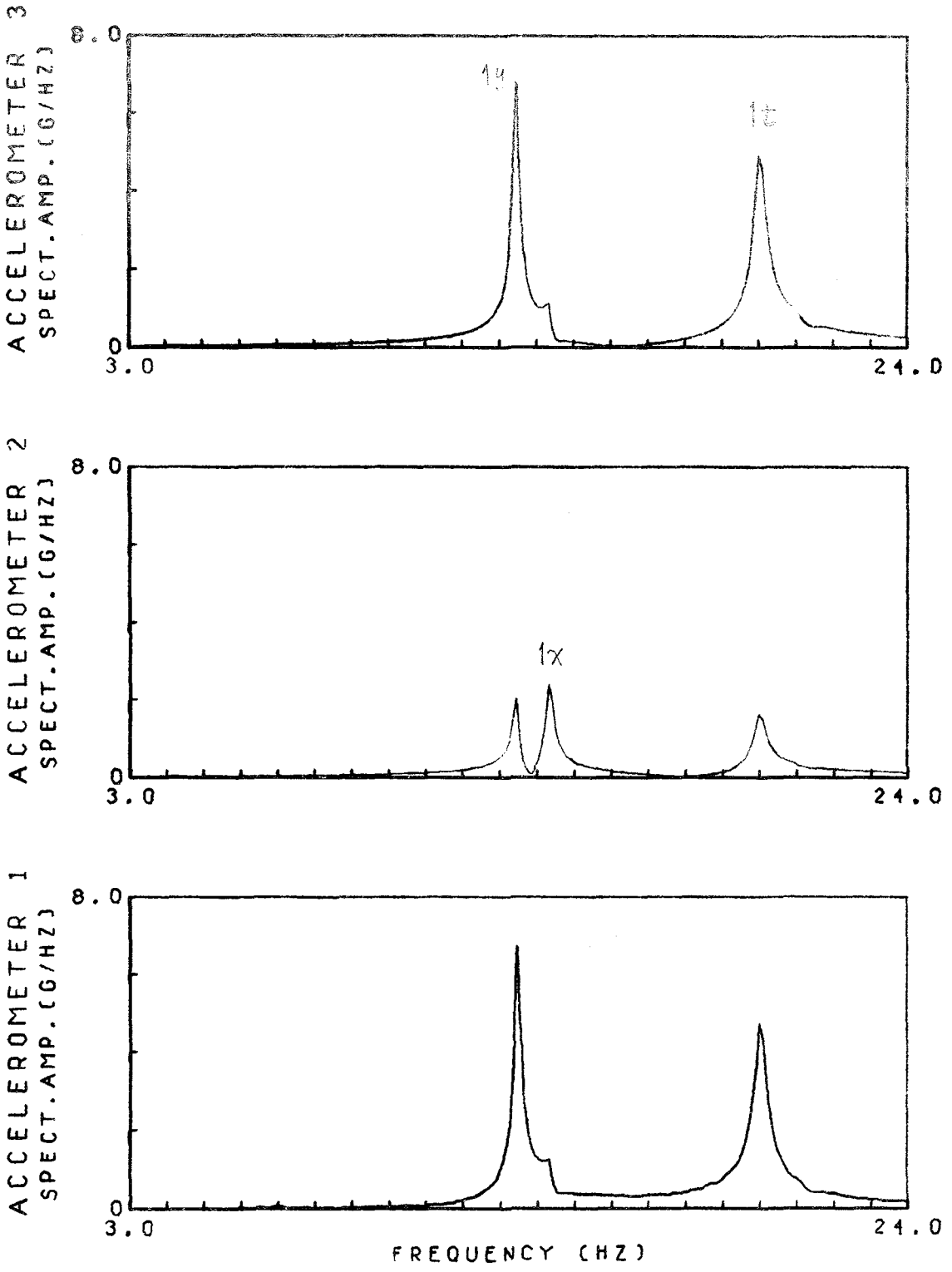

Fig. 4.13 TRANSIENT RESPONSE SPECTRA; MINIMUM DECK MASS CASE, Y-DIRECTION SHOCK ON DECK SIDE (S-Y, TEST 137)

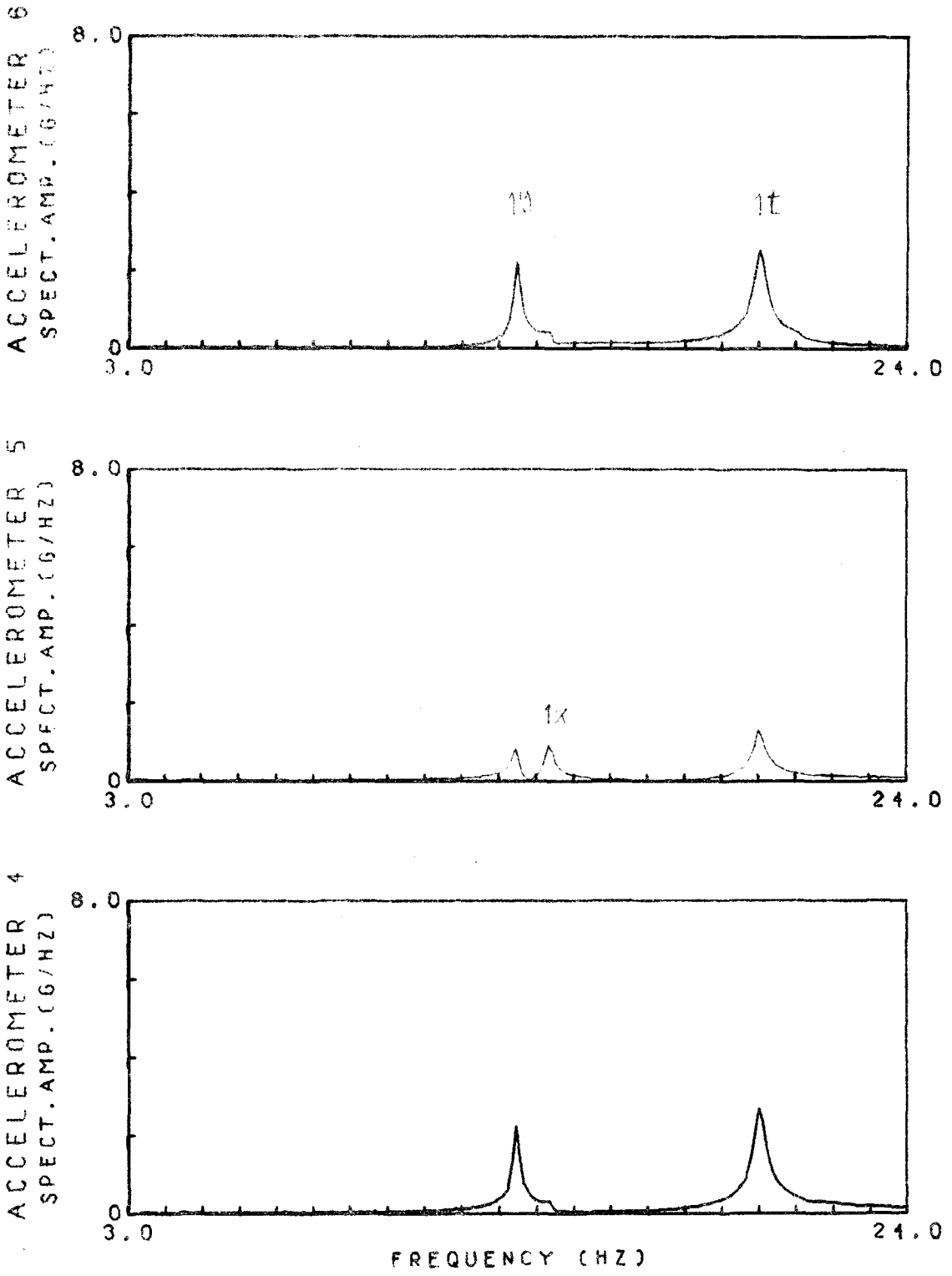

Fig. 4.14 TRANSIENT RESPONSE SPECTRA; MINIMUM DECK MASS CASE, Y-DIRECTION SHOCK ON DECK SIDE (S-Y, TEST 137)

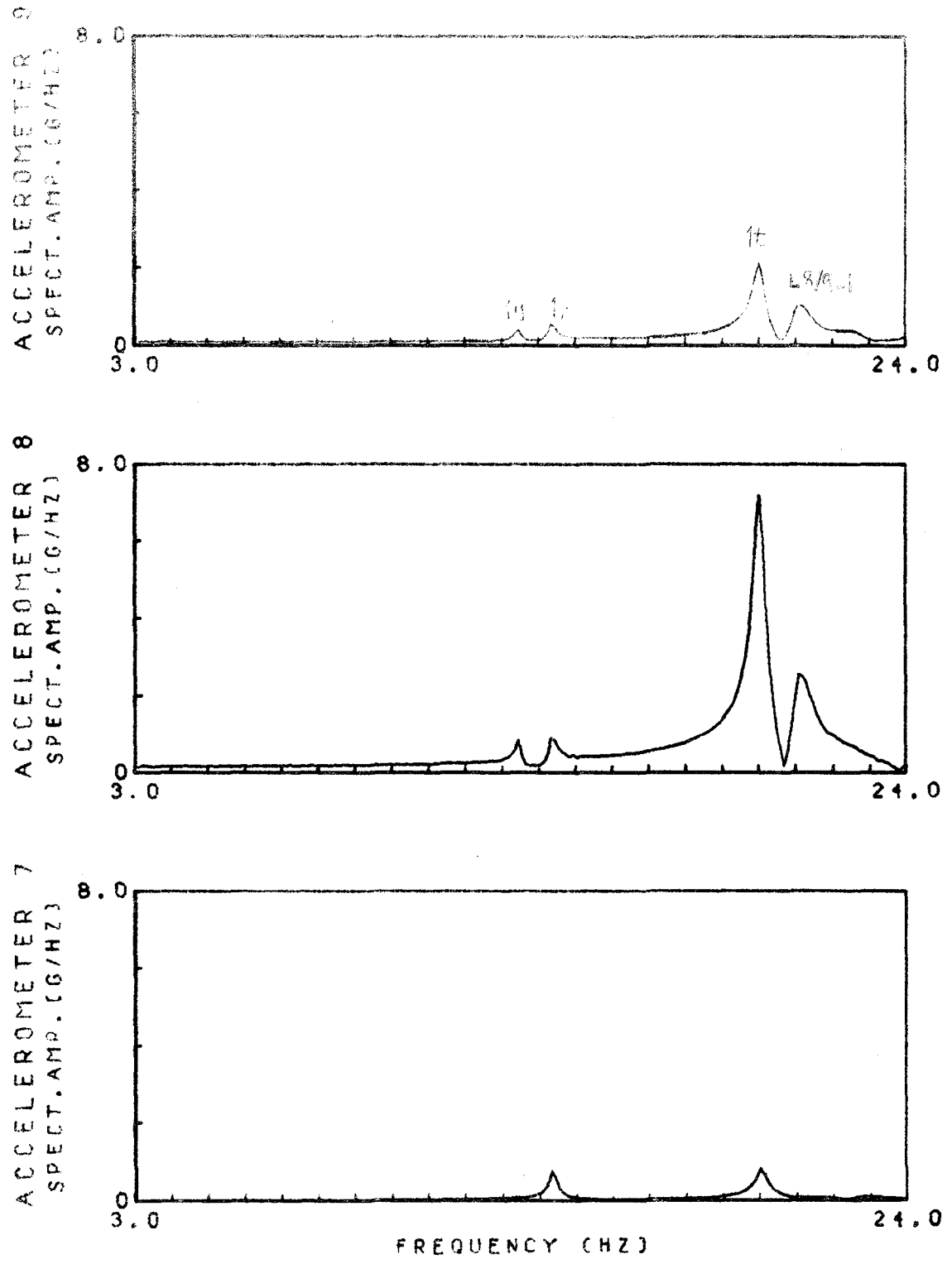

Fig. 4.15 TRANSIENT RESPONSE SPECTRA; MINIMUM DECK MASS CASE, Y-DIRECTION SHOCK ON DECK SIDE (S-Y, TEST 137)

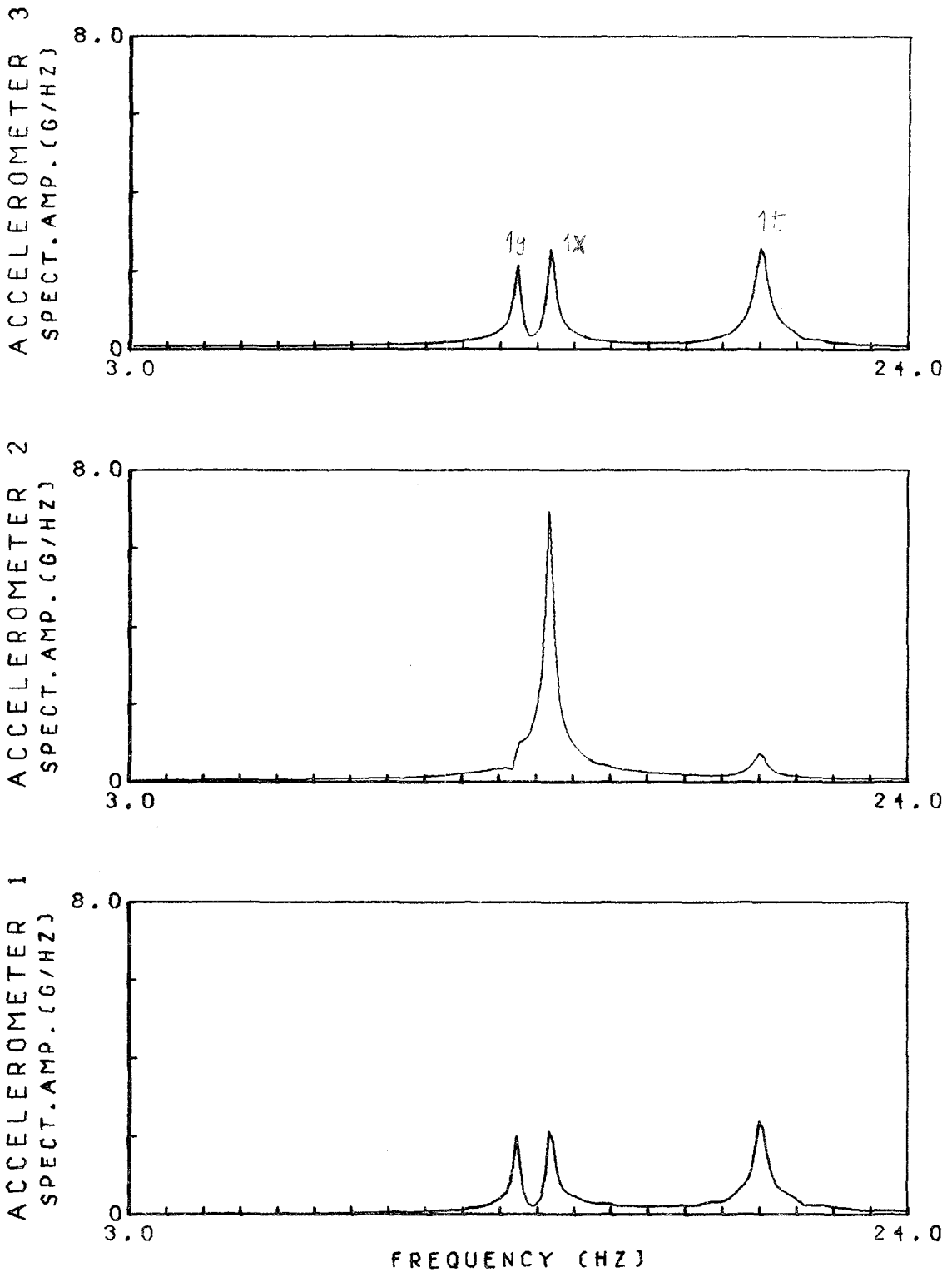

Fig. 4.16 TRANSIENT RESPONSE SPECTRA; MINIMUM DECK MASS CASE, X-DIRECTION SHOCK ON DECK SIDE (S-X, TEST 143)

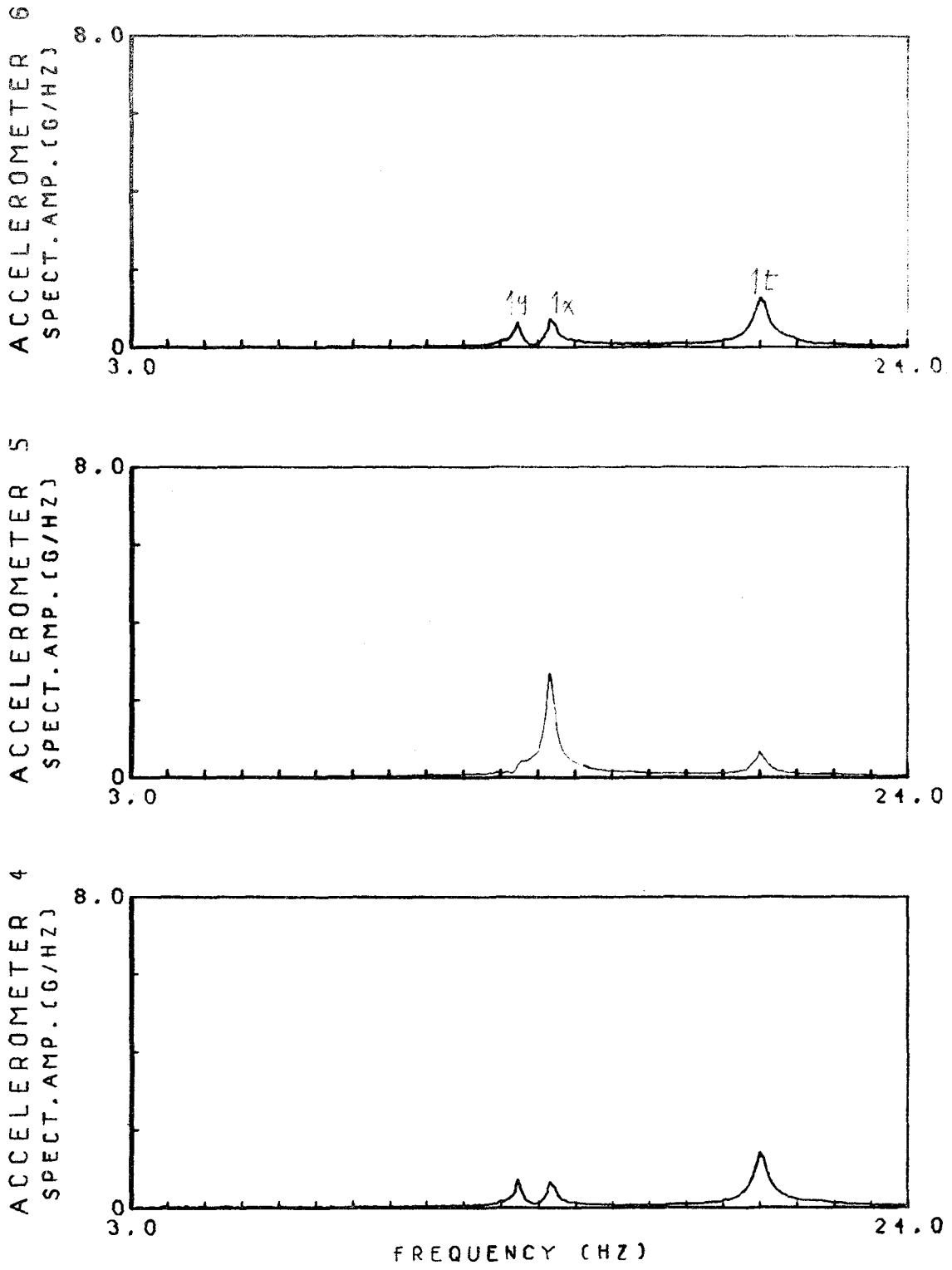

Fig. 4.17 TRANSIENT RESPONSE SPECTRA; MINIMUM DECK MASS CASE, X-DIRECTION SHOCK ON DECK SIDE (S-X, TEST 143)

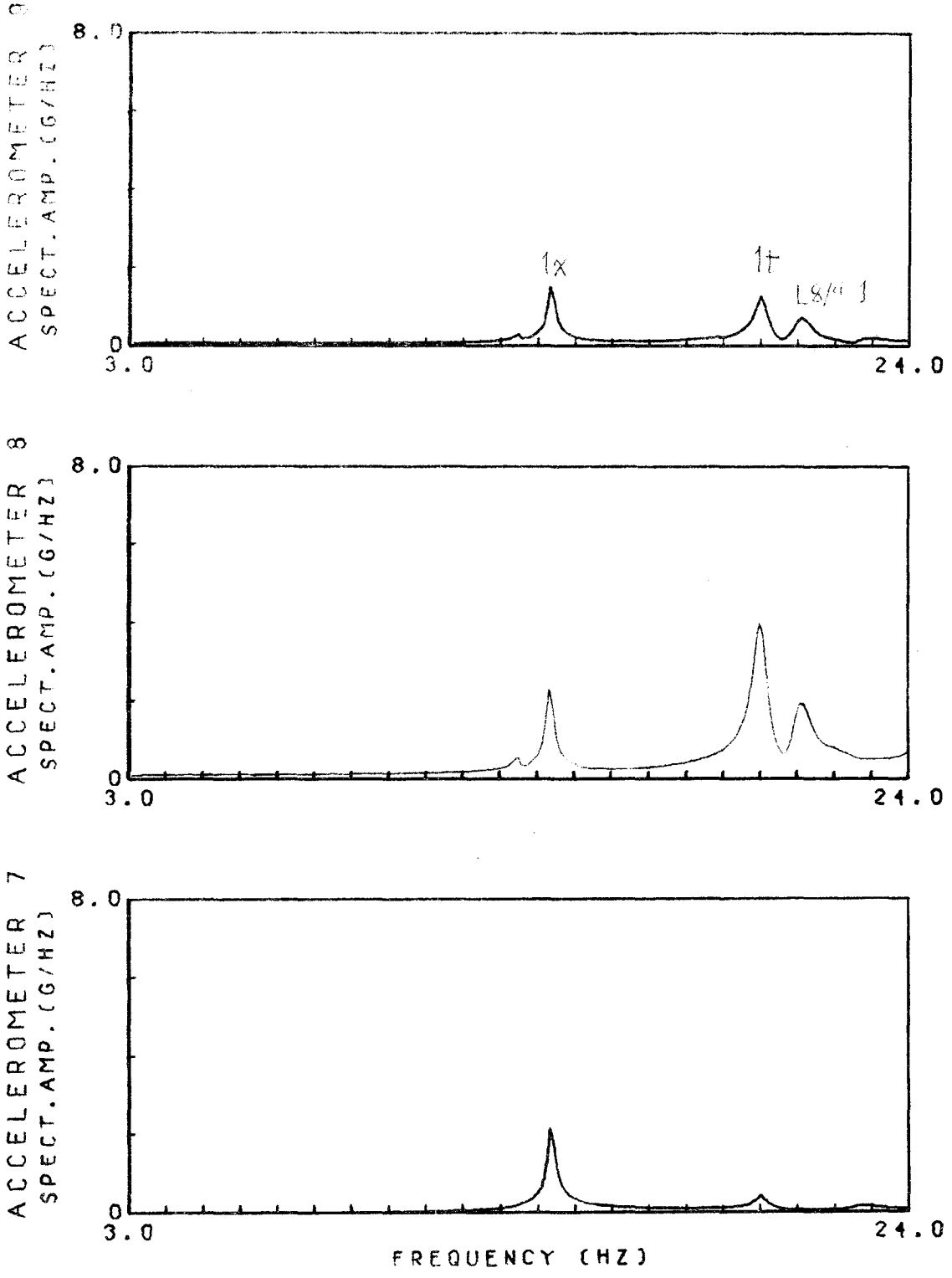

Fig. 4.18 TRANSIENT RESPONSE SPECTRA; MINIMUM DECK MASS CASE, X-DIRECTION SHOCK ON DECK SIDE (S-X, TEST 143)

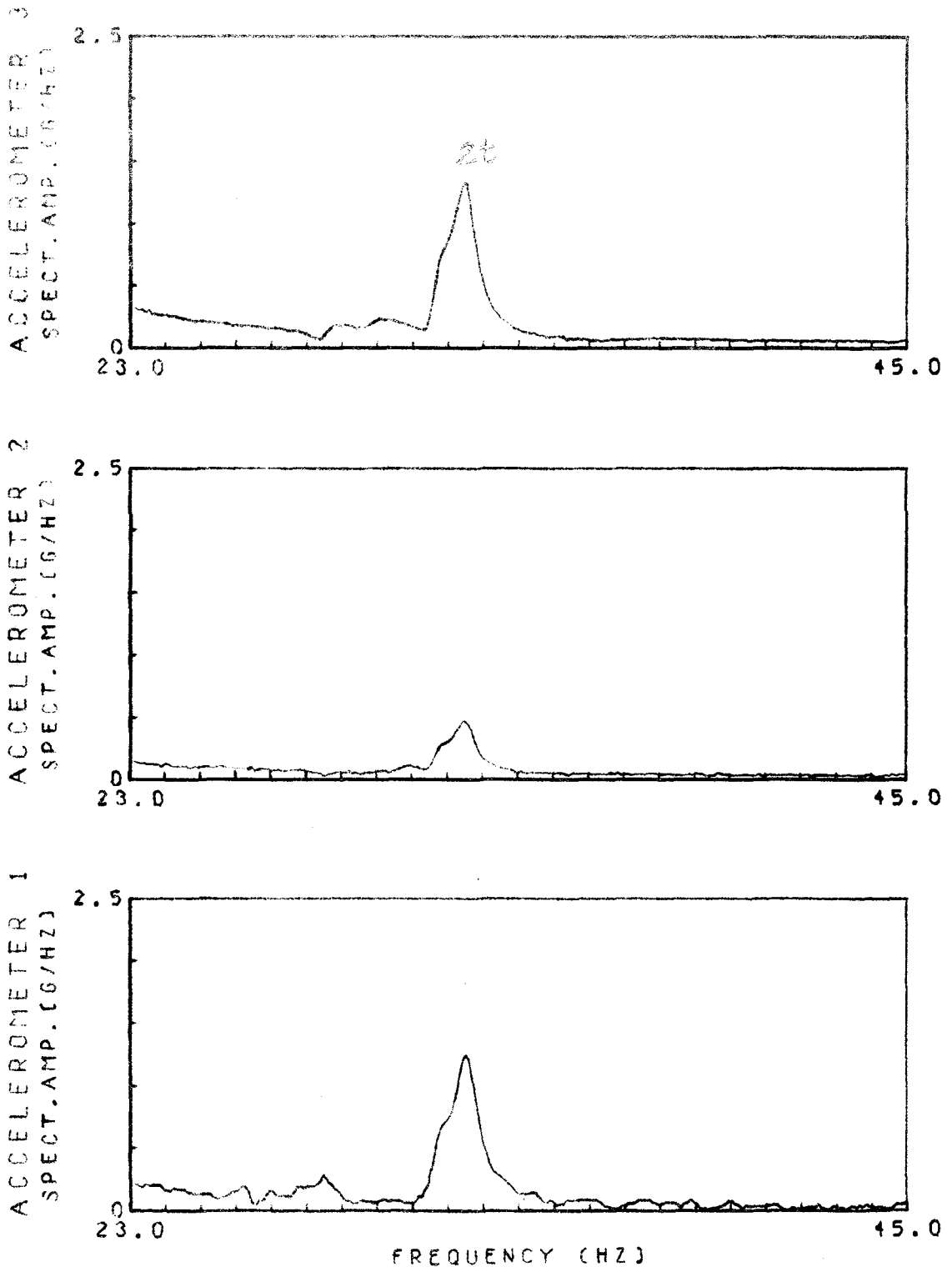

Fig. 4.19 TRANSIENT RESPONSE SPECTRA; MINIMUM DECK MASS CASE, Y-DIRECTION SHOCK ON DECK SIDE (S-Y, TEST 137)

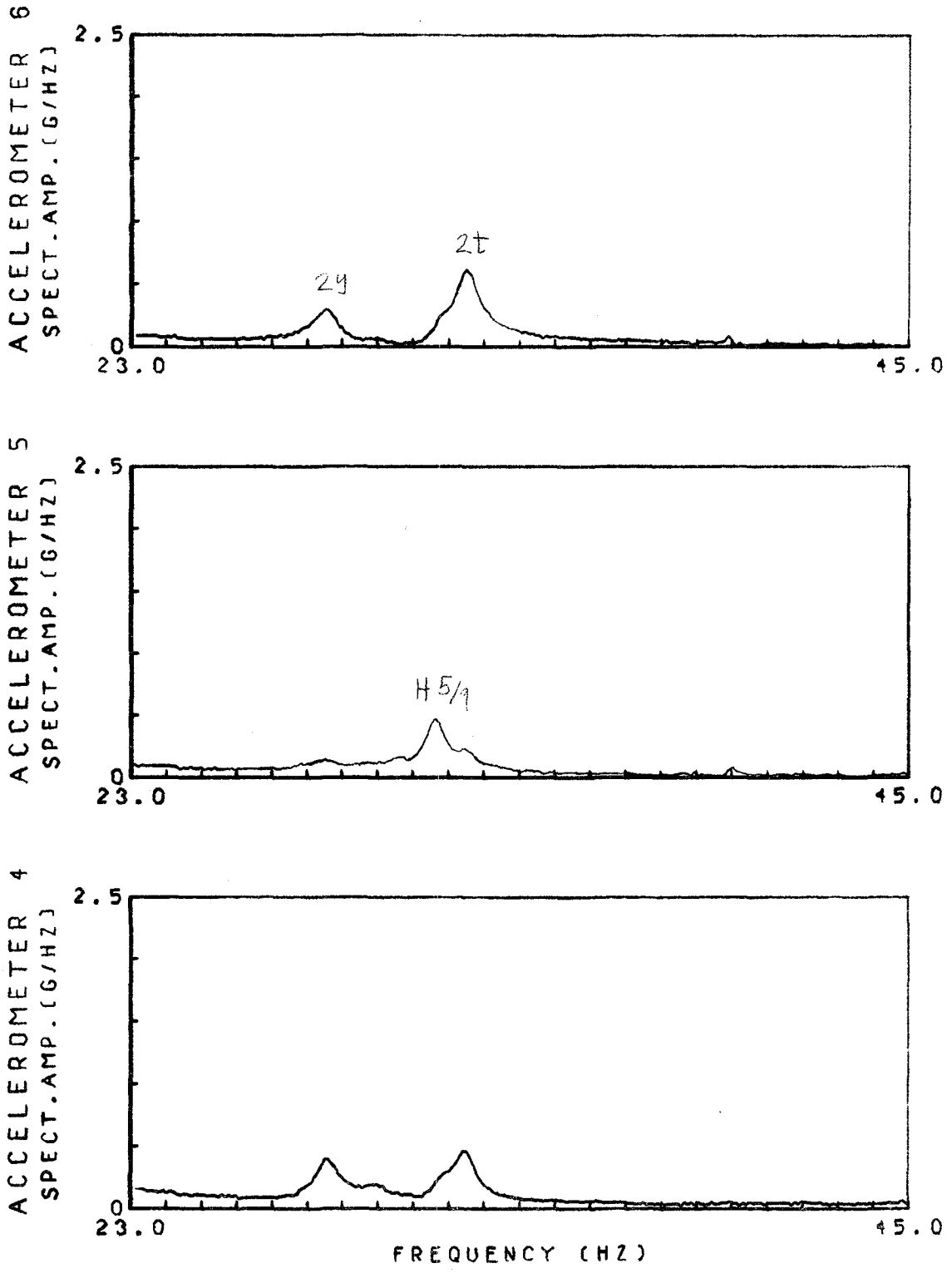

Fig. 4.20 TRANSIENT RESPONSE SPECTRA; MINIMUM DECK MASS CASE, Y-DIRECTION SHOCK ON DECK SIDE (S-Y, TEST 137)

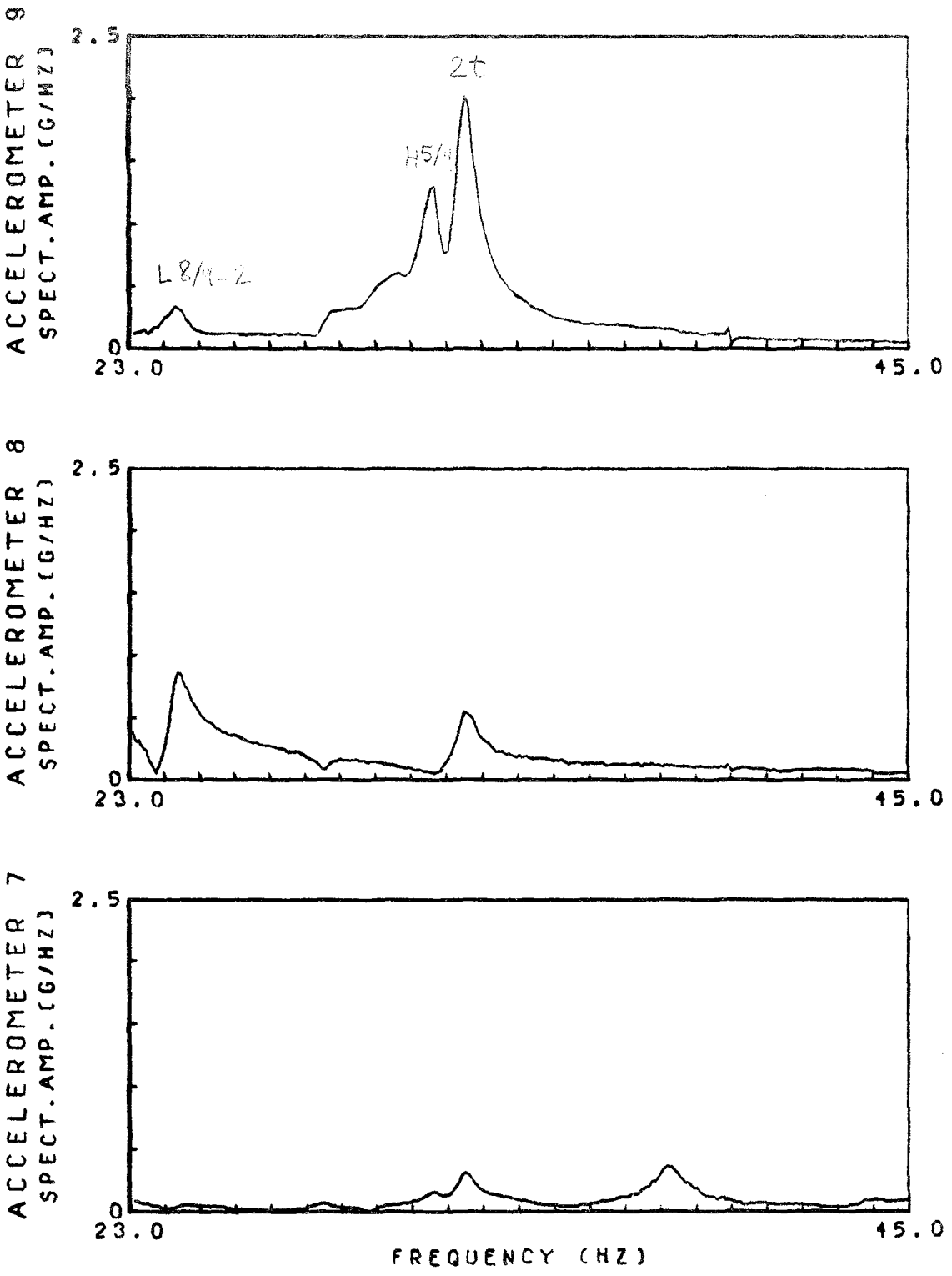

Fig. 4.21 TRANSIENT RESPONSE SPECTRA; MINIMUM DECK MASS CASE, Y-DIRECTION SHOCK ON DECK SIDE (S-Y, TEST 137)

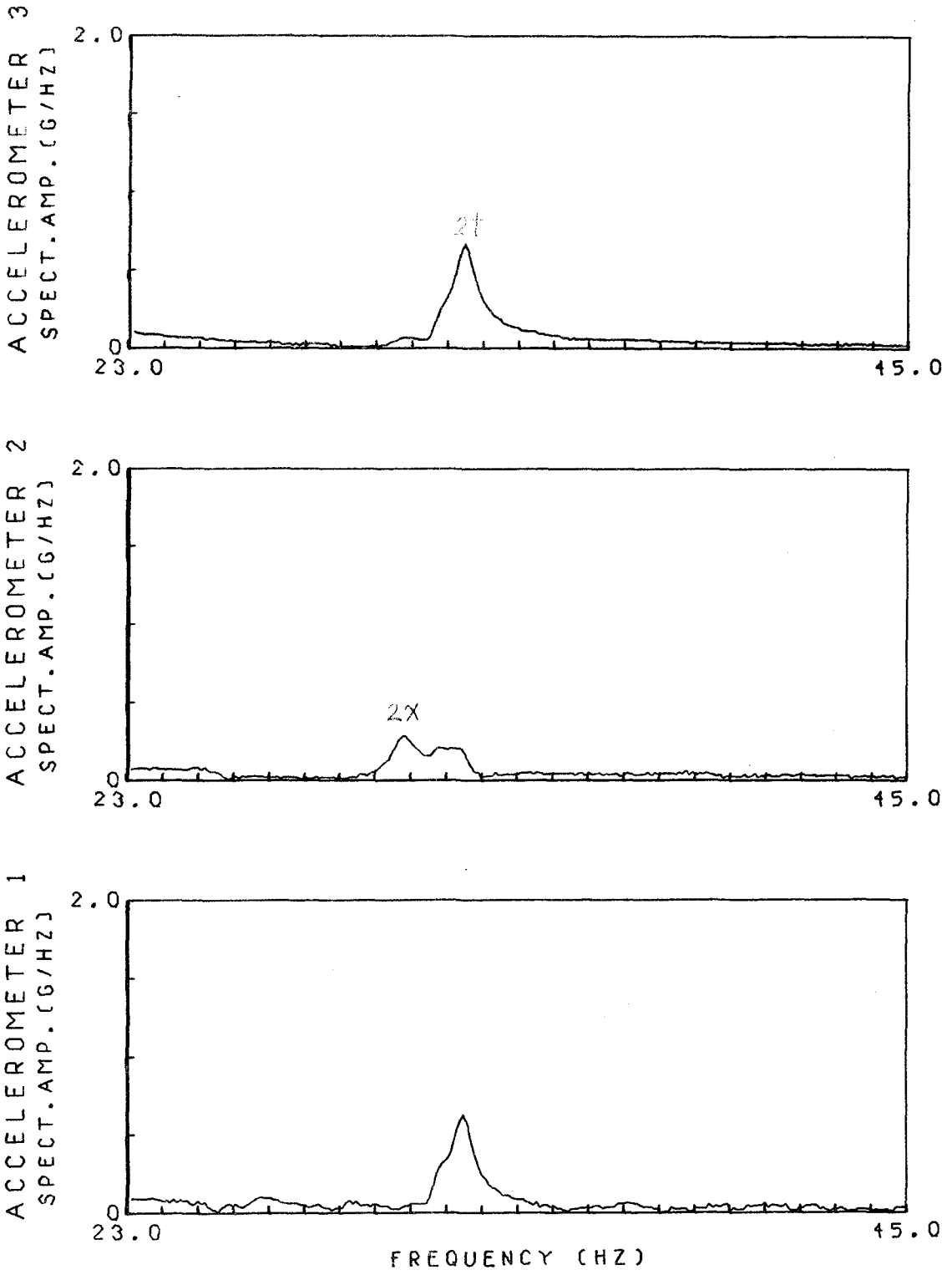

Fig. 4.22 TRANSIENT RESPONSE SPECTRA; MINIMUM DECK MASS CASE, X-DIRECTION SHOCK ON DECK SIDE (S-X, TEST 143)

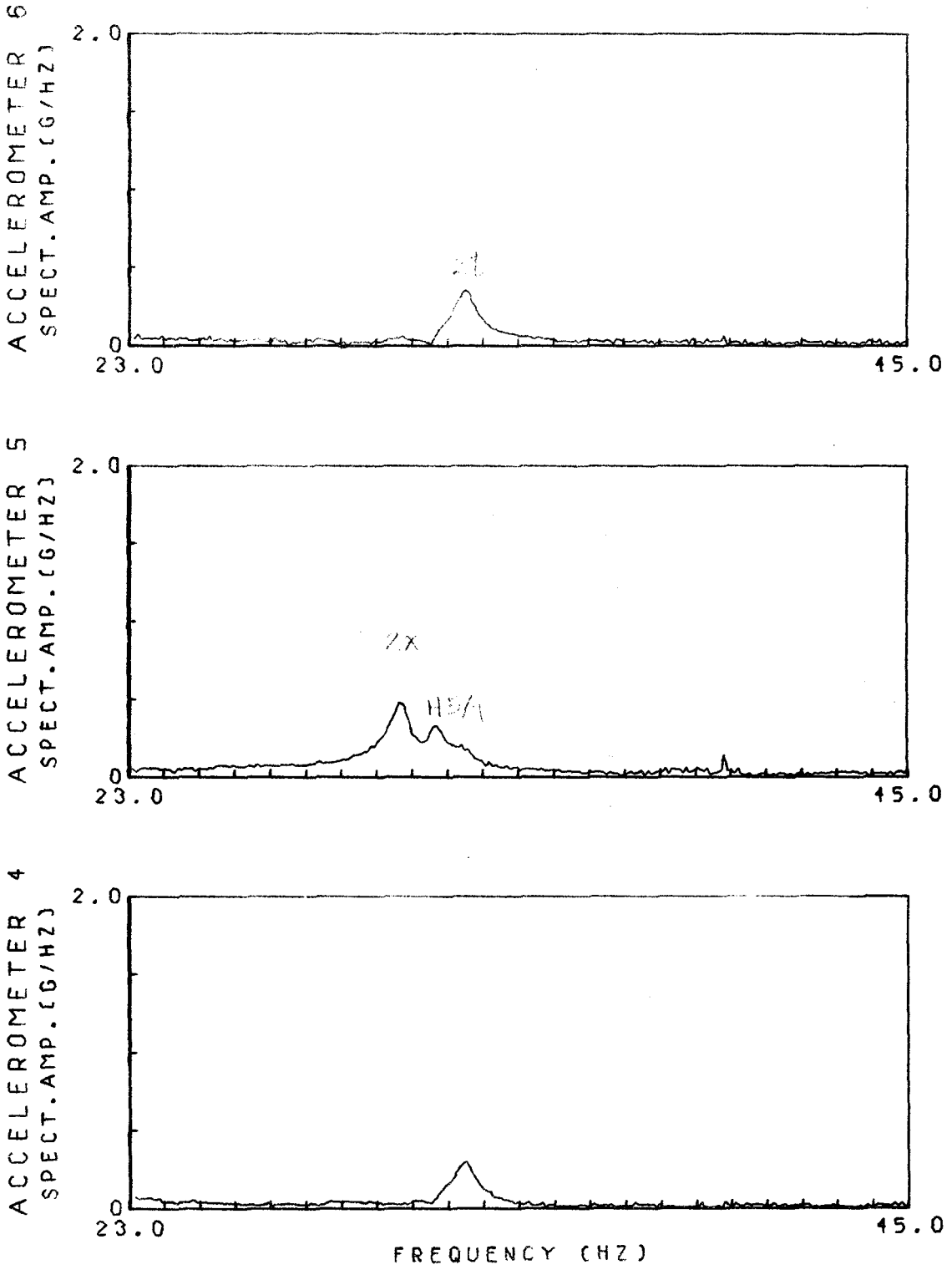

Fig. 4.23 TRANSIENT RESPONSE SPECTRA; MINIMUM DECK MASS CASE, X-DIRECTION SHOCK ON DECK SIDE (S-X, TEST 143)

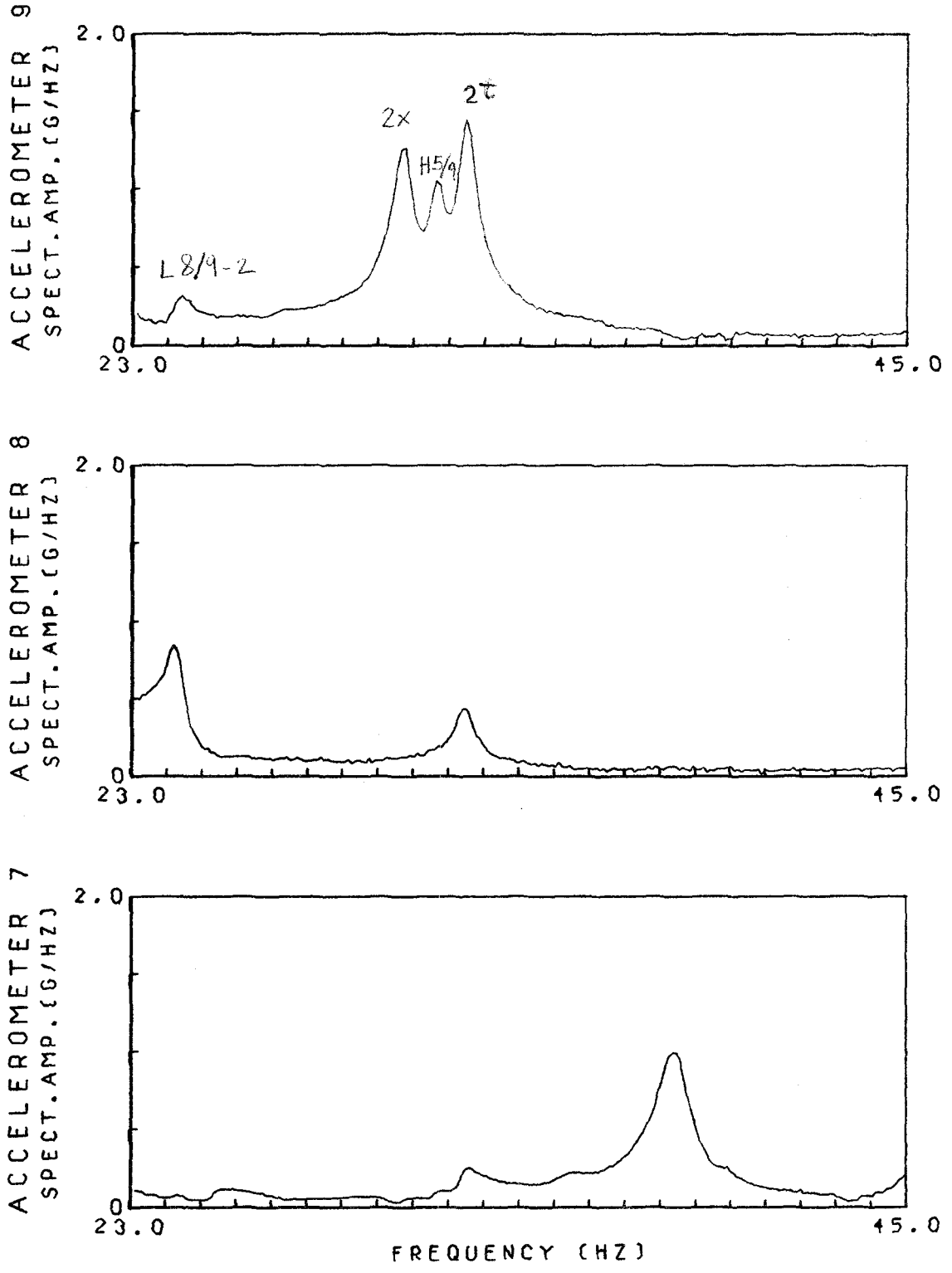

Fig. 4.24 TRANSIENT RESPONSE SPECTRA; MINIMUM DECK MASS CASE, X-DIRECTION SHOCK ON DECK SIDE (S-X, TEST 143)

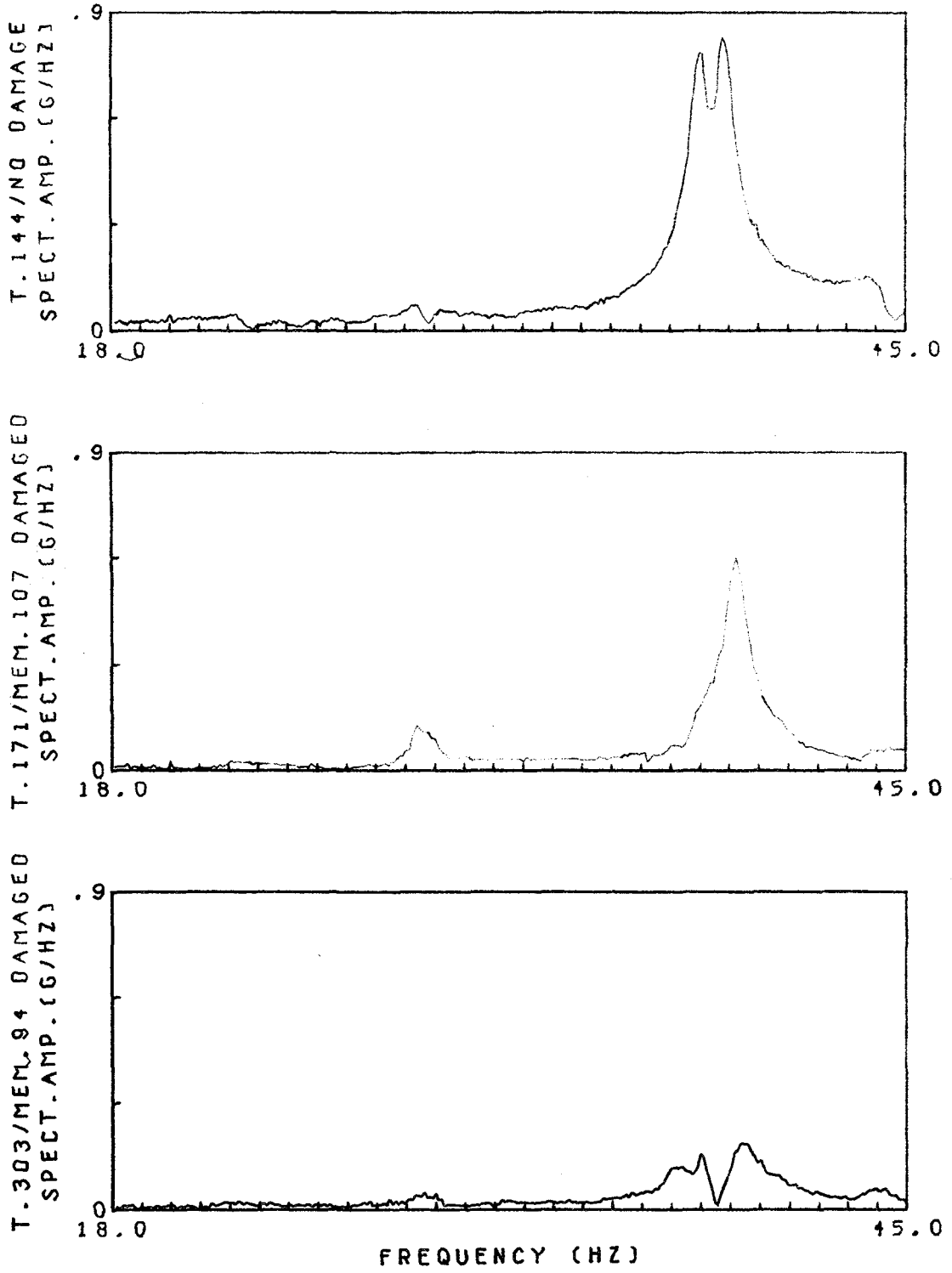

Fig. 4.25 TRANSIENT RESPONSE SPECTRA OF ACCELEROMETER NO.7; MAXIMUM DECK MASS CASE, Y-DIRECTION SHOCK ON DECK SIDE (S-Y TESTS)

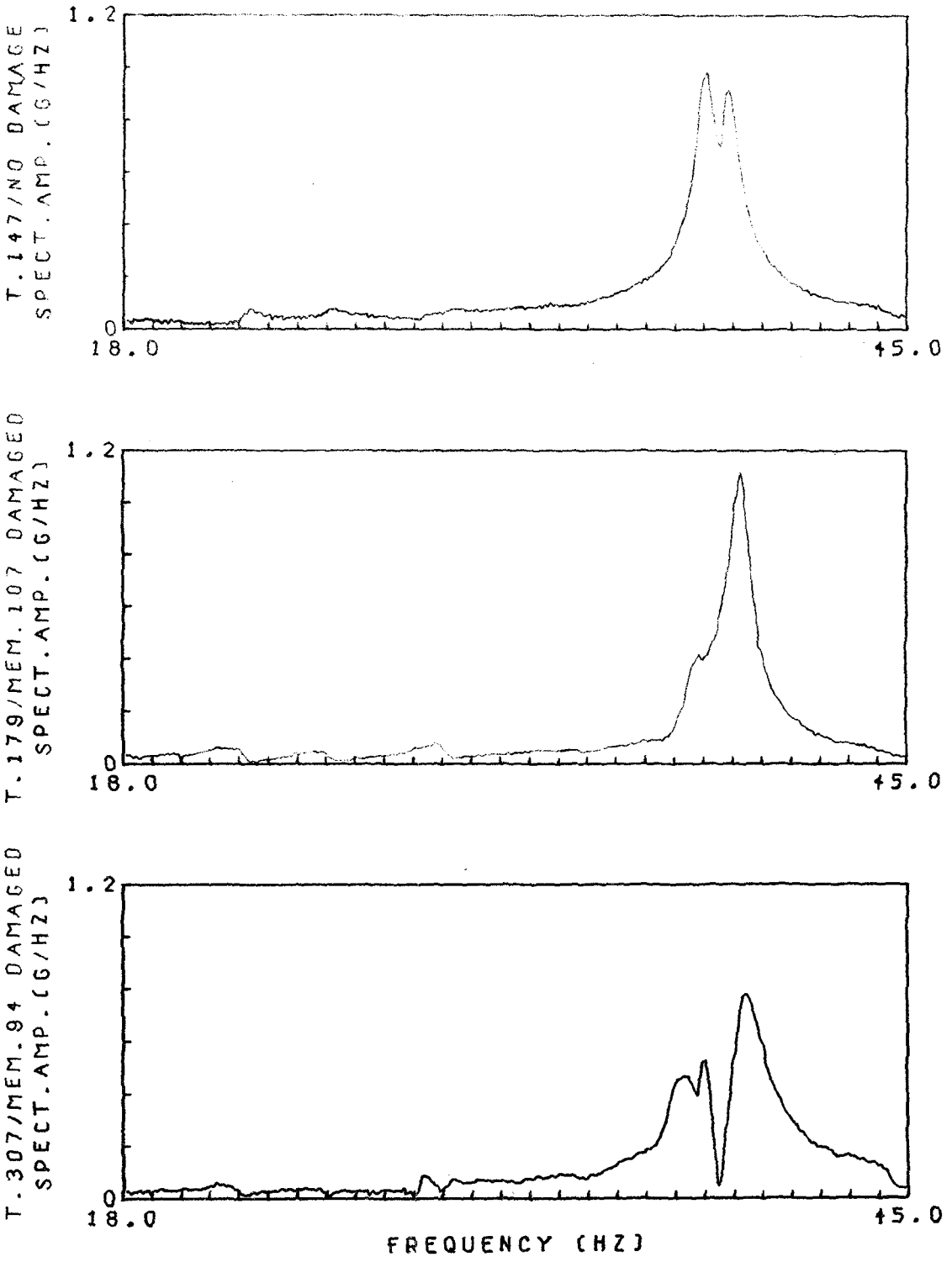

Fig. 4.26 TRANSIENT RESPONSE SPECTRA OF ACCELEROMETER NO.7; MAXIMUM DECK MASS CASE, X-DIRECTION SHOCK ON DECK SIDE (S-X, TESTS)

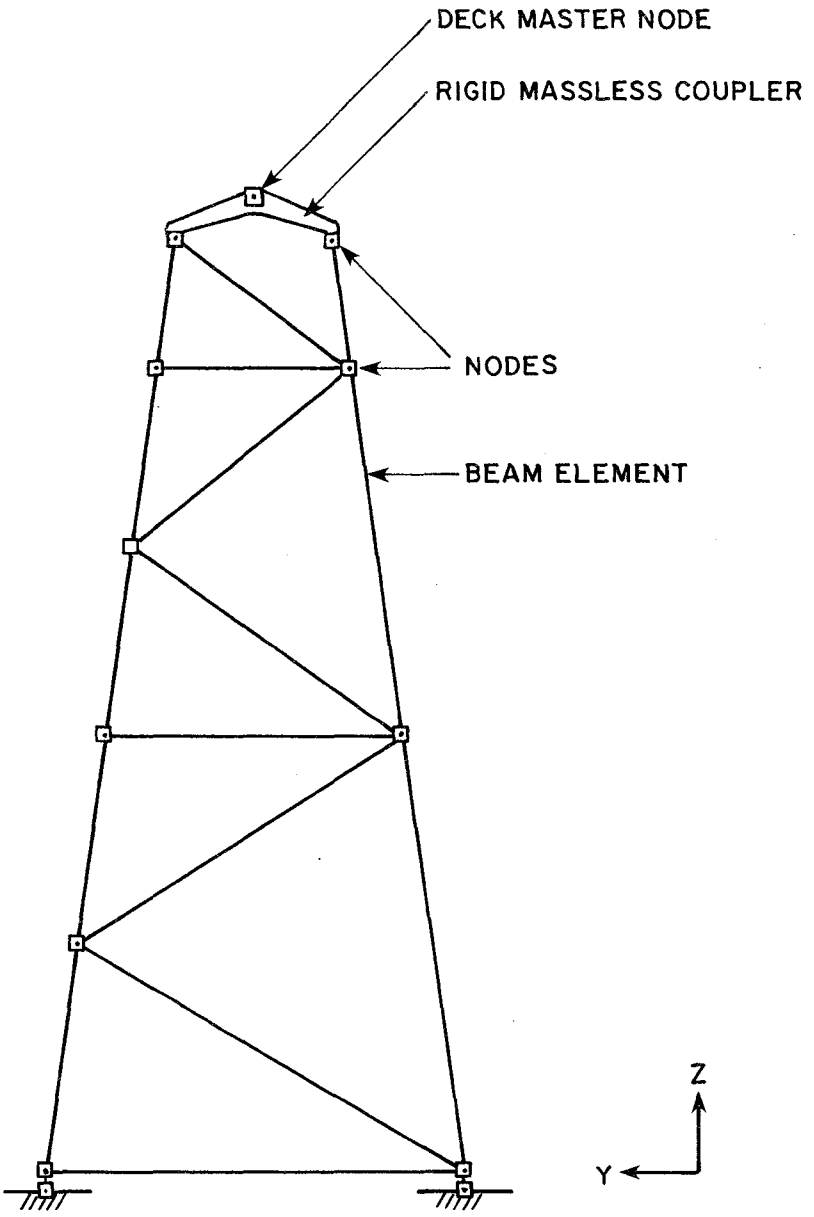

Fig. 5.1 Frame 4 of the structure in the finite element model

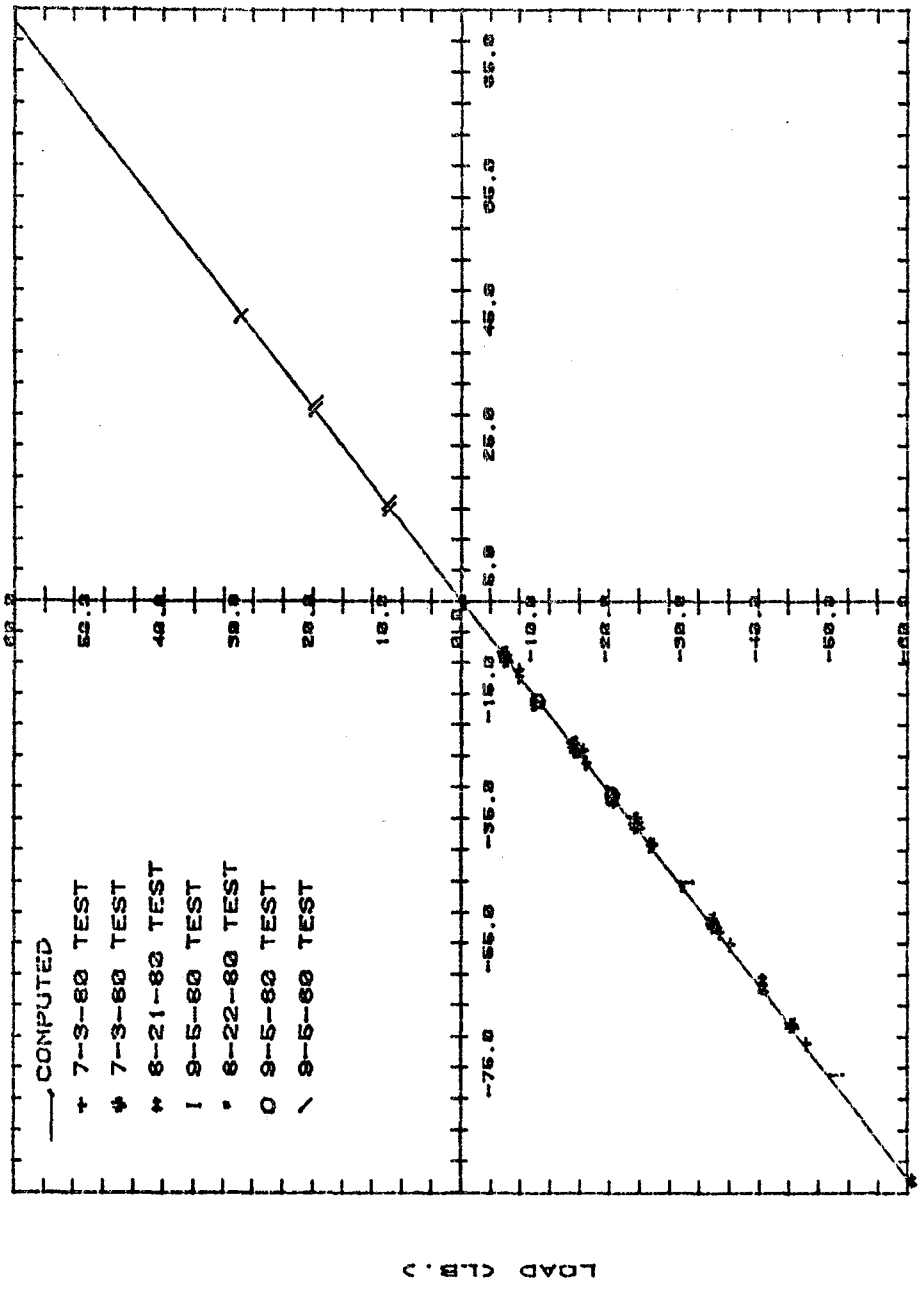

Fig. 5.2 DECK X-LOAD VS. X-DISPLACEMENT

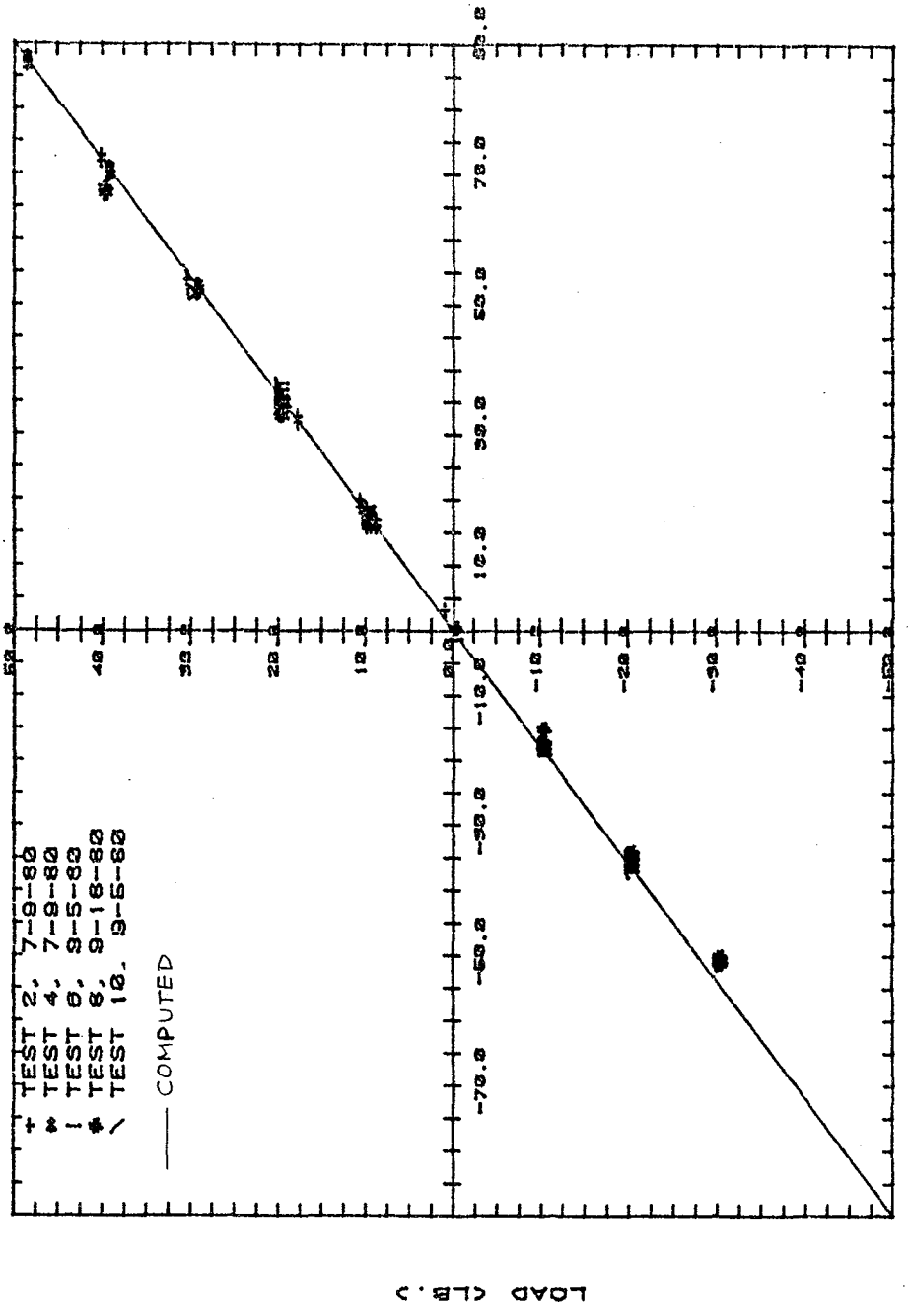

Fig. 5.3 DECK Y-LOAD VS. Y-DISPLACEMENT

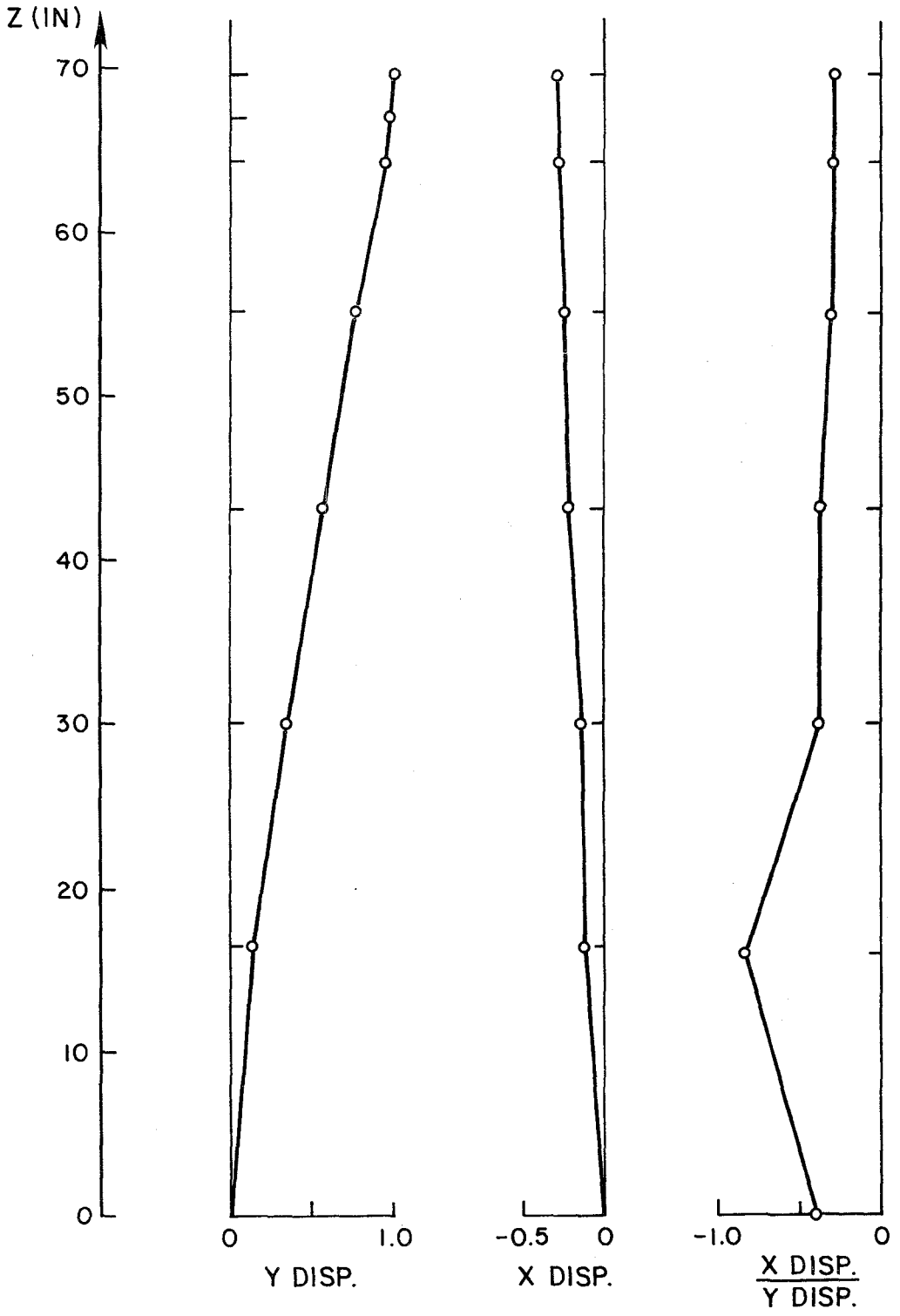

Fig. 5.4 Mode shape 1y, minimum deck mass case

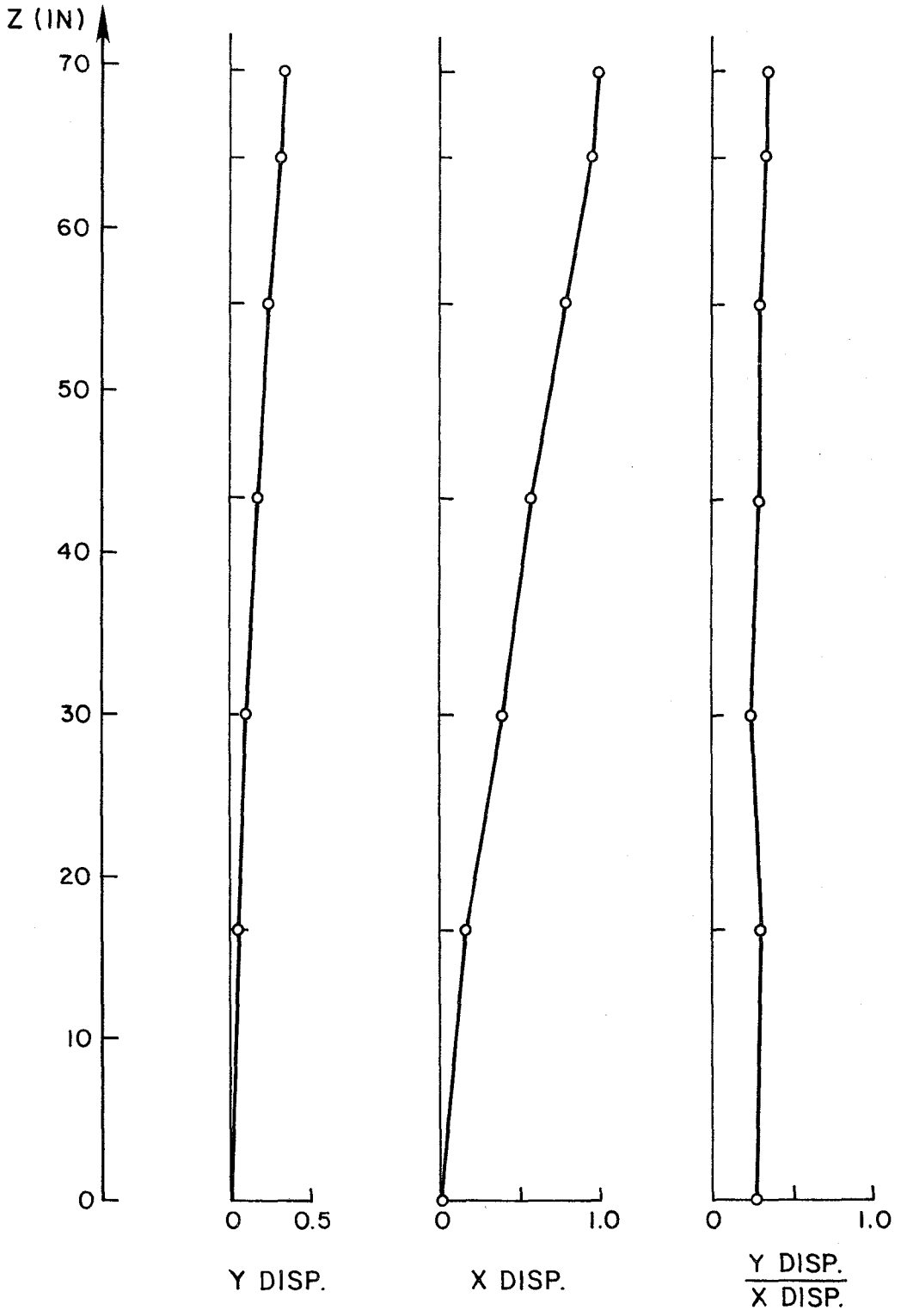

Fig. 5.5 Mode shape 1x, minimum deck mass case

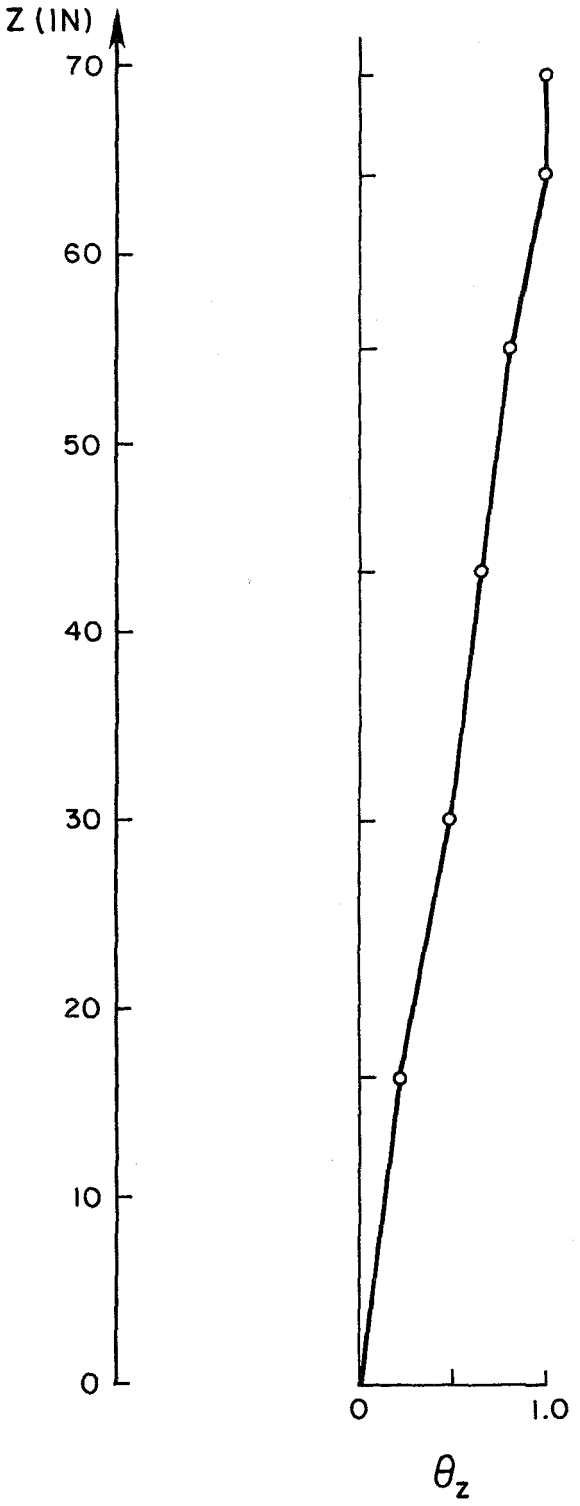

Fig. 5.6 Mode shape 1t, minimum deck mass case

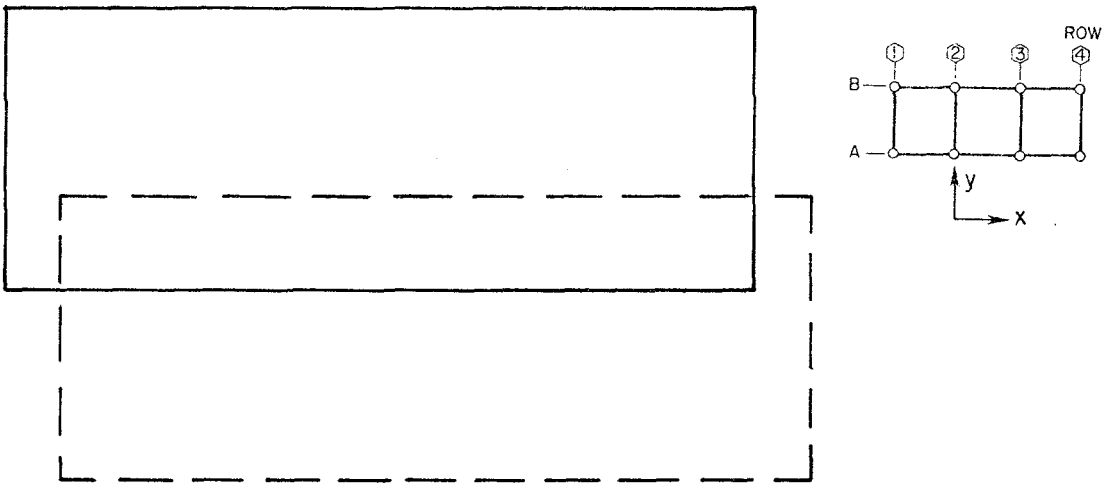

a) Mode 1y

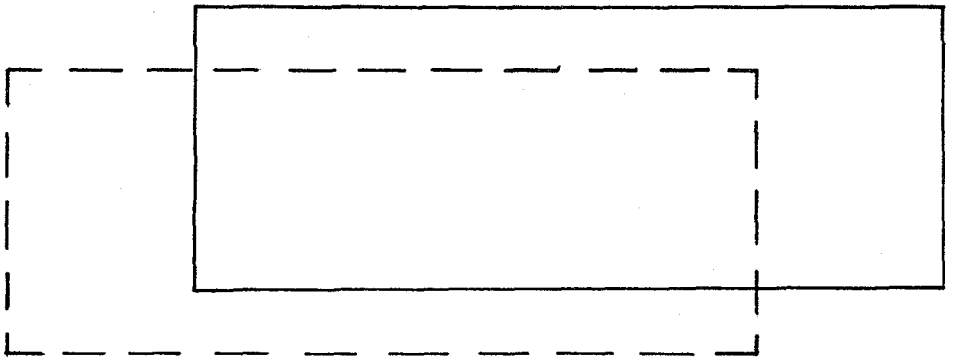

b) Mode 1x

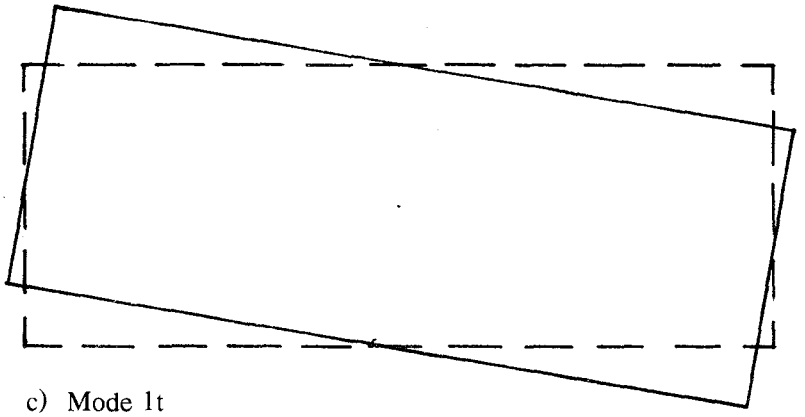

c) Mode 1t

Fig. 5.7 Analytical deck modal displacements for structure in water. Minimum deck mass case.

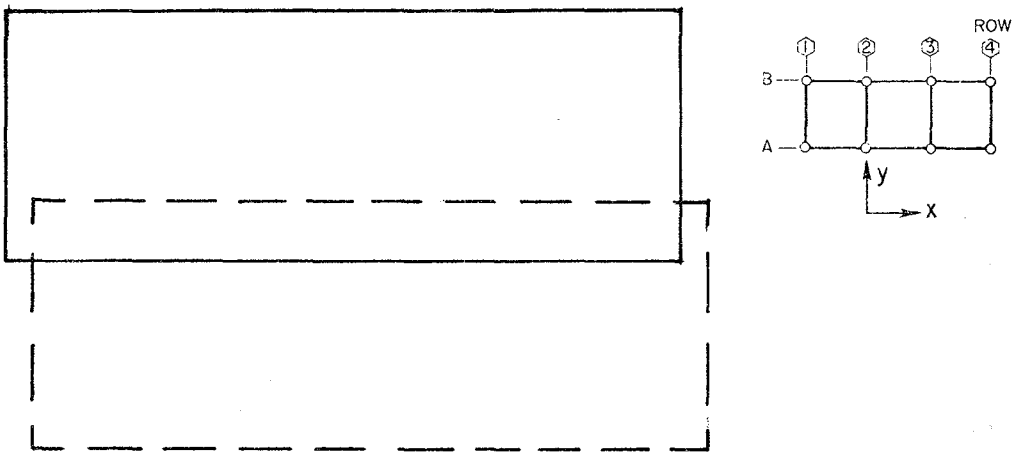

a) Mode 1y

b) Mode 1x

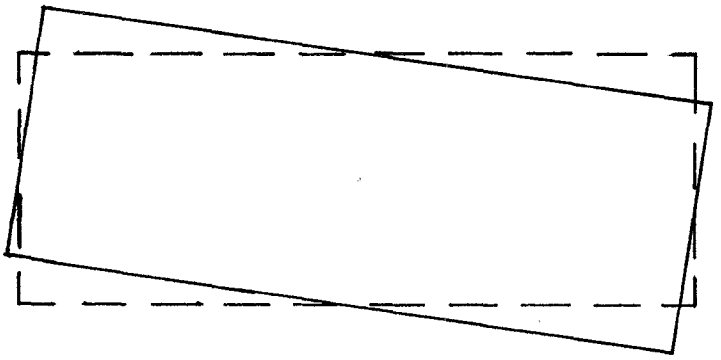

c) Mode 1t

Fig. 5.8 Analytical deck modal displacements for structure in water. Maximum deck mass case.

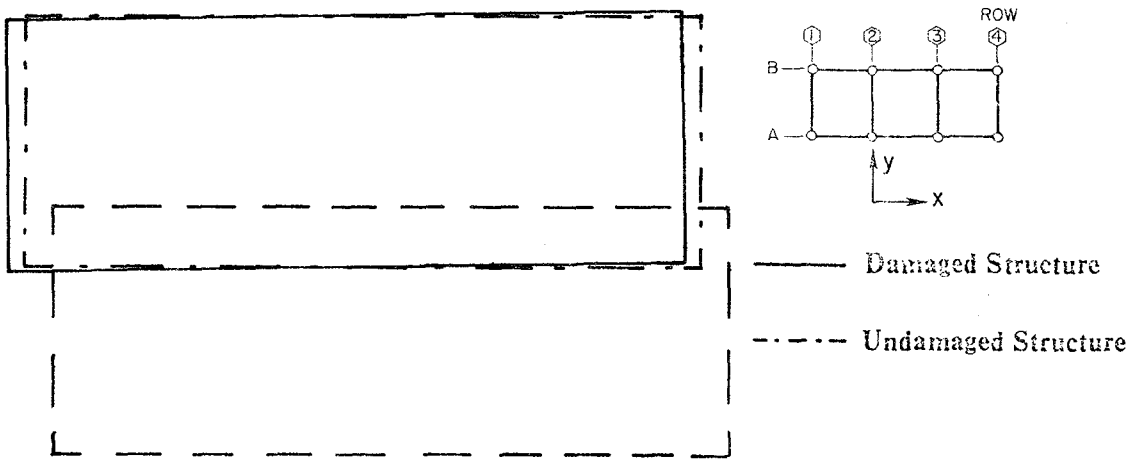

a) Mode 1y

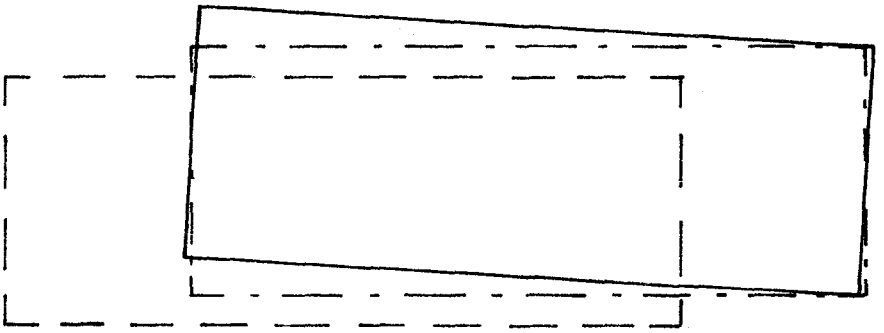

b) Mode 1x

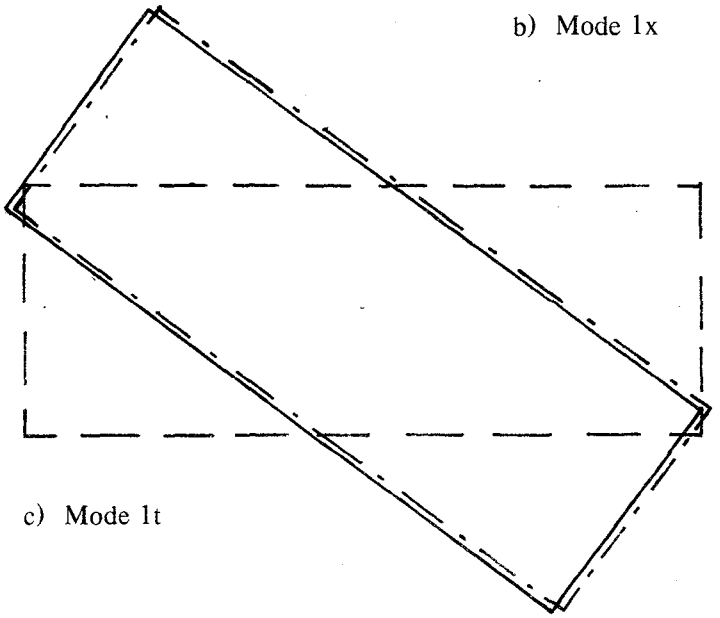

c) Mode 1t

Fig. 5.9 Analytical deck modal displacements for structure in water. Member 116 severed, maximum deck mass case.

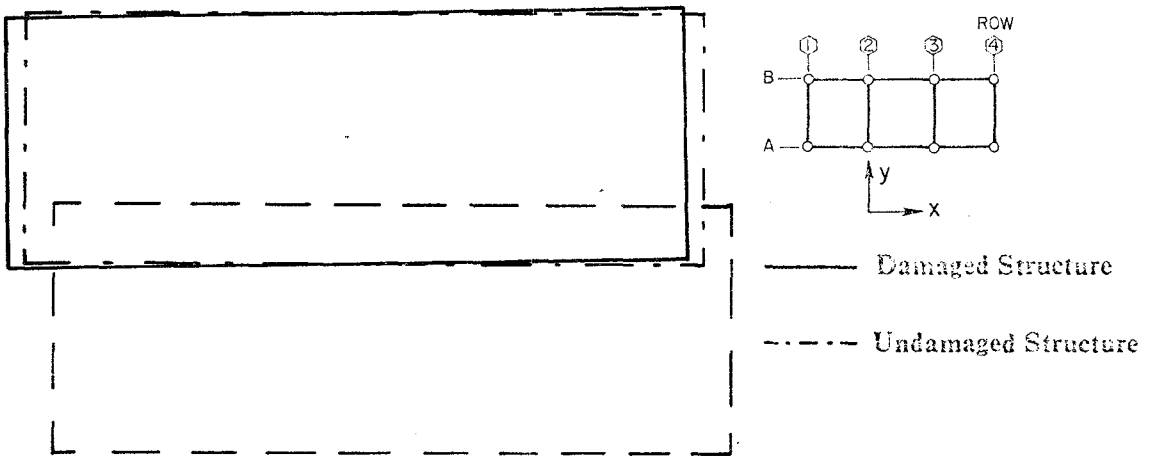

a) Mode 1y

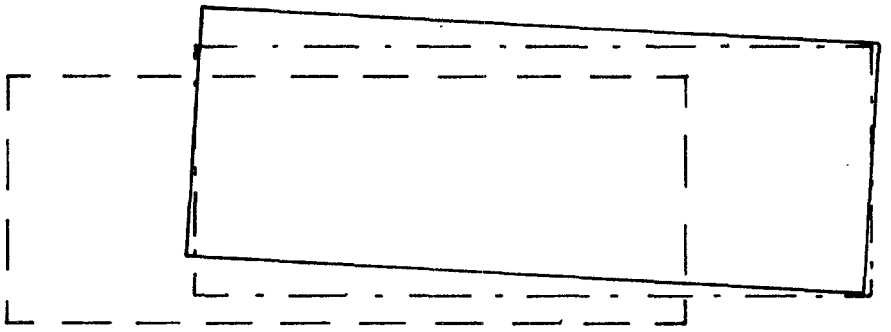

b) Mode 1x

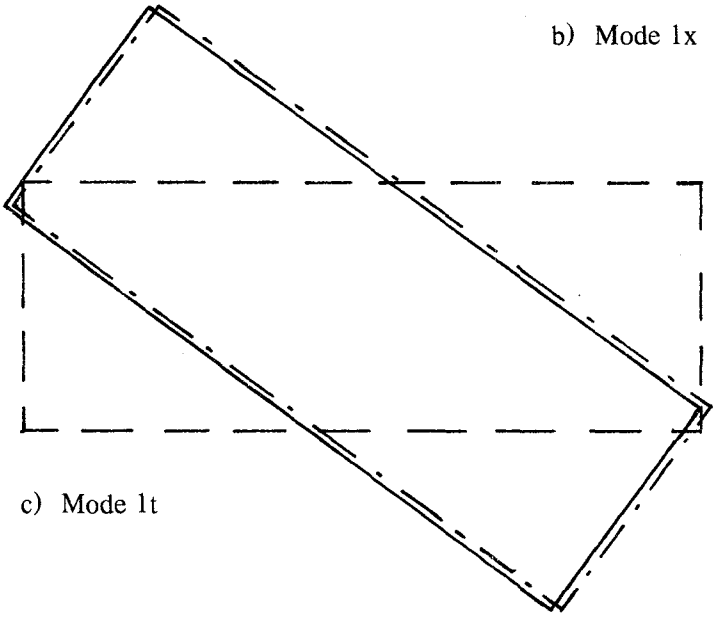

c) Mode 1t

Fig. 5.10 Analytical deck modal displacements for structure in water. Member 94 severed, maximum deck mass case.

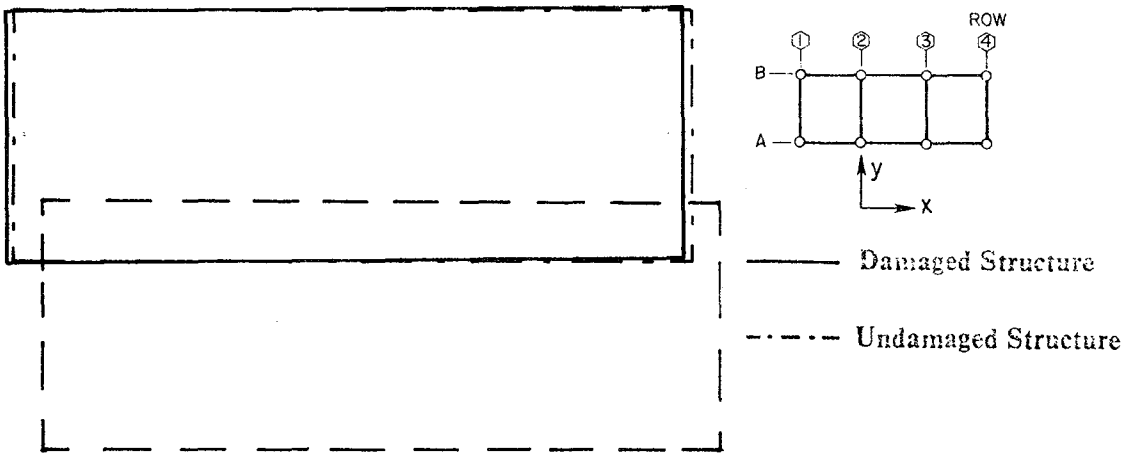

a) Mode 1y

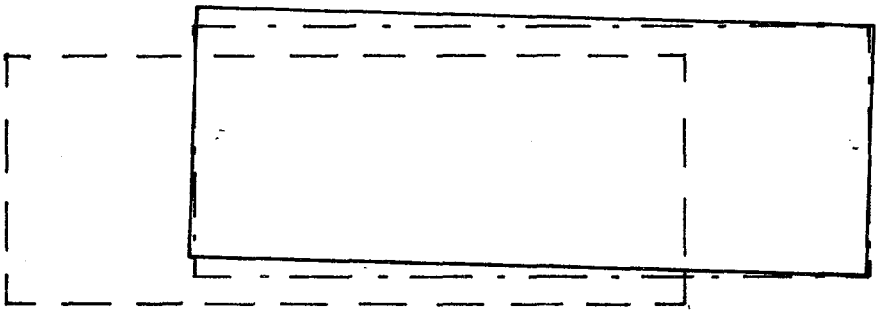

b) Mode 1x

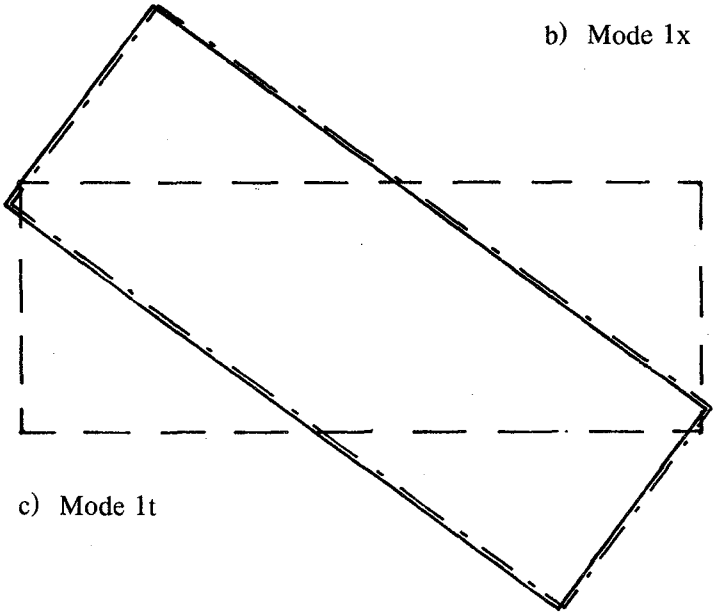

c) Mode 1t

Fig. 5.11 Analytical deck modal displacements for structure in water. Member 107 severed, maximum deck mass case.

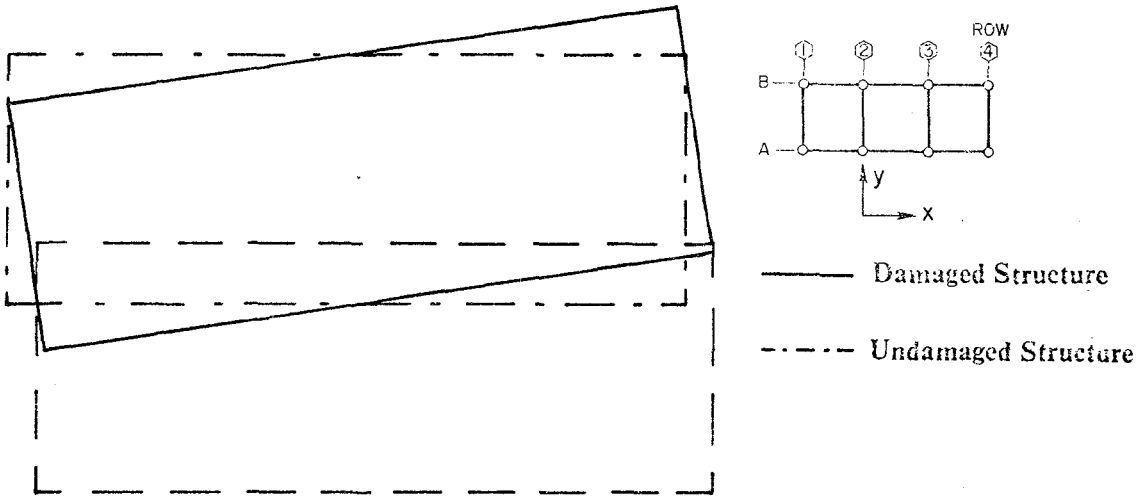

a) Mode 1y

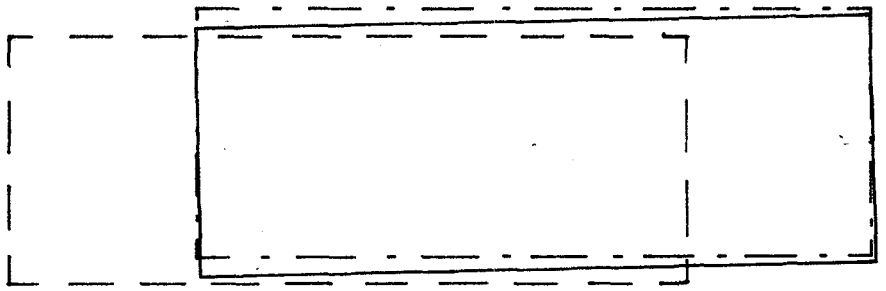

b) Mode 1x

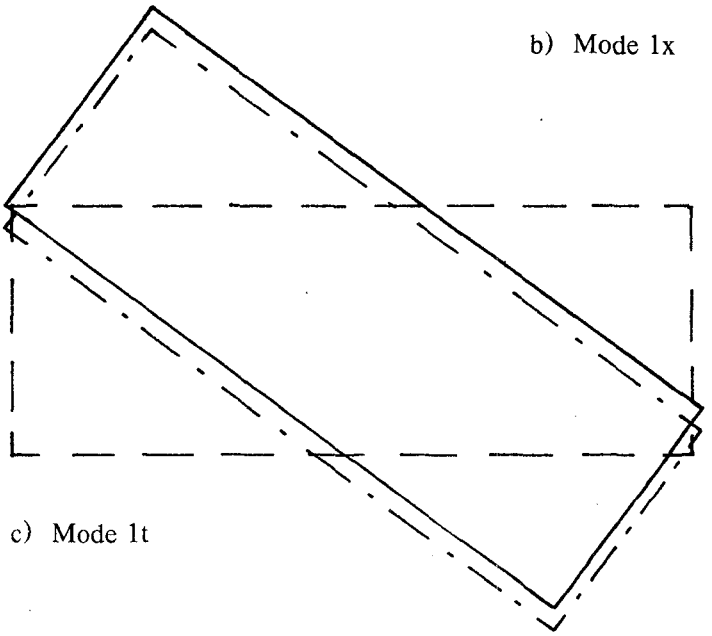

c) Mode 1t

Fig. 5.12 Analytical deck modal displacements for structure in water. Member 55 severed, maximum deck mass case.

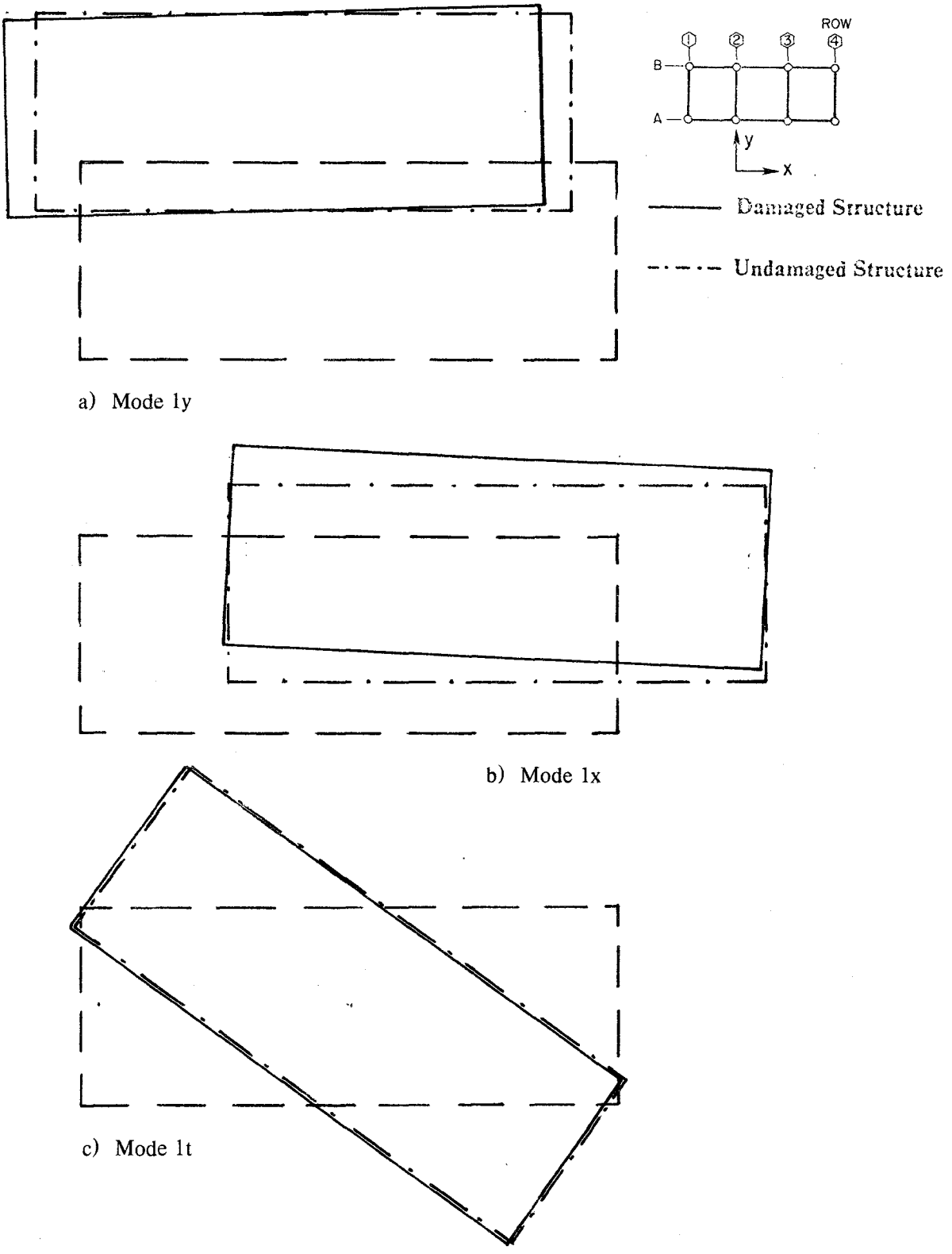

Fig. 5.13 Analytical deck modal displacements for structure in water. Member 116 severed, minimum deck mass case.

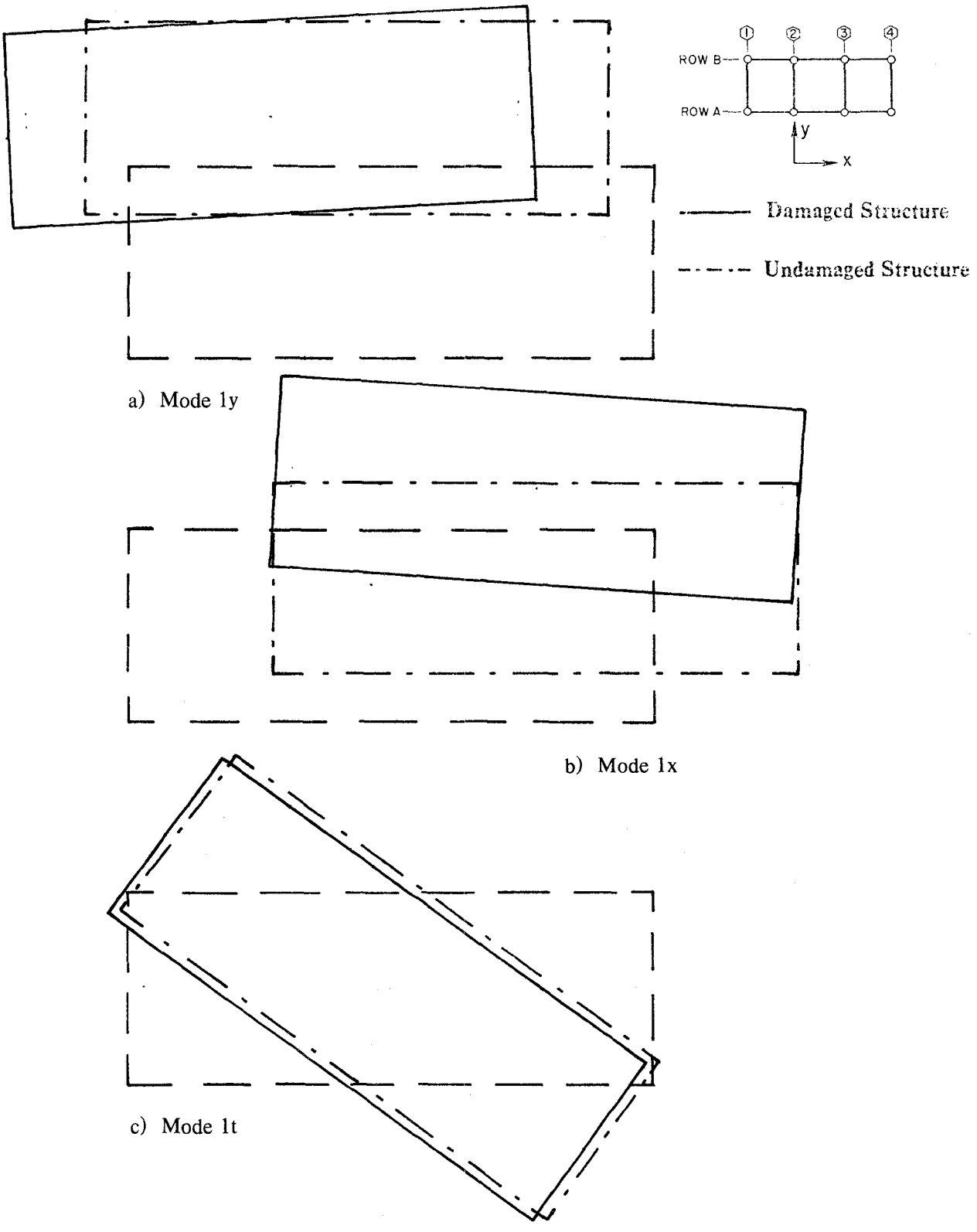

Fig. 5.14 Analytical deck modal displacements for structure in water. Member 94 severed, *minimum* deck mass case.

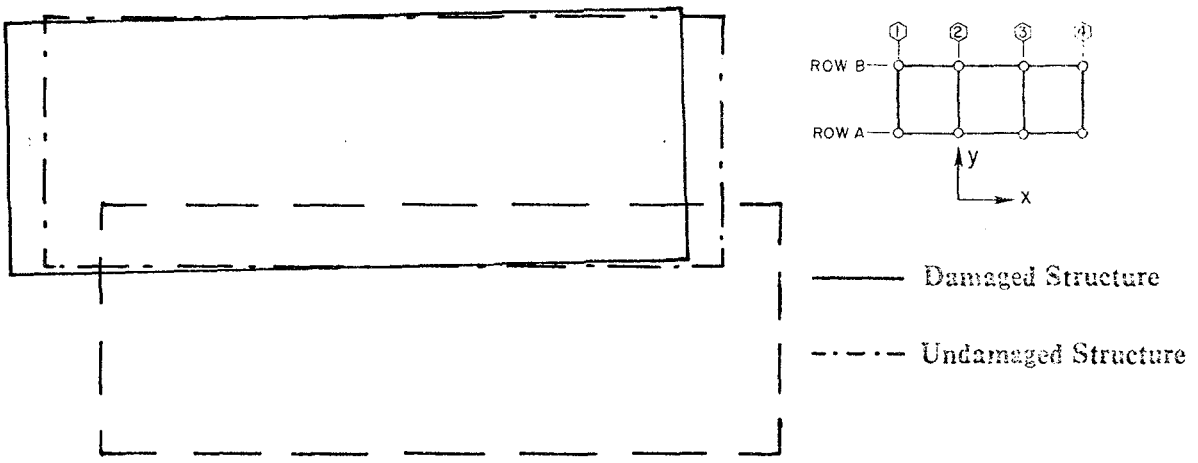

a) Mode 1y

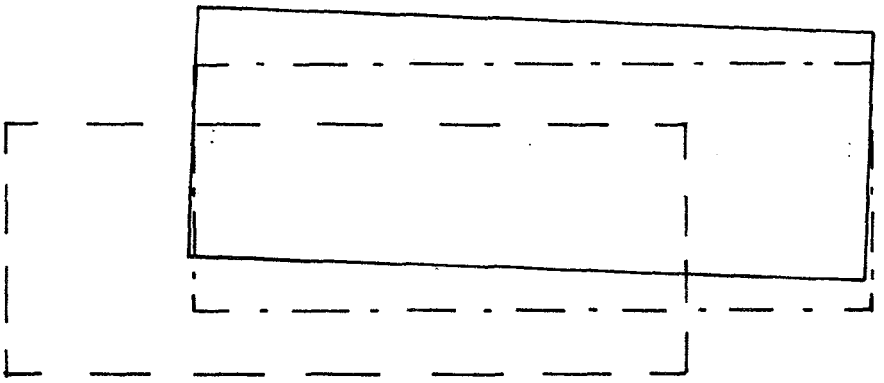

b) Mode 1x

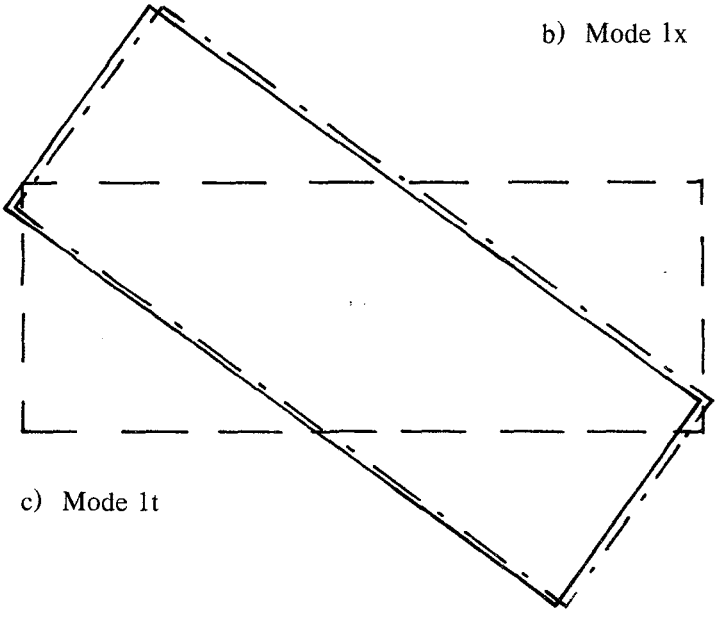

c) Mode 1t

Fig. 5.15 Analytical deck modal displacements for structure in water. Member 107 severed, minimum deck mass case.

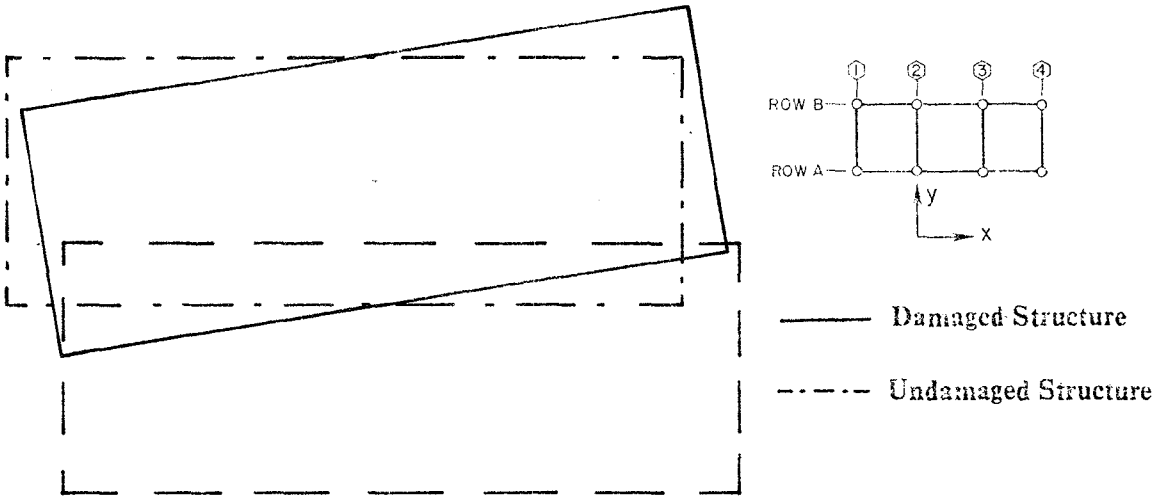

a) Mode 1y

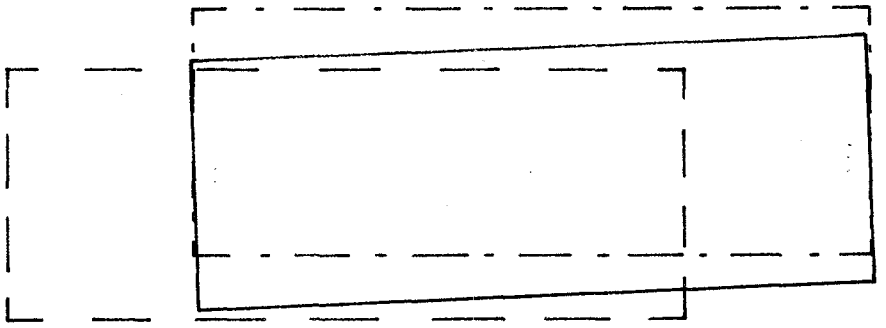

b) Mode 1x

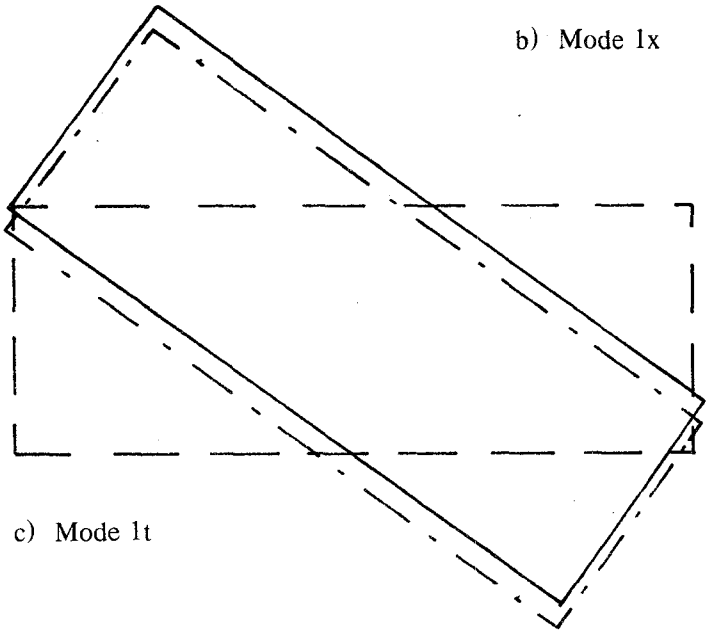

c) Mode 1t

Fig. 5.16 Analytical deck modal displacements for structure in water. Member 55 severed, minimum deck mass case.

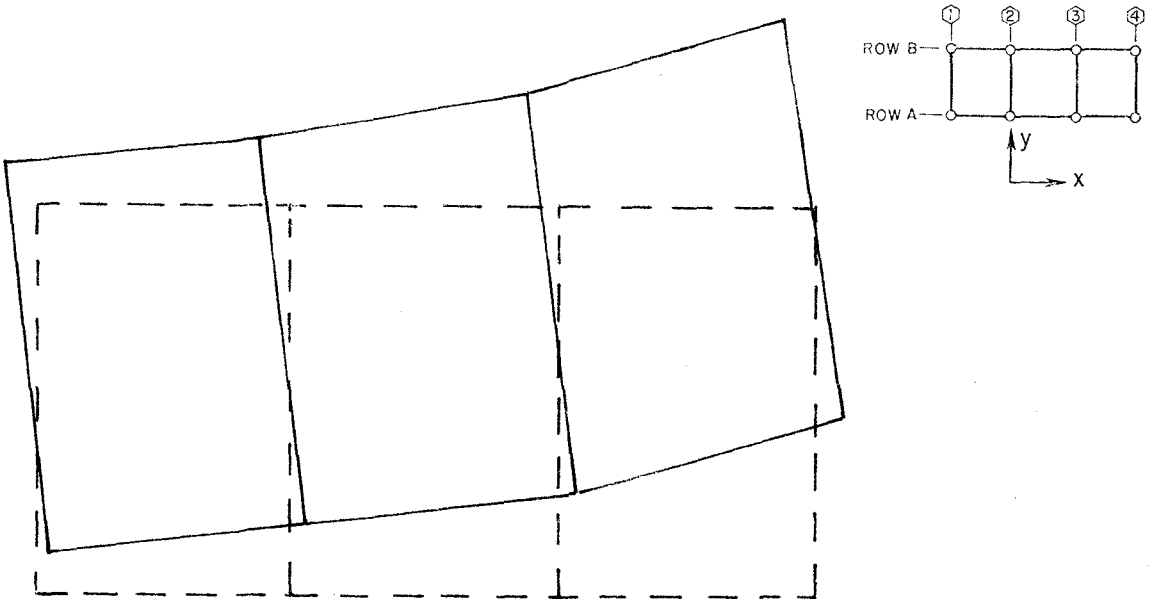

b) Minimum deck mass case

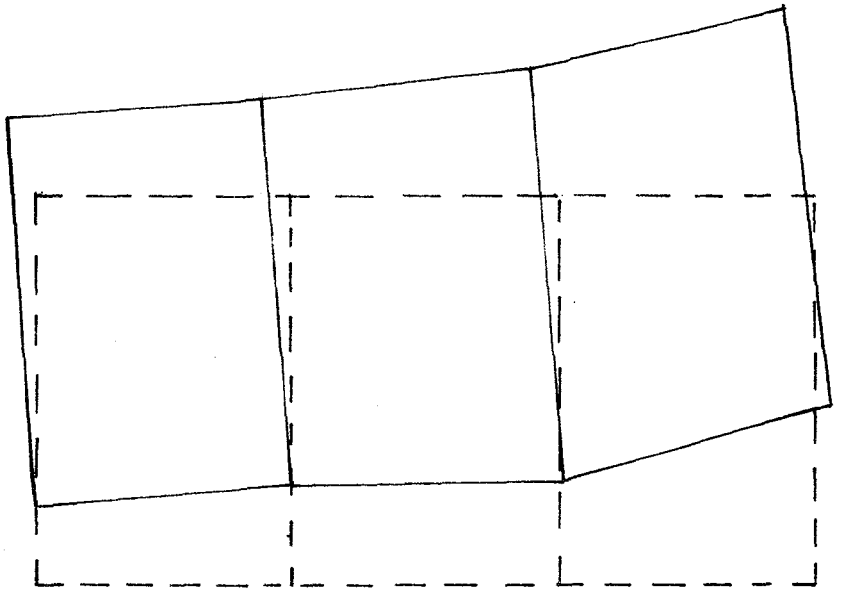

a) Maximum deck mass case

Fig. 5.17 Mode shape 1y at the 30" Elev. cross section of the structure as seen in plan view with Member 62 severed.

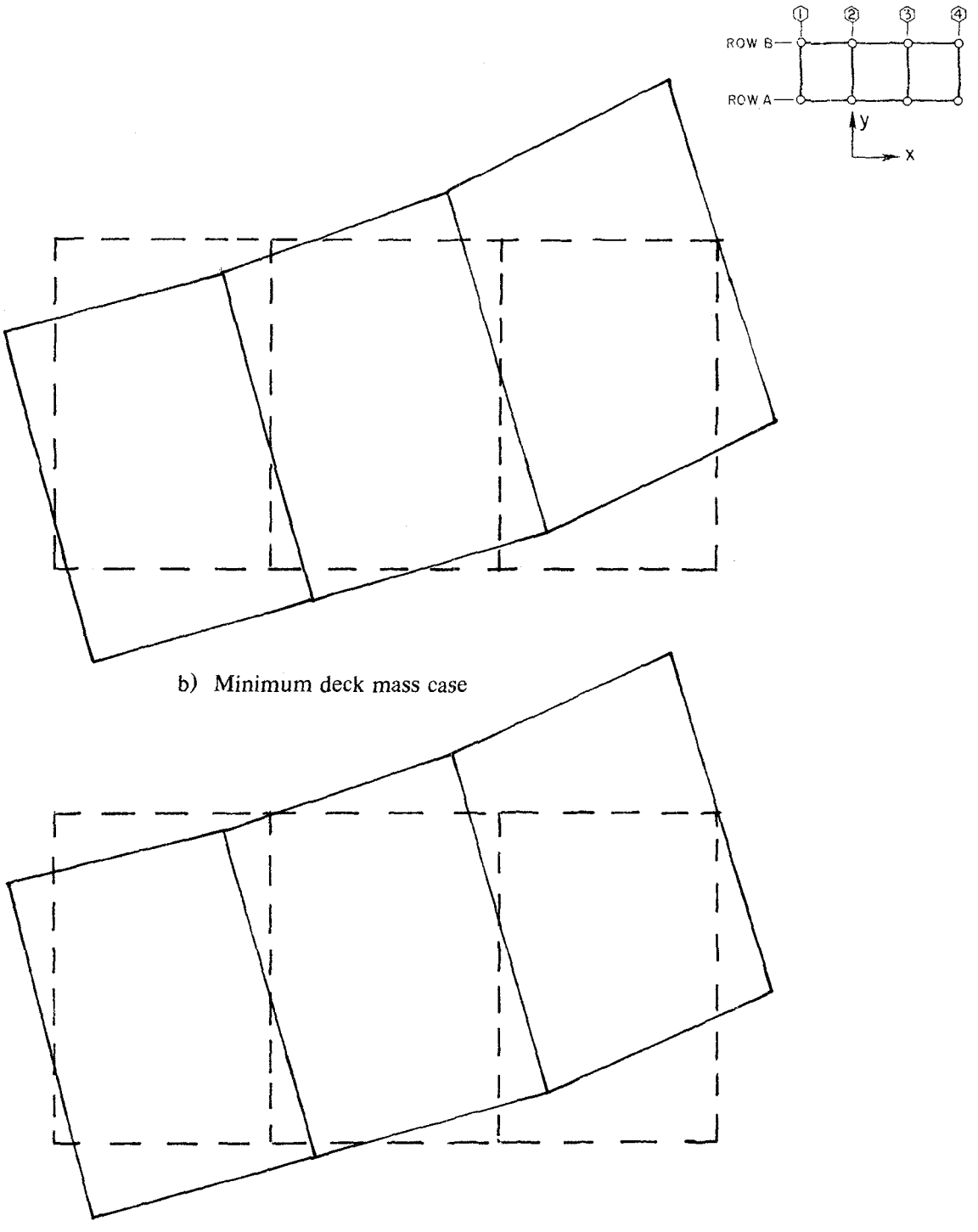

b) Minimum deck mass case

a) Maximum deck mass case

Fig. 5.18 Mode shape 1t at the 30" Elev. cross section of the structure as seen in plan view with Member 62 severed.

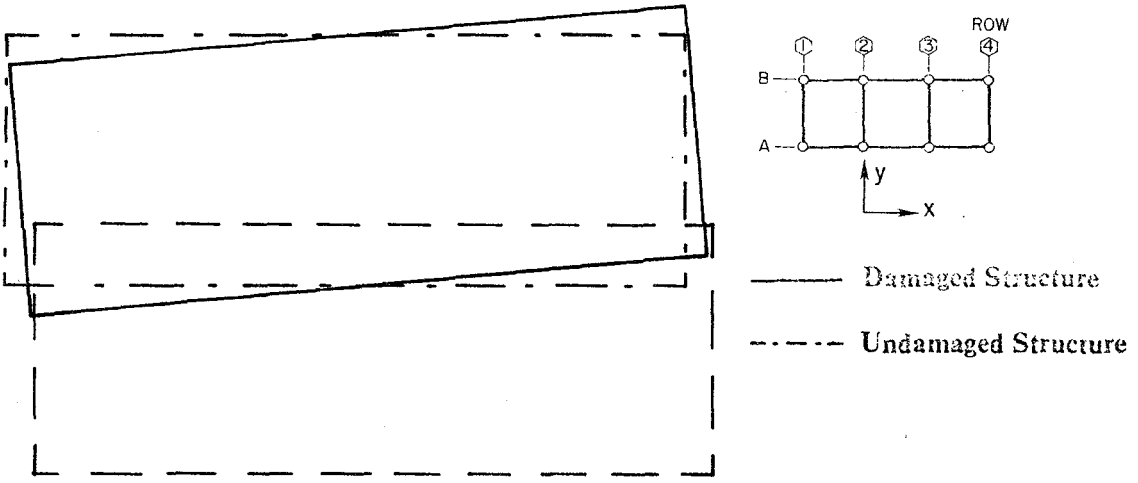

a) Mode 1y

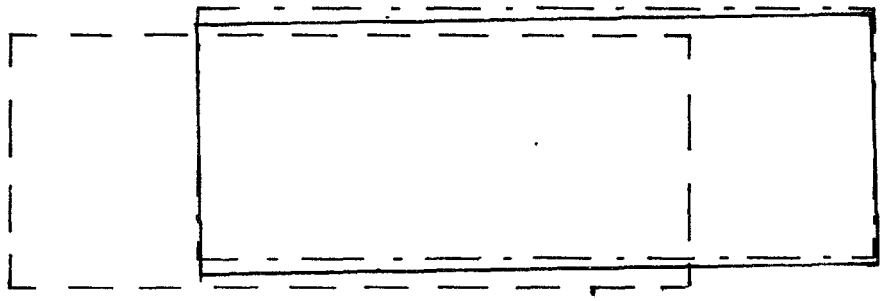

b) Mode 1x

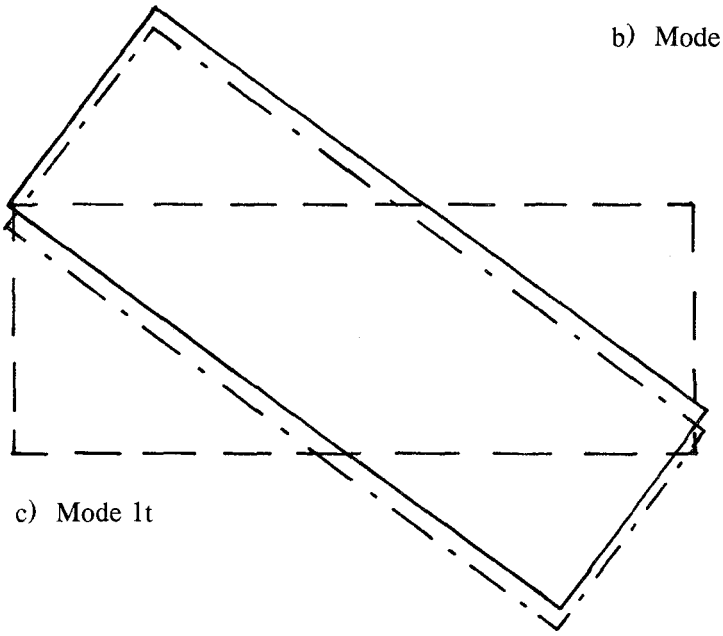

c) Mode 1t

Fig. 5.19 Analytical deck modal displacements for structure in water. Member 62 severed, maximum deck mass case.

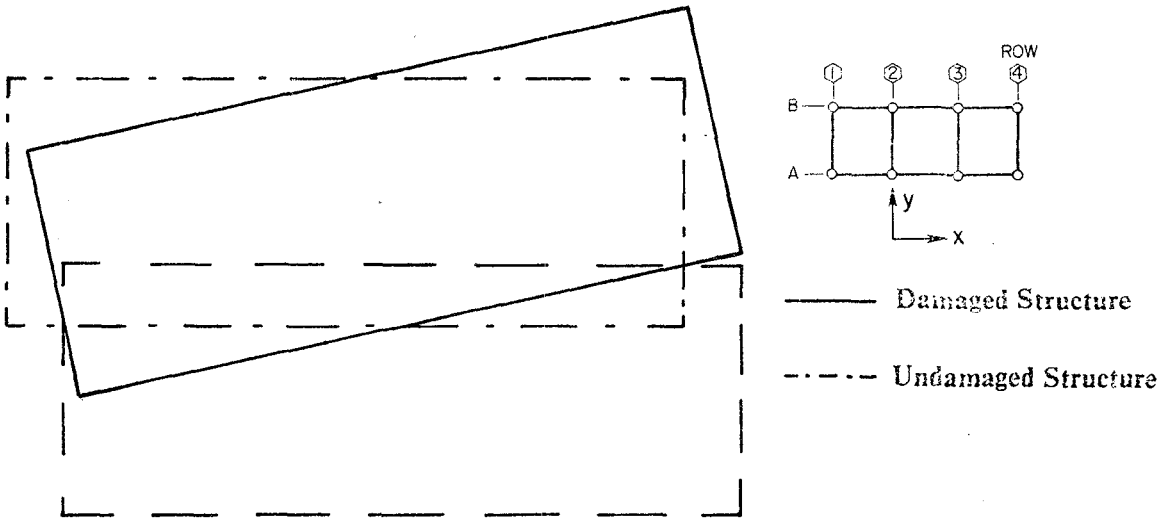

a) Mode 1y

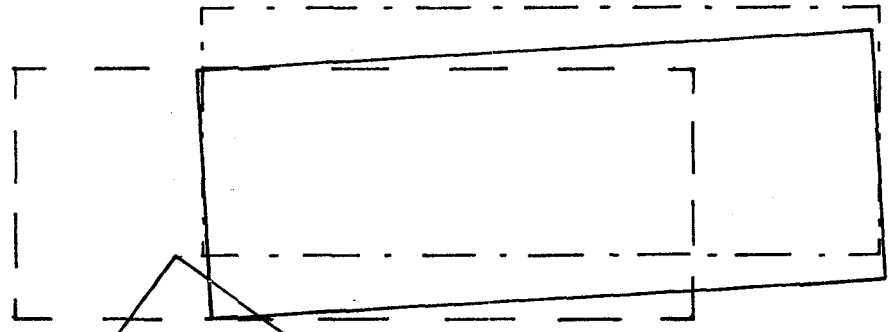

b) Mode 1x

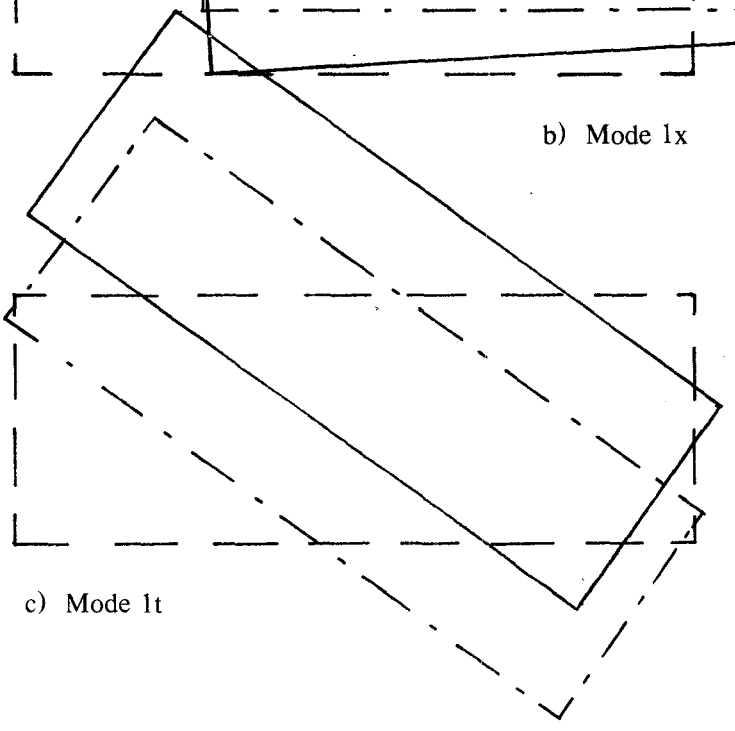

c) Mode 1t

Fig. 5.20 Analytical deck modal displacements for structure in water. Member 62 severed, minimum deck mass case.

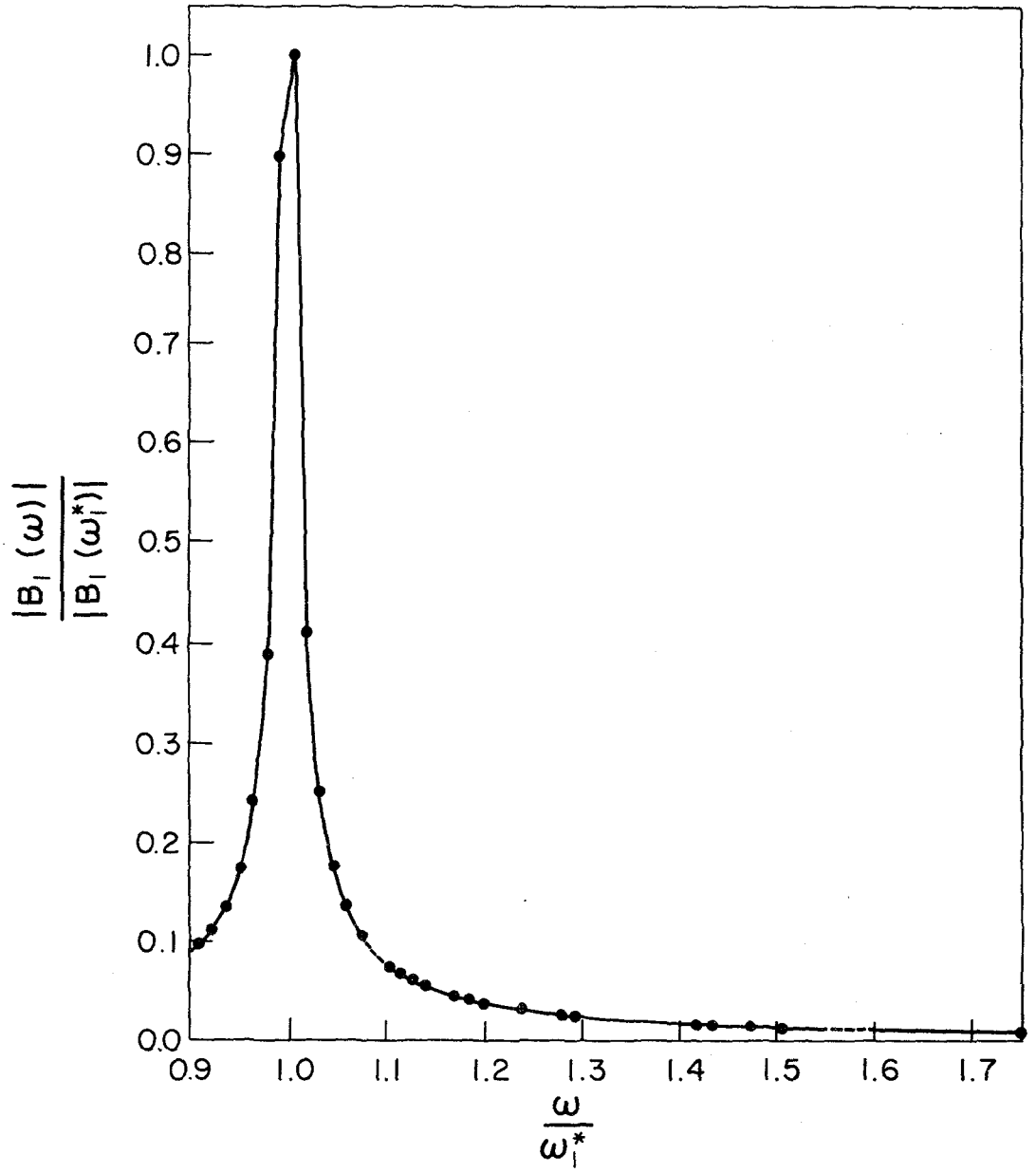

FIGURE A.1 PLOT OF $\frac{|B_1(\omega)|}{|B_1(\omega_1^*)|}$ VS. $\frac{\omega}{\omega_1^*}$

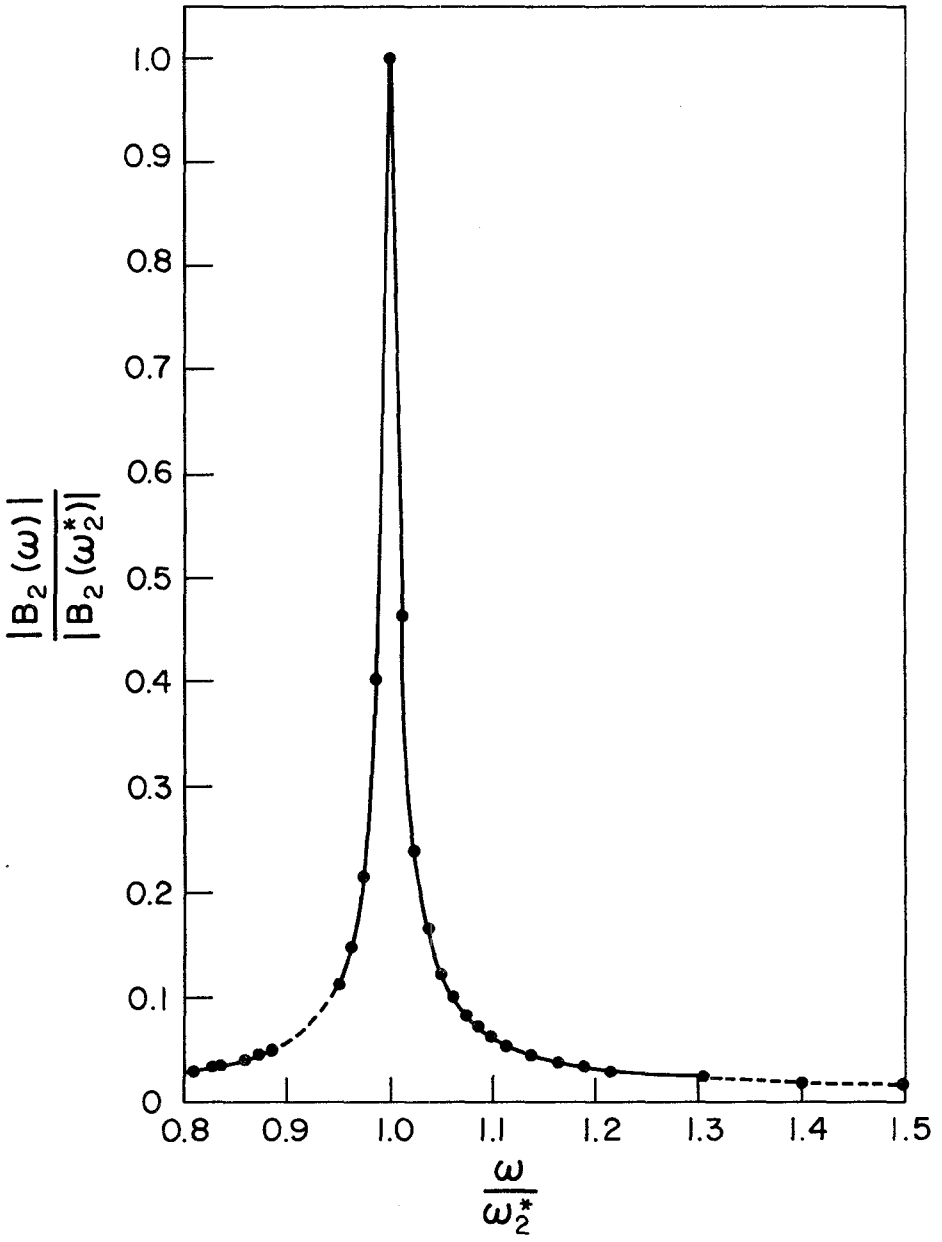

FIGURE A.2 PLOT OF $\frac{|B_2(\omega)|}{|B_2(\omega_2^*)|}$ VS. $\frac{\omega}{\omega_2^*}$

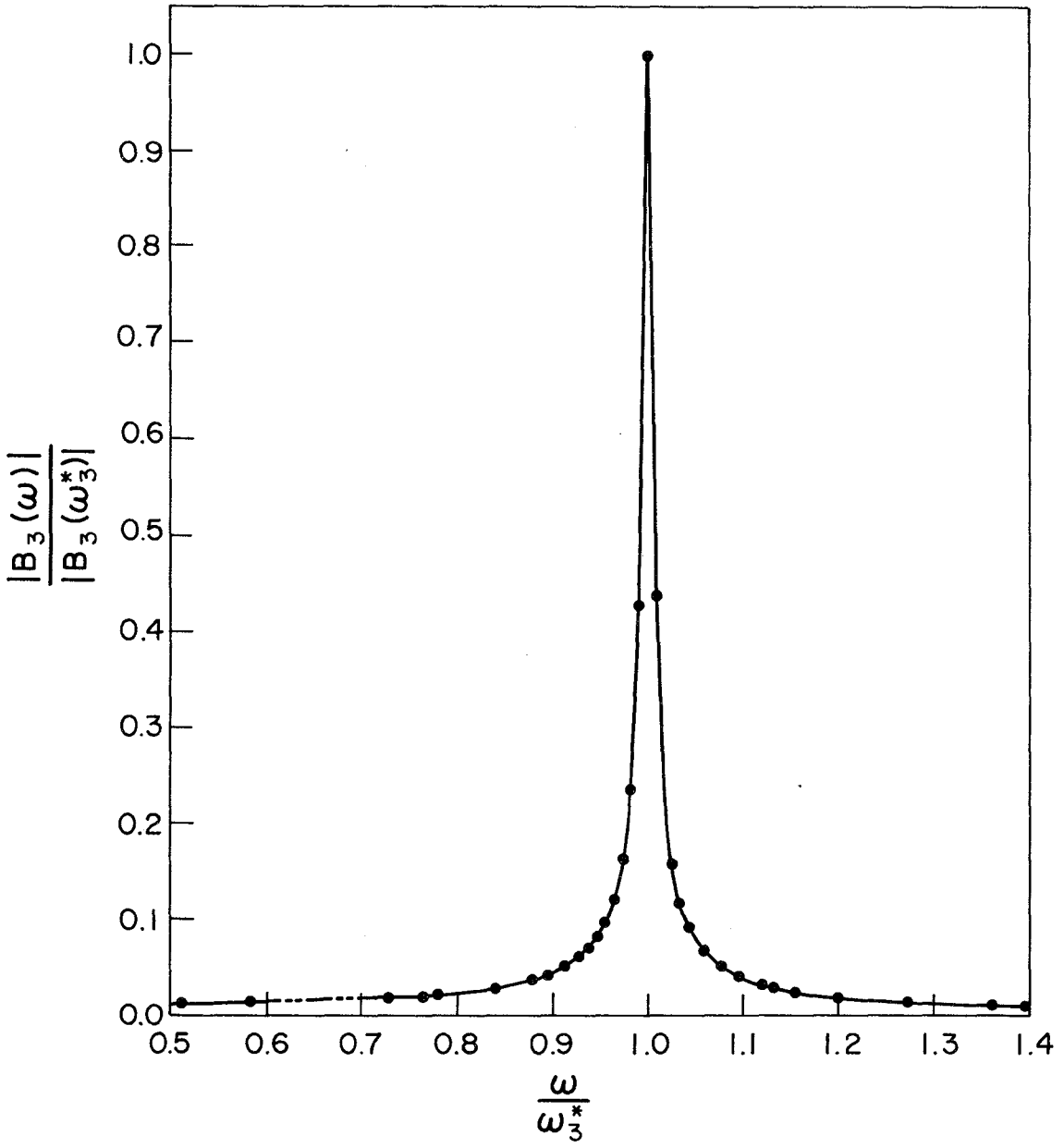

FIGURE A.3 PLOT OF $\frac{|B_3(\omega)|}{|B_3(\omega_3^*)|}$ VS. $\frac{\omega}{\omega_3^*}$

EARTHQUAKE ENGINEERING RESEARCH CENTER REPORTS

NOTE: Numbers in parentheses are Accession Numbers assigned by the National Technical Information Service; these are followed by a price code. Copies of the reports may be ordered from the National Technical Information Service, 5285 Port Royal Road, Springfield, Virginia, 22161. Accession Numbers should be quoted on orders for reports (PB --- ---) and remittance must accompany each order. Reports without this information were not available at time of printing. The complete list of EERC reports (from EERC 67-1) is available upon request from the Earthquake Engineering Research Center, University of California, Berkeley, 47th Street and Hoffman Boulevard, Richmond, California 94804.

UCB/EERC-77/01 "PLUSH - A Computer Program for Probabilistic Finite Element Analysis of Seismic Soil-Structure Interaction," by M.P. Romo Organista, J. Lysmer and H.B. Seed - 1977 (PB81 177 651)A05

UCB/EERC-77/02 "Soil-Structure Interaction Effects at the Humboldt Bay Power Plant in the Ferndale Earthquake of June 7, 1975," by J.E. Valera, H.B. Seed, C.F. Tsai and J. Lysmer - 1977 (PB 265 795)A04

UCB/EERC-77/03 "Influence of Sample Disturbance on Sand Response to Cyclic Loading," by K. Mori, H.B. Seed and C.K. Chan - 1977 (PB 267 352)A04

UCB/EERC-77/04 "Seismological Studies of Strong Motion Records," by J. Shoja-Taheri - 1977 (PB 269 655)A10

UCB/EERC-77/05 Unassigned

UCB/EERC-77/06 "Developing Methodologies for Evaluating the Earthquake Safety of Existing Buildings," by No. 1 - B. Bresler; No. 2 - B. Bresler, T. Okada and D. Zisling; No. 3 - T. Okada and B. Bresler; No. 4 - V.V. Bertero and B. Bresler - 1977 (PB 267 354)A08

UCB/EERC-77/07 "A Literature Survey - Transverse Strength of Masonry Walls," by Y. Omote, R.L. Mayes, S.W. Chen and R.W. Clough - 1977 (PB 277 933)A07

UCB/EERC-77/08 "DRAIN-TABS: A Computer Program for Inelastic Earthquake Response of Three Dimensional Buildings," by R. Guendelman-Israel and G.H. Powell - 1977 (PB 270 693)A07

UCB/EERC-77/09 "SUBWALL: A Special Purpose Finite Element Computer Program for Practical Elastic Analysis and Design of Structural Walls with Substructure Option," by D.Q. Le, H. Peterson and E.P. Popov - 1977 (PB 270 567)A05

UCB/EERC-77/10 "Experimental Evaluation of Seismic Design Methods for Broad Cylindrical Tanks," by D.P. Clough (PB 272 280)A13

UCB/EERC-77/11 "Earthquake Engineering Research at Berkeley - 1976," - 1977 (PB 273 507)A09

UCB/EERC-77/12 "Automated Design of Earthquake Resistant Multistory Steel Building Frames," by N.D. Walker, Jr. - 1977 (PB 276 526)A09

UCB/EERC-77/13 "Concrete Confined by Rectangular Hoops Subjected to Axial Loads," by J. Vallenas, V.V. Bertero and E.P. Popov - 1977 (PB 275 165)A06

UCB/EERC-77/14 "Seismic Strain Induced in the Ground During Earthquakes," by Y. Sugimura - 1977 (PB 284 201)A04

UCB/EERC-77/15 Unassigned

UCB/EERC-77/16 "Computer Aided Optimum Design of Ductile Reinforced Concrete Moment Resisting Frames," by S.W. Zagajeski and V.V. Bertero - 1977 (PB 280 137)A07

UCB/EERC-77/17 "Earthquake Simulation Testing of a Stepping Frame with Energy-Absorbing Devices," by J.M. Kelly and D.F. Tsztoo - 1977 (PB 273 506)A04

UCB/EERC-77/18 "Inelastic Behavior of Eccentrically Braced Steel Frames under Cyclic Loadings," by C.W. Roeder and E.P. Popov - 1977 (PB 275 526)A15

UCB/EERC-77/19 "A Simplified Procedure for Estimating Earthquake-Induced Deformations in Dams and Embankments," by F.I. Makdisi and H.B. Seed - 1977 (PB 276 820)A04

UCB/EERC-77/20 "The Performance of Earth Dams during Earthquakes," by H.B. Seed, F.I. Makdisi and P. de Alba - 1977 (PB 276 821)A04

UCB/EERC-77/21 "Dynamic Plastic Analysis Using Stress Resultant Finite Element Formulation," by P. Lukkunapvasit and J.M. Kelly - 1977 (PB 275 453)A04

UCB/EERC-77/22 "Preliminary Experimental Study of Seismic Uplift of a Steel Frame," by R.W. Clough and A.A. Huckelbridge 1977 (PB 278 769)A08

UCB/EERC-77/23 "Earthquake Simulator Tests of a Nine-Story Steel Frame with Columns Allowed to Uplift," by A.A. Huckelbridge - 1977 (PB 277 944)A09

UCB/EERC-77/24 "Nonlinear Soil-Structure Interaction of Skew Highway Bridges," by M.-C. Chen and J. Penzien - 1977 (PB 276 176)A07

UCB/EERC-77/25 "Seismic Analysis of an Offshore Structure Supported on Pile Foundations," by D.D.-N. Liou and J. Penzien 1977 (PB 283 180)A06

UCB/EERC-77/26 "Dynamic Stiffness Matrices for Homogeneous Viscoelastic Half-Planes," by G. Dasgupta and A.K. Chopra - 1977 (PB 279 654)A06

UCB/EERC-77/27 "A Practical Soft Story Earthquake Isolation System," by J.M. Kelly, J.M. Eidinger and C.J. Derham - 1977 (PB 276 814)A07

UCB/EERC-77/28 "Seismic Safety of Existing Buildings and Incentives for Hazard Mitigation in San Francisco: An Exploratory Study," by A.J. Meltsner - 1977 (PB 281 970)A05

UCB/EERC-77/29 "Dynamic Analysis of Electrohydraulic Shaking Tables," by D. Rea, S. Abedi-Hayati and Y. Takahashi 1977 (PB 282 569)A04

UCB/EERC-77/30 "An Approach for Improving Seismic - Resistant Behavior of Reinforced Concrete Interior Joints," by B. Galunic, V.V. Bertero and E.P. Popov - 1977 (PB 290 870)A06

UCB/EERC-78/01 "The Development of Energy-Absorbing Devices for Aseismic Base Isolation Systems," by J.M. Kelly and D.F. Tsztoo - 1978 (PB 284 978)A04

UCB/EERC-78/02 "Effect of Tensile Prestrain on the Cyclic Response of Structural Steel Connections, by J.G. Bouwkamp and A. Mukhopadhyay - 1978

UCB/EERC-78/03 "Experimental Results of an Earthquake Isolation System using Natural Rubber Bearings," by J.M. Eidinger and J.M. Kelly - 1978 (PB 281 686)A04

UCB/EERC-78/04 "Seismic Behavior of Tall Liquid Storage Tanks," by A. Niwa - 1978 (PB 284 017)A14

UCB/EERC-78/05 "Hysteretic Behavior of Reinforced Concrete Columns Subjected to High Axial and Cyclic Shear Forces," by S.W. Zagajeski, V.V. Bertero and J.G. Bouwkamp - 1978 (PB 283 858)A13

UCB/EERC-78/06 "Three Dimensional Inelastic Frame Elements for the ANSR-I Program," by A. Riahi, D.G. Row and G.H. Powell - 1978 (PB 295 755)A04

UCB/EERC-78/07 "Studies of Structural Response to Earthquake Ground Motion," by O.A. Lopez and A.K. Chopra - 1978 (PB 282 790)A05

UCB/EERC-78/08 "A Laboratory Study of the Fluid-Structure Interaction of Submerged Tanks and Caissons in Earthquakes," by R.C. Byrd - 1978 (PB 284 957)A08

UCB/EERC-78/09 Unassigned

UCB/EERC-78/10 "Seismic Performance of Nonstructural and Secondary Structural Elements," by I. Sakamoto - 1978 (PB81 154 593)A05

UCB/EERC-78/11 "Mathematical Modelling of Hysteresis Loops for Reinforced Concrete Columns," by S. Nakata, T. Sproul and J. Penzien - 1978 (PB 298 274)A05

UCB/EERC-78/12 "Damageability in Existing Buildings," by T. Blejwas and B. Bresler - 1978 (PB 80 166 978)A05

UCB/EERC-78/13 "Dynamic Behavior of a Pedestal Base Multistory Building," by R.M. Stephen, E.L. Wilson, J.G. Bouwkamp and M. Button - 1978 (PB 286 650)A08

UCB/EERC-78/14 "Seismic Response of Bridges - Case Studies," by R.A. Imbsen, V. Nutt and J. Penzien - 1978 (PB 286 503)A10

UCB/EERC-78/15 "A Substructure Technique for Nonlinear Static and Dynamic Analysis," by D.G. Row and G.H. Powell - 1978 (PB 288 077)A10

UCB/EERC-78/16 "Seismic Risk Studies for San Francisco and for the Greater San Francisco Bay Area," by C.S. Oliveira - 1978 (PB 81 120 115)A07

UCB/EERC-78/17 "Strength of Timber Roof Connections Subjected to Cyclic Loads," by P. Gülkan, R.L. Mayes and R.W. Clough - 1978 (HUD-000 1491)A07

UCB/EERC-78/18 "Response of K-Braced Steel Frame Models to Lateral Loads," by J.G. Bouwkamp, R.M. Stephen and E.P. Popov - 1978

UCB/EERC-78/19 "Rational Design Methods for Light Equipment in Structures Subjected to Ground Motion," by J.L. Sackman and J.M. Kelly - 1978 (PB 292 357)A04

UCB/EERC-78/20 "Testing of a Wind Restraint for Aseismic Base Isolation," by J.M. Kelly and D.E. Chitty - 1978 (PB 292 833)A03

UCB/EERC-78/21 "APOLLO - A Computer Program for the Analysis of Pore Pressure Generation and Dissipation in Horizontal Sand Layers During Cyclic or Earthquake Loading," by P.P. Martin and H.B. Seed - 1978 (PB 292 835)A04

UCB/EERC-78/22 "Optimal Design of an Earthquake Isolation System," by M.A. Bhatti, K.S. Pister and E. Polak - 1978 (PB 294 735)A06

UCB/EERC-78/23 "MASH - A Computer Program for the Non-Linear Analysis of Vertically Propagating Shear Waves in Horizontally Layered Deposits," by P.P. Martin and H.B. Seed - 1978 (PB 293 101)A05

UCB/EERC-78/24 "Investigation of the Elastic Characteristics of a Three Story Steel Frame Using System Identification," by I. Kaya and H.D. McNiven - 1978 (PB 296 225)A06

UCB/EERC-78/25 "Investigation of the Nonlinear Characteristics of a Three-Story Steel Frame Using System Identification," by I. Kaya and H.D. McNiven - 1978 (PB 301 363)A05

UCB/EERC-78/26 "Studies of Strong Ground Motion in Taiwan," by Y.M. Hsiung, B.A. Bolt and J. Penzien - 1978 (PB 298 436)A06

UCB/EERC-78/27 "Cyclic Loading Tests of Masonry Single Piers: Volume 1 - Height to Width Ratio of 2," by P.A. Hidalgo, R.L. Mayes, H.D. McNiven and R.W. Clough - 1978 (PB 296 211)A07

UCB/EERC-78/28 "Cyclic Loading Tests of Masonry Single Piers: Volume 2 - Height to Width Ratio of 1," by S.-W.J. Chen, P.A. Hidalgo, R.L. Mayes, R.W. Clough and H.D. McNiven - 1978 (PB 296 212)A09

UCB/EERC-78/29 "Analytical Procedures in Soil Dynamics," by J. Lysmer - 1978 (PB 298 445)A06

UCB/EERC-79/01 "Hysteretic Behavior of Lightweight Reinforced Concrete Beam-Column Subassemblages," by B. Forzani, E.P. Popov and V.V. Bertero - April 1979(PB 298 267)A06

UCB/EERC-79/02 "The Development of a Mathematical Model to Predict the Flexural Response of Reinforced Concrete Beams to Cyclic Loads, Using System Identification," by J. Stanton & H. McNiven - Jan. 1979(PB 295 875)A10

UCB/EERC-79/03 "Linear and Nonlinear Earthquake Response of Simple Torsionally Coupled Systems," by C.L. Kan and A.K. Chopra - Feb. 1979(PB 298 262)A06

UCB/EERC-79/04 "A Mathematical Model of Masonry for Predicting its Linear Seismic Response Characteristics," by Y. Mengi and H.D. McNiven - Feb. 1979(PB 298 266)A06

UCB/EERC-79/05 "Mechanical Behavior of Lightweight Concrete Confined by Different Types of Lateral Reinforcement," by M.A. Manrique, V.V. Bertero and E.P. Popov - May 1979(PB 301 114)A06

UCB/EERC-79/06 "Static Tilt Tests of a Tall Cylindrical Liquid Storage Tank," by R.W. Clough and A. Niwa - Feb. 1979 (PB 301 167)A06

UCB/EERC-79/07 "The Design of Steel Energy Absorbing Restrainers and Their Incorporation into Nuclear Power Plants for Enhanced Safety: Volume 1 - Summary Report," by P.N. Spencer, V.F. Zackay, and E.R. Parker - Feb. 1979(UCB/EERC-79/07)A09

UCB/EERC-79/08 "The Design of Steel Energy Absorbing Restrainers and Their Incorporation into Nuclear Power Plants for Enhanced Safety: Volume 2 - The Development of Analyses for Reactor System Piping,""Simple Systems" by M.C. Lee, J. Penzien, A.K. Chopra and K, Suzuki "Complex Systems" by G.H. Powell, E.L. Wilson, R.W. Clough and D.G. Row - Feb. 1979(UCB/EERC-79/08)A10

UCB/EERC-79/09 "The Design of Steel Energy Absorbing Restrainers and Their Incorporation into Nuclear Power Plants for Enhanced Safety: Volume 3 - Evaluation of Commercial Steels," by W.S. Owen, R.M.N. Pelloux, R.O. Ritchie, M. Faral, T. Ohhashi, J. Toplosky, S.J. Hartman, V.F. Zackay and E.R. Parker - Feb. 1979(UCB/EERC-79/09)A04

UCB/EERC-79/10 "The Design of Steel Energy Absorbing Restrainers and Their Incorporation into Nuclear Power Plants for Enhanced Safety: Volume 4 - A Review of Energy-Absorbing Devices," by J.M. Kelly and M.S. Skinner - Feb. 1979(UCB/EERC-79/10)A04

UCB/EERC-79/11 "Conservatism In Summation Rules for Closely Spaced Modes," by J.M. Kelly and J.L. Sackman - May 1979(PB 301 328)A03

UCB/EERC-79/12 "Cyclic Loading Tests of Masonry Single Piers; Volume 3 - Height to Width Ratio of 0.5," by P.A. Hidalgo, R.L. Mayes, H.D. McNiven and R.W. Clough - May 1979(PB 301 321)A08

UCB/EERC-79/13 "Cyclic Behavior of Dense Course-Grained Materials in Relation to the Seismic Stability of Dams," by N.G. Banerjee, H.B. Seed and C.K. Chan - June 1979(PB 301 373)A13

UCB/EERC-79/14 "Seismic Behavior of Reinforced Concrete Interior Beam-Column Subassemblages," by S. Viwathanatepa, E.P. Popov and V.V. Bertero - June 1979(PB 301 326)A10

UCB/EERC-79/15 "Optimal Design of Localized Nonlinear Systems with Dual Performance Criteria Under Earthquake Excitations," by M.A. Bhatti - July 1979(PB 80 167 109)A06

UCB/EERC-79/16 "OPTDYN - A General Purpose Optimization Program for Problems with or without Dynamic Constraints," by M.A. Bhatti, E. Polak and K.S. Pister - July 1979(PB 80 167 091)A05

UCB/EERC-79/17 "ANSR-II, Analysis of Nonlinear Structural Response, Users Manual," by D.P. Mondkar and G.H. Powell July 1979(PB 80 113 301)A05

UCB/EERC-79/18 "Soil Structure Interaction in Different Seismic Environments," A. Gomez-Masso, J. Lysmer, J.-C. Chen and H.B. Seed - August 1979(PB 80 101 520)A04

UCB/EERC-79/19 "ARMA Models for Earthquake Ground Motions," by M.K. Chang, J.W. Kwiatkowski, R.F. Nau, R.M. Oliver and K.S. Pister - July 1979(PB 301 166)A05

UCB/EERC-79/20 "Hysteretic Behavior of Reinforced Concrete Structural Walls," by J.M. Vallenas, V.V. Bertero and E.P. Popov - August 1979(PB 80 165 905)A12

UCB/EERC-79/21 "Studies on High-Frequency Vibrations of Buildings - 1: The Column Effect," by J. Lubliner - August 1979 (PB 80 158 553)A03

UCB/EERC-79/22 "Effects of Generalized Loadings on Bond Reinforcing Bars Embedded in Confined Concrete Blocks," by S. Viwathanatepa, E.P. Popov and V.V. Bertero - August 1979(PB 81 124 018)A14

UCB/EERC-79/23 "Shaking Table Study of Single-Story Masonry Houses, Volume 1: Test Structures 1 and 2," by P. Gülkan, R.L. Mayes and R.W. Clough - Sept. 1979 (HUD-000 1763)A12

UCB/EERC-79/24 "Shaking Table Study of Single-Story Masonry Houses, Volume 2: Test Structures 3 and 4," by P. Gülkan, R.L. Mayes and R.W. Clough - Sept. 1979 (HUD-000 1836)A12

UCB/EERC-79/25 "Shaking Table Study of Single-Story Masonry Houses, Volume 3: Summary, Conclusions and Recommendations," by R.W. Clough, R.L. Mayes and P. Gülkan - Sept. 1979 (HUD-000 1837)A06

UCB/EERC-79/26 "Recommendations for a U.S.-Japan Cooperative Research Program Utilizing Large-Scale Testing Facilities," by U.S.-Japan Planning Group - Sept. 1979(PB 301 407)A06

UCB/EERC-79/27 "Earthquake-Induced Liquefaction Near Lake Amatitlan, Guatemala," by H.B. Seed, I. Arango, C.K. Chan, A. Gomez-Masso and R. Grant de Ascoli - Sept. 1979(NUREG-CR1341)A03

UCB/EERC-79/28 "Infill Panels: Their Influence on Seismic Response of Buildings," by J.W. Axley and V.V. Bertero Sept. 1979(PB 80 163 371)A10

UCB/EERC-79/29 "3D Truss Bar Element (Type 1) for the ANSR-II Program," by D.P. Mondkar and G.H. Powell - Nov. 1979 (PB 80 169 709)A02

UCB/EERC-79/30 "2D Beam-Column Element (Type 5 - Parallel Element Theory) for the ANSR-II Program," by D.G. Row, G.H. Powell and D.P. Mondkar - Dec. 1979(PB 80 167 224)A03

UCB/EERC-79/31 "3D Beam-Column Element (Type 2 - Parallel Element Theory) for the ANSR-II Program," by A. Riahi, G.H. Powell and D.P. Mondkar - Dec. 1979(PB 80 167 216)A03

UCB/EERC-79/32 "On Response of Structures to Stationary Excitation," by A. Der Kiureghian - Dec. 1979(PB 80166 929)A03

UCB/EERC-79/33 "Undisturbed Sampling and Cyclic Load Testing of Sands," by S. Singh, H.B. Seed and C.K. Chan Dec. 1979(ADA 087 298)A07

UCB/EERC-79/34 "Interaction Effects of Simultaneous Torsional and Compressional Cyclic Loading of Sand," by P.M. Griffin and W.N. Houston - Dec. 1979(ADA 092 352)A15

UCB/EERC-80/01 "Earthquake Response of Concrete Gravity Dams Including Hydrodynamic and Foundation Interaction Effects," by A.K. Chopra, P. Chakrabarti and S. Gupta - Jan. 1980(AD-A087297)A10

UCB/EERC-80/02 "Rocking Response of Rigid Blocks to Earthquakes," by C.S. Yim, A.K. Chopra and J. Penzien - Jan. 1980 (PB80 166 002)A04

UCB/EERC-80/03 "Optimum Inelastic Design of Seismic-Resistant Reinforced Concrete Frame Structures," by S.W. Zagajeski and V.V. Bertero - Jan. 1980(PB80 164 635)A06

UCB/EERC-80/04 "Effects of Amount and Arrangement of Wall-Panel Reinforcement on Hysteretic Behavior of Reinforced Concrete Walls," by R. Iliya and V.V. Bertero - Feb. 1980(PB81 122 525)A09

UCB/EERC-80/05 "Shaking Table Research on Concrete Dam Models," by A. Niwa and R.W. Clough - Sept. 1980(PB81 122 368)A06

UCB/EERC-80/06 "The Design of Steel Energy-Absorbing Restrainers and their Incorporation into Nuclear Power Plants for Enhanced Safety (Vol 1A): Piping with Energy Absorbing Restrainers: Parameter Study on Small Systems," by G.H. Powell, C. Oughourlian and J. Simons - June 1980

UCB/EERC-80/07 "Inelastic Torsional Response of Structures Subjected to Earthquake Ground Motions," by Y. Yamazaki April 1980(PB81 122 327)A08

UCB/EERC-80/08 "Study of X-Braced Steel Frame Structures Under Earthquake Simulation," by Y. Ghanaat - April 1980 (PB81 122 335)A11

UCB/EERC-80/09 "Hybrid Modelling of Soil-Structure Interaction," by S. Gupta, T.W. Lin, J. Penzien and C.S. Yeh May 1980(PB81 122 319)A07

UCB/EERC-80/10 "General Applicability of a Nonlinear Model of a One Story Steel Frame," by B.I. Sveinsson and H.D. McNiven - May 1980(PB81 124 877)A06

UCB/EERC-80/11 "A Green-Function Method for Wave Interaction with a Submerged Body," by W. Kioka - April 1980 (PB81 122 269)A07

UCB/EERC-80/12 "Hydrodynamic Pressure and Added Mass for Axisymmetric Bodies," by F. Nilrat - May 1980(PB81 122 343)A08

UCB/EERC-80/13 "Treatment of Non-Linear Drag Forces Acting on Offshore Platforms," by B.V. Dao and J. Penzien May 1980(PB81 153 413)A07

UCB/EERC-80/14 "2D Plane/Axisymmetric Solid Element (Type 3 - Elastic or Elastic-Perfectly Plastic) for the ANSR-II Program," by D.P. Mondkar and G.H. Powell - July 1980(PB81 122 350)A03

UCB/EERC-80/15 "A Response Spectrum Method for Random Vibrations," by A. Der Kiureghian - June 1980(PB81 122 301)A03

UCB/EERC-80/16 "Cyclic Inelastic Buckling of Tubular Steel Braces," by V.A. Zayas, E.P. Popov and S.A. Mahin June 1980(PB81 124 885)A10

UCB/EERC-80/17 "Dynamic Response of Simple Arch Dams Including Hydrodynamic Interaction," by C.S. Porter and A.K. Chopra - July 1980(PB81 124 000)A13

UCB/EERC-80/18 "Experimental Testing of a Friction Damped Aseismic Base Isolation System with Fail-Safe Characteristics," by J.M. Kelly, K.E. Beucke and M.S. Skinner - July 1980(PB81 148 595)A04

UCB/EERC-80/19 "The Design of Steel Energy-Absorbing Restrainers and their Incorporation into Nuclear Power Plants for Enhanced Safety (Vol 1B): Stochastic Seismic Analyses of Nuclear Power Plant Structures and Piping Systems Subjected to Multiple Support Excitations," by M.C. Lee and J. Penzien - June 1980

UCB/EERC-80/20 "The Design of Steel Energy-Absorbing Restrainers and their Incorporation into Nuclear Power Plants for Enhanced Safety (Vol 1C): Numerical Method for Dynamic Substructure Analysis," by J.M. Dickens and E.L. Wilson - June 1980

UCB/EERC-80/21 "The Design of Steel Energy-Absorbing Restrainers and their Incorporation into Nuclear Power Plants for Enhanced Safety (Vol 2): Development and Testing of Restraints for Nuclear Piping Systems," by J.M. Kelly and M.S. Skinner - June 1980

UCB/EERC-80/22 "3D Solid Element (Type 4-Elastic or Elastic-Perfectly-Plastic) for the ANSR-II Program," by D.P. Mondkar and G.H. Powell - July 1980(PB81 123 242)A03

UCB/EERC-80/23 "Gap-Friction Element (Type 5) for the ANSR-II Program," by D.P. Mondkar and G.H. Powell - July 1980 (PB81 122 285)A03

UCB/EERC-80/24 "U-Bar Restraint Element (Type 11) for the ANSR-II Program," by C. Oughourlian and G.H. Powell July 1980(PB81 122 293)A03

UCB/EERC-80/25 "Testing of a Natural Rubber Base Isolation System by an Explosively Simulated Earthquake," by J.M. Kelly - August 1980(PB81 201 360)A04

UCB/EERC-80/26 "Input Identification from Structural Vibrational Response," by Y. Hu - August 1980(PB81 152 308)A05

UCB/EERC-80/27 "Cyclic Inelastic Behavior of Steel Offshore Structures," by V.A. Zayas, S.A. Mahin and E.P. Popov August 1980(PB81 196 180)A15

UCB/EERC-80/28 "Shaking Table Testing of a Reinforced Concrete Frame with Biaxial Response," by M.G. Oliva October 1980(PB81 154 304)A10

UCB/EERC-80/29 "Dynamic Properties of a Twelve-Story Prefabricated Panel Building," by J.G. Bouwkamp, J.P. Kollegger and R.M. Stephen - October 1980(PB82 117 128)A06

UCB/EERC-80/30 "Dynamic Properties of an Eight-Story Prefabricated Panel Building," by J.G. Bouwkamp, J.P. Kollegger and R.M. Stephen - October 1980(PB81 200 313)A05

UCB/EERC-80/31 "Predictive Dynamic Response of Panel Type Structures Under Earthquakes," by J.P. Kollegger and J.G. Bouwkamp - October 1980(PB81 152 316)A04

UCB/EERC-80/32 "The Design of Steel Energy-Absorbing Restrainers and their Incorporation into Nuclear Power Plants for Enhanced Safety (Vol 3): Testing of Commercial Steels in Low-Cycle Torsional Fatigue," by P. Spencer, E.R. Parker, E. Jongewaard and M. Drory

UCB/EERC-80/33 "The Design of Steel Energy-Absorbing Restrainers and their Incorporation into Nuclear Power Plants for Enhanced Safety (Vol 4): Shaking Table Tests of Piping Systems with Energy-Absorbing Restrainers," by S.F. Stiemer and W.G. Godden - Sept. 1980

UCB/EERC-80/34 "The Design of Steel Energy-Absorbing Restrainers and their Incorporation into Nuclear Power Plants for Enhanced Safety (Vol 5): Summary Report," by P. Spencer

UCB/EERC-80/35 "Experimental Testing of an Energy-Absorbing Base Isolation System," by J.M. Kelly, M.S. Skinner and K.E. Beucke - October 1980(PB81 154 072)A04

UCB/EERC-80/36 "Simulating and Analyzing Artificial Non-Stationary Earthquake Ground Motions," by R.F. Nau, R.M. Oliver and K.S. Pister - October 1980(PB81 153 397)A04

UCB/EERC-80/37 "Earthquake Engineering at Berkeley - 1980," - Sept. 1980(PB81 205 374)A09

UCB/EERC-80/38 "Inelastic Seismic Analysis of Large Panel Buildings," by V. Schricker and G.H. Powell - Sept. 1980 (PB81 154 338)A13

UCB/EERC-80/39 "Dynamic Response of Embankment, Concrete-Gravity and Arch Dams Including Hydrodynamic Interaction," by J.F. Hall and A.K. Chopra - October 1980(PB81 152 324)A11

UCB/EERC-80/40 "Inelastic Buckling of Steel Struts Under Cyclic Load Reversal," by R.G. Black, W.A. Wenger and E.P. Popov - October 1980(PB81 154 312)A08

UCB/EERC-80/41 "Influence of Site Characteristics on Building Damage During the October 3, 1974 Lima Earthquake," by P. Repetto, I. Arango and H.B. Seed - Sept. 1980(PB81 161 739)A05

UCB/EERC-80/42 "Evaluation of a Shaking Table Test Program on Response Behavior of a Two Story Reinforced Concrete Frame," by J.M. Blondet, R.W. Clough and S.A. Mahin

UCB/EERC-80/43 "Modelling of Soil-Structure Interaction by Finite and Infinite Elements," by F. Medina - December 1980(PB81 229 270)A04

UCB/EERC-81/01 "Control of Seismic Response of Piping Systems and Other Structures by Base Isolation," edited by J.M. Kelly - January 1981 (PB81 200 735)A05

UCB/EERC-81/02 "OPTNSR - An Interactive Software System for Optimal Design of Statically and Dynamically Loaded Structures with Nonlinear Response," by M.A. Bhatti, V. Ciampi and K.S. Pister - January 1981 (PB81 218 851)A09

UCB/EERC-81/03 "Analysis of Local Variations in Free Field Seismic Ground Motions," by J.-C. Chen, J. Lysmer and H.B. Seed - January 1981 (AD-A099508)A13

UCB/EERC-81/04 "Inelastic Structural Modeling of Braced Offshore Platforms for Seismic Loading," by V.A. Zayas, P.-S.B. Shing, S.A. Mahin and E.P. Popov - January 1981(PB82 138 777)A07

UCB/EERC-81/05 "Dynamic Response of Light Equipment in Structures," by A. Der Kiureghian, J.L. Sackman and B. Nour-Omid - April 1981 (PB81 218 497)A04

UCB/EERC-81/06 "Preliminary Experimental Investigation of a Broad Base Liquid Storage Tank," by J.G. Bouwkamp, J.P. Kollegger and R.M. Stephen - May 1981(PB82 140 385)A03

UCB/EERC-81/07 "The Seismic Resistant Design of Reinforced Concrete Coupled Structural Walls," by A.E. Aktan and V.V. Bertero - June 1981(PB82 113 358)A11

UCB/EERC-81/08 "The Undrained Shearing Resistance of Cohesive Soils at Large Deformations," by M.R. Pyles and H.B. Seed - August 1981

UCB/EERC-81/09 "Experimental Behavior of a Spatial Piping System with Steel Energy Absorbers Subjected to a Simulated Differential Seismic Input," by S.F. Stiemer, W.G. Godden and J.M. Kelly - July 1981

UCB/EERC-81/10 "Evaluation of Seismic Design Provisions for Masonry in the United States," by B.I. Sveinsson, R.L. Mayes and H.D. McNiven - August 1981

UCB/EERC-81/11 "Two-Dimensional Hybrid Modelling of Soil-Structure Interaction," by T.-J. Tzong, S. Gupta and J. Penzien - August 1981(PB82 142 118)A04

UCB/EERC-81/12 "Studies on Effects of Infills in Seismic Resistant R/C Construction," by S. Brokken and V.V. Bertero - September 1981

UCB/EERC-81/13 "Linear Models to Predict the Nonlinear Seismic Behavior of a One-Story Steel Frame," by H. Valdimarsson, A.H. Shah and H.D. McNiven - September 1981(PB82 138 793)A07

UCB/EERC-81/14 "TLUSH: A Computer Program for the Three-Dimensional Dynamic Analysis of Earth Dams," by T. Kagawa, L.H. Mejia, H.B. Seed and J. Lysmer - September 1981(PB82 139 940)A06

UCB/EERC-81/15 "Three Dimensional Dynamic Response Analysis of Earth Dams," by L.H. Mejia and H.B. Seed - September 1981 (PB82 137 274)A12

UCB/EERC-81/16 "Experimental Study of Lead and Elastomeric Dampers for Base Isolation Systems," by J.M. Kelly and S.B. Hodder - October 1981

UCB/EERC-81/17 "The Influence of Base Isolation on the Seismic Response of Light Secondary Equipment," by J.M. Kelly - April 1981

UCB/EERC-81/18 "Studies on Evaluation of Shaking Table Response Analysis Procedures," by J. Marcial Blondet - November 1981

UCB/EERC-81/19 "DELIGHT.STRUCT: A Computer-Aided Design Environment for Structural Engineering," by R.J. Balling, K.S. Pister and E. Polak - December 1981

UCB/EERC-81/20 "Optimal Design of Seismic-Resistant Planar Steel Frames," by R.J. Balling, V. Ciampi, K.S. Pister and E. Polak - December 1981

UCB/EERC-82/01 "Dynamic Behavior of Ground for Seismic Analysis of Lifeline Systems," by T. Sato and A. Der Kiureghian - January 1982 (PB82 218 926) A05

UCB/EERC-82/02 "Shaking Table Tests of a Tubular Steel Frame Model," by Y. Ghanaat and R. W. Clough - January 1982 (PB82 220 161) A07

UCB/EERC-82/03 "Experimental Behavior of a Spatial Piping System with Shock Arrestors and Energy Absorbers under Seismic Excitation," by S. Schneider, H.-M. Lee and G. W. Godden - May 1982

UCB/EERC-82/04 "New Approaches for the Dynamic Analysis of Large Structural Systems," by E. L. Wilson - June 1982

UCB/EERC-82/05 "Model Study of Effects of Damage on the Vibration Properties of Steel Offshore Platforms," by F. Shahrivar and J. G. Bouwkamp - June 1982